

Viktor Myrvågnes

Analyses and Characterization of Fossil Carbonaceous Materials for Silicon Production

Thesis for the degree philosophiae doctor

Trondheim, January 2008

Norwegian University of Science and Technology
Faculty of Natural Sciences and Technology
Department of Materials Science and Engineering



NTNU

Norwegian University of Science and Technology

Thesis for the degree philosophiae doctor

Faculty of Natural Sciences and Technology
Department of Materials Science and Engineering

© Viktor Myrvågnes

ISBN 978-82-471-6471-6 (printed version)
ISBN 978-82-471-6485-3 (electronic version)
ISSN 1503-8181

Doctoral theses at NTNU, 2008:30
IMT-Report 2008:30

Printed by NTNU-trykk

PREFACE

The PhD work presented in this thesis was carried out at the department of Materials Science and Engineering at the Norwegian University of Science and Technology from August 2003 to November 2007.

The doctoral work has been part of the CarboMat project which was funded by The Norwegian Research Council, The Norwegian Ferroalloy Producers Research Organization (FFF), Norwegian aluminium producers, Statoil and Elkem Carbon. Financial support from these organizations is greatly acknowledged.

Completion of this work would not have been possible without the assistance from a great many people. First and foremost, I would like to thank my supervisor, Professor Tor Lindstad, for the assistance he has provided throughout these years. Even though he is now retired, he has always been available for discussions and meetings. If there has been a problem he could not answer, his web of contacts always allowed him to send me in the right direction for help. I am deeply indebted for your patience and guidance – thank you very much.

I would also like to express gratitude to my good friend and office colleague through most of this work, Jakub Kaczorowski. Dr. Jakub finished his PhD work in 2006 and parts of his work also included coal and coke related subjects. It has been a tremendous support to have a fellow PhD student to discuss both scientific problems and every day life subjects. In addition, we have taken part in the same training with regard to characterizing coals and coke and accompanied each other on educational trips. Thank you for the company Jakub.

Professor Norbert Volkmann has been an invaluable source of knowledge and help during this PhD work. His enthusiasm regarding petrology and petrography is contagious. I would like to express my sincere gratitude for introducing petrographic techniques, providing us with his microscopes and staff for our education, proofreading and bringing “small gifts” from Germany on your many visits to Norway. Thank you very much for all the help Professor, and hope to see you a lot in the future as well.

Ralph Gray has been working with coal and coke his whole life and is an authority in the field. I am grateful for taking part in his lifelong experiences, and would also like to thank his son Daniel for assistance during the non-maceral and coke petrographic course in their private laboratory in Monroeville, USA.

The progress of this work has been closely monitored by my advisory group. I would like to thank Edin Myrhaug (Elkem), Birger Andresen (Fesil) and Ola S. Raaness (SINTEF) for many fruitful discussions and engagement in the problems addressed during the course of this work.

I would also like to thank the PhD students in the Carbomat project for help in practical matters, but especially for social events and common seminars. The Carbomat team

consisted of: Sten Yngve Larsen, Jakub Kazcorowski, Lina Jonasson, Kristin Vasshaug, Per Anders Eidem, Jafar Safarian, Michal Tkáč, Juraj Chmelar and Mohammed Ibrahim. In addition to these, my office neighbors Przemysław Szczygieł and Andreas Westermoen should also be mentioned.

I also appreciate the help from Steinar Prytz with reactivity measurements; Stein Rørvik with image analysis and Dr. Sean Gaal for helping with miscellaneous matters. In addition Łukasz Jarosz – my summer student from Poland – deserves a special attention for helping with taking microphotographs of both coal and coke samples.

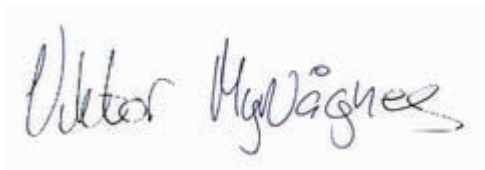
During the course of this work a number of coal and coke samples have been investigated under the petrographic microscope, and I sincerely appreciate the work of the “in house” coal preparation technicians Birgitte and Tone. The course in Freiberg really paid off – sehr gut und hertzlich dank meine Fräuleins.

A major part of this work has involved characterization of coal properties and understanding the factors influencing these. I would thus like to thank Henry Hansen and Sandra Todd for facilitating a visit to one of the Blue gem coal mines where we could observe the underground extraction of a very thin coal seam as well as the coal processing plant and accompanying laboratories.

In addition to the previously mentioned, I would like to thank the staff at both NTNU and SINTEF in Alfred Getz vei for being good colleagues and friends throughout this period.

Finally I would like to thank my wonderful partner Sandra and the most beautiful son in the whole wide world (Elias) for providing me with a sanctuary completely free from subjects even closely related to metallurgy and carbon thus liberating energy needed in order to finish this work. You are the best little family I could have ever hoped for and I love you both very very much.

Trondheim, November 2007

A handwritten signature in black ink, reading "Viktor Myrvågnes". The signature is written in a cursive style with a long horizontal stroke at the end.

Viktor Myrvågnes

ABSTRACT

Production of high silicon alloys is carried out in submerged arc furnaces by reduction of silicon bearing oxides (typically quartz) with carbon materials. Carbonaceous materials like coal, coke, charcoal and woodchips are commonly used as reduction materials in the process. Primarily based on historical prices of charcoal compared to fossil reduction materials, the Norwegian Ferroalloy Industry has mostly been using coal and coke (char) as the source of carbon. From a process point of view, the most important role of the carbonaceous material is to react with SiO gas to produce SiC. The ability of the reduction materials to react with SiO gas can be measured and the value is recognized as the reactivity of the carbon source. Reactivity is one of the most important parameters in the smelting process and is commonly acknowledged to strongly affect both productivity and specific energy consumption. The main objectives of this work has been to establish methods to characterize the material properties of fossil carbonaceous reduction materials used in the silicon process and to evaluated how these properties affect the reactivity towards SiO gas.

In order to accomplish these objectives, three run of mine (ROM) single seam coals which are particularly well suited for ferroalloy production were selected. Two Carboniferous coals from USA (Blue Gem) and Poland (Staszic) with similar rank, but significantly different composition as well as a Permian coal from Australia (Peak Downs) have been characterized by chemical- and petrographical methods. Blue Gem is a homogeneous coal, low in mineral inclusions and macerals of the inertinite group and determined to have a random vitrinite reflectance of 0.71 %. Staszic has a similar reflectance of vitrinite (0.72 %), but is determined to be a very inhomogeneous coal with both inertinite macerals and minerals embedded in the vitrinite matrix. Peak Downs has a random reflectance of vitrinite of 1.32 % and is hence the coal sample of highest rank. The highest amount of ash has been analyzed in this sample (11.6 %) and morphological studies of the sample revealed numerous clastic quartz inclusions throughout the coal matrix.

As constituents (macerals and minerals) in coal act differently upon carbonization, the ROM coals have been separated into different density fractions in order to obtain fractions with varying composition. Density fractions of the same coals proved to have significantly different petrographic composition, but were to some degree dependant upon the heterogeneity of the ROM coals.

The coals were carbonized according to a procedure simulating conditions the coals experience when charged to an industrial furnace. Both structure and texture of the resultant chars have been thoroughly examined. Petrographic examinations have been used to find the ratio of filler- and binder phase carbon forms in the carbonized samples. Generally, the correlation between fusible and infusible macerals in the coal samples agreed well with the ratio of binder- and filler phase carbon forms in the chars. A high amount of depositional carbons were however quantified in the Blue Gem sample which is due to a combination of carbonization procedure and nature of the coal sample.

Reactivity of the carbonized samples towards SiO gas was assessed by the SINTEF SiO reactivity procedure. To quantify the degree of conversion, a combination of weight increase of the carbon material following reaction with SiO gas and petrographic examinations of the reacted samples was used.

Results from the SINTEF test did reveal that Peak Downs was the most reactive material of the tested samples, and it was not possible to differentiate between the density fractions. The reason for the observed behavior of Peak Downs is due to the abundant quartz inclusions in the coal matrix. These inclusions will react with carbon at the reaction temperature of 1650°C to produce SiC and CO. In addition, the reaction will increase porosity and surface area of the material thus contributing to easier access for reacting gases which in turn will result in an increased reactivity and degree of conversion. Petrographic examinations of the reacted samples did in fact conclude with a degree of conversion close to 100 %.

Both density fractions of Blue Gem came out with similar reactivity values from the SINTEF test, and are termed intermediate of the tested materials. Blue Gem is a homogeneous coal, and there were no significant differences with regard to the petrographic composition of the density fractions. The effect of maceral composition on the reactivity towards SiO gas was thus hard to evaluate based on these samples. A degree of conversion between 80 – 90 % is estimated for the Blue Gem samples.

Staszic has been characterized as an inhomogeneous coal and the highest amount of infusible macerals and minerals are identified in the heaviest density fraction. The SINTEF SiO reactivity test revealed that there was a significant difference in reactivity between the two fractions. The highest density fraction of Staszic is the least reactive of all the tested materials and has a *R10 corrected* value more than 40 % higher than the lowest density fraction. As both fractions are of identical rank, the observed reactivity difference has to be caused by the higher amount of filler phase in the highest density fraction. The higher amount of filler phase did not affect the degree of conversion as values between 85 – 95 % was estimated for the Staszic samples.

Petrographic analyses have been extensively used throughout this work to characterize coal, carbonized coals and finally reacted samples. In order to fully understand the complexity of the coal samples, a combination of standard maceral analyses, non-maceral analyses and morphological studies is recommended. Petrographic analyses of the carbonized samples can give valuable information about the carbonization procedure and has in this work revealed massive formation of depositional carbon in the Blue Gem samples. Studies of the reacted samples under a petrographic microscope can render information about degree of conversion as well as which carbon forms are most reactive to SiO gas and preferential areas for condensation reactions.

CONTENTS

PREFACE	i
ABSTRACT	iii
CONTENTS	v
NOMENCLATURE	ix
1. CARBOTHERMIC PRODUCTION OF SILICON	1
1.1 Introduction	1
1.2 The Silicon Furnace	2
1.3 Main Compounds and Chemical Reactions	4
1.3.1 <i>Outer Reaction Zone</i>	6
1.3.2 <i>Inner Reaction Zone</i>	8
1.4 Carbonaceous Reduction Materials	10
1.4.1 <i>Composition of carbon materials recipe</i>	10
1.4.2 <i>Reduction materials</i>	11
2. REACTIONS BETWEEN SiO GAS AND CARBON	13
2.1 Introduction	13
2.2 Kinetic Models for Gas - Solid reactions	13
2.2.1 <i>Shrinking core model</i>	14
2.2.2 <i>Grain model</i>	17
2.3 Former studies of the reaction between SiO gas and Carbon Materials	20
2.3.1 <i>Gas analysis techniques</i>	20
2.3.2 <i>Thermogravimetric procedures</i>	22
2.3.3 <i>Correlations of material properties and reactivity</i>	25
2.4 Conversion Profiles and Shape of Reactivity Curves	26
3. COAL, COKE AND CARBONIZATION	29
3.1 Coal Formation and Metamorphosis	29
3.1.1 <i>Paleogeography and tectonics</i>	30
3.1.2 <i>Flora and climate</i>	32
3.2 Coal Metamorphosis	33
3.2.1 <i>Peatification (Biochemical coalification)</i>	34

3.2.2	<i>Coalification (Geochemical coalification)</i>	35
3.3	Coal Rank	37
3.3.1	<i>Rank parameters</i>	40
3.4	Microstructure of Coal	43
3.4.1	<i>Vitrinite</i>	44
3.4.2	<i>Liptinite</i>	45
3.4.3	<i>Inertinite</i>	46
3.4.4	<i>Mineral matter and trace elements in coal</i>	48
3.5	Carbonization and Production of Metallurgical Coke	50
3.5.1	<i>The effect of coal rank on carbonization</i>	52
3.5.2	<i>The effect of coal type on carbonization</i>	53
3.5.3	<i>The effect of coal grade on carbonization</i>	55
3.5.4	<i>Industrial production of metallurgical coke</i>	56
3.5.5	<i>Pore development during carbonization</i>	58
4.	EXPERIMENTAL PROCEDURES AND SAMPLE MATERIAL	61
4.1	Chemical and Physical Properties of Coal	61
4.1.1	<i>Proximate analysis</i>	61
4.1.2	<i>Ultimate analysis</i>	63
4.1.3	<i>Plastic properties of coal</i>	64
4.2	Petrographic Examinations	65
4.2.1	<i>Maceral analysis</i>	66
4.2.2	<i>Vitrinite reflectance</i>	66
4.2.3	<i>Non-maceral analysis</i>	67
4.2.4	<i>Coke petrography</i>	69
4.3	Density Separation	70
4.4	Carbonization Procedure	70
4.5	Structure and Texture of Char	71
4.5.1	<i>Image analysis</i>	71
4.5.2	<i>X-ray diffraction</i>	71
4.5.3	<i>BET surface area and total porosity</i>	74
4.5.4	<i>Mercury porosimetry</i>	74
4.6	SINTEF SiO-Reactivity Test	74

4.6.1	<i>Apparatus</i>	75
4.6.2	<i>Test procedure</i>	77
4.6.3	<i>Reactivity measure</i>	77
4.7	Sample Materials	78
4.7.1	<i>Blue Gem</i>	79
4.7.2	<i>Peak Downs</i>	82
4.7.3	<i>Staszic</i>	85
5.	EXPERIMENTAL RESULTS	89
5.1	Chemical- and Plastic Properties of Run of Mine (ROM) Coals	90
5.2	Coal Morphological Studies	91
5.2.1	<i>Blue Gem</i>	92
5.2.2	<i>Peak Downs</i>	93
5.2.3	<i>Staszic</i>	94
5.3	Density Separation of the ROM Coal Samples	95
5.4	Petrographic Analyses of Coal Samples	96
5.4.1	<i>Maceral analysis</i>	97
5.4.2	<i>Vitrinite reflectance</i>	103
5.4.3	<i>Non-maceral analysis</i>	107
5.5	Carbonization	110
5.6	Characterization of the Carbonized Coal Samples	111
5.6.1	<i>Morphology of samples</i>	112
5.6.2	<i>Textural analysis</i>	115
5.6.3	<i>X-ray diffraction</i>	120
5.6.4	<i>Physical properties</i>	123
5.6.5	<i>Pore size distributions and thickness of pore walls</i>	125
5.7	SINTEF SiO-Reactivity	131
5.7.1	<i>CO-concentration as a function of time</i>	132
5.7.2	<i>Time adjusted corrected reactivity curves</i>	134
5.7.3	<i>R10 corrected values</i>	135
5.7.4	<i>Degree of conversion</i>	137
5.7.5	<i>Effect of heat treatment of Peak Downs</i>	145
5.7.6	<i>Tangent in point of inflection as alternative reactivity measure</i>	148

5.8 Kinetic Parameters	150
5.8.1 <i>Thermogravimetric experiments</i>	151
5.8.2 <i>SINTEF test with reduced particle size</i>	151
6. DISCUSSION	159
6.1 Carboniferous- and Permian Coal samples	159
6.1.1 <i>Blue Gem</i>	160
6.1.2 <i>Peak Downs</i>	163
6.1.3 <i>Staszic</i>	164
6.2 Effect of Different Carbonization Procedures	164
6.2.1 <i>Physical properties</i>	165
6.2.2 <i>Coke petrography</i>	167
6.2.3 <i>X-ray diffraction</i>	168
6.3 Material Properties and Reactivity towards SiO gas	169
7. CONCLUSIONS AND FURTHER WORK	173
BIBLIOGRAPHY	177
APPENDIX A: COAL CLASSIFICATION SYSTEMS	191
APPENDIX B: COAL ALBUM	193
APPENDIX C: STANDARDS USED IN THE ANALYSES OF COAL SAMPLES	211
APPENDIX D: NON-MACERAL MICROTEXTURES	213
APPENDIX E: SYSTEMS FOR COKE NOMENCLATURE	215
APPENDIX F: ALBUM OF MICROTEXTURES IN CARBONIZED SAMPLES	217
APPENDIX G: REACTIVITY PROFILES	223
APPENDIX H: EVALUATION OF KINETIC PARAMETERS	227
APPENDIX I: DATA FROM REACTIVITY EXPERIMENTS	231

NOMENCLATURE

Abbreviations

<i>Ash</i>	High ash fraction
<i>BG</i>	Blue Gem
<i>CAQ</i>	Coke Anisotropy Quotient
<i>CRI</i>	Coke Reactivity Index
<i>daf</i>	Dry ash free
<i>dmmf</i>	Dry mineral matter free
<i>FCT</i>	Intensity correction factor
<i>Fix C</i>	Fixed Carbon
<i>FSI</i>	Free Swelling Index
<i>FWHM</i>	Full Width Half Maximum
<i>HD</i>	High Density fraction
<i>IA</i>	Image Analysis
<i>LCB</i>	Lublin Coal Basin
<i>LD</i>	Low Density fraction
<i>LSCB</i>	Lower Silesian Coal Basin
<i>MD</i>	Medium Density fraction
<i>MM</i>	Mineral Matter
<i>PD</i>	Peak Downs
<i>ROM</i>	Run of Mine
<i>St</i>	Staszic
<i>USCB</i>	Upper Silesian Coal Basin
<i>vol</i>	volatile

Symbols

<i>A</i>	Absorption factor (X-ray)
<i>a</i>	Stoichiometric coefficient
<i>A^a</i>	Ash on an as-received basis [wt%]

NOMENCLATURE

A_g	Surface area of grain [m^2]
A_p	Surface area of particle or pellet [m^2]
B	Full width half maximum of the carbon peak (002) (X-ray) [deg]
b	Stoichiometric coefficient
b	Full width half maximum of the silicon peak (111) (X-ray) [deg]
B_{ash}	Basicity index (expressed by equation 5.1)
b_r	Breadth of the X-ray beam at the sample position (X-ray) [m]
c	Stoichiometric coefficient
C_C	Molar density of pure carbon
$C_{CO,B}$	Concentration of CO gas in the bulk phase [moles/m^3]
$C_{SiO,B}$	Concentration of SiO gas in the bulk phase [moles/m^3]
C_{free}	Concentration of free carbon
C_{tot}	Total concentration of carbon
d	Stoichiometric coefficient
d_{002}	Interlayer spacing [\AA]
D_E	Effective diffusivity of particle [m^2/s]
f_c	Atom scattering factor (X-ray)
F_g	Shape factor of grain
F_{max}	Maximum fluidity [ddpm]
F_p	Shape factor of particle or pellet
$g_{F_g}(X)$	Conversion function for chemical reaction of the grains
$g_{F_p}(X)$	Conversion function for chemical reaction of the particle or pellet
h_D	External mass transfer coefficient [m^2/s]
$I(2\theta)$	Experimentally observed intensity (X-ray)
K	Shape factor (X-ray)
k_I	Correction factor for condensation
K_{ax}	X-rays wave (X-ray)
k_C	Chemical reaction rate constant [m/s]
K_E	Equilibrium constant for reaction 1.5
L	Lorentz factor (X-ray)
L_a	Layer plane diameter [\AA]

L_c	Stack height [\AA]
m_1	Mass of particles before reaction [kg]
m_2	Mass of particles after reaction [kg]
Mm_i	Molar mass of species i [kg/kmol]
m_p	Mass of particle [kg]
m_{p0}	Mass of particle before conversion starts [kg]
N	Total number of counted points in the point counting procedure
P	Polarization factor (X-ray)
P	Porosity in coke [%]
P	Applied pressure in mercury porosimetry [dyn/cm^2]
p	Percentage of components identified during point counting [%]
$p_{F_g}(X)$	Conversion function for diffusion through product layer on the grains
$p_{F_p}(X)$	Conversion function for diffusion through product layer on the particle
$P_r(2\theta)$	Profile fitted by calculation profiled (X-ray)
P_t^a	Total phosphorous on an as-received basis
Q_{Ar}	Gas flow of Argon through the reactor chamber [m^3/s]
Q_s^a	Gross calorific value on an as-received basis [Btu/lb]
R	Repeatability related to determination of petrographic composition
R	Factor expressing goodness of fit (X-ray) [%]
r	Pore radius [cm]
$R10$	Reactivity measure from the SINTEF test [ml SiO]
$R10_{corr}$	Corrected Reactivity measure from the SINTEF test [ml SiO]
R_g	Characteristic dimension of grain [m]
R_g	Length of goniometer arm (X-ray) [m]
R_{max}	Maximum reflectance of vitrinite in oil [%]
R_{min}	Minimum reflectance of vitrinite in oil [%]
R_p	Characteristic dimension of particle or pellet [m]
R_r	Random reflectance of vitrinite in oil [%]
R_{tex}	Relative reactivity index
S_t^a	Total amount of sulfur on an as-received basis [wt%]
Sh^*	modified Sherwood number

NOMENCLATURE

T	Temperature [°C, K]
t	Time [s]
$t_{18\%}$	Time when CO concentration drops below 18 %
$t_{10\%}$	Time when CO concentration drops below 10 %
t_c	Sample thickness (X-ray) [m]
t_{end}	Time when CO concentration drops below 5.2 %
t_g^*	Dimensionless time for the grain model
T_m	Temperature of maximum fluidity [°C]
T_r	Solidification temperature [°C]
T_s	Temperature of initial softening [°C]
t_s^*	Dimensionless time for the shrinking core model
$V_{5..15}$	Vitrinoid types referring to the reflectance of vitrinite
V^a	Volatile matter on an as-received basis [wt%]
V^{daf}	Volatile matter on a dry ash free basis [wt%]
V_g	Volume of grain [m ³]
V_p	Volume of particle or pellet [m ³]
W^a	Moisture on an as-received basis [wt%]
w_{FC0}	Mass fraction of fixed carbon just before conversion starts
X	Degree of conversion
x	Fixed carbon content in charge mixture (carbon coverage)

Greek letters

α_C	Volume fraction of pure carbon
β	Width of divergence slit (X-ray) [m]
β_c	FWHM of diffraction profile corrected for broadening (X-ray)
$\Delta H_{R,T}$	Enthalpy of reaction at a given temperature [kJ/mol]
Δt	Change in time
θ	Diffraction angle (X-ray) [deg]
λ	Wavelength (X-ray) [nm]
μ'	Apparent absorption coefficient (X-ray)
ρ_A	Absolute density [kg/m ³]

ρ_s	Particle density [kg/m ³]
σ	Surface tension of mercury [dyn/cm]
$\hat{\sigma}$	Gas-solid reaction modulus for the grain model
$\hat{\sigma}_g$	Gas-solid reaction modulus for the grains in the grain model
$\hat{\sigma}_s$	Gas-solid reaction modulus for the shrinking core model
σ_t	Standard deviation for the count pointing procedure
φ	Contact angle between mercury and carbon [deg]

1. CARBOTHERMIC PRODUCTION OF SILICON

The most economically feasible way to produce metallurgical grade silicon is still by carbothermic reduction of quartz in electric submerged arc furnaces. In this chapter a short introduction to the commercial production of silicon will be given.

Schei, Tuset and Tveit (1998) have given a comprehensive overview of the silicon production, reactions in the process, applications of silicon and other aspects related to the process of producing silicon. The reaction between SiO gas and carbonaceous materials (in particular charcoal) is very well covered by **Myrhaug (2003)** in his Dr. ing thesis. An extensive review of the reactions in the system SiO₂ – C – SiC is provided by **Wiik (1990)**. Unless otherwise stated, the following chapter is based on these works.

1.1 Introduction

Although the computerized control systems, safety and environmental issues as well as supporting logistics have improved drastically during the last century, the basic process is still the same. Quartz is reduced by carbon in the form of coal, coke, charcoal, petroleum coke or woodchips and silicon is produced as predicted from the idealized gross reaction of the process:



The process is more complicated than expressed by *reaction 1.1*, and will be covered in more detail in section 1.3.

According to **Valderhaug (1992)**, a typical silicon plant can be divided into four main parts:

Raw material handling: Includes all the stages from the raw materials are unloaded until they are charged to the furnace. (i.e. transport, storing, mixing and weighing).

Furnace(s): A silicon plant usually contains more than one furnace. Although size and technological level might be very different, a silicon furnace includes electricity supply, equipment for adding raw materials, a furnace body (consisting of a shell and lining) and equipment for tapping the liquid metal from the lower part of the furnace body. The furnace is further described in the next section.

Energy recovery and waste gas purification The waste gas from the production leaves the furnace at very high temperatures and contains large quantities of condensed silica fume (0.2 – 0.4 tons per produced ton of metal). The condensed silica is usually separated from the gas in large bag-house filters. Energy in the off-gases

might be recovered as hot water or steam and subsequently transformed into electricity.

Metal processing: Includes refining, casting, crushing, sizing and sieving.

The principal parts of a modern silicon plant are illustrated in Figure 1.1.

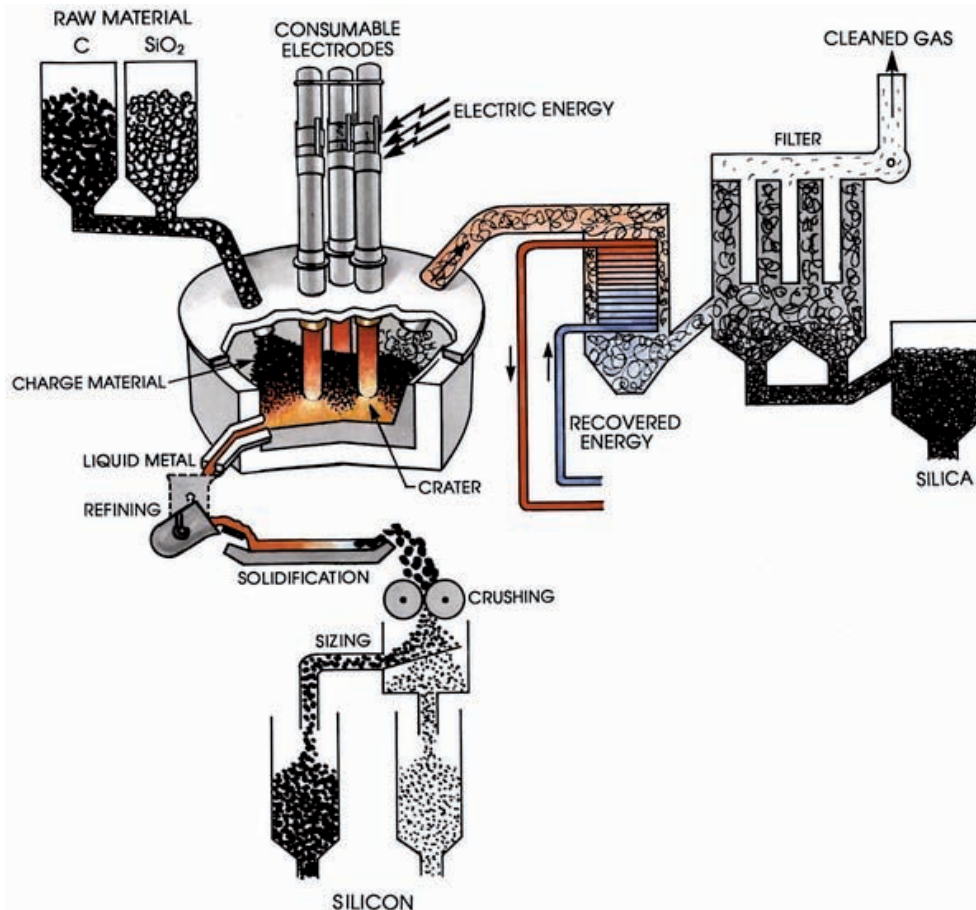


Figure 1.1: Principal parts of a modern silicon plant. After Schei et al. (1998).

Based on purity of the produced silicon, it is generally divided into grades with different applications. The three most common markets for metallurgical grade silicon are:

- Alloying of other metals (most common as an alloying element in aluminium alloys).
- Raw material for the chemical industry (production of silicones).
- Raw material for the semiconductor industry. (Required impurity levels for electronic devices and photovoltaic cells are respectively in the low ppb and ppm ranges).

1.2 The Silicon Furnace

The principal parts of a modern silicon plant are illustrated in Figure 1.1 and shortly described in the previous section. Even though the equipment has become more and

more sophisticated with time, the silicon furnace still remains the heart of a silicon plant. Silicon metal and high silicon ferroalloys are produced in submerged electric arc furnaces (EAF). They consist of furnace bodies in the shape of shallow crucibles made of steel shells and furnace linings that can withstand extremely high temperatures and attack by chemicals. Under operation, the furnace is filled to its rim by raw materials charged by gravity through a system of silos and charging tubes. In Figure 1.1 only one of the charging tubes are visible, but as evenly distributed raw materials throughout the cross sectional area of the furnace is of importance, there are several charging tubes contributing to fulfilling this criterion (see **Valderhaug (1992)**).

Energy needed for the smelting reactions is supplied as 3-phase alternating current through three electrodes which are positioned vertically and submerged deep into the charge mixture. As much as 90 – 95 % of the supplied energy is dissipated as heat from electric arcs in gas filled cavities surrounding the electrode tips.

An illustration of the inner structure of a silicon furnace is given in Figure 1.2.

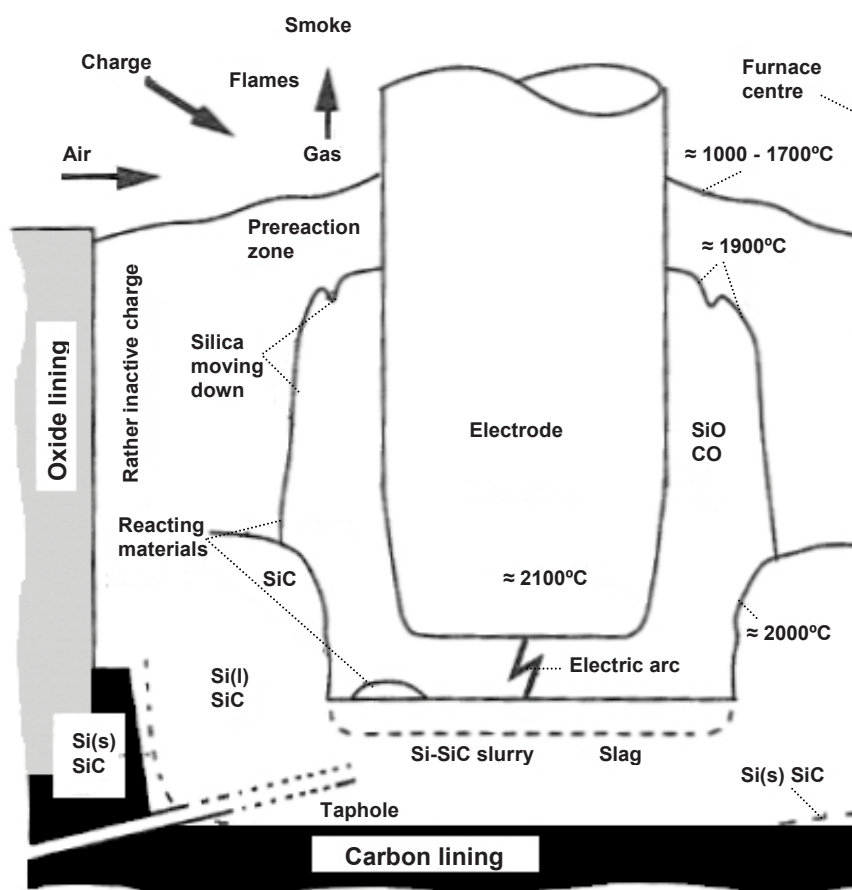


Figure 1.2: The inner structure of a silicon furnace. After Schei et al. (1998)

As most of the energy supplied is dissipated from the electrode tips, the temperature is highest in this part of the furnace, which can be seen in Figure 1.2. A furnace is thus typically divided into high- and low temperature zones which are also denoted as the inner- and outer reactions zones, respectively.

The metal forming reactions, which require temperatures exceeding 1800°C, are taking place in the inner reaction zone of the furnace. Liquid silicon metal is removed from the furnace in tapping channels through the furnace lining at the connection between the side walls and the bottom of the furnace. According to **Schei et al. (1998)**, the tapping procedure can be continuous or batch wise.

Reactions in the inner reaction zone are producing large amounts of gases which predominantly consist of CO and SiO. Formation of these gases is resulting in large gas filled cavities around each electrode which can be seen in Figure 1.2. These cavities are often referred to as craters. As SiO gas is an energy rich intermediate component in the process it needs to be recovered in the outer reaction zone. Most of the SiO gas is reacting with preheated and accessible carbon in the reduction materials under formation of solid SiC and CO gas. In the colder parts of the furnace some of the SiO gas will condense under formation of a condensate consisting for the most part of SiO₂ and Si. Some of the SiO gas will however not be recovered in the process and leaves the furnace with CO gas. As oxygen is available at the top of the furnace, SiO gas will oxidize producing amorphous SiO₂ (silica fume or microsilica) which is recovered in the filters (see Figure 1.1). Silica fume is sold as a valuable by-product of the process.

The craters surrounding each electrode are not connected, but separated by charge materials in various states of conversion. The craters are formed due to excessive generation of gases in the inner reaction zone combined with sticky condensate which are descending at a slower rate than actually consumed in the upper part of the gas filled cavities. The volume of the bed positioned straight above each crater is, according to **Andresen (1995)** referred to as the furnace shaft and is believed to confine the most active part of the charge. There are local variations when it comes to composition of the charge materials constituting the furnace shaft. These variations can affect gas distribution from the inner reaction zone and gas channels may develop. When a gas channel from the inner reaction zone is extending through the furnace shaft to the top of the charge, gas rich in SiO is released directly to the off gas system (see Figure 1.1) and the furnace is said to be blowing. During operation, the craters tend to expand in the vertical direction (i.e. decreasing thickness of the furnace shaft) thus increasing the possibilities for blowing. When the furnace is blowing, SiO gas is lost from the process thus decreasing the silicon recovery and increasing the specific energy consumption (section 1.3). In order to minimize the effect of blowing, the crater walls are broken by mechanical stokers at regular intervals and raw materials are added on top of the furnace to increase the furnace shaft thickness. The silicon process can thus be said to have a cyclic pattern.

1.3 Main Compounds and Chemical Reactions

The ideal gross reaction of the reduction of quartz by carbon is described by *reaction 1.1*. Carbon coverage in the charge is directly correlated to the silicon recovery. The carbon coverage can, according to **Schei and Halvorsen (1991)**, be defined by the parameter x in reaction with quartz: $SiO_2 + xC$. Depending on the carbon coverage both desired- and undesired reactions can occur:



The overall reaction for silicon production is given by *reaction 1.1* with x being equal to 2. An undercoked charge is characterized by a lower than optimal carbon coverage and will result in excessive formation of gas and hence reduced silicon recovery due to loss of SiO gas. This is expressed by setting x equal to 1 in *reaction 1.2*. Addition of too much carbon brings about an overcoked furnace which is expressed by *reaction 1.3* with x being equal to 3. A higher than optimal carbon coverage will result in accumulation of SiC in the furnace which is also causing a reduction in the silicon recovery. Correlation between carbon coverage and silicon recovery is illustrated in Figure 1.3.

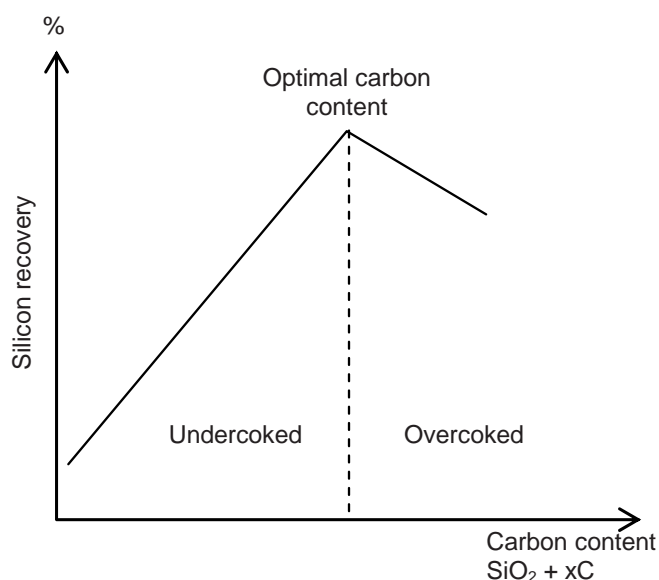
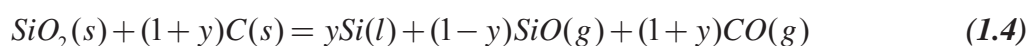


Figure 1.3: Silicon recovery as a function of the carbon content in the charge. Modified after Valderhaug (1992).

Assuming stoichiometric balance in the furnace, *reactions 1.1* and *1.2* can be combined to express the silicon recovery as:



The recovery of silicon is expressed as the amount of silicon in quartz that is recovered in the produced silicon metal. In *reaction 1.4*, y denotes the silicon recovery ($0 \leq y \leq 1$).

As mentioned in section 1.1, the chemistry of the process is however more complicated than expressed by *reactions 1.1 – 1.3*. The silicon producing reactions are taking place in the hottest parts of the furnace also referred to as the inner reaction zone. Recovery of

silicon in the form of SiO is however occurring in the upper part of the charge also denoted the outer reaction zone. A stoichiometric model first developed by **Motzfeldt (1961)** and later extended by **Schei and Halvorsen (1991)** is illustrating the main chemical reactions and material flows in the process. A sketch of the model is presented in Figure 1.4.

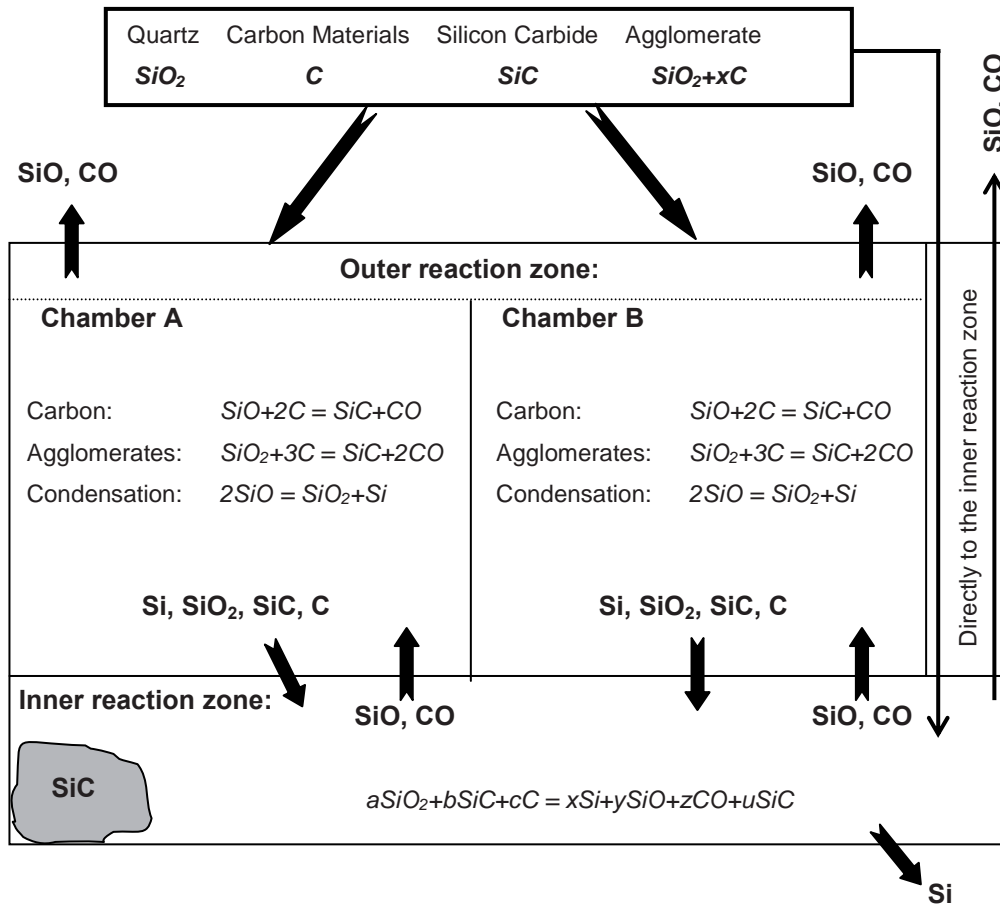


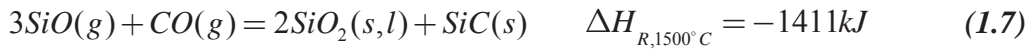
Figure 1.4: The stoichiometric model illustrating chemical reactions in the inner- and outer reaction zones as well as material flows. Modified after Schei and Halvorsen (1991).

1.3.1 Outer reaction zone

As much as 93 % of the energy required to reduce quartz to liquid silicon is fact used in the first reduction step to SiO gas. This implies that loss of SiO gas does not only have a negative effect on the recovery of silicon metal, but the specific energy consumption will also increase. As a result of these factors, it is essential to recover SiO gas which is produced in the inner reaction zone in the colder parts of the charge. **Schei and Halvorsen (1991)** have presented the following main reactions in the outer reaction zone:



Among others, **Motzfeldt (1961)** and **Otani et al. (1968)** claim that the following reactions also are taking place in this zone:



In order to have a better understanding of the reactions in the Si-O-C system and the stable phases depending on temperature and partial pressure of SiO gas, equilibrium relations of the main reactions in this system are presented in Figure 1.5.

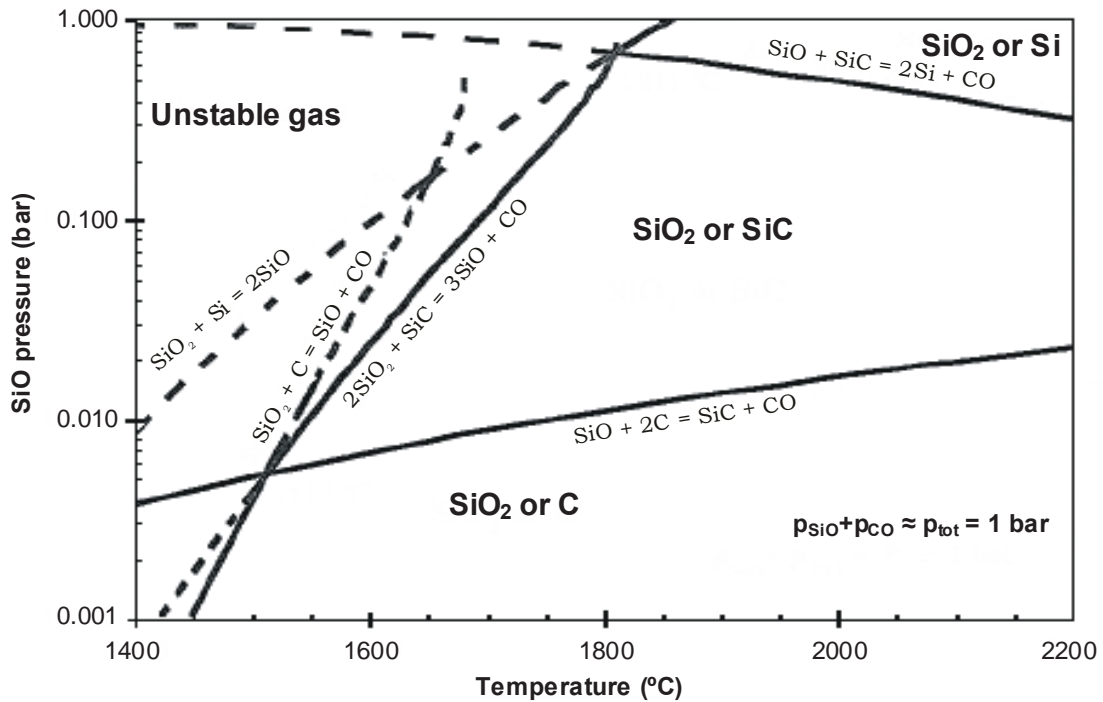


Figure 1.5: Equilibrium SiO-pressures above the condensed phase combinations C-SiC, SiO₂-C, SiO₂-SiC, SiC-Si and SiO₂-Si. Gas compositions corresponding to points above the condensation reactions are unstable. Broken lines indicate that the gas composition is in an unstable area. Total pressure in the system is 1 bar. After Schei et al. (1998).

Even though there is a temperature gradient in the furnace, temperatures about 1500°C are often assumed for the outer reaction zone. **Johansen et al. (1998)** have measured the temperature in the charge of an industrial silicon furnace and are reporting a value of up to 1300°C close to the surface. The reaction enthalpies have been calculated with HSC version 4.1 (**Roine 1997**). The bulk of the SiO gas generated in the inner reaction zone

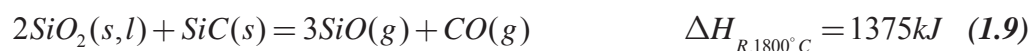
is recovered by reaction with carbonaceous reduction materials according to *reaction 1.5*. This is the most important reaction in the outer reaction zone as SiC is a product of the reaction. As can be seen from Figure 1.4, SiC is an intermediate product in the process which is essential for the silicon producing reactions in the inner reaction zone. The ability of the carbonaceous reduction materials to react with SiO gas according to this reaction is referred to as the reactivity in the silicon process. According to **Tuset and Raaness (1976)**, the reactivity of the reduction materials is one of the most important process parameters. One of the main objectives of the work presented in this thesis is to obtain a better understanding of how properties of fossil reduction materials used in the silicon process influence the reactivity expressed by *reaction 1.5*. From Figure 1.5 it can be seen that less than 1 % of the SiO gas would leave the furnace if this reaction is at equilibrium. The reaction is, according to **Schei et al. (1998)**, however slow at temperatures below 1500°C. Reactivity of carbonaceous materials in the silicon process has through the last decades received a great deal of attention and will be further elucidated in Chapter 2 of this thesis.

From *reaction 1.6* it can be seen that condensation of SiO gas is a highly exothermic reaction. The quantity of SiO gas that can be recovered as condensate is thus limited by the heat capacity of the charge and contributions from heat consuming reactions. Evaporation of moisture from the charged raw materials and gasification of volatiles from coal and woodchips are examples of such reactions. As SiO gas from the inner reaction zone passes through the colder charge, temperature of the gas drops and at temperatures below approximately 1500°C, condensation expressed by *reaction 1.6* is preferred above *reaction 1.5*. Even though condensation of SiO gas according to *reactions 1.7* and *1.8* are thermodynamically more stable than *reaction 1.6* (see Figure 1.5) at temperatures below approximately 1650°C, the latter has according to **Shei et al. (1998)** been proven by observations to dominate.

Quartz may react directly with carbon according to *reaction 1.3* at temperatures above approximately 1500°C. This reaction can be seen as a combination of *reaction 1.2* and *reaction 1.5*. Normally this reaction is considered to be negligible when lumpy raw materials are used. The reaction can proceed to some extent when agglomerates of intimately mixed quartz and carbon are used as part of the feed. Some fossil reduction materials do have a substantial amount of quartz inclusions embedded in the organic matrix and *reaction 1.3* might thus affect the process. The direct reaction between quartz and carbon is a strongly endothermic reaction (see *reaction 1.3*) and will increase the heat absorption capacity of the charge mixture in the outer reaction zone. This reaction is allowing more SiO gas to condense according to *reaction 1.6*.

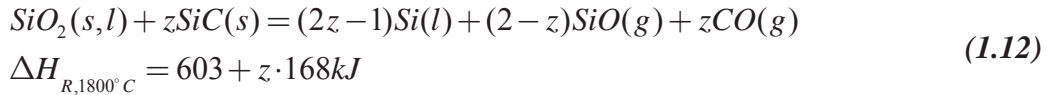
1.3.2 Inner reaction zone

The silicon producing reactions are taking place at higher temperatures. The intermediate product, SiC, produced in the outer reaction zone will react with SiO₂ in the inner reaction zone. **Schei and Halvorsen (1991)** have presented the following reactions to be of importance in this zone:





Combining these reactions results in the following:



where z is the amount of available SiC in the inner reaction zone ($0.5 \leq z \leq 1$). Both *reaction 1.9* and *reaction 1.12* are combinations of *reaction 1.10* and *reaction 1.11*. The enthalpies of reaction have been calculated at a temperature of 1800° by using HSC version 4.1.

From the above mentioned reactions, the importance of generation of SiC in the outer reaction zone is obvious as this compound is necessary for production of liquid silicon as expressed by *reaction 1.11*.

According to **Andresen (1995)**, the stable combination of condensed phases in the Si-O-C system above a temperature of 1514°C is SiO₂ and SiC when SiO₂ is in surplus of what is required from *reaction 1.3*. These compounds react following *reaction 1.9*, generating large amounts of gases. The equilibrium pressure of SiO gas is, as can be seen from Figure 1.5, increasing strongly with increasing temperature. At 1811°C it is reaching a level where liquid silicon can be formed as expressed by *reaction 1.11*. This is the lowest possible temperature for direct formation of silicon at a total partial pressure of SiO- and CO gas equal to one bar. Direct metal formation is dependant on a high partial pressure of SiO gas as well as high temperatures. From Figure 1.5, it can be seen that the reaction has a partial pressure of SiO at equilibrium of 0.67 bar at 1811°C while it is decreasing to a value of 0.5 bar at a temperature of approximately 2000°C.

The SiO generating reactions in the inner reaction zone are highly endothermic as can be seen by the reaction enthalpies in *reactions 1.9* and *1.10*. These reactions are thus consuming most of the heat generated by the electric arcs. They are believed to be the slowest of the proposed reactions and are not limited by chemical equilibrium.

As the silicon forming reaction in the inner reaction zone (*reaction 1.11*) is dependant upon a high partial pressure of SiO gas, reactions consuming SiO will tend to reduce the recovery of liquid silicon metal. Conversion of the carbon material in the outer reaction zone is thus of utter importance as unreacted carbon in the inner reaction zone will react with SiO gas according to *reaction 1.5*. According to **Schei et al (1998)**, the silicon recovery might drop from 100 % with fully converted carbon materials to 50 % with a conversion degree of 67 %.

1.4 Carbonaceous Reduction Materials

Quality of the carbonaceous reduction materials is considered to be of importance to achieve a high silicon yield in the silicon process. Reactivity and degree of conversion, as expressed by *reaction 1.5*, are directly affecting the silicon recovery as well as the specific energy consumption and thus process profitability. In addition to material parameters affecting the process, the level of mineral matter and trace elements are essential in order to produce metal of the required quality. Product specification of silicon is dependant upon the range of application (section 1.1).

1.4.1 Composition of carbon materials recipe

Composition of the reduction materials recipe is aspiring to fulfill both the process requirements and product specification with regard to amount and type of impurities. **Kallfeltz (2001)** have presented compositions for carbonaceous materials used as reductants in the silicon process for silicon smelters in different parts of the world. The compositions are presented in Figure 1.6.

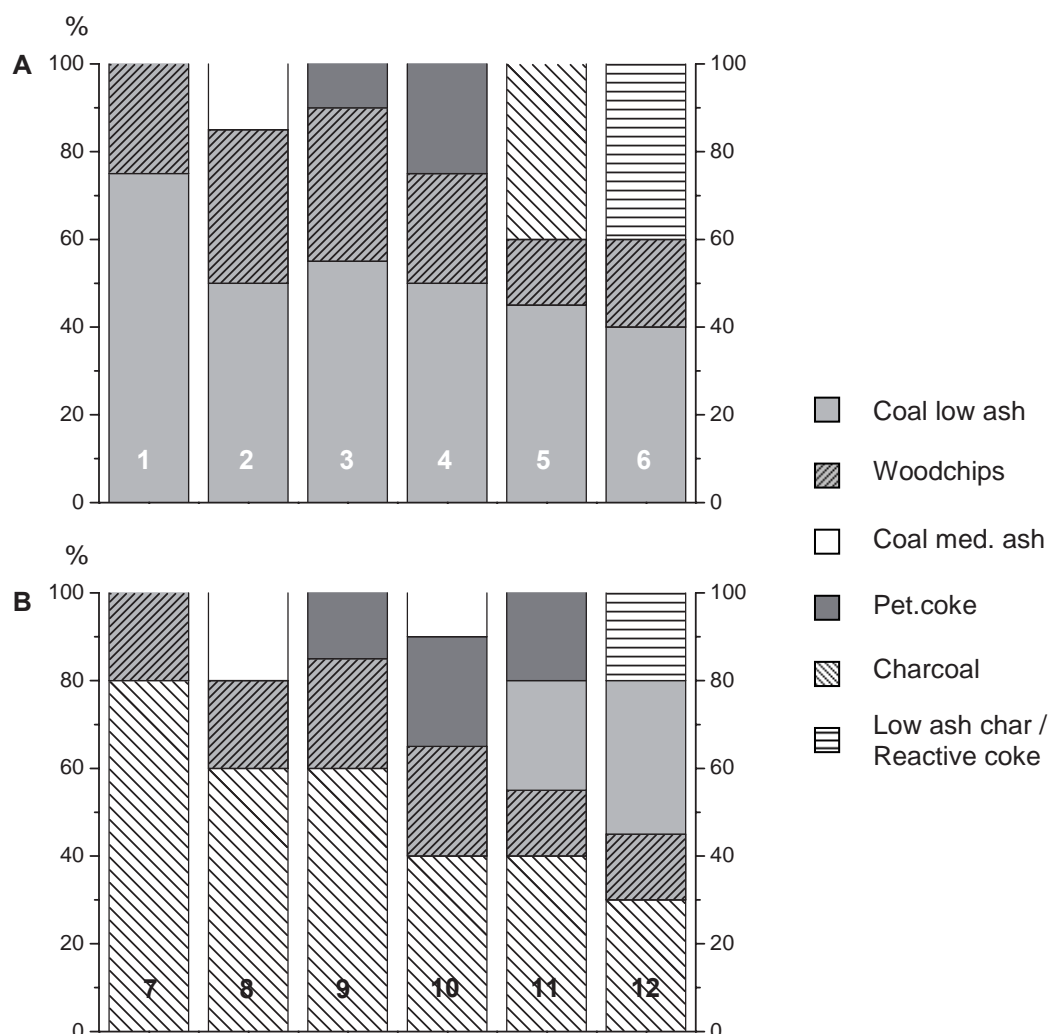


Figure 1.6: Compositions of carbonaceous reduction materials for silicon production with basis on fossil materials (A) and charcoal (B), respectively. Figure modified after Kallfeltz (2001).

From Figure 1.6, it can be seen that the only common reduction material for all silicon producers reported by **Kallfeltz (2001)** is woodchips. Woodchips are, as can be seen in section 1.4.2, added for process purposes. The author claims that the compositions are reflecting the availability of carbonaceous materials suitable for silicon production in different parts of the world as well as different experiences.

1.4.2 Reduction materials

In order to produce silicon metal, the silicon containing oxide (quartz) has to be reduced. The most common way to achieve this is by using carbonaceous materials as reductants in the process. Composition of the reduction materials depend upon several factors including availability of raw materials, process parameters and purity of the produced metal. In the following a short description of the most common carbonaceous materials used in the silicon process is given:

Coal: Coal is a fossil carbonaceous material that is fairly commonly used as a reductant in the silicon process. Properties of coal are determined by organic materials from which it is the solid product, conditions at the time of deposition and parameters that influence the maturity of coal. Main properties of coal affecting both the process and purity of the produced metal are: rank, maceral composition and amount and origin of mineral inclusions in the coal. Properties of coal and factors affecting these are thoroughly covered in Chapter 3 of this thesis.

Coke and char: Metallurgical coke is the solid residue after a controlled carbonization of bituminous coal. As most of the metallurgical coke is used in the blast furnace production of pig iron, main requirements are high strength and low reactivity towards CO_2 . Production of metallurgical coke and parameters influencing properties of the final product are described in section 3.5.

As properties of metallurgical coke do not correlate well with the requirements for reduction materials in the silicon process, char and reactive coke are more commonly used than metallurgical coke. According to **Byrne and Marsh (1995)**, char constitute carbonization products from wood, activated carbons or coal that do not pass through a plastic stage during pyrolysis and carbonization. Chars can be differentiated from metallurgical cokes by the level of anisotropy, with the former being isotropic while the latter are characterized by a high degree of anisotropy.

Charcoal: Charcoal is a biological reduction material and has been produced for centuries if not millenniums. Charcoal for the silicon process is produced by pyrolysis and carbonization of wood at moderate heating rates.

According to **Pinheiro et al. (2001)**, the process can be divided into the following main stages:

< 110°C	Heating and drying
110 - 270°C	Endothermic decomposition of wood
270 - 400°C	Exothermic decomposition of wood
~ 400°C	Charcoal containing some tar
~ 500°C	Carbonization complete
500 - 1000°C	Gasification and degradation of charcoal

Excellent reviews of charcoal production and properties are given by **FAO (1985)** and **Antal Jr. and Grønli (2003)**.

Petroleum-coke: Petroleum coke is often termed pet.coke or petrol coke and is as the name indicates a by-product of the oil refining process. Petroleum coke is generated in a process called delayed coking. In this process the heavy fractions from crude oil distillation are heated to approximately 500°C where they crack, generating hydrocarbons of lower molecular weight and a solid residue which is petroleum coke. Further information about delayed coking, parameters influencing the process and properties of the different types of petroleum coke (sponge-, shot- and needle coke) is given by **Ellis and Paul (1998)**.

Woodchips: Inclusion of woodchips in the raw materials recipe is resulting in a higher permeability in the furnace thus contributing to a better distribution of the gas flow through the burden and minimizing the effects of blowing.

2. REACTIONS BETWEEN SiO AND REDUCTION MATERIALS

According to **Szekely et al. (1976)**, reactions between solids and gases play a major role in a number of industrialized processes. Typical examples are: reduction of metal ores, combustion of solid fuels and coal gasification.

In the following chapter, a short introduction to gas – solid reactions will be given with emphasis on the reaction between carbon and SiO gas. The most relevant kinetic models for this reaction will be presented before a survey of previous studies on the SiO reactivity concludes this chapter.

2.1 Introduction

The ability of the carbonaceous reduction materials to react with SiO gas according to *reaction 1.5* is referred to as the SiO-reactivity. Reactivity of the carbonaceous materials in the outer reaction zone is affecting recovery of silicon metal, specific energy consumption and profitability of the process. This reaction has thus been subjected to special attention in the past decades (section 2.3).

2.2 Kinetic Models for Gas – Solid Reactions

According to **Sohn (1997)**, the most important reactions in metallurgical- and materials processing are those in which a fluid reacts with a solid, producing a coherent layer of porous products. These reactions can in general be expressed by equation 2.1:



Kinetic models describing the conversion of porous particles in a gaseous environment can generally be classified into the following categories:

1. The original homogeneous models, which treat both porous- and non-porous solids as continuums. These models were first proposed by **Ishida and Wen (1968)**.
2. The grain models which treat the porous solid as an agglomerate of solid grains. Reactant and product gases are transported to and from the non-porous grains by diffusion, and the grains are reacting according to the shrinking core model. The model was first presented by **Szekely and Evans (1970)** and has later been modified to include porous grains and distribution of grain sizes.
3. The pore models which treat the solid phase as a continuum with pores. The random pore model was in its original form presented by **Bhatia and Perlmutter (1980)**. The original model was extended in papers by **Bhatia and Perlmutter (1981 and 1983)**.

Based on previous studies of the reaction between carbon and SiO gas, the shrinking core- and grain models have proven to describe the relationship between degree of conversion and time well. In the following a more in-depth description of these models will be given.

2.2.1 Shrinking core model

The shrinking core model was first developed by **Yagi and Kunii (1955, 1961)**, and is conceptually a relatively simple model. An initially non-porous solid reactant is assumed to react with a gas from the outer surface. The chemical reaction proceeds in a topochemical manner from the outer surface towards the center, producing a product layer (ash) around the unreacted core of the solid reactant. The reaction is taking place at a sharp boundary between the two zones. An illustration of the shrinking core model is given in Figure 2.1. Based on the conceptual- and mathematical simplicity of the model, it has been extensively studied and applied to a wide range of reactions. According to **Levenspiel (1999)**, the reaction consists of five steps:

1. Diffusion of gaseous reactant through the gas film surrounding the particles.
2. Diffusion of gaseous reactant through the product layer to the surface of the unreacted core of solid reactant.
3. Chemical reaction according to *reaction 2.1*.
4. Diffusion of gaseous products through the product layer to the surface of the particle.
5. Diffusion of gaseous products through the gas film surrounding the particle.

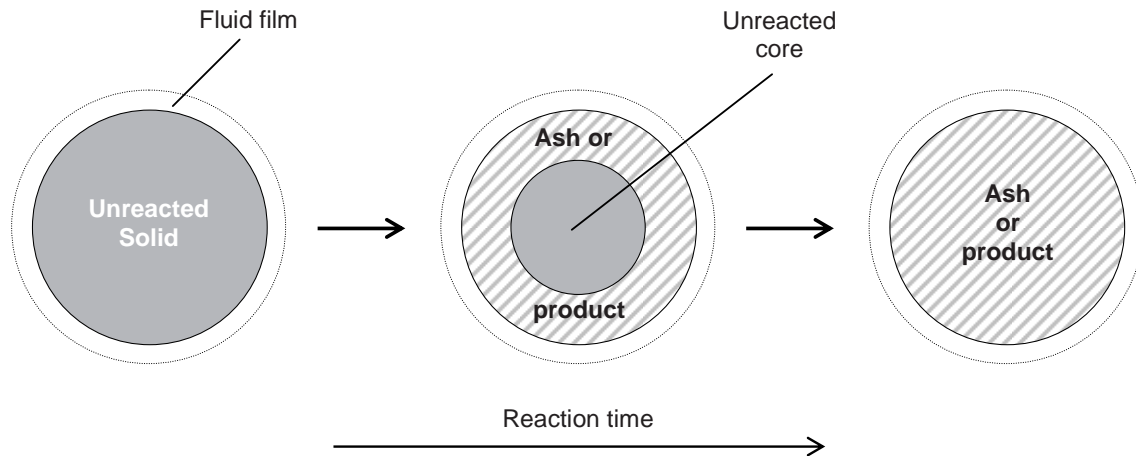


Figure 2.1: A gas - solid reaction proceeding with the formation of a shrinking unreacted core. Modified after Szekely et al. (1976).

External mass transfer, diffusion through the porous product layer and chemical reaction are all factors in a dimensionless equation presented by **Sohn (1997)** for the relation between degree of conversion and reaction time:

$$t_s^* = g_{F_p}(X) + \hat{\sigma}_s^2 \left(p_{F_p}(X) + \frac{4X}{Sh^*} \right) \quad (2.2)$$

In equation 2.2, X is the degree of conversion of the carbon particles according to *reaction 1.5*. $g_{F_p}(X)$ and $p_{F_p}(X)$ are conversion functions related to the chemical reaction and diffusion through the porous product layer, respectively. These functions are defined by equations 2.3 and 2.4:

$$g_{F_p}(X) = 1 - (1 - X)^{\frac{1}{F_p}} \quad (2.3)$$

$$p_{F_p}(X) = 1 - \frac{F_p(1 - X)^{\frac{2}{F_p}} - 2(1 - X)}{F_p - 2} \quad (2.4)$$

In addition to the degree of conversion and conversion functions given in equation 2.3 and 2.4, equation 2.2 includes a shape factor, F_p , of the particles. The shape factor attains values 1, 2 and 3 for a slab, long cylinder and sphere, respectively. When particles in the shape of long cylinders ($F_p = 2$) are adapted to the shrinking core model, the resulting equation 2.4 is given by the limit of the right hand side as $F_p \rightarrow 2$.

When the overall reaction rate is controlled by the chemical reaction, the term $g_{F_p}(X)$ applies, while $p_{F_p}(X)$ is dominating when the overall reaction rate is controlled by diffusion of SiO- and CO gas through the porous layer of solid SiC. Mass transfer of gaseous reactants and products through the gas film surrounding the reacting particles is incorporated in the shrinking core model by the term $4X/Sh^*$. The parameter Sh^* is a modified Sherwood number defined by equation 2.5:

$$Sh^* = 2 \frac{h_D R_p}{D_E} \quad (2.5)$$

where h_D and D_E are the mass transfer coefficient through the gas film and effective diffusivity, respectively. R_p is the characteristic dimension of the particle:

$$R_p = \frac{F_p V_p}{A_p} \quad (2.6)$$

where V_p and A_p are the volume- and area of the reacting particle, respectively. For a sphere, the characteristic dimension is equal to the radius of the particle.

The ratio between influence of chemical reaction rate and mass transfer (including both pore diffusion through the porous product layer and mass transfer from bulk gas to the particle surface) in the shrinking core model is determined by the gas-solid reaction modulus, $\hat{\sigma}_s$ which is defined in equation 2.7.

$$\hat{\sigma}_s^2 = \frac{k_C \left(1 + \frac{1}{K_E}\right)}{2F_p D_E} R_p \quad (2.7)$$

In this equation, k_C is the reaction rate constant and K_E is the equilibrium constant for reaction 1.5 while the other constants have been defined previously. According to **Szekely et al. (1976)**, the chemical reaction rate is dominating when $\hat{\sigma}_s^2 < 0.1$ (0.01), when the tolerable error is 10 % (1 %). On the other side, the system is controlled by diffusion through the porous product layer and external mass transfer when $\hat{\sigma}_s^2 > 10$ (100).

Equation 2.2 is expressing degree of conversion as a function of dimensionless time. Applying dimensionless time to the reaction between carbon and SiO gas (reaction 1.5) results in the following relationship:

$$t_s^* = \frac{bk_C}{\alpha_C C_C R_p} \left(C_{SiO,B} - \frac{C_{CO,B}}{K_E} \right) t \quad (2.8)$$

where b is the stoichiometric coefficient in equation 2.1 and equal to a value of 2 for the reaction between carbon and SiO gas. Bulk concentrations of gaseous reactant and product are denoted $C_{SiO,B}$ and $C_{CO,B}$, respectively. Constants referring to the volume fraction and molar density of pure carbon are respectively termed α_C and C_C while k_C is the reaction rate constant. In the original formulation by **Szekely et al. (1976)**, inerts and voids were included in the molar density of solid carbon (C_C). **Sohn (1997)** did however include the volume fraction (α_C) of solid carbon thus allowing these material properties to be incorporated in the shrinking core model.

A relationship between conversion and time can be deduced by substitution and combination of the equations 2.2 – 2.8. The full expression of the shrinking core model is given in equation 2.9:

$$t_s(X) = \frac{C_C}{b \left(C_{SiO,B} - \frac{C_{CO,B}}{K_E} \right)} \cdot \left(\frac{1}{k_C} \alpha_C R_p \left(1 - (1-X)^{\frac{1}{F_p}} \right) + \frac{1}{D_E} \cdot \frac{\alpha_C R_p^2}{2F_p} \cdot \left(1 + \frac{1}{K_E} \right) \cdot \left(1 - \frac{F_p (1-X)^{\frac{2}{F_p}} - 2(1-X)}{F_p - 2} \right) + \frac{1}{h_D} \cdot \frac{\alpha_C R_p}{F_p} \left(1 + \frac{1}{K_E} \right) X \right) \quad (2.9)$$

Even though the shrinking core model is attractive and has been widely used, **Sohn (1997)** states that the model in general is restricted to reactions of non-porous solids occurring at a well defined interface. Only when the reaction rate is limited by mass transfer ($\hat{\sigma}_s^2 > 10$), the mathematical expressions become identical for porous- and non-porous solids. Application of the shrinking core model to reactions for porous solids might result in misinterpretation of experimental data, and care should be taken.

2.2.2 Grain model

For non-porous solids following the shrinking core model, the reaction progress in a topochemical manner from the surface of the particle towards the centre and there is a sharp boundary between the unreacted core and the product layer. For porous particles there is, according to **Szekely et al (1976)**, a gradual change in the degree of conversion throughout the particles. The grain model was first proposed by **Szekely and Evans (1970)**. In this model, the porous solid (pellet) is imagined to be composed of solid grains. Both the pellet and grains of which the pellet is composed, can attain different geometries. In Figure 2.2 an illustration of a spherical pellet composed of spherical grains can be seen.

Similar to the shrinking core model, described in the previous section, a dimensionless relationship between time and degree of conversion is given in equation 2.10:

$$t_g^* = g_{F_g}(X) + \hat{\sigma}^2 \left(p_{F_p}(X) + \frac{4X}{Sh^*} \right) \quad (2.10)$$

where, similar to equation 2.2, total conversion of the carbon particles (pellets) is denoted by X and dimensionless time is given as t_g^* where the subscript g refers to *grain*. The conversion functions for chemical reaction control and mass transfer control are expressed by equations 2.11 and 2.4, respectively.

$$g_{F_g}(X) = 1 - (1-X)^{\frac{1}{F_g}} \quad (2.11)$$

As the grain model incorporates both pellets and grains, there are two shape factors to take into account. Shape factors of the grains are termed F_g while the pellets are referred to as F_p .

When the overall reaction rate is determined by the chemical reaction rate of the grains, $g_{F_g}(X)$ applies. In systems where diffusion of gaseous reactants and products through the porous network in the pellet to the surface of the grains is limiting the overall reaction rate, $p_{F_p}(X)$ is applicable. Possible effects from external mass transfer are incorporated in the grain model by the term $4X/Sh^*$. The modified Sherwood number was defined in the previous section.

In the same manner as for the shrinking core model, the ratio of influences by chemical reaction and mass transfer is determined by the gas-solid reaction modulus for the grain model:

$$\delta^2 = \frac{R_p^2}{R_g} \cdot \frac{\alpha_c k_c}{2F_p D_E} \left(1 + \frac{1}{K_E} \right) \quad (2.12)$$

where R_g is the characteristic dimension of the grain, defined by equation 2.13.

$$R_g = \frac{F_g V_g}{A_g} \quad (2.13)$$

When the gas-solid reaction modulus is small, the chemical reaction controls the overall reaction rate. Under such conditions, concentration of gaseous reactant is uniform throughout the particle and a situation illustrated in Figure 2.2 A) might arise. A large value of the gas-solid reaction modulus is implying that mass transfer controls the overall reaction rate. The concentration of the reacting gas species is limiting, and the chemical reaction is thus occurring in a narrow zone separating the unreacted core and the product layer. This situation is similar to the shrinking core model and is illustrated in Figure 2.2 B). In most systems, the gas-solid reaction modulus is not at either extreme, but rather takes an intermediate value where both chemical reaction and diffusion through the porous network are occurring at the same time in a diffuse zone. A system with an intermediate gas-solid reaction modulus can be seen in Figure 2.2 C).

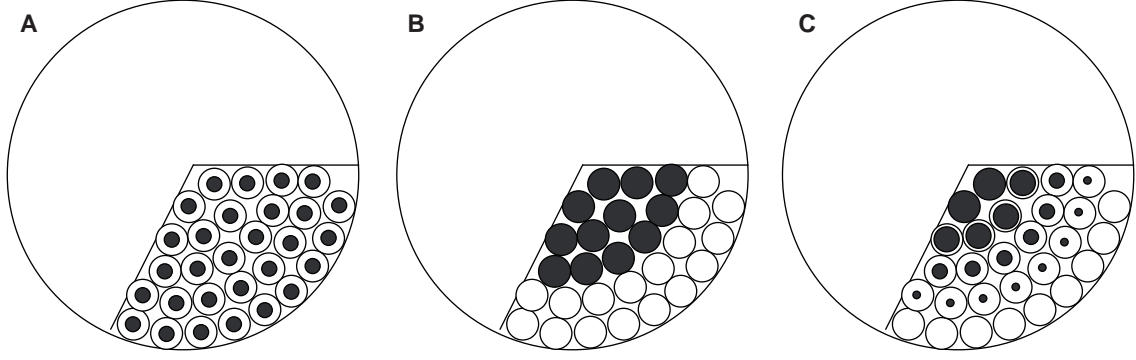


Figure 2.2: Graphical representation of the grain model with spherical particles and grains. Overall conversion rate is determined by chemical reaction rate (A), intragrain diffusion (B) and a combination of the two (C). Modified from Szekely et al. (1976).

Dimensionless time for the grain model is denoted t_g^* , and is defined by equation 2.14:

$$t_g^* = \frac{bk_c}{C_C R_g} \left(C_{SiO,B} - \frac{C_{CO,B}}{K_E} \right) t \quad (2.14)$$

in which all the variables and constants have been defined previously.

The effect of diffusion through the product layer on each grain has been assumed to be negligible in equation 2.10. An extension to the original grain model by applying the law of additive times, as described by **Sohn (1997)**, will include this effect:

$$t_g^* = g_{F_g}(X) + \hat{\sigma}_g^2 \cdot p_{F_g}(X) + \hat{\sigma}^2 \left(p_{F_p}(X) + \frac{4X}{Sh^*} \right) \quad (2.15)$$

where $\hat{\sigma}_g$ is the gas-solid reaction modulus describing the ratio between chemical reaction and diffusion through the product layer surrounding the grains, and is defined similar to the reaction modulus for the shrinking core model:

$$\hat{\sigma}_g^2 = \frac{k_c \left(1 + \frac{1}{K_E} \right)}{2F_g D_g} R_g \quad (2.16)$$

In equation 2.16, D_g is the effective diffusivity through the product layer of the grains. The conversion function for diffusion through the product layer of the grains is defined as follows:

$$p_{F_p}(X) = 1 - \frac{F_g (1-X)^{\frac{2}{F_g}} - 2(1-X)}{F_g - 2} \quad (2.17)$$

Substitution and combination into equation 2.15, is resulting in the full expression of the relationship between time and degree of conversion for the grain model. This relationship is given in equation 2.18:

$$t_g(X) = \frac{C_C}{b \left(C_{SiO,B} - \frac{C_{CO,B}}{K_E} \right)} \cdot \left(\begin{aligned} & \frac{1}{k_C} R_g \left(1 - (1-X)^{\frac{1}{F_g}} \right) + \\ & \frac{1}{D_g} \cdot \frac{R_g^2}{2F_g} \cdot \left(1 + \frac{1}{K_E} \right) \cdot \left(1 - \frac{F_g (1-X)^{\frac{2}{F_g}} - 2(1-X)}{F_g - 2} \right) + \\ & \frac{1}{D_E} \cdot \frac{\alpha_C R_p^2}{2F_p} \cdot \left(1 + \frac{1}{K_E} \right) \cdot \left(1 - \frac{F_p (1-X)^{\frac{2}{F_p}} - 2(1-X)}{F_p - 2} \right) + \\ & \frac{1}{h_D} \cdot \frac{\alpha_C R_p}{F_p} \left(1 + \frac{1}{K_E} \right) X \end{aligned} \right) \quad (2.18)$$

2.3 Former Studies of the Reaction Between SiO gas and Carbon Materials

Previous studies of the reaction between SiO gas and carbon can generally be classified according to the procedure in which the reaction has been monitored. In thermogravimetric experiments, the weight of the carbonaceous reducing agent is continuously monitored during reaction with SiO gas. Several studies have used this approach in order to assess the reactivity towards silicon monoxide, and some of these are referred to in section 2.3.2. Gas analysis techniques monitor composition of the effluent gas leaving a reaction chamber in which SiO gas has passed through a packed bed of carbonaceous material. A more in-depth discussion of these techniques is provided in section 2.3.1.

2.3.1 Gas analysis techniques

The most acknowledged test for assessing the reactivity of carbonaceous reduction materials towards SiO gas is the SINTEF SiO reactivity test. This test has been commercially available since the 1970's and the procedure was first published by **Tuset and Raaness (1976)**. The principle of the SINTEF test, and other reactivity tests based on the gas analysis technique, is that a gas with known concentration of SiO gas is passed through a packed bed with the reduction material to be tested. The carbon material will react with SiO gas according to reaction 1.5, and composition of the effluent gas is continuously monitored. The amount of SiO gas passing unreacted through the bed can thus be calculated and is used as a measure of reactivity. The

2.3 FORMER STUDIES OF THE REACTION BETWEEN SiO GAS AND CARBON MATERIALS

reactivity parameter in the SINTEF test is now denoted *R10 corrected* and is a measure of the volume of SiO gas which has passed unreacted through the packed bed as concentration of CO in the effluent gas decreases from 18 to 10 %. Even though advances have been made to the SINTEF test, of which the most recently are described by Lindstad et al. (2007) and Hansen (2005), the principle still remains the same. The apparatus and procedure used in the SINTEF SiO reactivity test is thoroughly described in section 4.6.

Reactivity parameters reported from experiments based on the gas analysis technique are calculated from CO versus time profiles as can be seen on the right hand side in Figure 2.3. The shape of these profiles contains information about the reactivity of the carbon materials which are tested. Gas entering the reaction chamber contains 13.5 % and 4.5 % of respectively SiO- and CO gas. Assuming that equilibrium with carbon is established at the reaction temperature (1650°C) within the sample, SiO gas will practically quantitatively convert to SiC according to reaction 1.5. This reaction will thus produce an effluent gas with 18 % CO. In the initial period of reaction, the supply of SiO gas is the overall rate controlling factor. The distribution of SiO- and CO gas through the reaction chamber for a reactive and less reactive coke is illustrated on the left hand side in Figure 2.3.

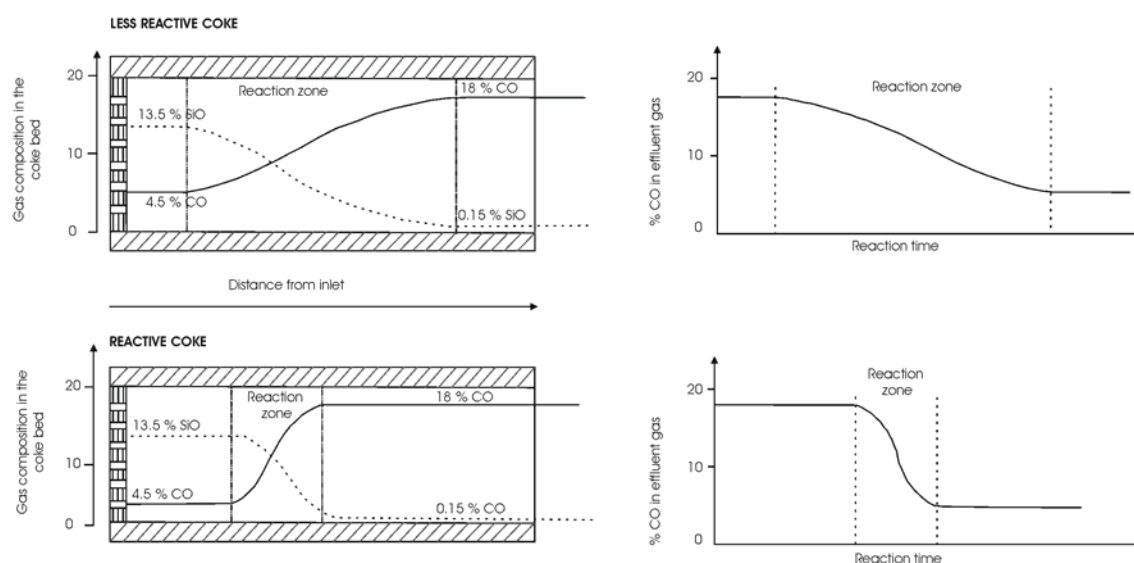


Figure 2.3: Reaction propagation in the reaction chamber and measured CO profiles for a reactive (bottom) and less reactive (top) coke from the SINTEF SiO test. Modified from Tuset and Raanes (1976).

Succeeding the initial period, a reaction front is established and with time this front will expand into a zone. Expansion of the reaction zone is a characteristic property of the reduction materials, and the thickness of the reaction zone is less than the total height of the reaction chamber for most materials. As the reaction front is propagating towards the top of the packed bed, the CO concentration in the effluent gas is dropping below 18 %. From this point in the test, the measured CO profile will reflect the compositional gradient through the reaction zone as is indicated in Figure 2.3.

The SINTEF test is well suited to classify reduction materials according to their reactivity towards SiO gas (low, medium and high). On the basis of the numerous tests performed in the SINTEF SiO reactivity test throughout the years, a classification of the different carbonaceous materials based on the reactivity towards SiO gas has been proposed. This classification is illustrated in Figure 2.4.

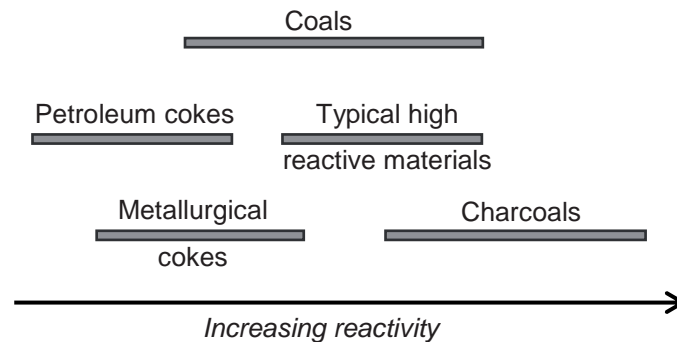


Figure 2.4: Classification of different carbonaceous materials used as reduction materials in the silicon process based on experiences from the SINTEF SiO reactivity test. Figure is modified from Tuset and Raaness (1976).

Paul and See (1978) presented an attempt to establish a similar gas analysis technique as the SINTEF SiO reactivity test. The authors have reported reactivity experiment with petroleum coke, metallurgical coke, charcoal and a highly reactive char. The results did however not have sufficient resolutions to separate the carbon materials according to their ability to react with SiO gas. The main cause was described as problems with stable concentration of SiO gas from the gas generator due to manual temperature control. As partial pressure of SiO gas is very sensitive to temperature in the temperature range in which the test is performed, this factor was detrimental for the reactivity experiments.

2.3.2 Thermogravimetric procedures

One of the first scientific works trying to characterize carbon materials according to their reactivity towards SiO gas was published by **Kozhevnikov et al. (1972)**. In this work discs (30 mm) of graphite, metallurgical coke and charcoal were subjected to SiO gas at temperatures from 1480 - 1680°C and the weight change with time was monitored at a constant temperature of 1680°C. The SiO gas was produced by heating briquettes of SiO₂ and Si to a temperature of 1680°C which according to the authors was sufficient to produce a constant amount of SiO gas for a reaction test period of one hour. Based on the experimental results, the authors conclude that the different reduction materials do not show significant differences in the investigated temperature range. Based on the presented plots indicating weight change with reaction time, there are some interesting results. The charcoal sample is slightly more reactive than the graphite sample especially in the initial reaction stage. Charcoal also seems to react with SiO gas at lower temperatures than both graphite and especially coke. Regarding the coke samples, the results indicate that the amount and type of ash components in the coke has a major impact on the registered weight change. An initial weight decrease observed for the coke sample is attributed to the reduction of quartz inclusions in the coke according to

2.3 FORMER STUDIES OF THE REACTION BETWEEN SiO GAS AND CARBON MATERIALS

reaction 1.3. Coke which was subjected to heat treatment previous to reaction with SiO gas attained a reaction rate similar to the other tested reduction materials.

Based on the results observed with the metallurgical coke, **Kozhevnikov et al. (1973)** were trying to determine the effect of oxides in the ash on the reactivity of carbon materials towards SiO gas. Even though it might not be what the silicon producers of today are looking for, the authors state that ash content up to 30 % will increase the reactivity due to higher porosity and surface area. They suggest to subject cokes with higher ash content than 15 % to a preliminary heat treatment in order to reduce losses of SiO gas.

A quite different thermogravimetric procedure is reported by **Videm (1995)**. In this procedure the gas generating agglomerate and carbon particles which are reacting with the produced SiO gas are contained in the same crucible. The apparatus used in the reactivity experiments is illustrated in Figure 2.5.

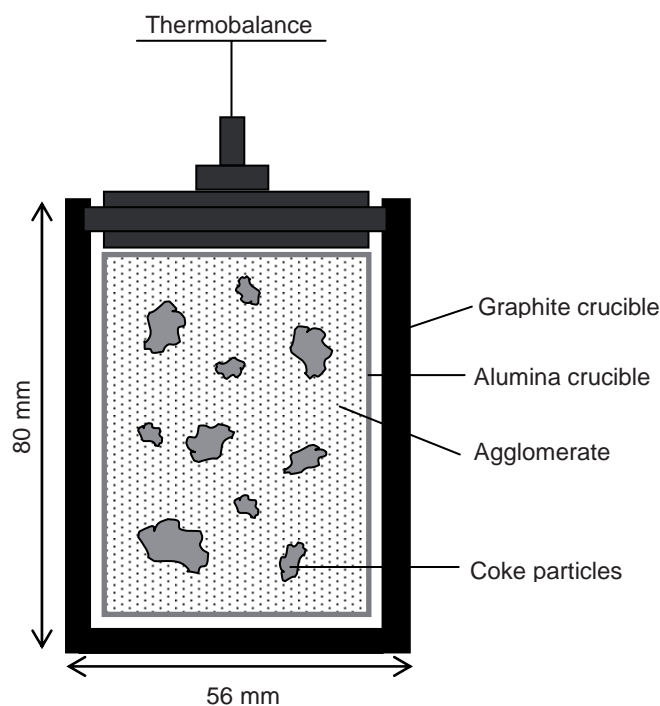


Figure 2.5: Apparatus for the reactivity test performed by Videm (1995).

The gas producing agglomerate is a mixture of finely ground quartz and silicon carbide producing SiO gas according to *reaction 1.10*. The carbon particles are in the size range 4 – 6.3 mm and the reaction temperature is 1690°C. The reactivity is observed as the weight change of the apparatus with time. The SiO producing agglomerate will experience a weight reduction with time according to *reaction 1.10* while the reaction of carbon with the produced SiO gas will contribute to a weight increase (*reaction 1.5*). The author claims that a combination of these reactions makes it possible to monitor the amount of carbon which has reacted. Reactivity from this test procedure is reported as percentage of the carbon material which has reacted (degree of conversion).

In a later study using the same apparatus, **Videm Buø et al. (1999)** were testing nine different cokes. The cokes were petrographically analyzed and a connection between the observed reactivity results and the petrographic properties were sought. The analyzed cokes had a wide distribution of binder- and filler phase components in the texture. All the cokes were produced from a narrow range of low rank coals as the degree of anisotropy is relatively low in all samples. According to this study, the main petrographic properties in the carbonized samples contributing to an increased reactivity towards SiO gas are:

- High content of binder phase components.
- Low amount of filler phase components.
- High amounts of structures derived from pseudovitrinite in coals.
- A relatively high degree of isotropic microtextures.

The property that was revealed to correlate best with the observed reactivity was however the bulk volume weight of the cokes. The volume weight is a function of porosity and surface area. These physical parameters can be argued to be functions of the petrographic composition of the coals from which the cokes are made.

During his doctoral work, **Myrhaug (2003)** prepared spheres of both charcoal, carbonized coal and metallurgical coke and monitored the weight increase of these as they reacted with SiO gas according to *reaction 1.5*. A simplified illustration of the apparatus used in his work is given in Figure 2.6.

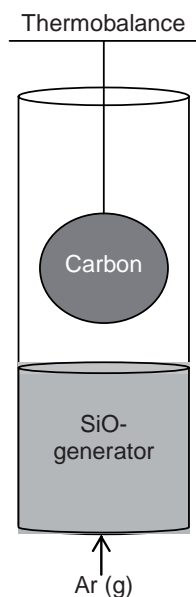


Figure 2.6: A simplified illustration of the thermogravimetric apparatus used by Myrhaug (2003).

The spheres had diameters in the range 8 – 25 mm and were connected to a thermobalance by a tungsten wire. Similar to the SINTEF SiO reactivity test, the SiO generator is placed below the reaction chamber. The SiO generator is filled with agglomerates of powdered quartz and α -SiC which produced SiO- and CO gas in the

2.3 FORMER STUDIES OF THE REACTION BETWEEN SiO GAS AND CARBON MATERIALS

ratio 3:1 according to *reaction 1.10*. The reaction temperature was set to 1650°C which is identical to the reaction temperature in the SINTEF procedure.

Analyses of the reduction materials combined with the recorded weight change during reaction made it possible to calculate the degree of conversion according to the following equation:

$$X = \frac{(m_p - m_{p0})}{w_{FC0} m_{p0} \left(\frac{Mm_{SiC} - 2Mm_C}{2Mm_C} \right)} \quad (2.19)$$

where m_p and m_{p0} are the actual- and initial weights of the sphere, respectively. w_{FC0} is the mass fraction of fixed carbon in the particle just before conversion starts and Mm_{SiC} and Mm_C are the molar masses of SiC and C respectively.

Based on the obtained relationship between reaction time and conversion of the tested carbonaceous reduction materials, several kinetic models were adapted to the experimental data. For the charcoal samples, the shrinking core model gave the best description of the reaction kinetics. In Figure 2.7 A), a microprobe picture from the cross section of a 50 % converted charcoal particle illustrates the similarities to the shrinking core model. For the fossil reduction materials which were tested, both the shrinking core model and the grain model gave satisfactory results. The shrinking core model did however prove to give the best description of the behavior in a packed bed. The cross section of a 50 % converted sphere of metallurgical coke is illustrated in Figure 2.7 B).

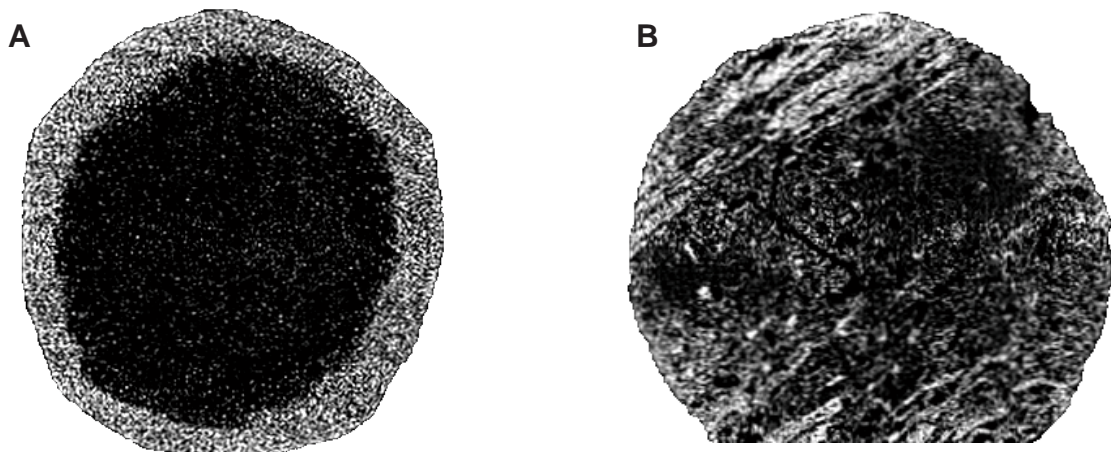


Figure 2.7: Cross sections of reacted spheres of charcoal (A) and metallurgical coke (B).
Microprobe pictures from Myrhaug (2003).

2.3.3 Correlations of material properties and reactivity

Raanes and Gray (1995) have selected eight coals acknowledged as suitable for the manufacture of silicon and silicon rich ferroalloys and tested them in the SINTEF SiO reactivity test. Preceding the reactivity tests, material properties of the coals were

evaluated including proximate analysis, petrographic composition and rank in terms of vitrinite reflectance. The coals were subsequently carbonized and microtextures of the produced chars were quantified by petrographic analysis. The most prominent petrographic parameter influencing reactivity of the tested sample materials is rank determined by reflectance of vitrinite. Increased rank, or maturity of the coals, tends to give a lower reactivity towards SiO gas.

The results presented by **Raanes and Gray (1995)** have been used in a multivariate analysis presented by **Patalsky et al. (1995)**. In addition to rank, the authors have evaluated the effect of maceral composition on reactivity towards SiO gas. They claim that presence of coarse inertinite macerals in the coals increase the reactivity while small sized macerals of this category tend to increase the pore wall thickness thus resulting in a lower reactivity. Macerals belonging to the liptinite group are contributing to increased pore development and are thus favorable for the reactivity. In terms of the microtextures in the carbonized coals, the authors claim that a high ratio of binder- to filler phase components in general is resulting in an increased reactivity in the silicon process.

Petrographic data from 35 coal samples have been correlated with the reactivity from the SINTEF SiO reactivity test by multivariate analysis in a paper by **Raanes et al. (1998)**. Majority of the coal samples were Carboniferous and covering a rank range from high- to low volatile bituminous. A widely used sub-bituminous coal source from South-America was also included in the tested materials. Based on the multivariate analysis, the authors reported the following parameters of coals to have the greatest effect on SiO reactivity:

- Vitrinite reflectance and distribution of V-Types.
- Amount and distribution of reactive macerals.
- Amount and distribution of inert macerals.

Based on the regression coefficients from the analysis, a high content of mineral matter tend to give a less reactive material. Composition of the mineral matter is however not part of the analysis. **Raanes (2001)** used the same data to simplify the model and thus make it more user-friendly.

To summarize the results from the quoted studies, the following parameters are most important in assessing SiO reactivity:

- Rank
- Ratio of fusible- to infusible macerals
- Volume weight
- Amount and composition of mineral matter

2.4 Conversion Profiles and Shape of Reactivity Curves

The CO profile from the SINTEF SiO reactivity test is a function of the material reactivity. A highly reactive carbonaceous material has a steep curve and hence a low value of *R10 corrected*. The reactivity curves are also believed to depend upon the

thickness of the reaction zone in the apparatus. A highly reactive material will have a narrow reaction zone and hence a steep CO profile while the opposite is true for a low reactive material (Figure 2.3). Mathematical expressions for conversion profiles through a packed bed have been developed based on different kinetic models and assumptions.

Both **Bakken (1969)** and **Moriyama (1971)** have deduced mathematical expressions for conversion profiles for gas - solid reactions following the shrinking core model in fixed bed reactors under isothermal conditions. The conversion profiles have sigmoid shapes after an initial time and transverse the reactor chamber. Mass transfer coefficients, reaction rate constants and effective diffusivities are all kinetic parameters included in the expressions.

Evans and Song (1974) have come up with a similar equation based on the grain model for spherical pellets where each grain is assumed to follow the shrinking core model. By using this model the conversion profiles take on a sigmoid shape after an initial time and travels down the fixed bed with unvarying profiles. Width of the reaction zone is increasing with an increasing reaction modulus (equation 2.12). The authors have assumed that diffusion of gaseous reactants through the product layer surrounding the grains is not the rate determining step. They are thus not using the extended grain model (equation 2.15), but rather the model presented in equation 2.10. This approximation might very well be justified in the first stages of reaction, but as the degree of conversion increases and the product layer becomes thicker, this step might very well be rate determining for the reaction between carbon and SiO gas.

Conversion profiles through the packed bed in the SINTEF apparatus were investigated at various periods of exposure to SiO gas by **Tuset and Raaness (1976)**. The experimental conversion profiles correlated fairly well with the profiles calculated by the procedure described by **Bakken (1969)**. Kinetic parameters like reaction rate constant and effective diffusivity were calculated based on the experimental conversion profiles through the reaction chamber. The procedure is however cumbersome, time consuming and not very accurate, thus not suitable to deduct kinetic constants for the reduction materials.

3. COAL, COKE AND CARBONIZATION

This chapter is based on the following references unless otherwise stated:

1. Organic Petrology, **Taylor et al, (1998)**
2. Stach's Textbook of Coal Petrology, **Stach et al, (1982)**
3. Sciences of Carbon materials, **Rodriguez-Reinoso and Marsh, (2000)**

Coal is defined by **Schopf (1956)** as a readily combustible rock containing more than 50 % by weight and 70 % by volume of carbonaceous material, formed from compaction or induration of variously altered plant remains similar to those of peaty deposits.

Coal can be characterized by three basic properties (**Speight 1994**):

Coal Grade: Is a measure of the purity of coal and composition of the mineral matter which is dispersed in the coal matrix. The coal grade might be very important for industrial applications. Factors contributing to the grade of coals are elucidated on in section 3.4.4.

Coal Type: Coal is primarily composed of organic material, and the coal type gives information about the plant material from which the coal was formed (macerals). More information on the coal type is given in sections 3.4.1 – 3.4.3.

Coal Rank: The rank of coal is a measure of the degree of maturation / coalification a coal has reached. Coal rank can be assessed both chemically and petrographically. More information on the coal maturation and degree of coalification can be found in section 3.3.

3.1 Coal Formation and Metamorphosis

All coal deposits around the world originate from peat deposited in mires. Mires are defined as wetlands where peat accumulates, and include terms as swamps, bogs, moors and more. In order for the peat beds to develop, there has to be a balance between the subsidence and the level of groundwater. The rate of subsidence of the mire has to be just right for the groundwater to be static at surface level in order to preserve organic material in an anaerobic environment. As additional organic material accumulates on top of the mire, the peat seam becomes thicker. The mire then had to have a subsidence which allowed additional organic material to be deposited without exposing it to oxygen.

Throughout geological history there have been three great eras of peat accumulation and hence coal formation. The first period stretches from the Carboniferous to the end of the Permian. The Carboniferous coals are mostly mined on the northern hemisphere, especially in Europe and North America. Permian coals on the other hand are more abundant in Australia, India, China and South Africa.

During the Jurassic and Cretaceous coal formation occurred in the western parts of USA and Canada as well as in China. The third era of coal formation had its peak during the Tertiary, and most of the low rank coals mined in the world today have their origin in this period.

3.1.1 Palaeogeography and tectonics

In comparison with the resources of oil and natural gas, the coal basins are more evenly distributed around the world (see Figure 3.1).

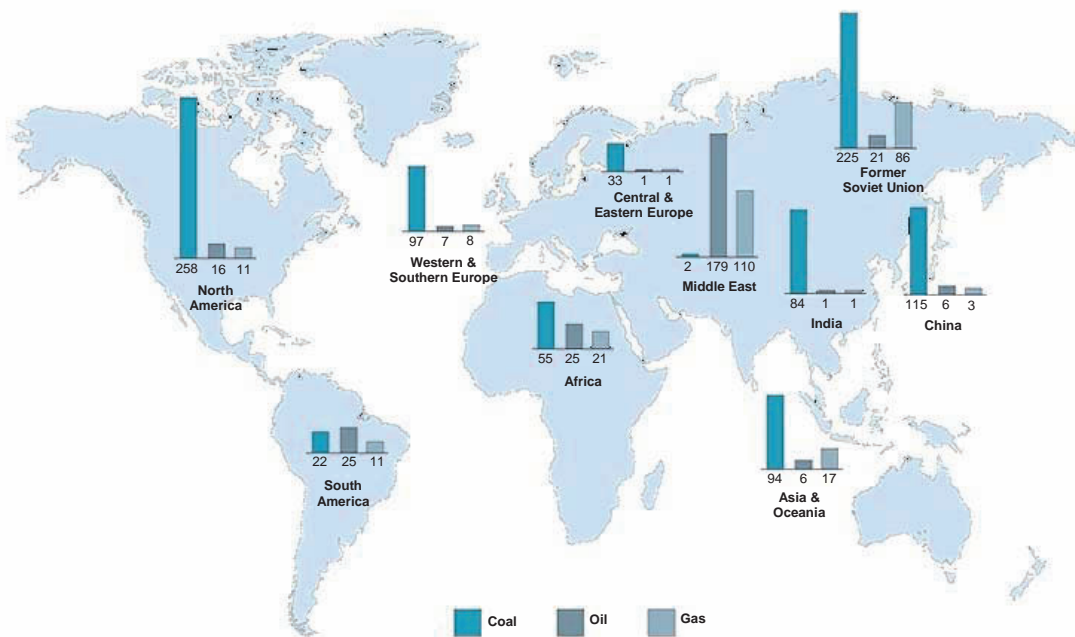


Figure 3.1: Reserves of fossil fuels in the world. Numbers are given as gigatons of coal equivalents. One coal equivalent is equal to the calorific value of 1 kg coal (7000 kcal / 29.3 MJ / 8.141 kWh). 1 kg oil = 1.52 and 1 m³ natural gas = 1.35 coal equivalents, respectively (ENS 2007). Figure is modified after Optima (2005).

Worldwide, coal is the most abundant of the fossil fuels, and its reserves are also the most widely distributed. Estimates of the world's total recoverable reserves of coal in 2003 were about 900 billion metric tons (EIA 2007). The resulting ratio of coal reserves to production is close to 150 years (WCI 2007), meaning that at current rates of production (and no change in reserves), coal reserves could in theory last for another century and a half. Carstens (2005) reported on new discoveries of coal on the Norwegian continental shelf which exceeds the total recoverable reserves in the world (see Figure 3.2). These resources are deposited far under the sea bed and are thus impossible to mine. They will be regarded as unrecoverable until technology for underground gasification makes it possible to utilize the coal where it is deposited.

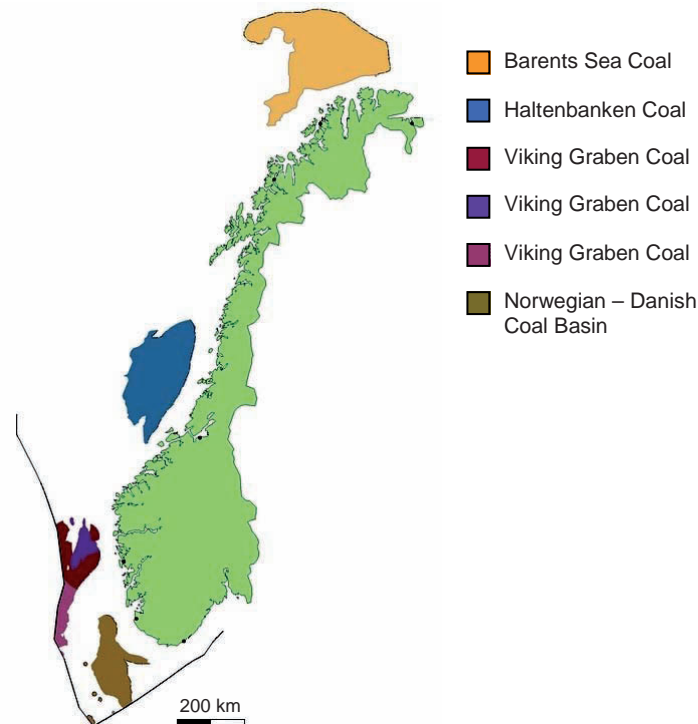


Figure 3.2: Coal deposits on the Norwegian Continental Shelf. (Kårstad 2006)

According to the Energy Information Administration (**EIA 2007**) the largest reserves of coal in the world are found in the United States (27 %) and Russia (17 %) which account for nearly half of the global coal reserves. China (13 %), Australia (9 %), South Africa (5 %), and Poland (2 %) also have significant amounts of the world's total recoverable coal reserves.

To explain this scattering of the coal deposits of the world, it is necessary to have an understanding of tectonic plate migration. Due to the convection in the mantle, the continents have migrated around the globe throughout geological time. Continents have collided, causing mountain formation or drifted apart generating vast oceans.

Regarding coal formation, the most significant event occurred in the Carboniferous period. At this time America, Europe and Africa collided and formed a single “supercontinent” called Pangea. This collision of the continents created an extensive zone of mountain formation. In Europe these mountains extended from east to west and are called the Viscarian Mountains, and in North America the Appalachian Mountains in the eastern USA were formed. The foreland basins of these mountains were located near the equator at that time (palaeo equator), and suitable conditions arose for the formation of luxuriant tropical peat swamps. These conditions led to the formation of the Carboniferous coals of Europe and eastern USA which have been of tremendous economical interest during the last two centuries.

At the time when the Carboniferous coals were being formed in the northern hemisphere, the southern part of Pangea (Gondwana) was centered close to the southern pole. When the Permian period was approaching, this land mass drifted northwards into

a sub-arctic too cool temperate climatic zone. This temperate peat forming vegetation formed the basis for the Permian coals of Australia, South-Africa, India and South-America.

During the Cretaceous period, Africa rifted from South-America – opening the South Atlantic Ocean, the Pacific Philippine plate separated from the Asian continental plate, India moved towards Asia and the Gulf of Mexico opened. These movements caused deformation, subduction and mountain formation providing excellent conditions for the final main phase of coal formation which extended from the Cretaceous- to the Tertiary period. The distribution of the continents in the most important times of coal formation is illustrated in Figure 3.3.

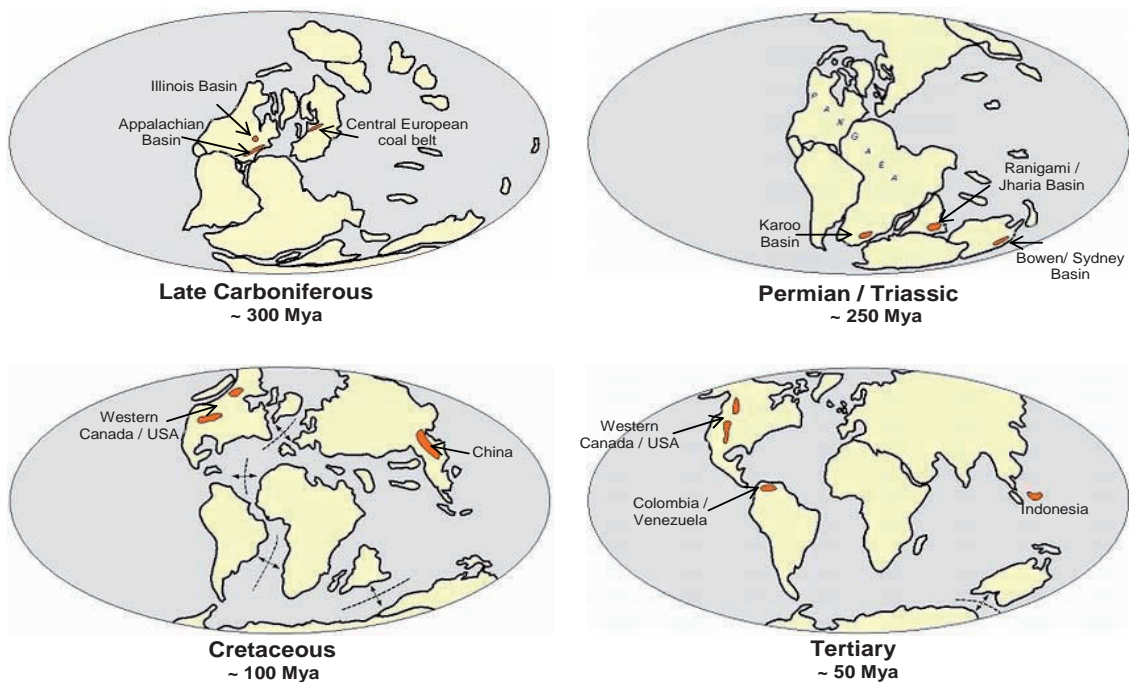


Figure 3.3: The major eras of coal formation and some of the most important basins. Modified after Condie (1989).

3.1.2 Flora and climate

Throughout geological history the climate has varied from ice ages to tropical conditions. The flora is naturally affected by climate and the resulting coal seams are again functions of the organic material from which they are the solid residue.

The carboniferous coals in Europe and North America were deposited under tropical or sub-tropical conditions, and the lack of growth rings in the flora is an indication of the tropical climate under which these coals were laid down. Flora in the northern hemisphere consisted of large trees (Lepidodendron, Sigillaria and Cordaites) with dense undergrowth.

Permian coals of the southern hemisphere (Gondwanaland) were however deposited under sub-arctic to cool temperate conditions, and the flora was characterized by stunted

trees and a wide range of plants with broad leaves (Glossopteris and Gangamopteris). An illustration of the most common coal forming species respectively in the Carboniferous and Permian is given in Figure 3.4.

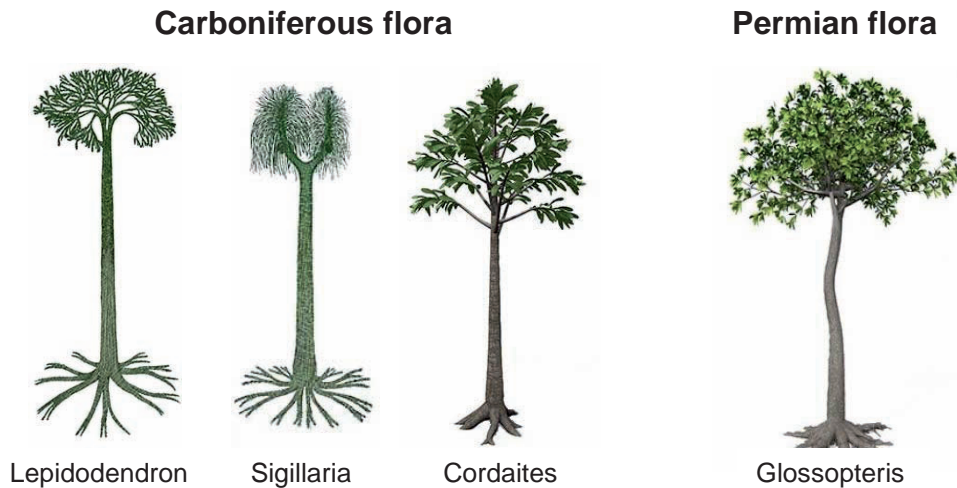


Figure 3.4: Illustrations of species that composed the flora in respectively carboniferous- and Permian times. Modified after Murphy (2007).

As geological time passed, the diversity and abundance of the plant kingdom increased, so the coal deposits from Cretaceous- and Tertiary times were formed from a wider range of species than Carboniferous- and Permian coals. Rapid development of the flora led to the rich angiosperms featuring Ginkgophyta, Cycadophyta and early Conifers. A comprehensive review of different coal forming plants through time in North America is given by **Cross and Phillips (1990)**. Development of coal measures from early Carboniferous to the Tertiary as functions of climate and continental position is reviewed by **Butler et al. (1988)**.

3.2 Coal Metamorphosis

The natural process of forming coal from organic material takes millions of years and is divided into two distinct processes; peatification and coalification. Environmental factors contributing to the conditions in the mire as well as an illustration of the two stages of coal metamorphosis is shown in Figure 3.5.

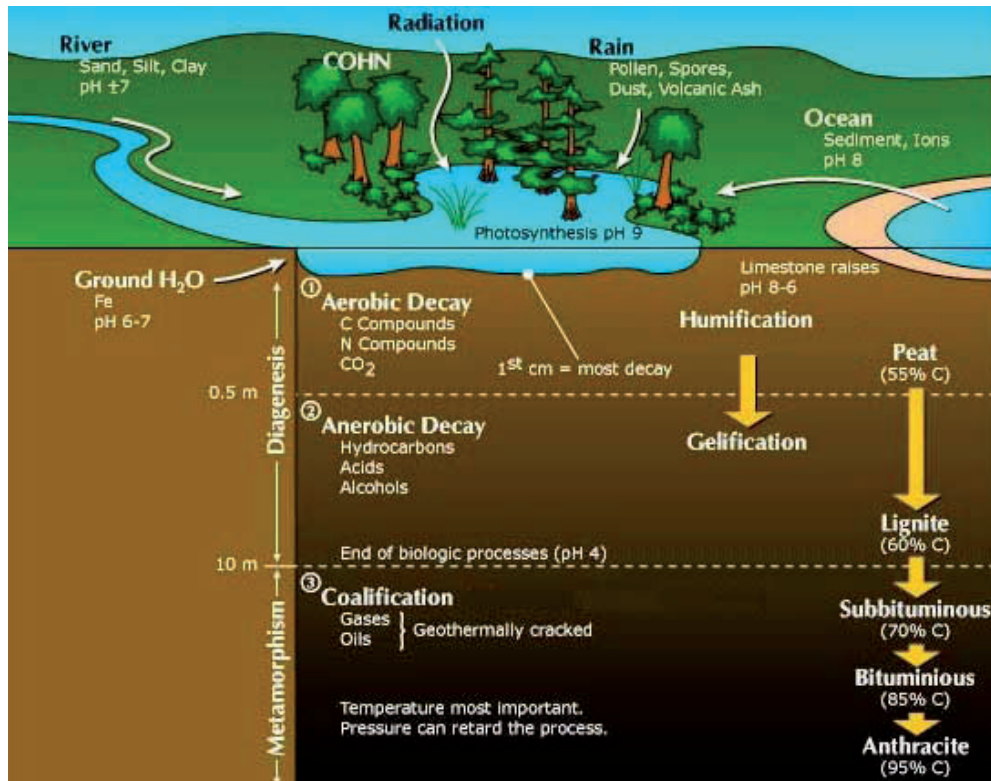


Figure 3.5: Illustration of the peatification and coalification stages in relation to a mire. After McClurg (2001).

3.2.1 Peatification (Biochemical coalification)

In order for coal to be formed, the organic matter first has to be transformed to peat. This transformation is termed *peatification* and includes the chemical, physical and biological processes taking place shortly after deposition of the organic material in the mires. The major alterations of the organic material are occurring from the surface of the mire to a depth of approximately 0.5 m. In this region aerobic bacteria and fungi are active and cause decomposition of cellulose, lignin and other carbohydrates, producing mobile humic substances and gases (CO₂, NH₃, CH₄ and H₂O). This process is called *humification* and is regarded as the most important process during peatification.

Biochemical *gelification* may follow the humification, and in this process the mobile humic substances undergo repolymerization and polycondensation producing humins. At increased depths, the oxygen content decreases and aerobic organisms are replaced by anaerobic bacteria. At depths below approximately 10 meters, only geochemical changes will occur as microbial life no longer exists.

Several factors have an effect on the peatification process:

Oxygen supply

The oxygen supply in the mire, or more correctly the red-ox potential, determines the path of transformation of the deposited organic material. Depending on the red-ox potential, the organic material can be totally degraded, transferred to peat, mould or hydrogen rich coals called sapropelic coals. This process is illustrated in Table 3.1.

Table 3.1: Paths of transformation of organic material in the mire depending on the oxygen supply. Modified from Patonié (1920).

	Process	Product	
↓ Decrease of O ₂ -supply ↓	Aerobic	Disintegration	No solid residue
		Mouldering	Mould
		Peatification	Peat
	Anaerobic	Putrefaction	Sapropel
			} Humic coals } Sapropelic coals

Temperature:

As bacterial and fungal life is enhanced by higher temperatures, plant remains in tropical mires are more degraded than in temperate mires provided all other factors are equal. According to **Jacob (1956, 1961)**, the optimum temperature for bacteria and fungi is approximately 40°C.

Nutrient supply

Some nutrients like Ca, P, K and N intensify bacterial life. Groundwater is usually richer in these nutrients than rainwater. Plant material in mires where the level of moisture is controlled by ground water (low moors) are thus more easily decomposed than mires where the water supply is controlled by rain water (high moors).

Acidity

Bacteria thrive best under neutral conditions while fungi can tolerate pH-values as low as 4. In practice, this implies that the rate of decomposition is a function of the pH-value in the mire and that neutral conditions will give the highest rate of degradation.

Type of organic material deposited

During the stage of peatification the easily hydrolysable and nitrogen rich components of the plants are decomposed i.e. parts rich in lignin and cellulose. These are the organic components that will be transformed into vitrinite later in the coalification process. Parts that are mainly composed of lignin are more resistant than cellulose rich materials towards degradation. Hydrogen rich plant material (liptinites) and plant material that has been oxidized (fusinites) are resistant towards the peatification process.

3.2.2 Coalification (Geochemical conversion)

After the biological processes cease, the peat must be buried under layers of sediments which act as an insulating blanket, trapping heat that otherwise would rise to the surface of the mire. The geochemical processes that follow peatification are termed coalification. During the coalification process, the organic material (peat) mainly undergoes two types of changes:

- Mobile products are driven off due to increasing temperature and pressure.
- Condensation of the solid residue due to aromatization.

The coal resources around the world are deposited at different times. The Carboniferous coals in the northern hemisphere are more than 300 million years old while the Tertiary deposits range in age from 10 – 65 million years. Since the time of peat formation the organic material has undergone degradation and maturation. The geological age of the coal does not necessarily give any information of how mature the coal is. The maturity of a coal is a measure of the degree of metamorphosis the coal has reached, and is usually termed the *rank* of the coal. There are several factors contributing to the rank, but the most important are: geological time, pressure and temperature. Figure 3.6 illustrates how an increase in pressure, temperature and time affects the rank of the coal, and the main factors are commented in more detail below.

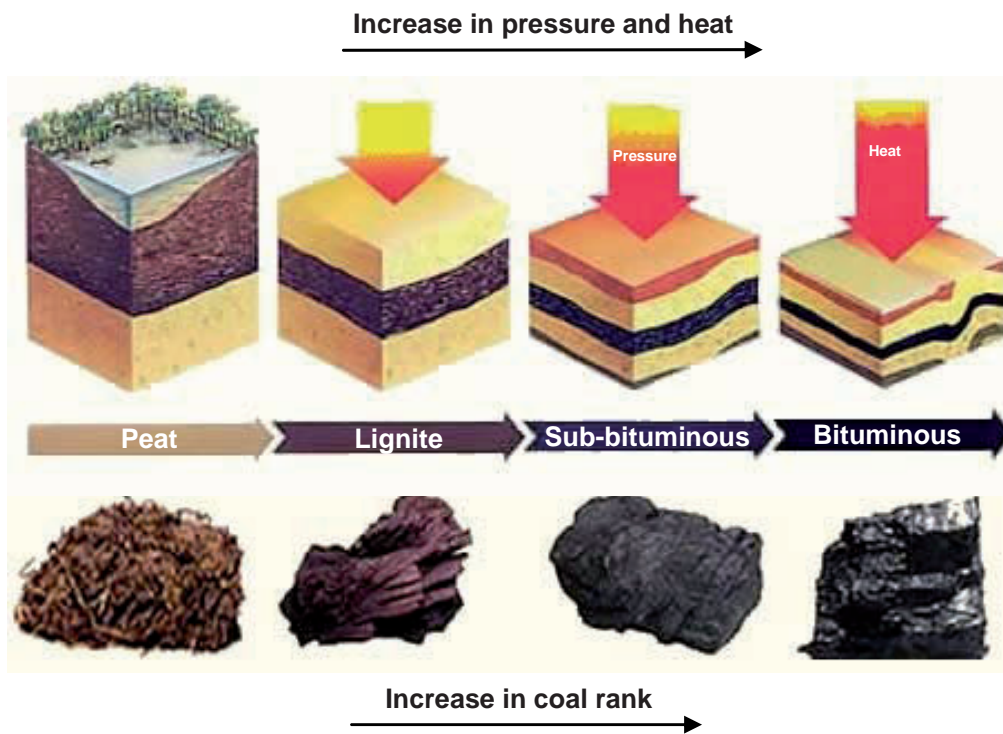


Figure 3.6: Increase in rank from peat to bituminous coals as a response to increasing pressure and temperature. Modified from ITAM (2003).

Temperature

Coalification and maturation depends mainly on the maximum rock temperature and the way the temperature has varied through geological time. The increase in coal rank with depth according to Hilt's Rule is due to the geothermal gradient which commonly is expressed as the increase in temperature per 100 meters ($^{\circ}\text{C}/100\text{m}$). The geothermal gradient is dependant upon the heat conductivity of rocks which again is a function of the mineral composition and porosity (amount of water). According to **Volkman (2004)**, the average geothermal gradient in Central Europe is about

3°C/100m which is in accordance with other reported values (Taylor et al. 1998, Price 2005). When the temperature reaches about 100°C, the bituminization process starts (generation of petroleum like substances). Typical coalification temperatures are 100 – 170°C for bituminous coals and 170 – 250°C for anthracites.

One of the most substantial evidences for the impact of temperature on coalification is that the relatively young coals which have been in contact with an intrusive body have an extraordinary high rank compared other the coals in the same region. Examples of the effect of intrusive bodies on coal rank can be found in coals from Sulfur Creek, Canada (Volkman 2004) and in the Upper Silesian Basin (Gabzdyl and Probierz 1987).

Time

The effect of time on the maturation of coals is dependant upon the temperature. The Lower Carboniferous (more than 300 Ma ago) lignite deposits of the Moscow Basin never subsided to a depth corresponding to more than approximately 25°C and is the perfect example of that time can be neglected if the temperature is too low. If the temperature is more than 130°C, the reactions proceeds at such high rate that time no longer has any significant effect on the degree of coalification. The conclusion must thus be that the effect of time is only of any importance as long as the temperature is in the range 70 – 100°C.

Pressure

The geostatic pressure is increasing as the amount of overlaying sediments is accumulating. According to Le Chatelier's principle, increasing pressure will retard chemical reactions involved during the maturation of coal – i.e. removal of liquid and gases. An increase in pressure will however promote some physical changes like loss of porosity and alignment of structural units, especially during compaction of peat until the early bituminous stage.

3.3 Coal Rank

The degree of metamorphism or coalification undergone by a coal, as it matures from peat to anthracite, has an important bearing on its physical and chemical properties, and is referred to as the rank of the coal. The classification of rank can be quite diverse as coal has been utilized in countries around the world since before the industrial revolution, and due to this fact many countries developed their own classification of coals. Table 3.2 illustrates the different coalification stages according to the American coal classification and some of the most important variables in order to asses coal rank. From Table 3.2 it is evident that the American classification divides coal into four major groups according to their degree of coalification: *lignite*, *sub-bituminous-* and *bituminous coal* and *anthracite*.

Lignite and sub-bituminous coals represent the lowest degree of coalification and are often referred to as brown coals or low rank coals. An example of how lignite and sub-bituminous coal might look like is provided in Figure 3.6. The most prominent changes during this stage are the formation of humic substances (see section 3.2.1) and the decrease in moisture content. The loss in moisture content is mainly a function of the increased pressure (loss of porosity), but also due to decomposition of hydrophilic

3 COAL, COKE AND CARBONIZATION

functional groups which subsequently reduces the O/C ratio. As the moisture content decreases, the calorific value of coals is increasing.

Table 3.2: Coalification stages according to the American coal classification, microscopic characteristics of the different rank stages and the applicability of the different rank parameters. After Teichmüller (1987).

Rank	Refl. R _{r oil}	Vol. M. d.a.f %	Carbon d.a.f Vitrite	Bed Moisture	Cal. Value Btu/lb (Kcal/kg)	Microscopic Characteristics	Applicability of Different Rank Parameters
Peat	0.2	68				free cellulose, details of initial plant material often recognisable, large pores	
Lignite	0.3	60	ca. 60	ca. 75	7200 (4000)	no free cellulose, plant structures still recognisable, cell cavities frequently empty, formation of rank inertinite	bed moisture (ash-free) calorific value (moist, ash-free)
Sub Bit C	0.4	52				geochemical gelification and compactation takes place, vitrinite is formed,	
Sub Bit B	0.48	48	ca. 71	ca. 25	9900 (5500)	formation of exudatinite, 1 st coalification jump of liptinites	Carbon (dry, ash-free)
C A	0.5	44				formation of micrinite	
B	0.6	40	ca. 77	ca. 8-10	12600 (7000)	2 nd coalification jump of liptinites, rapid rise of red/green quotient of sporinite fluorescence	
High Vol. Bituminous A	0.7	36					
	0.8	32					
Medium Volatile Bituminous	1.2	28	ca. 87		15500 (8650)	beginning of 3 rd coalification jump, rapid rise of liptinite reflectance	
	1.4	24				R _r sporinite = R _r vitrinite,	
Low Volatile Bituminous	1.6	20					
	1.8	16					
Semi-Anthracite	2.0	12					
	8		ca. 91		15500 (8650)	R _{max} liptinite > R _{max} vitrinite, R _{max} liptinite > R _{max} inertinite,	hydrogen (d.a.f) volatile matter (dry, ash-free) R _{max} reflectance of vitrinite R _r R _{min} moisture X-ray, electron diffraction
Anthracite	3.0	4				R _{max} vitrinite > R _{max} inertinite,	
Meta-A.	4.0						

The most prominent change during the sub-bituminous coal stage is the geochemical gelification (vitrinization). This occurs at the boundary between sub-bituminous C/B and transforms the humins into vitrinite which in turn makes the coal black and lustrous (see the silky luster of the bituminous coal compared to the sub-bituminous coal in Figure 3.6).

The moisture content is still decreasing corresponding to an increase in the calorific value during the progress of coalification in the high volatile bituminous coal stage. This stage is also characterized by the bituminization process. In this process bitumen (petroleum like substances) are formed by decarboxylation and reduction processes. The bitumen is responsible for the softening and agglomeration of coals dictating their coking ability. The onset of the bituminization process also corresponds to a distinct change in the lipid constituents which is known as the first coalification jump of liptinites.

During the bituminous coal stage the amount of volatile matter, which mainly consists of aliphatic components, is decreasing rapidly. **Levine (1993)** refers to this stage as the de-bituminization stage and claims that the volatile matter is composed mainly of low molecular weight hydrocarbons (methane) which causes the H/C ratio in coal to drop. A higher reflectivity of vitrinite is caused by the higher degree of ordering of the aromatic units. In the low volatile bituminous rank stage, the liptinites have attained the optical properties of vitrinite and the two maceral groups can not be distinguished (see Figure 3.9.A).

During the anthracitic stage a rapid fall of hydrogen, corresponding to a decrease in the H/C ratio, and a very strong increase in reflectivity and optical anisotropy are the characteristic features. At the border between low volatile bituminous coals and semi-anthracite, a sudden orientation of the aromatic units occurs. As anthracite represents the highest degree of metamorphosis and thus have experienced very high pressure due to the overburden, flattened pores are characteristic for the structure. The pore walls consists of stacks of 2 - 3 aromatic layers which are oriented parallel to the pore walls.

The molecular structure of the coals is continuously developing during coalification and is illustrated in Figure 3.7.

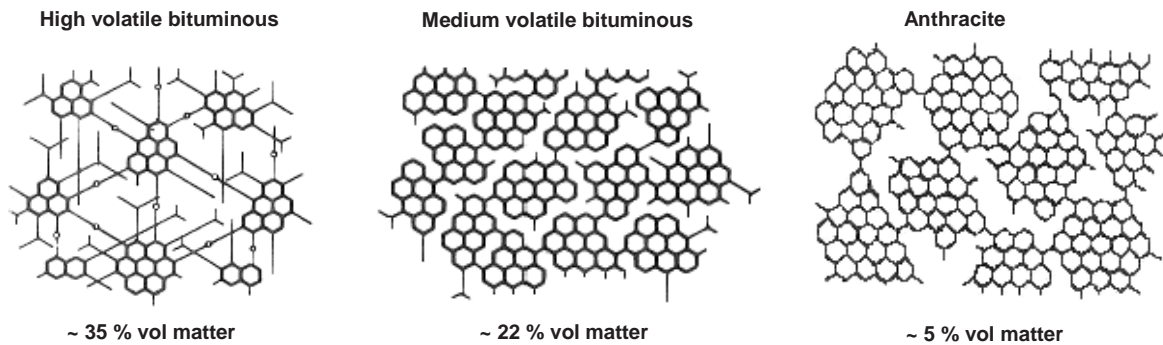


Figure 3.7: Changes in chemical structure from high volatile bituminous coal to anthracite. Notice the development of the aromatic structure. The hexagons represent the aromatic fraction and lines aliphatic components which are gradually removed during coalification.
After Teichmüller and Teichmüller (1968)

3.3.1 Rank parameters

In addition to the American classification of coals which is described above, there exist a number of coal classification systems around the world. Almost every coal producing country has its own classification. A comparison of the systems in Poland, Germany and USA in addition to the coal classification system proposed by the Economic Commission in Europe (ECE) is provided in Appendix A. The ECE coal classification was adopted by the United Nations in 1988 (**ECE-UN 1988**) and is an attempt to standardize all the existing systems.

Coal rank is regarded as the most important parameter in order to evaluate technological applications for coal. In assessing rank parameters of a coal, corrections have to be made for moisture and content of minerals. In Europe it is common to express these parameters on a dry ash free basis (*daf*), while it is more usual to report the results on a mineral matter free basis (*dmmf*) in the United States. An illustration of the relationship of thermally fixed and volatile matter in coal as well as a description of the different ways in which it is common to report rank parameters is provided in Figure 4.1.

To measure the degree of maturation in coals a few parameters have been introduced and widely used. For low rank coals the moisture content and especially the calorific value on a dry mineral matter free basis have commonly been used. As the moisture content stabilizes as the rank reaches the bituminous stage, other parameters have to be assessed in order to differentiate the hard coals. Volatile matter has traditionally been used to measure the rank for more mature coals.

The applicability of the different rank parameters are indicated at the right hand side in Table 3.2, and an illustration of how some of the most important rank parameters change with the degree of coalification is shown in figure 3.8.

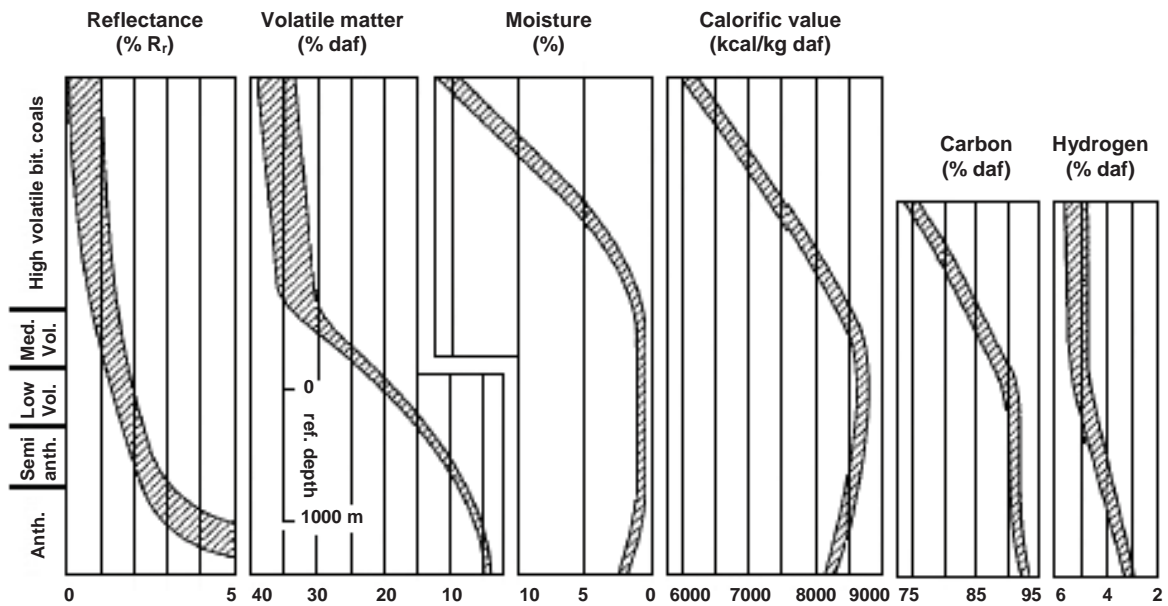


Figure 3.8 Increase in the degree of coalification affects the most used rank parameters differently. Modified after Teichmüller and Teichmüller (1979).

During the course of coalification there is an enrichment of carbon in coal as contents of oxygen and hydrogen decrease. In 1991, ASTM introduced a method of classification that relies on the fixed carbon content in coals. The fixed carbon content comes as a result of a proximate analysis (described in section 4.1.1) and is simply put the carbon residue after a defined heat treatment. Values of fixed carbon are however very dependant upon the mineral matter in coal and will thus not represent the degree of maturation of organic matter to a satisfactory degree. The fixed carbon content of a coal sample can be directly analyzed from bulk samples and is therefore a parameter that suites the industry well. Chemical rank parameters accepted by the International Committee for Coal Petrology (ICCP) are based on samples from vitrite. Vitrite comprises by definition of 95 % or more of vitrinite macerals in bands at least 50 μm thick. The carbon content of coal on a dry ash free basis (daf) is traditionally a widely used parameter in the western countries. The degree of coalification can however be misinterpreted as coals of the same maturity, but with a varying petrographic composition can give different values for total carbon.

Hydrogen is regarded as the best chemical rank parameter within the stage of anthracites as the level decreases due to release of methane.

Indisputably, reflectance of vitrinite is the most acknowledged measure of rank. Reflectance of a maceral is expressed as the percentage of incident vertical light intensity that is reflected from a polished surface of coal, using a petrographic microscope. The reflectance is related to the aromaticity of the organic compounds in coal which is increasing with rank as described in section 3.3.

Reflectance of vitrinite has been evaluated to be the best rank indicator as it is the most homogenous and dominant maceral in coal. Figure 3.9 shows that the reflectance of vitrinite is increasing linearly with rank (up to about 2 %), in contrary to the reflectance of liptinites and inertinites.

The measured reflectance of vitrinite is dependant upon the refractive and absorption indices. As the degree of aromatization is increasing, the refractive index, which is related to the very fine structure, is also increasing. The absorption index is dependant upon the number of delocalized electrons and as the electron mobility is increasing with the size of the aromatic lamella, it is also increasing with rank.

Anisotropy of coals is due to orientation of the aromatic complexes mostly as a consequence to the increasing load pressure. The process of alignment of the aromatic layers is especially noticeable during the formation of bitumen. This is the process which makes the coals fluid and corresponds to the liquid phase during carbonization. The degree of anisotropy in coals is increasing with rank, and can be evaluated when the maximum and minimum reflectance of vitrinite is measured (see section 4.2.2). Then the level of anisotropy will be the difference between the maximum- and minimum reflectance ($R_{max} - R_{min}$). The increasing anisotropy with rank as well as the relationship between maximum (R_{max}) and random reflectance (R_r) of vitrinite is illustrated in Figure 3.9.B.

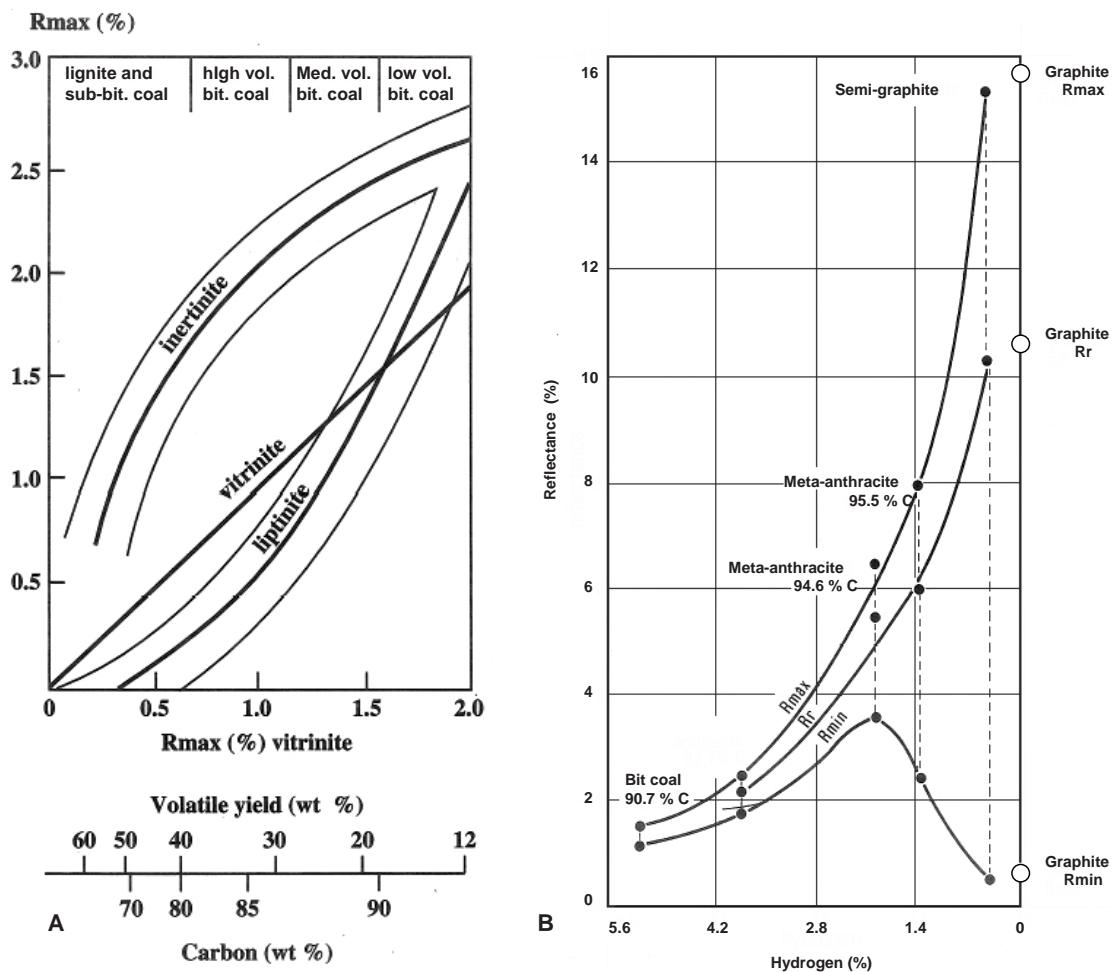


Figure 3.9: A) Reflectance of vitrinite, liptinite and inertinite with increasing rank. B) Increasing degree of anisotropy during the rank stage from bituminous coals to graphite.

Modified from Teichmüller (1989) and Ragot (1977).

The procedure for determining vitrinite reflectance is described in section 4.2.2.

3.4 Microstructure of Coal

Coal can in general be said to consist of two parts - an inorganic- and organic part. The inorganic part is what is recognized as mineral inclusions in the coal and will be covered further in section 3.4.4. The organic part of the coal can on the other hand be divided into different groups of macerals.

The term maceral was introduced by **Stopes (1935)** as an analogy to the minerals in inorganic rocks. Macerals are the smallest microscopically observable entities in the coal which represents the coalified remains of various plant derived substances existing at the time of peat formation. Even though macerals are compared to minerals in rocks, the chemical composition and the physical properties of the former vary over a significant range and they have no defined crystal structure. These properties will also change with the degree of coalification (rank). The original plant material, the level of decomposition and the degree of coalification are of fundamental importance in the genesis, development and properties of macerals. Macerals can only be observed under the microscope and are identified and recognized on behalf of their reflectance, color, shape, hardness (relief), size and association with other macerals. Some of the macerals have retained the cell structure and can be traced back to the original plant material from which they are derived, while other macerals are degradation products which are so altered that their plant origin can not be determined.

The composition of coal texture is represented in Figure 3.10.

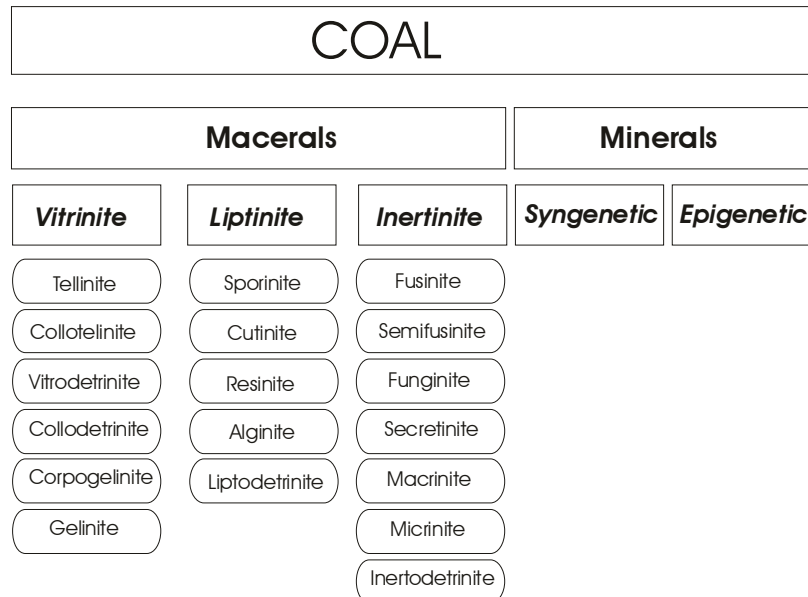


Figure 3.10: Composition of coal texture with the maceral groups, individual macerals and types of minerals

As can be seen from Figure 3.10, all the names of the macerals end in *-inite* and are grouped in three groups of macerals: *Vitrinite*, *Liptinite* and *Inertinite*. These groups all contain individual macerals which have similar chemical, physical and petrographical properties. Universal acceptance is given to the classification of the International

Committee for Coal and Organic Petrology (ICCP). As the identification of macerals is subjective, the ICCP has formulated some rules for petrographic microscopy which provide that the description of macerals should be in terms of their appearance in reflected light with oil immersion objectives with 25 – 50x magnification.

Formation of macerals from organic matter during the stage of peat formation depends on a number of factors. In addition to the type of organic material and the climate, there are also some factors of the depositional environment (the mire) such as: the bacterial activity, acidity, redox potential, water flow and supply of nutrients that affects the formation of macerals (see section 3.2.1).

3.4.1 Vitrinite

Vitrinite is the main maceral group in most hard coals. It usually constitutes the matrix of the coal texture with liptinites and inertinites embedded in the vitrinite. Vitrinite originates from lignin and cellulose in the cell walls of the organic material. Depending on the process of decomposition, degree of gelification and rank, some macerals will have well preserved cell structures while others are very homogenous. Typical examples of the origin are: tree trunks, branches, roots, leaf tissue and bark of the trees. Vitrinite is a group of macerals that do not exist in low rank coals. In lignite and sub-bituminous coals, the vitrinite is classified as huminite. It is during the first coalification jump (see Table 3.2) that vitrinite is formed from huminites. In terms of the ECE classification (ECE–UN 1988) of coals as low, medium- and high rank coals, the transition between huminite and vitrinite is set at a random reflectance of 0.6 %. According to the new vitrinite classification (ICCP System 1994) (ICCP 1998), vitrinite is defined as a group of macerals whose color is grey in reflected white light and with reflectance between liptinite and inertinite over the rank range where all maceral groups can be recognized. The chemical composition will be dependent upon rank, but vitrinite is rich in carbon (77 – 96%) relative to the other maceral groups.

According to the ICCP System 1994, macerals belonging to the vitrinite group are characterized based on degree of degradation and are subdivided into the following groups:

Telovitrinite

Vitrinite macerals categorized in the telovitrinite subgroup have preserved botanical cell structures which may or may not be visible in reflected white light. Telovitrinite comprises the macerals *tellinite* and *collotellinite* which can be distinguished based on their degree of geochemical gelification. Tellinite clearly has recognizable cell walls while collotellinite is more or less homogenous. Collotellinite is the principal reactive maceral of the vitrinite group in terms of carbonization and liquefaction. Wet conditions with a low pH-value during the peat stage which results in a high degree of cell preservation will generate large amounts of telovitrinite.

Pseudovitrinite is an informal name for a variety of vitrinite which is derived from the same plant material as telovitrinite. It has a slightly higher reflectance (minimum 0.025 %) than telovitrinite and is characterized by visible cell structure, small slits (comma slits) in the structure and stepped edges, but does not always display all these

characteristics. It is generally free from pyrite inclusions and is generally very homogenous.

Detrovitrinite

This subgroup of vitrinite macerals consists of finely fragmented vitrinitized plant remains and consists of the macerals *vitrodetrinite* and *collodetrinite*. The former describes clearly visible and isolated particles of vitrinite (particle size < 10 µm) while collodetrinite describes aggregates or a groundmass of vitrinite where the boundaries of individual particles no longer are visible due to gelification. A large amount of detrovitrinite is an indication of a neutral to weakly alkaline and oxidizing depositional environment.

Gelovitrinite

Colloidal infillings of vitrinitic material in former voids makes up the gelovitrinite subgroup. *Corpogelinite* and *gelinite* are the two macerals comprising this subgroup. Corpogelinite describes primary infillings in cell lumens while secondary homogenous infillings in microfissures, cleats or other formerly empty spaces are termed gelinite. Gelovitrinite is derived from humic fluids formed during decay or diagenesis of plant tissues and subsequently precipitated as gels within voids or cavities in the source material.

As vitrinite is a major component in most coals, the properties of vitrinite affect most industrial processes utilizing coal. In bituminous coals, vitrinite fuses and becomes fluid upon heating, and this is a very important property in the production of metallurgical coke (see section 3.5.4). During storing of coals, vitrinite will oxidize and hence deteriorate the thermoplastic properties.

3.4.2 Liptinite

Liptinites are derived from hydrogen rich components of the organic material such as resins, waxes, spores, pollens and cuticles. In contrast to vitrinite and inertinite, liptinite contains a relatively large amount of aliphatic constituents.

The following categorization of the liptinite macerals are from **Taylor et al. (1998)**.

Sporinite

It is the most common maceral of the liptinite group in humic coals and originates from the waxy coatings of fossil spores and pollens. The size may vary in the range 10 – 2000 µm and it can be classified as micro-, macro- and mega spores. (The largest spores are of female origin while the smallest are male.)

Cutinite

This maceral is observed in most coals, but is not very abundant. The origin is from the waxy coatings of leaves, roots and stems. Cutinites are composed of polyesters which are relatively resistant to mechanical and chemical degradation.

Resinite

Resinite is common in most coals and is usually observed in the form of oval bodies. The principal precursors of resinite are waxes and resins, but may also be balsams,

latexes, oils and fats. This maceral is most common in Tertiary coals due to the development of the resin producing plants.

Alginite

It is rarely observed in humic coals, but one of the main components of sapropelic coals. Alginite originates as the name indicates from a resistant oil rich algae and is best observed under fluorescent light.

Liptodetrinite

Fragmentation products of other liptinites are termed liptodetrinites and occur as small dispersed particles in coals.

3.4.3 Inertinite

Most of the inertinites are of the same origin as vitrinite (cellulose and lignin), but have been altered in some way either by forest fires before being deposited in the mire (charring), oxidation or by bacterial attack (fusinitization). Formerly the macerals of the inertinite group were believed not to soften during carbonization, and were thus regarded more or less non-reactive. Based on these observations, the macerals were grouped under the term inertinite. Later research has proven that much of the inertinite macerals actually contributes significantly to the fusion of coking coals (see paragraph 3.5.2), but the inertinite term is still in use.

Because the inertinite macerals have a high degree of aromatization and condensation, the reflectivity of these macerals is substantially higher than the vitrinite macerals even though the origin is the same. Under the microscope, inertinite macerals will appear white to bright grey compared to vitrinite and liptinite.

Secondary inertinite is formed from other macerals during the course of coalification, of which micrinite is an example.

During coalification the inertinite macerals alter very little. The main reason for this is that the macerals to some extent are pre-coalified.

The inertinite macerals are in general harder, with the exception of micrinite, than the other macerals and will thus show a positive relief in polished samples for microscopic investigations.

The following classification of the inertinite macerals are taken from the ICCP System 1994 (**ICCP 2000**).

Fusinite

Fusinite is one of the macerals in the inertinite group with visible plant cell structures. According to the definition in the ICCP System 1994, fusinite is showing highly reflecting, well preserved cellular structure. Some fusinite is the result of wild fires which resulted in the formation of fossil charcoal, denoted as *pyrofusinite*. According to **Taylor et al. (1998)**, the fusinite group can be further divided according to the genesis into *pyro-*, *rank-*, *degrado-* and *primaryfusinite*.

Semifusinite

This maceral is similar to fusinite in origin. According to the definition, reflectance and structure of semifusinite is between that of vitrinite and fusinite in the same coal. Semifusinite is formed by weak humification, red-ox processes and/or dehydration during the peat stage. Wild fires, which are responsible for the genesis of pyrofusinite, may also be the origin of semifusinite. Temperature and / or residence time have however been too low for formation of fusinite. Some Gondwana coals may be rich in semifusinite partly formed from leaves.

Funginite

Highly reflecting fungal remains comprise the funginite maceral. This maceral have visible cell walls under the microscope. Fungi have been a part of the flora of the world since long before any coal was deposited, so we can expect funginite to be present in peats and coals of all ages (although in small amounts).

The reflectance of funginite is normally higher than the corresponding vitrinite up to about 1.6 % random reflectance (R_r).

Secretinite

Secretinite is a high reflecting maceral with a round to oblong shape that shows no cellular structure. The dimension of secretinite is usually 60 – 400 μm in cross section, but it might be as large as 2000 μm in elongated form. It can show fractures and have an oxidized rim of lower reflectance. The origin of this maceral is believed to be from oxidized resin.

Macrinite

Macrinite is defined as a relatively large and compact maceral without cell structure. It does not have a defined shape, and might appear as a groundmass or in discrete lenses. The reflectance is close to semifusinite in the same coal. Flocculated humic substances that underwent dehydration and red-ox processes due to temporarily lowered groundwater level is the origin of macrinite.

Micrinite

Micrinite occurs as very fine rounded grains with high reflectance in the coal ground mass and has an upper size limit of 2 μm . Based on the small size of individual grains, micrinite is hard to account for during a standard maceral analysis. Only aggregates of micrinite can be properly accounted for.

Some micrinite is defined as a secondary maceral in the sense that it is formed from liptinites during the course of coalification. It might also originate from peatification or strong fragmentation of other inertinite macerals.

Inertodetrinite

Inertinitic fragments without microscopically recognizable structure is denoted inertodetrinite. The dimension of inertodetrinite is less than 10 μm (maximum dimension for compact grains and minimum direction for thread shaped fragments). As particles less than 2 μm are referred to as micrinite, the size range for inertodetrinite is

2 – 10 μm . In general the size and shape of the inertodetrinite particles are functions of desiccation, mechanical crushing and attrition to which the inertinites were exposed to before and during decomposition and compaction.

3.4.4 Mineral matter and trace elements in coal

Mineral matter is unavoidable in coals, and although it is a minor constituent of most coals it can affect the technical utilization to a great deal. After both carbonization- and combustion processes mineral matter in coal can be oxidized or transformed, and is further referred to as ash.

For coal combustion processes mineral matter decreases the calorific value of the coal as there is less carbon available. Composition of the mineral matter might also be a problem as effective removal of ash is a key requirement for boiler operation (sticky ash, fouling). Ash fusion temperature is used as an indication of how the ash behaves at elevated temperature in either reducing or oxidizing conditions.

A high level of mineral matter in coals used for cokemaking consequently results in high ash content in the final coke. This will further affect both the performance in the blast furnace (or production of ferroalloys) and the metal quality. As an example, potassium has been proven to act as a catalyst for gasification of coke in the production of manganese ferroalloys (**Kaczorowski 2006**) causing higher consumption of both raw materials and energy.

According to **Taylor et al. (1998)**, mineral matter in coal can be classified in three groups according to their origin:

1. **Syngenetic** mineral matter which was present in the organic material from which the coal was formed. This group of mineral matter is often referred to as *inherent mineral matter* (or ash). Plants need nutrients in order to grow and inorganic components are often dissolved in the media from which these nutrients are absorbed. Amount and type of mineral matter absorbed by plants is dependant upon the soil and type of environment of the mire in which they grow. Grasses require large amounts of silica while lycopods need alumina in order to grow. The major component in coal originates from wood (vitrinite), and in general wood of any tree contains less than one percent of mineral matter, leaves contain about three percent while the bark of a tree can contain as much as twenty percent of mineral components (**Todd and Hansen 1995**).
2. **Syngenetic** inorganic material which was present in the peat at the time of deposition or inorganic / organic complexes that formed during the early stages of peat formation (see Figure 3.5.)
3. **Epigenetic** minerals which were formed after consolidation of the coal by crystallization in cracks, fissures or cleats from solutions that have been in contact with the consolidated coal seam. Epigenetic minerals can also be formed by transformation of syngenetic minerals.

Epigenetic minerals can readily be removed from the coal by coal preparation techniques (e.g. density separation) while syngenetic mineral matter is harder to remove as the inclusions often are small and well distributed within the organic matrix.

Both the amount of mineral matter and the composition is a function of the depositional environment of the coal seam. *Paralic* coals deposits that were open to marine inclusions during the time of deposition generally have a higher level of mineral matter and sulfur than *limnic* coal deposits which were laid down under continental (intramountain regions) conditions. According to **Goodzardi and Swaine (1994)**, the Boron content in coal can be an indicator of the marine influence during early coalification where paralic coals have a higher level of Boron ($B > 110$ ppm) than fresh water influenced coals ($B < 50$ ppm).

Regarding the supply of nutrients and types of moors, low moors are generally higher in mineral matter due to the level of nutrients in ground water compared to high moors which were dependant upon rain water for moisture and thus adequate growth (ombrotrophic moors). The depositional environment may develop from low- to high moors during the time of peat formation. An illustration of the different types of peat swamps (moors) is provided in Figure 3.11.

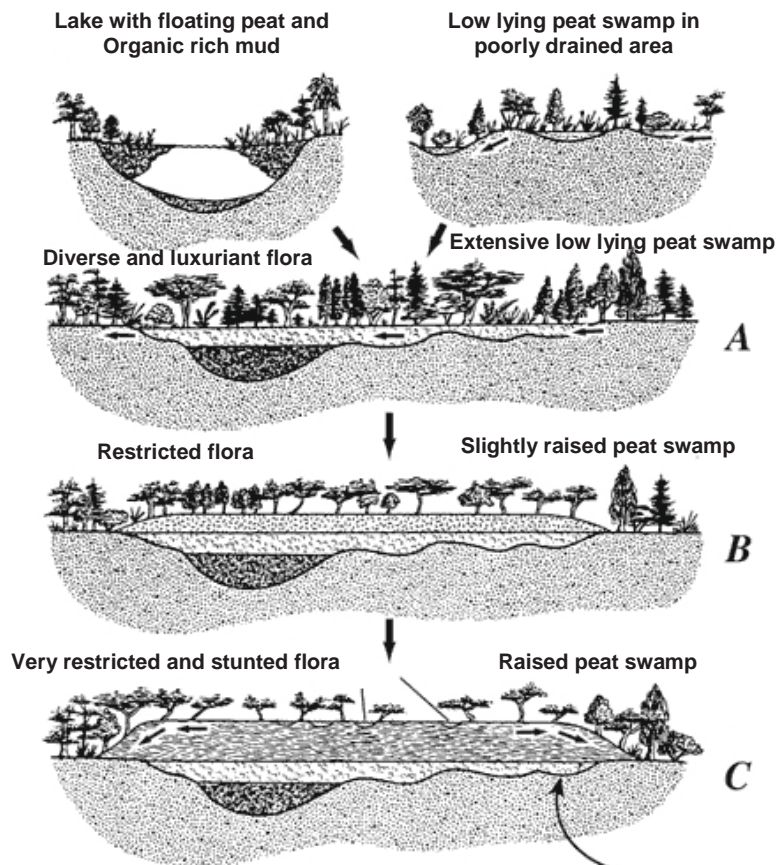


Figure 3.11: Different types of peat swamps (mires) that affect both the diversity of the flora and the amount and composition of the mineral matter in coal (Schweinfurth 2003).

Trace elements can be associated with both the organic- and inorganic part of coal. In general trace elements are associated with silicon rich minerals (clays), carbonate minerals, sulfide minerals, oxides and phosphates (**Swaine 1994**). There are however some trace elements that are believed to be organically combined, as for instance B, Be, Ge and Sb.

The most common groups of minerals in coals include clays, carbonates, iron sulfides and silicas and are listed in Table 3.3 according to their origin.

Table 3.3: Minerals in coal. After Crelling (1987).

Mineral Group	Syngenetic Formation		Epigenetic Formation	
	Inherent	Detrital	Deposited	Transformed
Clay minerals	Kaolinite, Illinite, Sericite, Montmorillonite, Tonstein, Mixed layer clays			Illinite, Chlorite
Carbonates		Siderite, Dolomite, Ankerite, Calcite	Ankerite, Dolomite, Calcite	
Sulphides		Pyrite, Marcasite, Melnikovite	Pyrite, Marcasite, Sphalerite, Galena, Chalcopyrite	Pyrite (from Siderite)
Oxides		Hematite	Goethite, Lepidocrocite	
Quartz	Quartz grains (clastic quartz)	Chalcedony Quartz	Quartz	
Phosphates	Apatite	Phosphorite, Apatite		

Microphotographs of macerals and minerals identified during the course of this work are presented in the form of an album in Appendix B.

3.5 Carbonization and Production of Metallurgical Coke

The two main commercial consumers of coal are coal fired power plants and producers of metallurgical coke. Both processes include subjecting the coal to high temperatures, but the conditions are quite different. According to **Callcott and Callcott (1990)**, the most important coal properties for electricity generation are: calorific value, consistent deliveries, relatively low ash content (without the need for coal processing) and ash fusion temperature.

Production of metallurgical coke is carried out by carbonizing coal or coal blends under controlled conditions, and the process sets three requirements to the coal properties.

Rank: Coals used for cokemaking should fall within the bituminous rank range. These coals are often referred to as *caking coals* (0.5 – 1.9 % R_r) as they soften, become plastic and coalesce into

a solid mass which swells and re-solidifies upon heating. There exists a subclass of the caking coals which is especially suitable for producing coke, and it is conveniently called *coking coals* (1.1 – 1.7 % R_r). According to the American coal classification system, the coking coals mainly fall within the medium volatile bituminous rank range. Coals that do not meet the rank requirements can only be used as blend components as they do not meet the product specifications (low rank coals) or cause operational problems (high rank coals).

- Type:* Not all macerals soften and become plastic upon heating (see section 3.4). In order to produce a sufficiently strong coke, the coal must contain a minimum of fusible macerals (mainly vitrinite).
- Grade:* As most of the mineral matter and trace elements in coal will be contained in the produced coke, there are limits to the amount of inorganic matter in coal.

The International Committee for Characterization and Terminology of Carbon (ICCTC) defines carbonization as: *A process of formation of material with increasing carbon content from organic material, usually by pyrolysis, ending with an almost pure carbon residue at temperatures up to 1600 K. (ICCTC 1982)*

Depending on the feed coal and process parameters, the final product of carbonization might be either coke or char. The **ICCTC (1983)** defines char as a carbonization product which has not passed through a fluid stage during carbonization. Thus, according to the definition, a char can be produced by carbonizing coals other than bituminous in rank, or by applying a very high heating rate which is the case in coal fired power plants.

Most of the metallurgical coke produced in the world is used in the blast furnace production of pig iron, but minor amounts are also utilized in producing ferroalloys and carbides. An extensive review of the requirements and role of coke in the blast furnace is given by **Poveromo (2005)**. In short, coke is fulfilling three roles in the furnace: Coke acts as a fuel providing energy for the endothermic reactions and for the melting of iron and slag. It is also providing reducing gases for the iron ore reduction. The third role of coke is to maintain permeability of the furnace and supporting the furnace burden.

During the last few decades there has been a trend in constructing larger blast furnaces as well as the use of pulverized coal injection (PCI) as an alternative source of heat. Due to these changes more emphasis have been put on coke properties that help support the burden and create permeability rather than as a fuel.

3.5.1 The effect of coal rank on carbonization

Based on studies on the coal to coke conversion during the last century, it is well known that rank of the feed coal affects the coke yield and the size and shape of the anisotropic domains in the coke texture. As discussed above, not all coals are suitable for cokemaking as they do not fuse and become plastic. The plastic properties of coals are usually measured using the Gieseler plastometer test which is described in section 4.1.3, and are depending on rank of the coals.

The molecular structure of low rank coals are characterized by covalent bonds. As discussed in section 3.3, coalification in the sub-bituminous to high volatile bituminous stage is essentially a decarboxylation process in the course of which the O/C ratio decreases. Medium volatile bituminous coals have lost most of the covalent bonds which are due to the relatively high oxygen content and are replaced by hydrogen bridges which are weaker. This results in a higher degree of thermoplasticity. The anthracitic rank stage is characterized by development of relatively large amounts of methane and thus a reduced H/C ratio. The diminishing level of hydrogen leads to the end of thermoplasticity and strong covalent carbon to carbon bonds are developing.

The petroleum like substances formed during the bituminization process have several functions in the developing thermoplasticity of coals. They act as a solvating medium for the aromatic units and a hydrogen donor to stabilize the free radicals formed by bridge cleaving.

During the plastic stage, the mixture of fluids and dispersed solids (infusible macerals or minerals, see section 3.5.2) is resulting in a molecular ordering by coalescence of the aromatic clusters. This process is similar to the liquid crystal theory described by **Marsh and Clarke (1986)**. Molecular mobility is determining the degree of coalescence of the aromatic units and hence determining the size and shape of the aromatic domains in the final coke. Dimensions of a single carbon crystal are determined by X-ray diffraction (described in section 4.5.2) while the size and shape of the anisotropic domains in the final coke are evaluated manually by microscopy. The correlation between a single carbon crystal and the anisotropic domains in coke is shown in Figure 3.12.

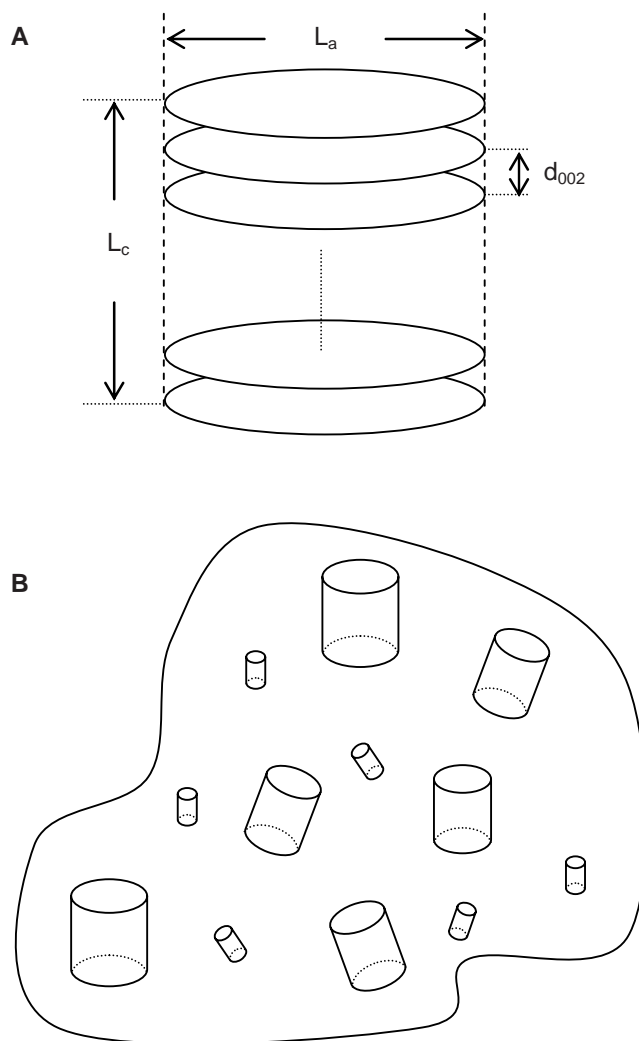


**Figure 3.12: Dimensions of a single carbon crystal (A) and orientation of these during the plastic stage of carbonization producing the characteristic anisotropic domains in coke (B).
From Gundersen (1998).**

There are several systems of nomenclature for description of optical texture, and some of these are listed in Appendix E. Size and shape of the anisotropic domains in coke are functions of molecular mobility during the plastic stage of carbonization which again is a function of the degree of metamorphosis the coal has reached (rank). As the rank of the coal increases, the aromatic to aliphatic ratio is also increasing. This is, according to **Sakurovs (1987)**, causing a more stable molecular structure during the plastic stage which is responsible for the larger anisotropic domains in medium volatile- compared to high volatile coals. Coke made from coals higher in rank will produce even larger anisotropic entities. This is due to the increasing molecular ordering of the coals and not to mesophase mobility which is reduced at rank stages higher than medium volatile coals.

3.5.2 The effect of coal type on carbonization

In the period 1957 to 1960 U.S. Steel conducted thermal studies of coal macerals. The results of these studies were first published by **Schapiro and Gray (1960)** and

elucidated by **Schapiro and Gray (1964)**. They defined the macerals that fused upon heating as reactive, and this group included vitrinite, liptinite and varying amounts of semifusinite depending on coal rank ($1/3$ when $R_{\max} < 1.35$ and $1/5$ in higher rank coals). Fusinite, inertodetrinite, macrinite, micinite and the remainder of semifusinite did not fuse when heated and were thus included in the group named inerts. The studies on coal to coke transformations conducted by Schapiro and Gray in this period made the basis for the U.S. Steel coke strength prediction which is the precursor for the ASTM coke stability curves (see Figure 3.13.).

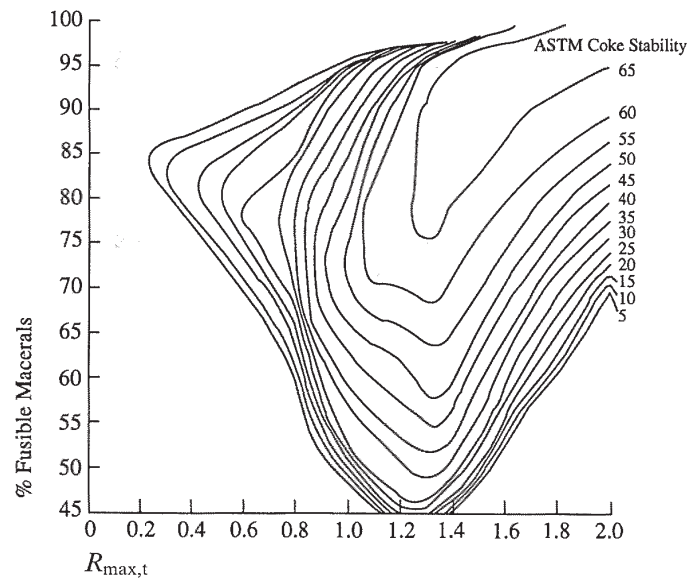


Figure 3.13: Coke stability as a function of maximum reflectance of vitrinite and the amount of total inerts. Figure after Brown et al. (1982).

Coke stability is a measure of how strong the coke is, and is a very important material parameter as the dimensions of the blast furnaces keep increasing. The ASTM stability index is a function of coal rank in terms of maximum vitrinite reflectance and coal type on basis of total amounts of inerts.

The Schapiro-Gray system is more than 40 years and although it has been widely used to predict coke stability, it has not remained unchallenged. The system was based on coal samples from the Appalachian basin and is excellent for these coals and similar Carboniferous coals. There are however large differences in coal properties depending on the depositional conditions. Australian coking coals proved to have a higher stability than predicted by the Schapiro-Gray method (**Gray and Bowling 1994**). The reason for this is believed to be that a higher portion of inertinite macerals in Gondwana coals actually fuses during carbonization and thus contributes to the reactives compared to the inerts (see Figure 3.13). In Australia it is common to perform a full maceral reflectogram in order to assess coal rank and all macerals below 1.8 % random reflectance are regarded as reactive. **O'Brien et al. (2003)** give a very good summary of the procedure and argues that automated image analysis also can be used to identify and quantify macerals in coal.

Based on the developments and research on coal type during heating, macerals are still quantified as fusible (reactives) and infusible (inerts).

Macerals of the inertinite group can be infusible, partially fusible or completely fusible. Fusinite and highly reflecting semifusinite constitute the infusible macerals and they retain their shape and size during carbonization and will form filler phase in the coke matrix. Partially fused inert macerals can be identified, but boundaries to the coke matrix are diffuse because of partial melting. Medium to low reflecting macrinite and semifusinite are the main sources of this category. Macerals of the inertinite group that are completely fusible upon heating are often hard to distinguish from the vitrinite based fused matrix and are part of the binder phase in the coke texture. Low reflecting inertinites are the main components in this category.

Liptinite macerals are usually relatively resistant upon change during biochemical coalification, but due to their high content of aliphatic components large amounts of gases are produced during carbonization. This enhances fluidity and contributes to the swelling properties of coals without leaving a large amount of solid residue.

Vitrinite is the maceral group contributing most to the formation of coke as it fuses and re-solidifies to constitute the binder phase of the coke matrix. According to Bethlehem Steel Corporation, pseudovitrinite should partially be considered as an inert during carbonization (Gray 1982). Pseudovitrinite resembles telovitrinite and is easily recognized during petrographic examinations. Microphotographs of pseudovitrinite can be seen in Appendix B.

3.5.3 The effect of coal grade on carbonization

Coal grade involves the amount and type of mineral inclusions in coal. The mineral matter in feed coal for coke production has to be kept within certain limits as it affects coke quality and at later stages also the total impurity level in the metal produced. In addition to the quality concerns, most authorities have set limitations to the total emissions of sulfur and other compounds from the production thus putting further attention to the level of potential polluting species in the charged coal. In order to assure that the mineral inclusions in coal do not exceed the limits, the run-of-mine (ROM) coal is usually processed before it is sent to the coking plant.

The most common way to process ROM coal before it is shipped to the coking plant is by taking advantage of the different densities of the constituents in coal. Mineral inclusions have a higher density (typically set as 2.5 g/cm³) than the organic material, but also macerals vary in density and can be separated. Figure 3.14 shows how the maceral densities vary with rank.

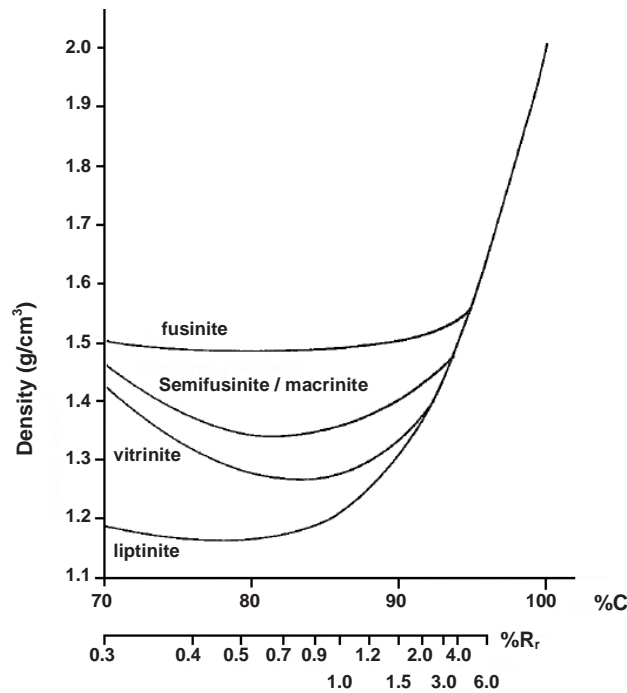


Figure 3.14: Density distribution of some macerals and maceral groups as a function of rank. The reported values are true density (excluding pores).

After van Krevelen (1961), Dyrkacz et al. (1984) and Diessel & Wolff-Fischer (1986).

The main target for coal preparation plants is to decrease the amount of mineral inclusions, but for some coals it might also be desirable to increase the content of reactive macerals by removing some of the inertinite. In addition to crushing and screening, most coal preparation plant employ density separation of the ROM coal into a high- and low ash fraction. Due to the heterogeneity of coal and the intergrowth of macerals and minerals, a certain amount of mineral inclusions must be tolerated in the clean fraction and the organic content in the ash rich tailings can reach 40 %.

Two properties of metallurgical coke that determines the suitability for use in the blast furnace are strength and reactivity towards CO_2 . Petrographic properties such as rank and maceral composition are important in determining these properties. The amount and composition of mineral matter in coke is also important as some minerals will catalyze the Boudouard reaction (Kaczorowski 2006). Grigore et al. (2005, 2006 and 2007) and Sakurovs et al. (2007) have done several studies to quantify and identify mineral matter in cokes and their parent coals. As the production of coke involves heating the coal to more than 1000°C , transformations of the original mineral matter in coal is expected. The authors have investigated transformation of mineral matter during carbonization by applying a low temperature ashing (LTA) procedure.

3.5.4 Industrial production of metallurgical coke

The history of making coke for metallurgical purposes stretches back several centuries. It has been firmly established that coke was used as the source of fuel in a blast furnace in England in the beginning of the 18th century. Coke was at this point in time produced by storing coal in piles and covering the piles with wet leaves, straws and dirt to reduce the supply of oxygen. Some of the coal was then ignited to supply the heat needed to

convert the remainder of the coal to coke. The production facilities and technology used for production of metallurgical coke throughout the centuries is reviewed in an article by **Kobus (2005)**.

Today most of the metallurgical coke is produced in coke oven batteries consisting of up to 80 retorts or ovens, and coking plants usually have several batteries. One oven is often referred to as a slot oven and typical dimensions are: width 0.4 – 0.6 m, length 10 – 20 m and height 4 – 6 m (**Olsen, Tangstad and Lindstad 2007**). Heat required for carbonization is supplied by combustion of coke oven gas in combustion chambers located between adjacent slot ovens. An industrial manufacturer of metallurgical coke usually blends at least three different coals in order to meet the coke specifications. The coal blend is washed, crushed and charged to the coking chamber. Charged coal is heated from two sides by the red hot silica brick walls. Coal in contact with the walls is rapidly carbonized resulting in swift melting and release of volatiles. The remainder of the coal charge is transformed into coke as the two heat fronts from the walls are advancing towards the oven centre. As the temperature reaches 350 - 380°C, the coal fuses and produces a plastic layer which separates the solidified semi-coke from the coal that still has not reached the softening temperatures. The carbonization process is illustrated in Figure 3.15.

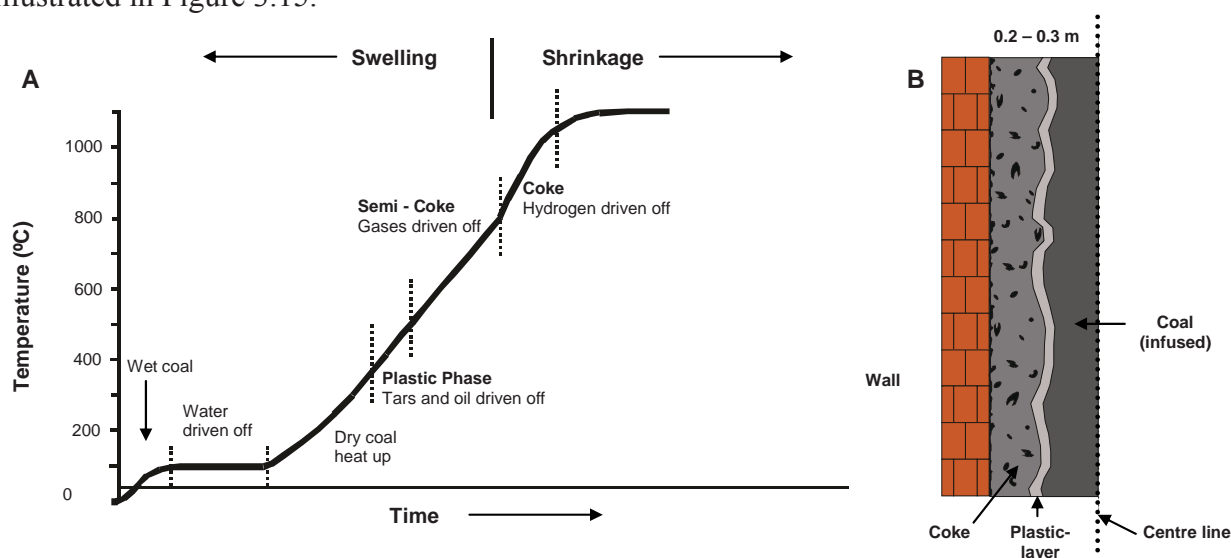


Figure 3.15: Temperature dependant processes leading to the formation of metallurgical coke (A). Illustration of a coking chamber during carbonization (B). Coke is produced close to the walls and the plastic layer is separating the infused coal mass at the centre of the chamber and the solidified semi-coke. Modified from Price (2005)

Figure 3.15 (A) is a schematic representation of the stages in coal carbonization as a function of time and temperature. As discussed above, the coal close to the walls is quickly heated thus losing water and become plastic in a relatively short time. During the plastic stage organic tars and aromatic hydrocarbons are generated and driven off. As the plastic layer is relatively impermeable, about 80 – 90 % of the volatile matter escapes through fissures and pores in the semi-coke / coke (see Figure 3.16). A further increase in temperature (450 - 500°C) will cause re-polymerization of the plastic matter into semi-coke. During the re-solidification, methane and other volatile gases are driven

off. As the temperature is increased to 1000°C, the semi-coke contracts and fissures generating methane and hydrogen as it is transformed into coke. According to **Todoschuk (2005)**, the final coke temperature should be 950°C or higher. In order to make sure that the coal charge is fully transformed into coke, the industrial practice is to leave the coke for an additional time. The time between the coke has reached 950°C to it is pushed out of the slot oven is referred to as the soak time.

Due to the high temperature gradient close to the hot walls the plastic layer is quite thin in this region, but becomes thicker as it migrates towards the oven centre. The volatile matter generated during pyrolysis is substantially heated on its way through the hot coke. The high temperature causes cracking which is producing lighter gases and pyrolytic carbon. Pyrolytic carbon is defined as the solid form of carbon deposited on a hot surface by cracking of gaseous or liquid hydrocarbons (**Rodriguez-Reinoso and Marsh 2000**). The pyrolytic carbon has a structure similar to carbon black and is relatively resistant to attack by CO₂. An illustration of the distribution of volatile matter during cokemaking is given in Figure 3.16.

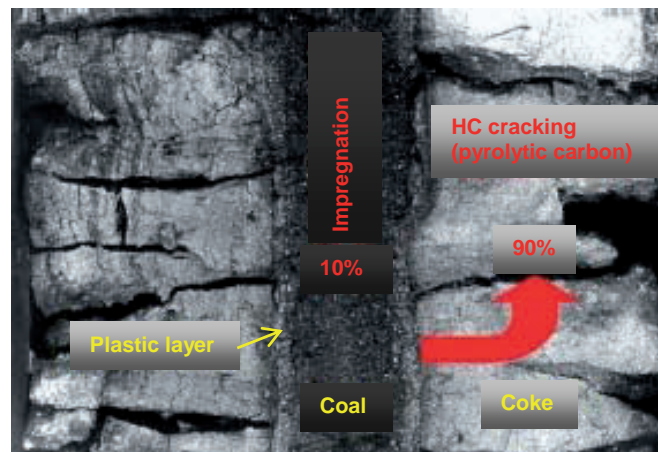


Figure 3.16: 90% of the volatile matter generated during pyrolysis is escaping through fissures and pores in the coke where they are subjected to high temperatures which causes cracking and thus producing pyrolytic carbon. The remaining 10% is causing impregnation of the coal due to re-condensation. (Steller et al. 2006).

Extensive formation of pyrolytic carbon during the carbonization process is an indication of too high wall temperatures.

3.5.5 Pore development during carbonization

Physical properties of the carbonized materials such as total porosity, pore size distribution and surface area can have a significant effect upon the reactivity of the carbonaceous material as well as its strength. The porosity and microstructure in coke is fixed by volatile components trapped in the plastic layer during re-solidification. Coke porosity can be placed in three categories according to their size.

Coarse pores: These pores are larger than 10 µm and are created by gas bubbles trapped in semi-coke during re-condensation. Coarse pores are best evaluated using image analysis techniques.

Macropores: The size of these pores is in the range 10 nm – 10 μm and is usually evaluated by mercury intrusion porosimetry.

Micropores: Microporosity in coke is generated by small gas molecules which are products of cracking reactions in the temperature range 500 - 800°C. The sizes of the voids are about the same magnitude as the molecules that are produced (CH₄, CO, H₂S, H₂O and H₂), typically about 0.5 nm.

The porosity in the final coke is a function of petrographic and rheological properties of the coal as well as process parameters like heating rate, coal size and bulk density. High volatile bituminous coals tend to produce the largest amounts of volatile matter and have the lowest coke yield, but also make a porous coke with plentiful fissures. Medium volatile bituminous coals produce cokes with moderate porosities and relatively thick pore walls. Low volatile bituminous coals would generate an excessive pressure on the coke chamber walls, and are thus seldom coked alone.

Size of the coal grains also has an effect upon pore size distribution in the coke. Larger coal particles will generate more volatile gases, and these will exert a pressure causing the particle to swell. Short pathways to the surface and small quantities of gas volume generated are the reasons why small coal grains are not forced into a pressure driven pore formation. A decrease in the coal size will however tend to maximize the particle interaction and create a more homogenous coke microstructure. Studies on porosity in coke as a function of the charged coal size do however indicate an increase in porosity with increased degree of crushing. **Fomin et al. (1973)**.

Coals with a high Gieseler fluidity will produce more porous cokes with thinner pore walls compared to coals with lower fluidity.

Regarding the process parameters, an increase in the bulk density of the charged coal will give less porosity in the final coke. Some coke manufacturers actually stamp the coal mass before it is charged to the slot ovens in order to increase the bulk density and thus reducing the porosity (increasing strength). A higher heating rate during carbonization generally results in a more porous coke with a lot of fissures.

The industrial practice is to blend coals with the required properties, so commercial cokes have porosities in the range of 45 – 55 %. According to **Price (2005)**, the total porosity of a coke can be calculated based on the true and apparent densities:

$$P(\%) = 100 \left(1 - \frac{\rho_s}{\rho_A} \right) \quad (3.1)$$

where ρ_s is the apparent density (particle density) and ρ_A is the true or absolute density of the coke.

As mentioned in section 1.4.2, the requirements of coke in the silicon- and ferrosilicon process are quite different from the blast furnace production of pig iron. Production of metallurgical coke is primarily concerned about fulfilling the stability criterion from the

blast furnace production. Although dimensions of the submerged arc furnaces used for production of high silicon alloys are quite considerable, coke stability is not the main concern. Reactivity towards SiO gas and degree of conversion according to *reaction 1.5* as well as amount and type of impurities are more important. Metallurgical coke does not fulfill these criteria to a satisfactory degree. From Figure 1.6, it can be seen that some producers are using char or reactive coke in the charge mixture. These materials are however produced in a way securing consistency with requirements of the silicon process.

4. EXPERIMENTAL PROCEDURES AND SAMPLE MATERIAL

4.1 Chemical and Plastic Properties of Coal

The Run Of Mine (ROM) coal samples were air dried for three days before representative amounts were sent to an externally accredited laboratory (The Institute for Chemical Processing of Coal) for basic analyses. As the laboratory is located in Zabrze, Poland, the analyses were conducted according to Polish Norms (PN). These are, however in most cases identical with the ISO standards. Further information about the Polish Norms used and the corresponding ISO- and ASTM standards are given in Appendix C. The Institute for Chemical Processing of Coal (IChPW) performed proximate- and ultimate analysis as well as determining composition of the ash. In addition, the plastic properties of the coals were measured using the Gieseler method.

There exist different ways of reporting the results from coal analyses. Figure 4.1 shows the relationship between the volatile- and the thermally fixed components of coal as well as the basis for reporting the results.

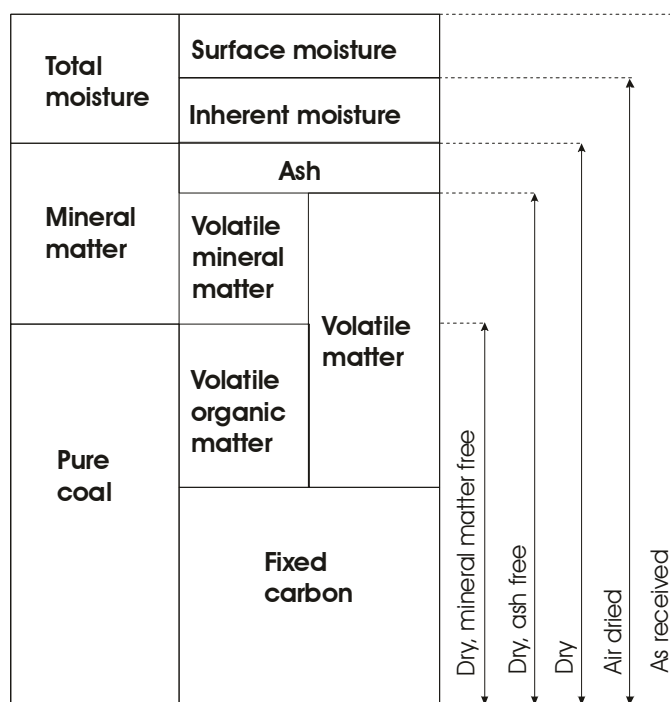


Figure 4.1: Alternative ways of reporting analytical results. After van Krevelen (1993).

4.1.1 Proximate analysis

The proximate analysis covers determination of volatile matter, moisture and ash. In addition, Fixed Carbon (Fix C) is calculated by difference. A graphical illustration of the proximate analysis is provided in Figure 4.3.A.

Moisture: Moisture is usually determined by drying the sample following two procedures. One split of the sample is dried at a specified room temperature and relative humidity and the other split is dried at 110°C under inert atmosphere. The *total moisture* is the difference between the as-received sample and the residue after drying at 110°C until the weight is constant. *Inherent moisture* is the difference between the as received sample before and after drying at specified room temperature. The difference between the total moisture and the inherent moisture is referred to as the *free moisture* (see Figure 4.2).

Volatile: matter The amount of volatile matter in coal is determined by heating a small quantity (1 g) of air dried coal to a temperature of about 900°C in absence of air. The volatile matter is determined as the weight loss corrected for moisture content.

Ash: The content of inorganic matter in coal is determined by heating a predefined amount of coal under oxidizing conditions to a temperature of 750 – 815°C until a constant weight is obtained (ASTM: 750°C).

Fixed: carbon Fixed Carbon is determined by difference, and is not equal to the total carbon content. Carbon present in ash and volatile matter do not contribute to the amount of fixed carbon (see Figure 4.3.A).
$$\text{Fix C (\%)} = 100 - \text{Moisture (\%)} - \text{Volatile matter (\%)} - \text{Ash (\%)}$$

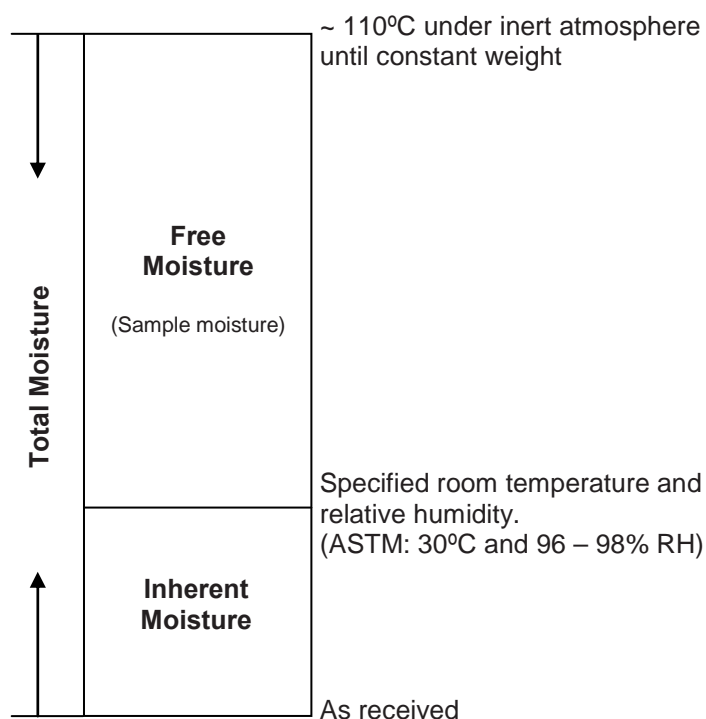


Figure 4.2: Analytical procedures for determining moisture in coal.

4.1.2 Ultimate analysis

Ultimate analysis describes elemental composition of the most common elements present in coal i.e. C, H, N, O and S. The content of ash is also a part of the ultimate analysis and is determined in the same way as described under proximate analysis. Direct analytical methods are used in order to determine the content of C, N, H, and S while the concentration of oxygen is usually calculated by difference and is hence the value most liable to error.

In this work C and H were determined simultaneously as CO_2 and H_2O (combustion products) were analyzed by absorption. Nitrogen was quantified using the Dumas method in which the organic material is mixed with a copper oxide and then heated to release nitrogen. A Leco CHN-1000 was used to analyze Carbon, Hydrogen and Nitrogen, and the amount of total Sulfur was determined by the total combustion method.

A schematic representation of the ultimate analysis is given in Figure 4.3.B.

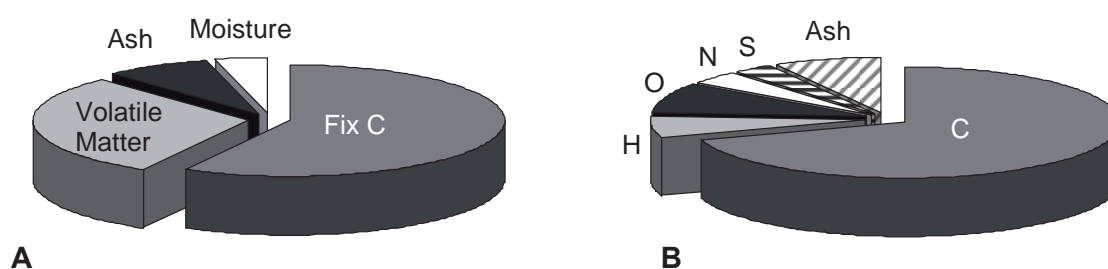


Figure 4.3: A graphical illustration of the output from respectively proximate analysis (A) and ultimate analysis (B).

The amount of ash determined from the proximate- and ultimate analysis is not equal to the amount of mineral matter originally present in the coal. Heating the coal under oxidizing conditions in order to remove the carbon also causes structural changes to the mineral matter. Carbon dioxide is removed from carbonate minerals and other minerals can be oxidized. In order to assess the original mineral matter in coal, a low temperature ashing procedure can be employed. There are several formulas correlating the mineral matter in coal with the output from the ultimate analysis. The Parr formula given in equation 4.1, gives a relationship between the mineral matter in coal and the ash and total sulfur yield from the ultimate analysis:

$$\%MM = 1.08A^a + 0.55S_t^a \quad (4.1)$$

Where $\%MM$ is the mineral matter in coal, A^a and S_t^a is the amount of ash and total sulfur from the ultimate analysis on an as received basis.

4.1.3 Plastic properties of coal

Rheological properties of coal include both plastic- and swelling properties. These properties are of uttermost importance to evaluate in order to make a good coke. There are a number of tests available to assess the swelling properties of coal, and the producers of coke can choose from Free Swelling Index (FSI), Roga Tests and Gray-King Assay depending on which test(s) correlates best with the performance of the coal and the final quality of the coke.

In this work the plastic properties of the coal have been measured by the Gieseler plastometer test. A simplified schematic of the Gieseler plastometer is given in Figure 4.4 A. This test gives information about the rheological properties of coal in its plastic state.

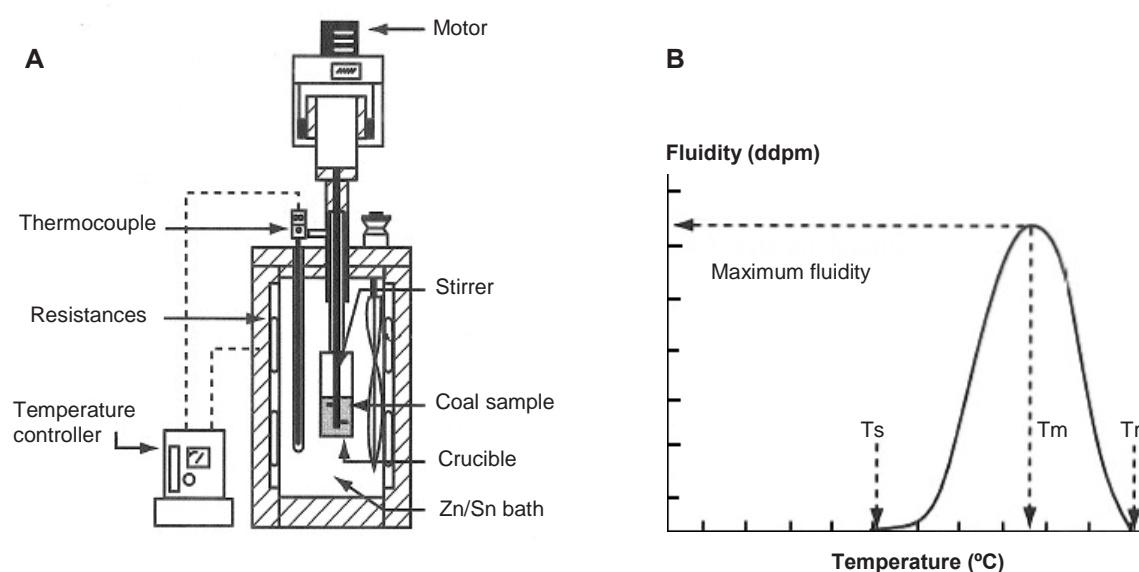


Figure 4.4: A simplified Gieseler plastometer (A) and a typical plastometer curve (B).
Modified from Rodriguez-Reinoso and Marsh (2000).

About 5 grams of air dried coal ($< 850 \mu\text{m}$) is placed in a crucible containing a stirrer and immersed in a bath. The stirrer is connected to a motor which provides a constant torque. As the temperature of the bath is increasing uniformly, the coal begins to soften and the stirrer starts rotating. The number of intervals per minute is recorded, and the output from the test is a plastometer curve of which there is given an example in Figure 4.4 B. From the plastometer curve we get information about when the coal softens and the stirrer starts rotating. This temperature is referred to as *the initial softening temperature*, and is denoted T_s in Figure 4.4.B. When the stirrer reaches its maximum rotation velocity, both *the maximum fluidity temperature* (T_m) and the maximum fluidity are reported. Usually the maximum fluidity is reported as dial divisions per minute (ddpm) (which is the number of rotations of the stirrer in one minute). As the temperature of the bath further increases, the coal will transform into solid coke and the stirrer will stop moving. The temperature at which this happens is referred to as *the solidification temperature* (T_r).

High volatile bituminous coals usually have lower temperatures of initial softening and re-solidification than higher rank bituminous coals, but are usually more fluid (higher value of $ddpm$) than coals higher in rank. This is mainly caused by generation of large amounts of gases and liquids due to the higher level of volatile components in this rank of coals. Medium volatile bituminous coals have the widest plastic range ($T_r - T_s$). As could be seen in Chapter 3.5, it is common for the producers of metallurgical coke to blend coals of different rank in order to have optimal coking conditions. To produce a strong uniform coke, the plastic ranges of the coals in the blend have to overlap. The Gieseler plastometer test gives information that can ensure the cokemakers that the plastic properties of the coal blend is in the specified range in order to make good coke.

4.2 Petrographic Examinations

During this work a number of petrographic analyses have been carried out on samples of both coal and char (coke). All the examinations have been performed with the use of a reflected light petrographic microscope. Following sample reduction, the polished pellets were prepared following the ASTM standard for preparing polished samples for petrographic examinations (ASTM D2795 1999). The standard suggests to use a pressure device (hydraulic- or screw presses) to reduce the voids in the pellet. This prevents gravity separation and results in a quicker preparation. As there was no pressure device for this purpose available, a vacuum of approximately 100 mbar was employed to the mixture of epoxy and particles by using an Epovac.

The petrographic analyses performed in this work have been carried out on a Leitz Orthoplan microscope. A MPV-SP intensity counter was attached to the photomultiplier of the microscope for reflectance measurements. Pictures presented in this work have been taken by a Kappa CF 20 DXC digital camera that was attached to the microscope. Set up of the petrographic unit used in this work is presented in Figure 4.5.

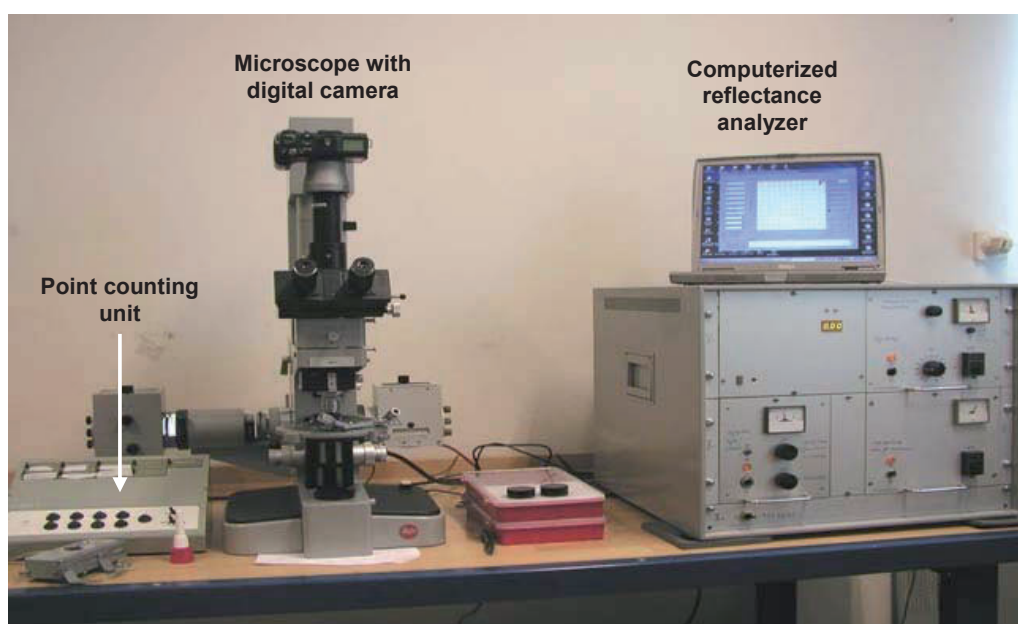


Figure 4.5: Setup for the petrographic equipment

In the petrographic examinations of coal and char (coke), three oil immersion objectives of magnification 20-, 32- and 50x were used. As the oculars had a magnification of 10x, the total magnification was 200 – 500x. Lower magnification would give insufficient resolution, while higher magnifications would result in poor image quality. To prevent loss of intensity reflected from the specimen, oil immersion objectives have been used. As light passes from one material to another with a different refractive index, it bends causing loss of intensity. In order to avoid this loss, the immersion oil has a refractive index equal to the glass in the objective (1.515). The difference between a microphotograph taken by the use of dry objective and oil immersion objective is illustrated in Figure 4.6.

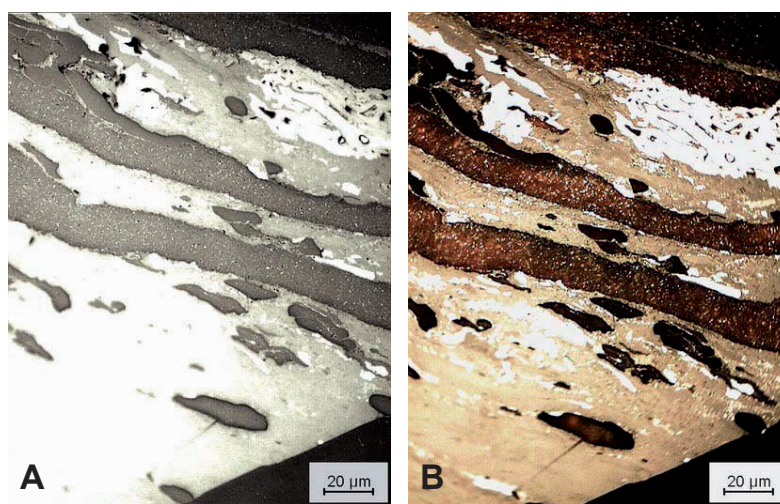


Figure 4.6: Coal under white light microscopy respectively using dry (A) and oil immersion lenses (B). Notice the increased level of details by using oil immersion objectives.

4.2.1 Maceral analysis

Standard maceral analyses are based on the Delesse relationship which states that the total area of a constituent, measured on a random plane surface, is proportional to the volume of this constituent. The point count method was used to quantify the macerals and mineral inclusions in the coal sample in this work. This procedure was first described by **Glagolev (1934)**, and a point counter generated a uniformly spaced grid of the specimen. According to the ASTM standard (**ATSM D2799 1999**), the grid spacing should be approximately half the size of the largest particles in the polished pellet. Macerals are identified based on their size, shape, color, structure, relief and association with other macerals. A crosshair in the eyepiece of the microscope ensured that most of the points counted coincided with only one grid point. A minimum of 500 points were counted on two separate pellets for each sample. The macerals are described in Chapter 3.4.1 – 3.4.3 and a catalog of the macerals identified during this work is presented in Appendix B.

4.2.2 Vitrinite reflectance

Determination of vitrinite reflectance has become the most acknowledged measure of rank and maturation of sedimentary organic matter. Vitrinite reflectance is performed on

a single maceral group (vitrinite) and is expressed as the fraction of perpendicularly incident light returning from a polished surface expressed in percent.

The reflectance of vitrinite is increasing with rank, and **McCartney and Teichmüller (1972)** showed that the reflectance was directly proportional to the size of the aromatic complexes. Due to the aromaticity of coals, there are two ways in which the reflectance of vitrinite can be reported:

When maximum reflectance of vitrinite (R_{max}) is reported, orientation of the aromatic lamellae is taken into consideration. A polarizer and a rotating sample stage are employed as the reflectance is continuously measured during rotating the sample 360°. The maximum value during the rotation is taken as one reading. The difference between the highest and lowest reflectance values during one rotation is a measure of the anisotropy of the coal sample. Anisotropy of coal is a property which is increasing with rank (see Figure 3.9.B).

Following the procedure for measuring random reflectance of vitrinite (R_r), orientations of the aromatic clusters are discarded and hence a rotating sample stage is not needed. There exist several correlations between random- and mean – max reflectance, and **Price (2005)** states that this relationship is given by equation 4.2. **Komorek and Morga (2002)** have tested 189 coal samples from the Upper Silesian Coal Basin in Poland, and have presented the relationship given in equation 4.3.

$$R_{max} = 1.061 \cdot R_r \quad (4.2)$$

$$R_{max} = 1.090 \cdot R_r - 0.052 \quad (4.3)$$

Koch and Günther (1995) argue that some of the relationships between maximum and random reflectance of vitrinite is only applicable up to $R_{max} = 1.8\%$. This is due to the non-linear increase in R_{max} (see Figure 3.9.B).

In this work random reflectance of vitrinite (R_r) has been measured on single grains of vitrinite. In order to do this according to the prescribed standards (**ASTM D2798 1999**), power was stabilized using a Straton rectifier, light from the halogen lamp was filtered at 547 nm and the light in the laboratory was dimmed during the analysis. Before the coal samples were analyzed, the photomultiplier was calibrated using two calibration standards of respectively 0.588 % and 1.720 % reflectance in oil. For reflectance measurements on single seam coal samples, a total of 100 readings is recommended. More inhomogeneous samples of coal need a higher number of readings and 500 are suggested for coal blends. (**Taylor et al. 1998**). As the coal samples in this work were of known origin, 100 - 200 readings were recorded and presented as histograms (Figure 5.7).

4.2.3 Non-maceral analysis

As a supplement to the maceral analysis and the reflectance measurements, **Gray (1982)** proposed a non-maceral analysis. This analysis has been further elucidated

and illustrated by **Gray and Gray (2005a)**. The analysis was developed in order to produce petrographic data that can be used in the utilization of coal (**Gray 1991**). The non-maceral analysis includes important materials that are not included in a standard maceral analysis. The non-maceral analysis divides the observed microstructures in coal into normal coal, pseudovitrinite, fines, oxidation, microbrecciation, mineral matter and miscellaneous. The relative amount of these microstructures will have an effect upon the utilization of coal, whether it is to be used for coke making, directly in the production of ferroalloys as a reduction material or in combustion processes. The analysis is carried out on the same pellets used for maceral counting and vitrinite reflectance (particle size < 850 μm). A minimum of 500 points were counted under a total magnification of 500x. A predefined grid of the polished pellet is acquired by using a mechanical point counter, and step size was set to more than the required minimum (425 μm).

Compared to using the cross hair in the maceral analysis, a whipple disc is inserted in the eyepiece of the microscope and employed in the counting procedure of non-maceral microstructures. The whipple disc has 100 squares with 10 on each side and one square is further divided into 25 subsquares. An illustration of the whipple disc is provided in Figure 4.7. For single maceral or mineral particles the corner angles of the whipple disc define the count points.

Heterogeneous coal is referred to as attrital coal and follows a slightly different counting procedure. For attrital coal the corner angles are considered as centres of a circle with a radius of 2.5 squares (25 μm). Each circle is evaluated in order to assess the heterogeneity of the coal, and depending on the amount of vitrinite the count point are recorded as bright (vitrinite $\geq 75\%$), intermediate ($75\% > \text{vitrinite} > 50\%$) or dull (vitrinite $\leq 50\%$) coal.

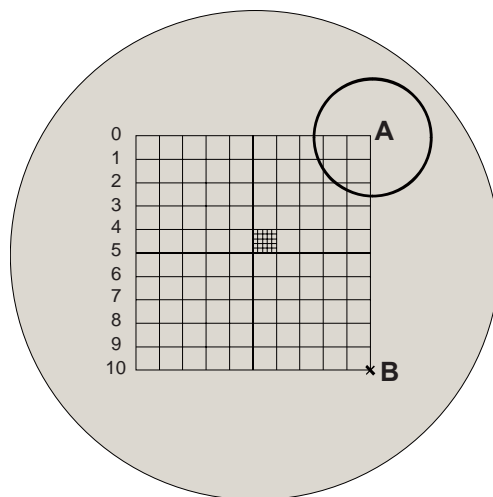


Figure 4.7: Whipple disc used for assessing the non-maceral microstructures. Attrital coal is counted according to the content of vitrinite in a circle (A) and single macerals and minerals are counted as illustrated by point B.

Homogenous particles of vitrinite, pseudovitrinite, semifusinite or fusinite in the size range 10 – 50 μm were counted as single macerals.

All particles less than 10 μm were regarded as fines.

One of the advantages of the non-maceral procedure compared to normal maceral counting, is that features of coal that might have direct impact on the utilization are identified. Examples of non-maceral microstructures not included in the standard maceral procedure:

Attrital coal: Quantifies the degree of homogeneity of the coal.

Oxidized coal: Reveals coal that has been exposed to air and / or water.

Brecciation: Fractured particles due to tectonically movements in the coal seam.

Cenospheres: Indication of high temperature on mining equipment or driers.

Fines: Amount of fines is an indication of coal rank, degree of oxidation and amount of brecciation.

Non-maceral microstructures identified in the coal samples used in this work are presented in Appendix D.

4.2.4 Coke petrography

Even though the carbonized coal samples in this work are categorized as chars, a standardized coke petrography procedure was employed in order to assess the microtexture of the char samples. Microtextures are the carbon forms that make up the porewalls. The microtextures in coke are primarily determined by rank and type of coal(s) used to produce the coke. The petrographic procedure is conducted under polarized light following the ASTM standard (ASTM D5061 1997). The microtextures were categorized as binder phase, filler phase or miscellaneous according to the nomenclature proposed by **Gray and Devanney (1986)** and later adopted by ASTM. There are several systems of nomenclature of coke texture in use and some of them are given in Appendix E.

Binder phase carbons originate from what is referred to as fusible (reactive) coal macerals and are determined based on the size and shape of the anisotropic domains.

Filler phase textural components originate from infusible (inert) macerals or minerals in coal. Inert coal macerals are usually isotropic in polarized light and retain their shape during carbonization and are thus easily recognizable. The macerals that are partially fused are harder to identify, but can still be recognized even though the boundaries towards the binder phase are more diffuse (see section 3.5.2). Minerals in the carbonized product can be both isotropic and anisotropic, but are distinctly different from the organic material and can hence be recognized. As the size of the filler phase components are determining the thickness of the porewalls, both organic- and inorganic filler phase constituents are categorized as fine or coarse with the limit being 50 μm (**Gray and Devanney 1986**).

4.3 Density Separation

In order to separate the coal samples into density fractions with different maceral constitution, the coal was first crushed to minimum amount of fines and sieved to a size fraction between 3.35 – 9.50 mm. A total amount of 10 – 20 kg of coal was washed in order to secure consistency with the ASTM standard procedure (ASTM D4371 1998). Aqueous solutions of $ZnCl_2$ with specific density 1.25, 1.35 and 1.50 g/cm^3 were prepared according to the solubility data in Lide (2002) and used as separating media. The densities of the solutions were controlled with a pycnometer. The coal fractions were separated using the traditional sink – float procedure illustrated in Figure 4.8.

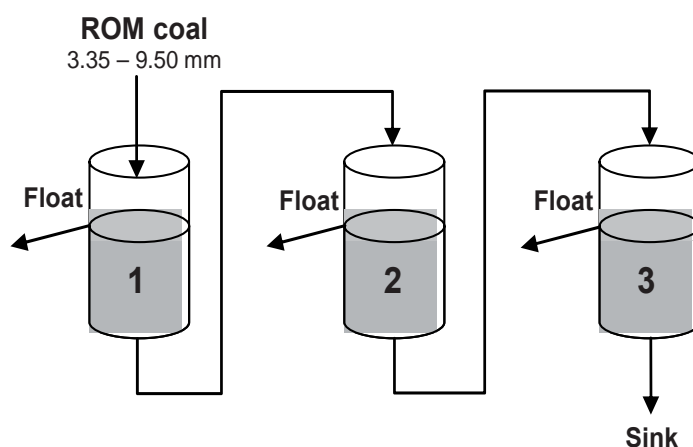


Figure 4.8: An illustration of how the sink - float washability test was performed. The density of the solution increased in the order $1 < 2 < 3$

Following the separation, all coal fractions were rinsed in fresh water until the concentration of Cl^- was under a specific limit. The chloride concentration was measured by a chloride sensitive electrode – WTW Cl 800 connected to a WTW pH/Ion 340i pocket meter.

The density separation of the coal samples could maximum give four density fractions of each ROM coal (Table 5.2).

More information about industrial coal processing techniques is given in section 3.5.3. The density distribution of some macerals and maceral groups as a function of rank is shown in Figure 3.14.

4.4 Carbonization Procedure

The carbonization procedure was originally designed to simulate the conditions the coal experiences when charged to an industrial electrical submerged arc furnace. A graphite crucible is heated to $1200^{\circ}C$ in an induction heated laboratory furnace (ASEA). The temperature is manually controlled by regulating the input power. When the temperature reaches $1200^{\circ}C$, 300 g of dried coal (+ 4.00 – 9.50 mm) is charged to the graphite crucible. As the coal is charged, the temperature drops to $600 - 700^{\circ}C$. Subsequent input of power will again increase the temperature to $1200^{\circ}C$ and the coal is kept at this

temperature for 20 minutes before cooling in an air sealed container. The yield of char is recorded based on the weight difference between the coal and the produced char.

4.5 Structure and Texture of Char

4.5.1 Image analysis

In order to measure the pore size distribution of large pores ($> 5 \mu\text{m}$) and the thickness of the pore walls, an image analysis procedure was used. Two polished samples of the char particles in a size range 3.35 – 4.75 mm were prepared. In order to increase the contrast between the carbon matrix and the resin, a fluorescent epoxy (Epodye) was employed in preparation of the samples. A metallurgical inverted reflected light microscope (Leica MeF3A) was used for the image analysis. The microscope was equipped with an analog 3-chip Charge Coupled Device (CCD) camera for acquisition of images. The procedure was controlled from a computer which was connected to the camera and a moving sample stage. The computer software was a modified version of the analysis program NIH Image version 1.62.

The samples were examined under ultraviolet light. The analysis program automatically captured 384 adjacent images of the samples at 80x magnification and stitched them together. This procedure also enables large pores, covering several frames, to be evaluated. More information about the image analysis technique can be found in **Øye et al. (2000)**.

4.5.2 X-ray diffraction

In order to obtain information about the structural parameters of the produced chars, the carbonized coal samples were subjected to X-ray diffraction. Char particles in the size range 3.35 – 4.75 mm were ground in a ball mill until all the material passed a 106 μm test sieve (ASTM No 140). Finely ground ultra pure silicon (purity $> 99.99999\%$) was added to the powder and mixed using a pestle and mortar. Silicon was added as a reference so the diffraction profiles could be precisely adjusted based on the known position of the silicon peak. The powder mix, containing 10 wt% of silicon, was transferred to two sample holders for parallel measurements. The diameter of the sample holder was 25 mm while the sample thickness was approximately 1.5 mm.

X-ray diffraction profiles were collected for all the samples using a Siemens D5005 X-ray diffractometer. Nickel filtered $\text{CuK}\alpha$ X-ray was used. The accelerating voltage was 40 kV with a current of 50 mA. Step scanning was performed from 15° to 35° with a step size of 0.02° and 5 seconds acquisition time. The radius of the goniometer was set to 205 mm and the symmetrical divergence slit to 2° .

All of the resulting diffraction profiles showed the steep silicon peak (111) and the broad carbon peak (002). According to **Iwashita (2004)**, a shift to the lower angle side as well as a broadening of the diffraction profile is observed for carbon materials. This is caused by the low absorption coefficient and necessitates the use of a high purity silicon standard in the samples. Instrument and sample dependant factors like Lorentz

(L), polarization (P), absorption (A) and atom scattering (f_c) are functions of 2θ and will cause a shift in the observed profiles to the lower angle side.

The diffraction profiles were corrected by dividing each reflection by the intensity correction factor (FCT).

$$FCT = L \cdot P \cdot A \cdot f_c^2 \quad (4.4)$$

$$L = \frac{1}{\sin^2 \theta \cos \theta} \quad (4.5)$$

$$P = \frac{1 + \cos^2 2\theta}{2} \quad (4.6)$$

$$A = \left(1 - \frac{\sin(2\theta)}{2\mu' b_r}\right) \cdot \left(1 - \exp\left(\frac{-2\mu' t_c}{\sin \theta}\right)\right) + \frac{2t_c \cos \theta}{b_r} \cdot \exp\left(\frac{-2\mu' t_c}{\sin \theta}\right) \quad (4.7)$$

$$f_c = 2.261 \cdot \exp(-22.691 \cdot s^2) + 1.562 \cdot \exp(-0.066 \cdot s^2) + 1.051 \cdot \exp(-9.756 \cdot s^2) + 0.839 \cdot \exp(-55.595 \cdot s^2) + 0.287 \quad (4.8)$$

In these equations μ' is the apparent absorption coefficient which is equal to 10 cm^{-1} when 10 wt% of silicon is present in the sample mixture. The sample thickness, t_c , is 0.15 cm, b_r is the breadth of the X-ray beam on the sample expressed by equation 4.9 and the expression for s is given in equation 4.10.

$$b_r = R_g \cdot \sin \beta \quad (4.9)$$

where R_g and β are the radius of the goniometer (205 mm) and the width of the divergence slit (2°), respectively.

$$s = \frac{\sin \theta}{\lambda} \quad (4.10)$$

The wavelength of the X-ray, λ , is 1.541838 \AA for $\text{K}\alpha_1$.

The intensity correction factor is dependant upon instrument settings and sample dimensions and is hence just a function of 2θ . The effect of intensity correction for a sample of carbonized Blue Gem is demonstrated in Figure 4.9. Shifting of the carbon peak (002) slightly to the right is clearly illustrated.

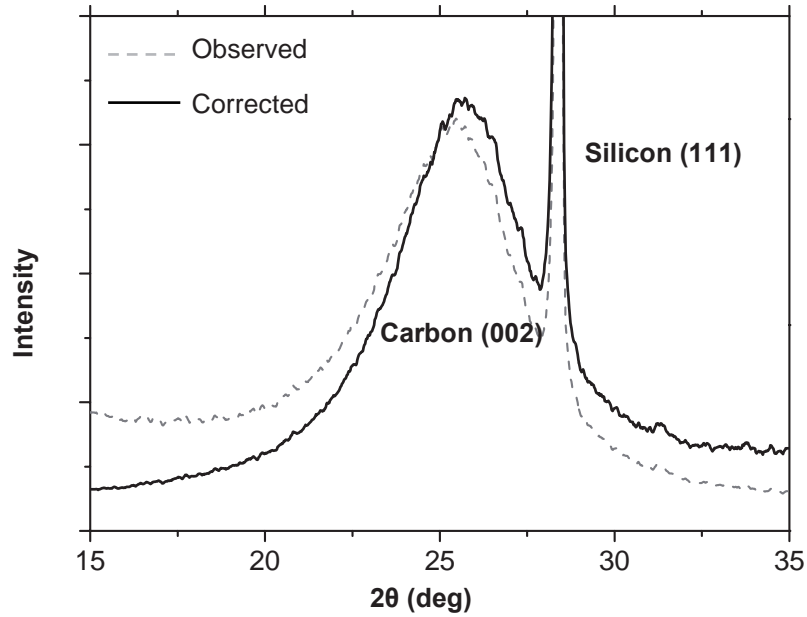


Figure 4.9: X-ray diffraction profile for a Blue Gem char sample before and after FCT correction. The profiles are smoothed using the Savitzky-Golay method

The corrected diffraction profiles were adjusted for the angle displacement in the EVA program. The angle displacement was found from the difference in diffraction angle between the observed silicon peak (111) and the theoretical peak of the silicon standard (28.467°). A linear background was subtracted and a Pseudo-Voigt function was then fitted to each of the shifted and corrected diffraction profiles by using the Profile software. The goodness of the fit was automatically examined by the program according to equation 4.11.

$$R = \frac{\sum_{2\theta} |I(2\theta) - P_r(2\theta)|}{\sum_{2\theta} I(2\theta)} \cdot 100\% \quad (4.11)$$

According to **Iwashita (2004)**, the R factor should be less than 10 %, and for all the samples tested in this work the values were below 5 %.

The curve fitting procedure automatically calculated two parameters which enabled further evaluation of the crystallite size (see Figure 3.12.A). The corrected 2θ position for the carbon peak (002) was used to calculate the d_{002} interlayer spacing of the carbonized coal samples from the Bragg equation:

$$2 \cdot d_{002} \cdot \sin \theta = \lambda \quad (4.12)$$

The average crystallite size, L_c , was calculated according to the Scherrer equation:

$$L_c = \frac{K \cdot \lambda}{\beta \cdot \cos \theta} \quad (4.13)$$

where the shape factor, K , was taken as 0.9 according to **Rodriguez-Reinoso and Marsh (2000)** and β is the Full Width Half Maximum ($FWHM$) corrected for broadening according to equation 4.14

$$\beta = \sqrt{B^2 - b^2} \quad (4.14)$$

where B is the $FWHM$ for the carbon peak (002) and b is the $FWHM$ of the silicon reflection (111).

4.5.3 BET surface area and total porosity

The physical properties were measured using standard procedures. Surface area of the char samples was evaluated using a FlowSorb II 2300 instrument according to the BET method (DIN 66131). A mixture of 70 % helium and 30 % nitrogen by volume was used as adsorbing medium. For surface area measurements there was a limitation in the particle dimensions so the char samples were reduced in size to less than 2 mm.

Absolute densities were measured with a gas displacement instrument (AccuPyc 1330) and total porosities were assessed by using AccuPyc 1330 and GeoPyc 1360 pycnometers. The particle size in these analyses was 3.35 – 4.75 mm.

4.5.4 Mercury porosimetry

As the resolution of the camera used in the image analysis method is not sufficient to analyze pores less than approximately 2 μm , mercury intrusion porosimetry (C. Erba Porosimeter Mod. 2000) was applied to the char samples to determine the pore size distribution for pores less than 1 μm . A representative selection of the char samples was ground and sieved to a size fraction of 250 – 600 μm for analysis.

The principle of the mercury intrusion porosimetry is that the sample is suspended in mercury and by applying pressure the mercury will penetrate the pores. All the pores are assumed to be symmetrical, and the radius is a function of the pressure required to force mercury into the pores. This relationship is given by the Washburn equation (**Marsh 1989**):

$$r = -\frac{2\sigma \cdot \cos\phi}{P} \quad (4.15)$$

where σ is the surface tension of mercury, ϕ is the contact angle, r is the radius of the pores and P is the applied pressure. In this work 140° and 480 dyn/cm have been used as values for respectively the wetting angle and surface tension of mercury (**Stenstad 2006**).

4.6 SINTEF SiO-Reactivity Test

The most acknowledged reactivity test for reduction materials in the production of ferrosilicon, silicon metal and to some degree silicon carbide was developed by Tuset and Raaness in the 1970's (**Tuset and Raaness 1976**). This test is called the SINTEF SiO-reactivity test and has been the only commercially available test to investigate the

ability of the reduction materials to react with SiO gas since the test was established. The principle of the test has remained the same over the years, but lately SINTEF has automated the procedure securing consistency and repeatability. In addition, the degree of conversion is analyzed chemically and not by weight increase of the reacted samples. The description and figures of the test are primarily based on the original publication by Tuset and Raaness and an article describing the modifications made by Lindstad et al. (2007).

4.6.1 Apparatus

An illustration of the reactor used in the SINTEF SiO-reactivity test is given in Figure 4.10. It is placed in a vacuum graphite tube resistance furnace and comprises three main sections:

SiO-generator: The generator contains pellets made up of ground quartz (SiO_2) and α -SiC powder. When the pellets are heated to the correct temperature they react to produce 4.5 % CO and 13.5 % SiO according to *reaction 1.10*.
In addition to the gas produced by the pellets, argon is used as a carrier gas at a constant flow rate (320 ml/min).



Reaction chamber: The sample to be tested is placed in the reaction chamber (20 cm^3). The gas mixture from the SiO-generator is passed through the reaction chamber and the carbon sample reacts according to the reaction:



Condensing chamber After the gases have passed through the reaction chamber, the product gases enter the condenser where they are cooled. The condensing chamber is filled with alumina tubes to provide surface area for any unreacted SiO gas to condense (see reaction 1.6), and it also provides additional cooling to the product gases.



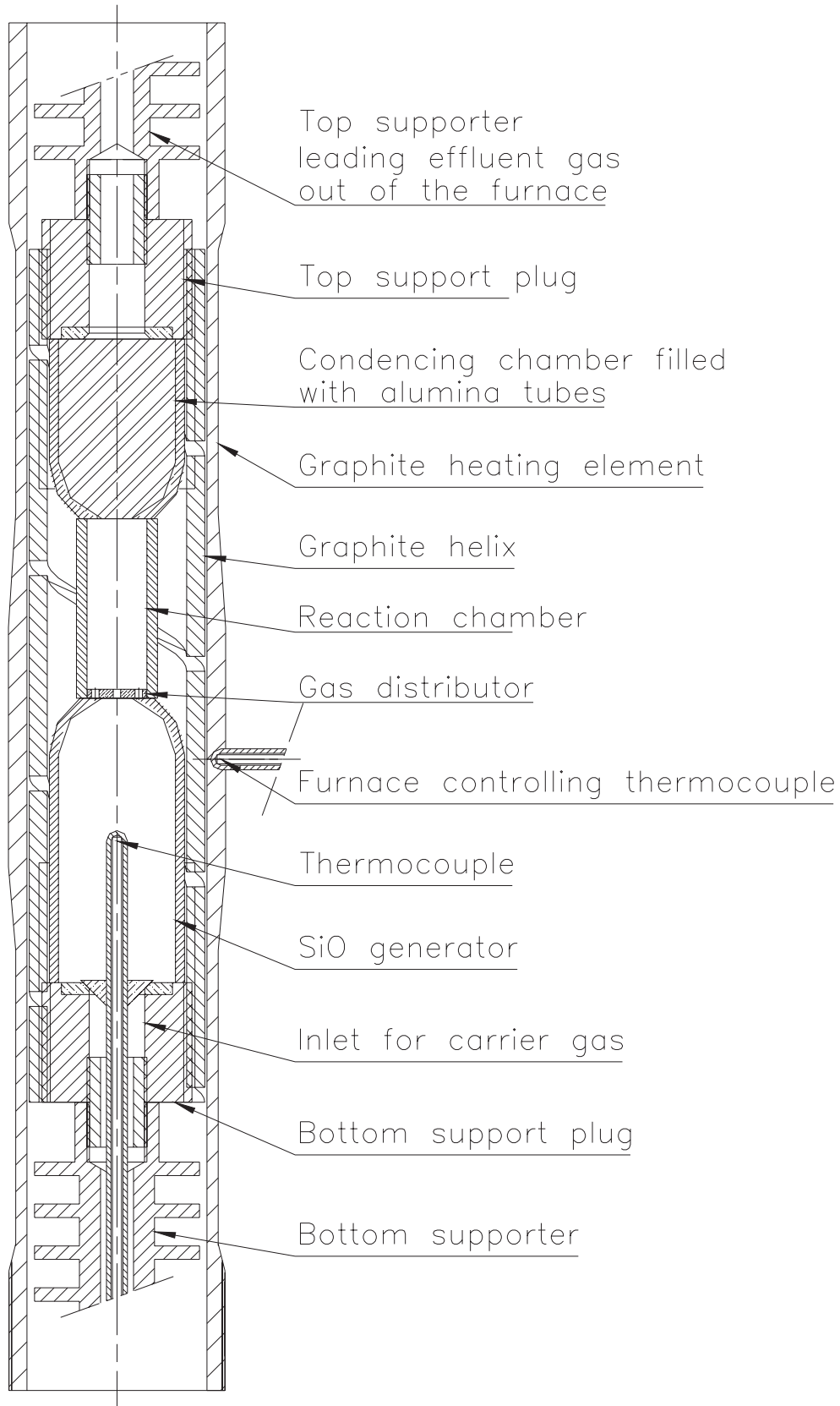


Figure 4.10: The SINTEF SiO reactor (Illustration by Jensen 2006)

All these parts are made of re-crystallized alumina, with graphite support plugs on each end connecting the components to the helix. As any leaks in the apparatus would be detrimental to the test results, alumina components are joined together with Al-Fix glue while the graphite support plugs are sealed to the alumina by gaskets made up of graphite paper. The reactor is compressed and aligned by the graphite helix. The temperature is measured at the top of the SiO-generator with a type B thermocouple (Pt/Pt Rh). The temperature in the sample is however not measured directly during the test, but profiles of the apparatus are frequently checked in order to ensure that there is a slight increase in temperature from the SiO-generator to the reaction chamber. The thermocouple close to the graphite heating element is used to control the furnace.

4.6.2 Test procedure

The carbonized sample (see section 4.4) is crushed and sieved to a particle size of 4.00 – 6.30 mm. 20 cm³ of the sample is then placed in the reactor chamber. The reactor is heated to 1500°C according to a defined procedure and controlled by a Eurotherm temperature controller. At this temperature the maximum amount of ash is reduced without significant formation of SiO-gas in the generator. When the CO-level drops below 5 %, most of the oxides are reduced and the temperature is quickly increased to 1650°C where the sample reacts with the gas mixture from the SiO-generator. At the reaction temperature (1650°C) and set flow rate of carrier gas, the equilibrium corresponds to 13.5 % SiO, 4.5 % CO and 80 % of the carrier gas (Ar). The concentration of CO is measured with an infrared analyzer at the outlet of the reactor and the test is stopped when the concentration drops below 5.2 % which is defined as the end point of the test.

4.6.3 Reactivity measure

As pointed out in section 4.6.2 the concentration of CO in the effluent gas stream is measured continuously during the test. The direct output from the SINTEF SiO-reactivity test is a curve showing the CO concentration as a function of time. Historically the reactivity has been calculated directly from this curve where the SiO reactivity number was given as the amount of SiO gas which had passed through the reaction chamber unreacted before the CO content in the exit gas drops below 10 %. This reactivity number is calculated from the equation:

$$R_{10} = \sum_{18 \rightarrow 10} \frac{Q_{Ar}(18 - \%CO)}{82 - 0.82 \cdot \%CO} \cdot \Delta t \quad (4.16)$$

A plot of a typical output from the test is provided in Figure 4.11.

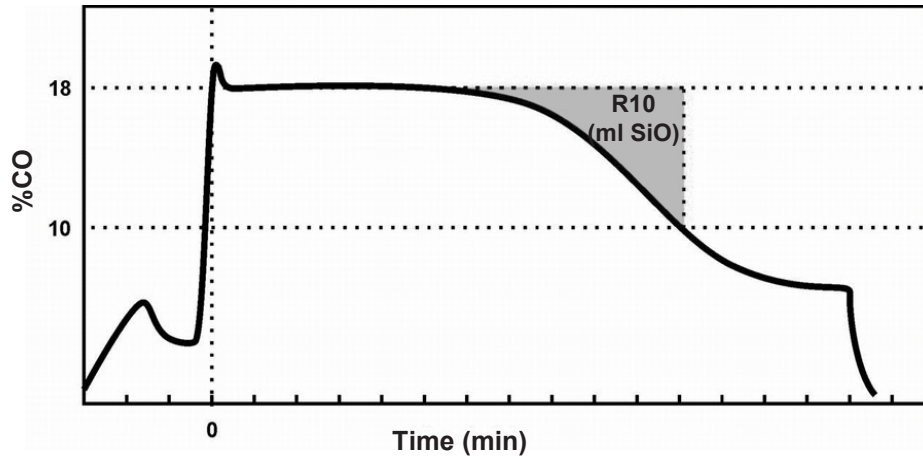


Figure 4.11: A plot of an idealized CO profile as a function of time. The shaded area is the reactivity measure R10 given as amount SiO-gas that escapes the reactor in ml. Figure from Gaal (2007).

As some of the CO produced in the reaction chamber (*reaction 1.5*) will react with the silicon that is produced in the condenser (*reaction 1.6*) according to the reaction:



The measured CO concentration in the gas stream from the condenser will be lower than what is actually produced by *reaction 1.5*. By assuming that the degree of condensation increases linearly with time, a corrected CO concentration can be calculated:

$$\%CO_{corrected} = \left[1 + k_1 \left(\frac{t - t_{18\%}}{t_{end} - t_{18\%}} \right) \right] \cdot \%CO_{analyzed} \quad (4.17)$$

where $\%CO_{corrected}$ and $\%CO_{analyzed}$ are the corrected and analyzed concentrations of CO, respectively. The correction factor for condensation, k_1 , was determined experimentally to be 0.21. $t_{18\%}$ and t_{end} are the times during the test where respectively the CO level drops below 18 % and 5.2 %.

The reactivity measure used in this work is based on the corrected CO curves and calculated in the same manner as equation 4.16.

$$R10_{corr} = \sum_{18 \rightarrow 10} \frac{Q_{Ar} (18 - \%CO_{corr})}{82 - 0.82 \cdot \%CO_{corr}} \cdot \Delta t \quad (4.18)$$

4.7 Sample Material

In order to investigate how the microstructure in coals of different origin and rank influence the reactivity towards SiO, three ROM (Run Of Mine) coal samples have been acquired for studies in this work. The samples cover a wide range in petrographic properties - both maceral composition and rank. Selection of these samples was based

on the importance of these particular coal bearing regions for the metallurgical industry in Norway. An amount of 50 – 100 kg was received of each sample which were air dried and stored in air sealed plastic containers. In order to prevent oxidation and to have a reference sample of the ROM coals, approximately 5 kg of each coal were stored in air sealed buckets at – 25°C.

4.7.1 Blue Gem

There are vast resources of coal in North America and according to **WCI (2007)**, USA is the second largest producer of hard coal in the world. The major coal basins in the USA are illustrated in Figure 4.12.

Availability of the Carboniferous coals from Illinois- and Appalachian Basin was one of the reasons for establishing the massive steel production in the Eastern USA. The coal measures of the Illinois Basin are of Pennsylvanian (Upper Carboniferous) age and according to the American terminology, of bituminous rank (high- and medium volatile). The Illinois Basin is covering large parts of Illinois, the western part of Indiana and the north western part of Kentucky. **Hatch and Affolter (2002)** have given an extensive assessment of the coal measures in the Illinois basin.

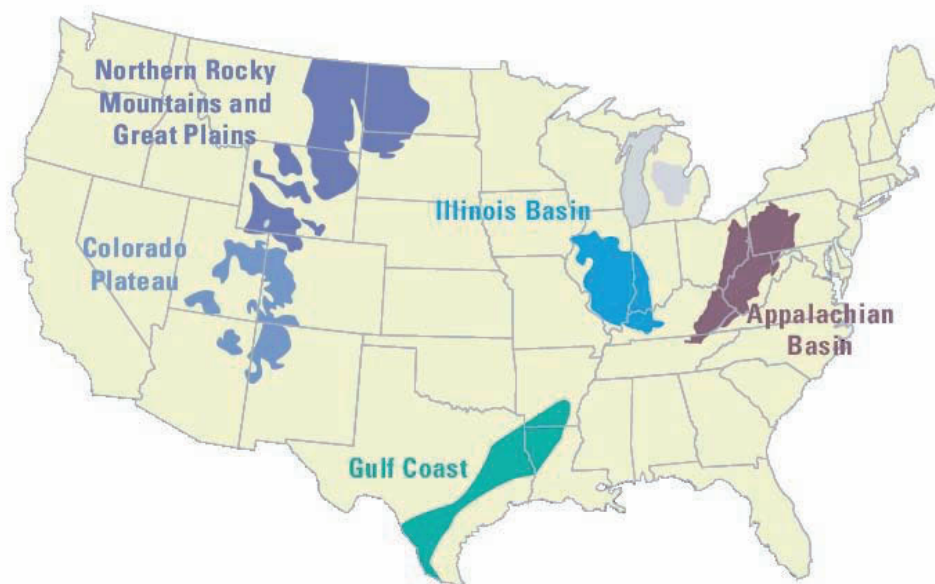


Figure 4.12: Coal basins in the USA. Figure modified after Ruppert et al. (2001).

The coal resources from the Northern Rocky Mountains and Great Plains are of Tertiary age. While the highly productive Powder River Basin in Wyoming and Montana is of sub bituminous rank, the Fort Union region in North- and South Dakota is consisting of lignite. More information on the low rank coals from this region can be found in **Flores et al. (1999)**.

According **Kirschbaum et al. (2000)**, about 85 % of the Cretaceous coal in the Colorado Plateau is being used for generation of electrical power. The coal measure is

covering parts of Utah, Colorado, Arizona and New Mexico and is sub-bituminous to medium volatile bituminous in rank. An extensive report about the coal in the Colorado Plateau is given by **Kirschbaum et al (2000)**.

The Tertiary coal measure in the Gulf region is covering a large geographical area and is consisting of lignite.

The Appalachian Basin

The Appalachian Basin is one of the most important coal producing regions in the United States. The coal basin covers a large geographical area from Pennsylvania in the North to Alabama in the South, and is divided into three regions based on regional geological structure and stratigraphy. Figure 4.13 illustrates the geographical extent of the Appalachian basin as well as the division into sub-regions.

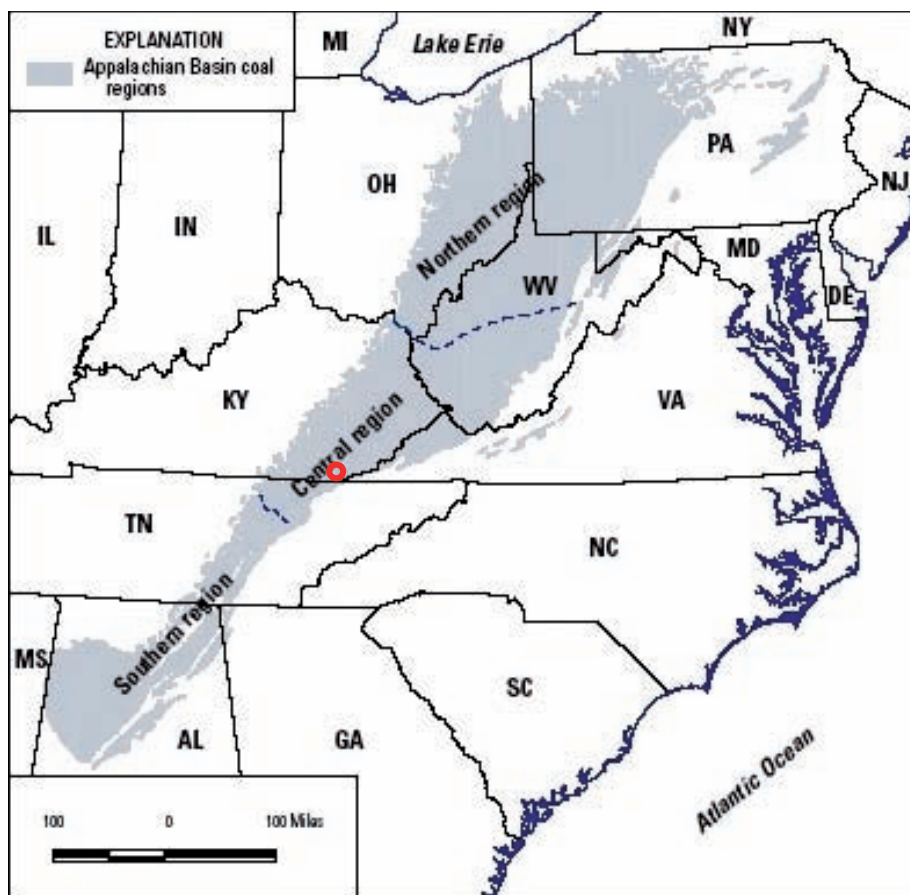


Figure 4.13: Map showing the northern-, central- and southern Appalachian coal regions. The red circle indicates the position of the Blue Gem coal bed.

Figure modified after Ruppert et al. (2001).

The Appalachian Basin was formed along the eastern edge of the North American continental plate after a collision with the European and African (Gondwana) continental plates. This collision was also responsible for the formation of the Variscan mountains and subsequently the coal belt in central Europe. The collision of the continental plates led to an uplift of the eastern shore of North America causing a

massive transport of sediments westwards into the subsiding Appalachian basin, and extensive coal forming swamps developed in this area.

The Appalachian basin consist of bituminous coals of Carboniferous age.

According to the annual coal report for 2005 presented by the Energy Information Administration (EIA) (EIA 2005), there were 1230 mines in operation in the Appalachian Basin, and the total tonnage in the region is only exceeded by the output from the Powder River Basin.

Blue Gem Coal Bed

The Blue Gem coal bed is a part of the central Appalachian coal region located in the south – eastern part of Kentucky (Knox, Bell and Whitley counties) and is an important low ash, low sulfur coal resource. Due to the high quality of the coal, Blue Gem coal is heavily mined even though the seam thickness rarely exceeds 70 centimeters. Based on the low thickness of the seams, untraditional mining operations must be used. According to Rimmer et al. (2000), the coal is high volatile bituminous in rank from middle Pennsylvanian era with vitrinite reflectance ranging between 0.72 – 0.95 (% R_{max} , in oil). Stratigraphically the Appalachian basin can be quite difficult to interpret as various terminologies are used in the different states the basin is covering. The Blue Gem coal measures can be found in the Pond Creek coal zone which is part of the Pottsville group (Breathitt formation in Kentucky). The stratigraphy of the northern- and central Appalachian Basin is illustrated in Figure 4.14.

SYSTEM	SERIES	GROUP	ASSESSED COAL BED or ZONE
PENNSYLVANIAN	UPPER	Monongahela Group	Pittsburgh coal bed
		Conemaugh Group	
	MIDDLE	Allegheny Group	Upper Freeport coal bed
			Lower Kittanning coal bed
	LOWER	Pottsville Group	Fire Clay coal zone
			Pond Creek coal zone
			Pocahontas No. 3 coal bed

Figure 4.14: Stratigraphy of the central Appalachian coal region. The Blue Gem coal bed is part of the Pond Creek coal zone in the Pottsville Group (Locally this is referred to as the Breathitt formation in Kentucky). After Ruppert et al. (2001).

According to Hower et al. (1991), the low ash content together with the upwards decrease in trace elements is an indication that the Blue Gem peat swamp received nutrients solely from rain water (ombrotrophic) in at least part of its geological history.

In order to elucidate on these findings **Rimmer et al. (2000)** investigated the petrography and palynology of the Blue Gem coal bed in Knox County, and revealed that the coal bed is divided into two distinct zones. The lower and middle part of the coal bed is enriched in well preserved vitrinite with arborescent lycopods and fusinite rich layers. The upper part of the seam contains greater amounts of degraded macerals. The conclusion from these investigations is that the peat swamp initially was diverse and well nourished (higher ash content at the base of the seam). At this stage the swamp was planar. The low ash and sulfur content in the middle of the seam indicates that the swamp may have domed slightly. In the final stages of peat accumulation, the swamp was domed and characterized by a more diverse flora and greater levels of degradation of the organic material.

4.7.2 Peak Downs

Australia is the leading coal exporter of hard coals in the world. The geographical locations of the coal basins in Australia are shown in Figure 4.15.

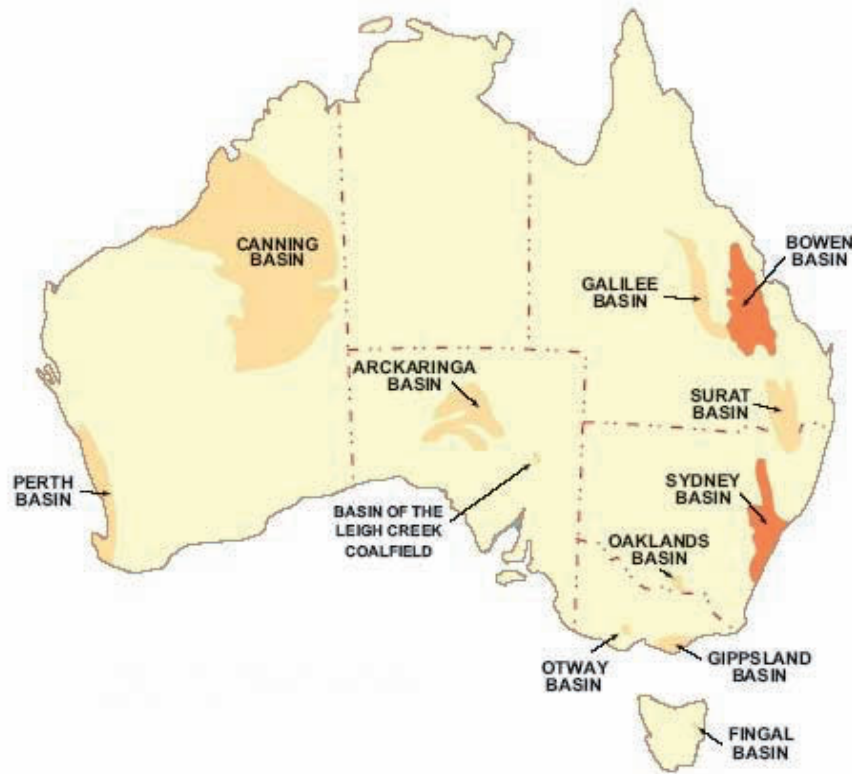


Figure 4.15: Coal basins in Australia (ITAM 2003)

Although coal is mined throughout Australia, the quality and properties of the coals vary widely.

Coals from Sydney-Gunnedah Basin in New South Wales and Bowen Basin in Queensland are premium coking coals from the late Permian period and are to a large degree exported (mostly to Japan). According to **ITAM (2003)**, the Permian coals on

the eastern margins of Australia are formed from the remains of the extinct seed-fern *Glossopteris* (see figure 3.4).

Low rank coals from the Triassic- and Tertiary periods are important locally in some states and are mostly used for electricity generation.

According to **Gurba and van Schagen (2003)**, there are extensive resources of sub-bituminous coal in the Surat Basin. These coal measures are of Jurassic period, but are not mined to any great extent.

Bowen Basin

According to **Kahraman and Esterle (2001)**, the Bowen Basin is one of the most important coal basins in the world and comprises of Permian coals. The total resources can amount to 28.5 billion metric tons. Crustal plate collisions on the eastern margins of the Australian continent led to the formation of both the Bowen- as well as the Sydney-Gunnedah basins. The major coal bearing sedimentary system of the Bowen basin is called the Blackwater group. The group is of late Permian age and is divided into three coal bearing formations. Stratigraphy of the Blackwater group is illustrated in Figure 4.16.

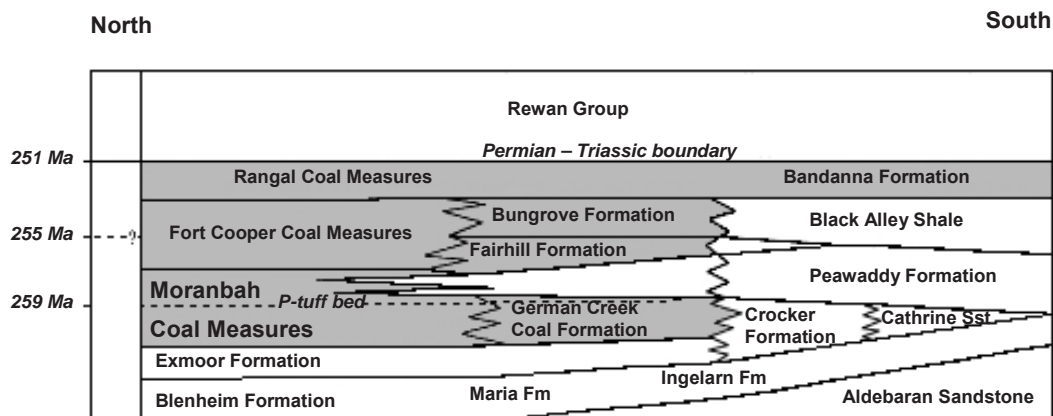


Figure 4.16: Stratigraphy of the coal bearing formation in the Bowen basin. Peak Downs is part of the Moranbah coal measure. Figure modified after **Michaelsen (2002)**.

The Rangel coal measure is the youngest of these formations, and reflects the product of a long lived peatland system which came to a sudden termination at the Permian – Triassic boundary. Climate, fauna and geological setting in the northern Bowen basin at this stage are some of the factors discussed by **Michaelsen (2002)**.

The Moranbah coal formation is the oldest and most extensive in the Blackwater group. Extensive mining operations are present at the western part of this formation due to the thick, relatively clean and continuous seams of medium to low volatile bituminous coal (**Michaelsen and Henderson 2000**). To the south the Moranbah formation coincides with the German Creek coal formation and the McMillan formation. According to **Michaelsen and Henderson (2000)** the strong development of growth rings in petrified wood indicates that the deposition in the Moranbah formation occurred in cold climate. The P-tuff bed is a large (1 - 2 meters thick) deposit of pyroclastic units that is present

in most of the formation. The bed is the product of a large scale volcanic eruptive period and can be seen in open cut coal mines (among these Peak Downs).

Peak Downs Mine

The Peak Downs coal mine is located on the western margin of the central Bowen basin (see map in Figure 4.17) and is operated by BHP Billiton. The Peak Downs coal is part of the Moranbah coal formation in the Blackwater group and was deposited under fresh water fluvial environment.

Peak Downs is a large, open cut mining operation of medium volatile bituminous coal seams which average thickness is 4 – 5 meters (BMA Coal 2007).

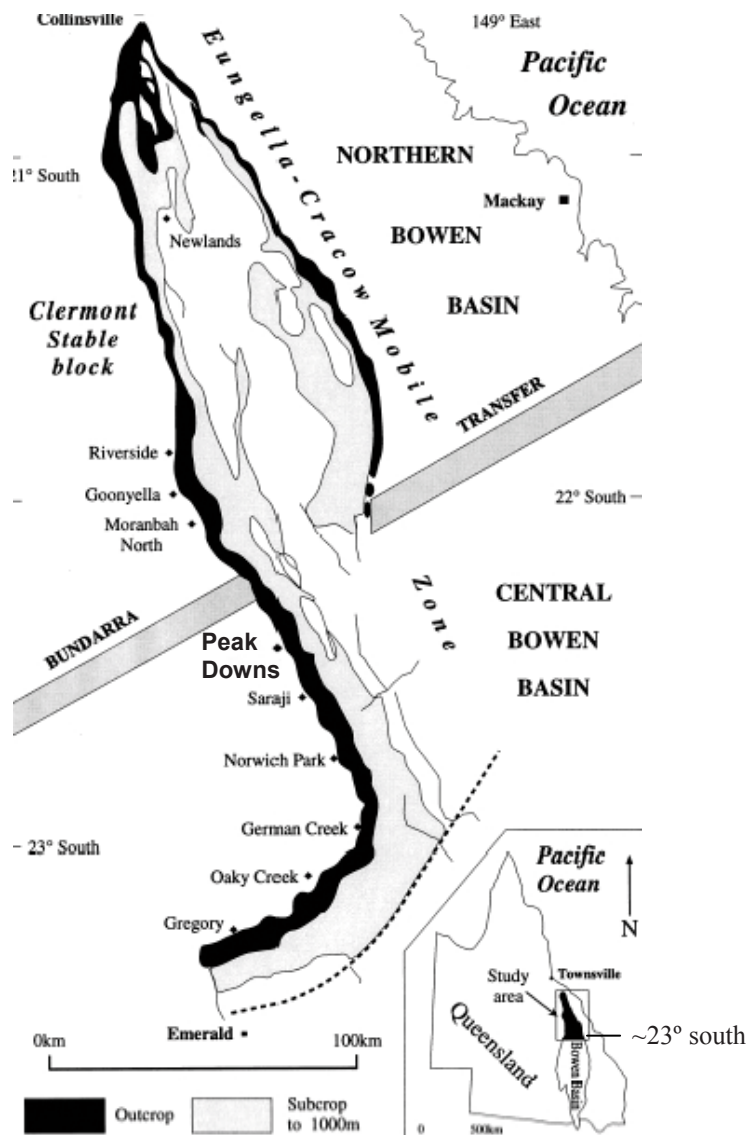


Figure 4.17: Map showing the northern- and central Bowen Basin and the position of the Peak Downs coal mine. Figure modified after Michaelsen and Henderson (2000).

For the purpose of this work, an amount of about 100 kg of Peak Downs coal was received from the SSAB coking plant in Luleå. Size of the coal ranged from fine coal

dust to lumps of 40 mm. The coal was divided into fractions above and below 3.35 mm, dried and stored in air sealed plastic containers.

4.7.3 Staszic

Poland is according to The World Coal Institute (**WCI 2007**) ranked as the largest producer of coal in Europe (number eight in the world). Coal has been one of the largest industries in Poland and accounted for 92 % of the electricity generation in the country in 2005. Although the resources of coal are large in Poland, the production has declined during the last 25 years. From 1979 when the coal production had a peak with a total output of more than 200 million tons (**USEPA 1995**), a drop by more than 100 million tons was experienced as the estimated numbers for 2006 were 95 Mt (**WCI 2006**).

The major reason for the decline in the coal production in Poland is due to less accessible coal seams which in turn increase the costs of mining. In addition, the Polish government has during the last decade reformed the coal producing sector which also included closing down inefficient mines.

In Poland resources of bituminous coal occur exclusively in the Upper Carboniferous strata and can be found in three coal basins. Geographical location of the bituminous coal resources as well as two lignite fields in Poland is illustrated in Figure 4.18.



Figure 4.18: A map showing the coal deposits in Poland. The shaded areas indicate the resources of high rank coals. Lignite deposits located in Bełchatów and Turów are marked in black.
Figure modified after Kotarba and Lewan (2004).

The Lower Silesian Coal Basin (LSCB) is located in an intermountain depression in the Sudetes. The Upper Carboniferous coal measures of the LSCB are grouped in two lithostratigraphical units which are mainly of Pennsylvanian age. There is a wide range in coal rank from the LSCB due to plentiful magmatic intrusions in the strata. The LSCB is the smallest coal basin in Poland and although mining in this area is documented back to the mid 1300's, there is currently no activity (**Nowak 2004**).

The Lublin Coal Basin (LCB) is associated with a platform depression located in the south-east of Poland. LCB covers a large geographical area and consists of four lithostratigraphical productive units from Upper Mississippian and Pennsylvanian age. Although there are 7.6 billion tons of documented coal reserves in the LCB (USEPA 1995), mining is not widespread in the region (Only one active mine - Bogdanka).

Upper Silesian Coal Basin (USCB)

The Upper Silesian Coal Basin (USCB) is the largest coal basin in Poland based on its coal resources (55.5 billion tons according to **Kotarba and Lewan 2004**). The USCB is a foredeep basin located in the south of Poland extending into the Ostrava-Karvina region in the Czech Republic. The coal bearing formations of the USCB is divided into four lithostratigraphical units which are shown schematically in Figure 4.19.

Chronostratigraphical division		Lithogenetic complexes	Lithostratigraphical Member		Boundary Levels	Thickness in m /maximum/	
CARBONIFEROUS SILESIA	WESTPHALIAN	Coal-bearing arthamolasse	Craów sandstone series	Libiaz Beds	Horizon 119	560	
				Laziska Beds	Horizon 209 Horizon of facial change	1080	
			Siltstone series	Orzesze Beds	XX Tuffite horizon	2000	
				Zeleeze Beds	Horizon 401		
			Upper Silesian sandstone series	Ruda Beds	Fresh water fauna horizon	810	
	Anticlinial Beds	Horizon 501 Horizon 510		290			
	NAMURIAN	Molasse association	Coal-bearing paramolasse	Paralic series = Marginal Beds	Poleba Beds	Goebler horizon	1100
					Jaklovec Beds	Barbara horizon	380
				Lower Marginal Beds	Hrusov Beds	Enna horizon	1300
					Pettkovice Beds	XX Honestone horizon	760
Zalas Beds				Stur horizon	1500		
DINATIAN	Flysch Association	Flysch Association	Malinowice Beds				
			Zalas Beds				
UPPER VISEAN	Go 1 Go 2						
PENDLEIAN	ARNBERGIAN	Molasse association	Coal-bearing arthamolasse				
NAMURIAN	WESTPHALIAN	Coal-bearing arthamolasse	Siltstone series				
WESTPHALIAN	NAMURIAN	Coal-bearing arthamolasse	Craów sandstone series				
WESTPHALIAN	NAMURIAN	Coal-bearing arthamolasse	Siltstone series				
WESTPHALIAN	NAMURIAN	Coal-bearing arthamolasse	Craów sandstone series				
WESTPHALIAN	NAMURIAN	Coal-bearing arthamolasse	Siltstone series				
WESTPHALIAN	NAMURIAN	Coal-bearing arthamolasse	Craów sandstone series				

Figure 4.19: Stratigraphy of the productive series in the Upper Silesian Coal Basin (USCB).
Figure modified after Roman (1990).

The lower part of the productive series (*The Paralic Series*) is comprised of clastic and phytogenic sediments deposited in both marine and limnic environments (Roman 1990). The Paralic series contain 3 – 4 % coal and the seams are relatively thin. An extensive review of the Namurian deposits in the USCB is given by Havlena (1982).

The Upper Silesian Sandstone Series mainly consists of sandstones and conglomerates, but also thick coal seams. The series can further be divided into *the Anticlinial Beds* and *the Ruda Beds*. Coals seams in the Anticlinial Beds can attain thicknesses up to 24 meters. There is a lack of marine horizons in the series and several fresh water environments have been noticed in the Ruda Beds.

The Siltstone Series mainly consists of fine grained clastic rocks. There are also numerous coal seams, but they are relatively thin. Luxurious flora is characterizing the series and horizons with fresh water fauna have been observed.

The upper part of the productive USCB, the Cracow Sandstone Series, is consisting of continental sediments rich in coarse grained material and is deposited in limnic-fluvial environments.

The Staszic Mine

The Staszic mine is located in the southeastern part of Katowice and is operated by the Katowice Holding Company (KWK). The total mining area is 21 square kilometers and production started in 1964 even though coal was discovered already in 1955. A map of the Staszic mine is presented in Figure 4.20.

The Staszic concession is crossed by several faults. The greatest displacement occurs along the Klodnicki fault and strata south of this fault are downthrown as much as 100 meters. Most of the mining occurs north of this fault. According to information given on the internet of KHC (www.kwkstaszic.pl), the mining is longwall mining operated underground. The mine has two working levels located 500 and 720 meters under the surface and the coal seams can reach a thickness of 3.3 meters. Rank of the coal ranges from sub-bituminous to high volatile A bituminous.

For the purpose of this work, about 100 kg of coal in the form of lumps (30 – 70 mm) was received from the Staszic mine. This coal was mined from the Anticlinal beds, but no information regarding the seam number (seam 501 or 510) was supplied.



Figure 4.20: A map of the mining concessions at the Polish side of the USCAB. The Staszic concession is shaded in black. Figure modified after USEPA (1995).

5. EXPERIMENTAL RESULTS

Even though **Chen et al. (2000)** claim that an electrochemical method for reduction of SiO_2 to silicon metal will be both more energy efficient and environmentally friendly, the carbothermic production is still the only commercial process of producing silicon alloys. In this process, carbonaceous materials are used in order to reduce the metal bearing ore, typically quartz in the production of silicon metal and quartzite in the ferrosilicon process. Proper carbonaceous materials must be selected in order to obtain desired production yield and metal quality.

Amount and nature of the mineral inclusions in the carbonaceous materials play an important role in determining the purity of the produced metal. Purity of the silicon metal is of utter importance when it is to be utilized in the semi - conductor industry or for producing photovoltaic cells.

Regarding the operational process, the most important parameters of the reductants are:

- A high reactivity towards SiO gas.
- A high degree of conversion.

In the present work, the main focus was to investigate how the properties of fossil carbonaceous reductants influence the reactivity in the silicon process. The progress of the work can be divided into three main parts which are illustrated in Figure 5.1.



Figure 5.1: Progress of this work can be divided into three distinct parts: 1) Evaluating material properties of the selected coals. 2) Carbonizing coals and determining material properties of the carbonized material. 3) Testing the carbonized materials in the SINTEF SiO reactivity apparatus and evaluating the results.

The experimental results which are presented in this section follow the progress illustrated in Figure 5.1, and contain the following sections:

- Determination of coal properties.
- Coal processing and carbonization.
- Determination of properties of the carbonized coal samples.
- Reactivity studies.
- Correlation of material properties and reactivity results.

Throughout this chapter a number of tables and graphs will be presented, and in some of them the following abbreviations for sample names are used: Blue Gem (BG), Peak Downs (PD) and Staszic (St).

5.1 Chemical- and Plastic Properties of the Run of Mine (ROM) Coals

Results from proximate- and ultimate analyses as well as plastic properties and ash composition of the ROM coals are presented in Table 5.1.

Table 5.1: Proximate- and ultimate analyses, plastic properties and ash composition for the Run Of Mine (ROM) coals.

		Blue Gem		Peak Downs		Staszic	
		Value	Uncertainty	Value	Uncertainty	Value	Uncertainty
Proximate Analysis [wt%]							
Moisture	W ^a	2.4	0.1	0.9	0.1	2.5	0.1
Ash	A ^a	1.5	0.2	11.6	0.2	5.9	0.2
Volatile matter	V ^a	36.14	0.11	19.8	0.33	31.76	0.33
	V ^{daf}	37.61	0.17	22.63	0.39	34.67	0.39
Fixed C	Fix C ^a	59.96	0.25	67.7	0.4	59.84	0.4
Ultimate Analysis [wt%]							
Carbon	C _t ^a	80.5	0.3	77.1	0.3	75.8	0.3
Sulfur	S _t ^a	0.73	0.15	0.58	0.15	0.47	0.15
Hydrogen	H _t ^a	5.29	0.1	4.34	0.1	4.74	0.1
Nitrogen	N ^a	1.98	0.03	1.68	0.03	1.27	0.03
Oxygen	O ^a	10	0.42	4.7	0.42	11.82	0.42
Phosphorous	P ^a	0.003	0.002	0.057	0.002	0.029	0.002
Plastic properties							
T _s	°C	386	4	410	4	390	4
T _m	°C	429	3	464	3	429	3
T _r	°C	448	3	496	3	447	3
F _{max}	ddpm	9	1	124	9	4	1
Ash composition [wt%]							
SiO ₂		31.24	2.22	53.23	2.22	30.44	2.22
Al ₂ O ₃		22.96	1.4	30.98	1.4	24.16	1.4
Fe ₂ O ₃		17.41	0.16	9.03	0.16	16.26	0.16
CaO		9.88	0.07	0.94	0.07	9.74	0.07
MgO		2.36	0.08	0.7	0.08	5.06	0.08
K ₂ O		1.83	0.03	1.67	0.03	1.09	0.03
P ₂ O ₅		0.53	0.08	1.14	0.08	1.13	0.08
SO ₃		9.82	0.16	0.32	0.16	8.59	0.16
Mn ₃ O ₄		0.04	0.01	0.19	0.01	0.15	0.01
TiO ₂		1.21	0.05	1.36	0.05	0.72	0.05
BaO		0.83	0.07	n.a	-	n.a	-
SrO		0.52	0.01	n.a	-	n.a	-
Na ₂ O		1.12	0.02	0.6	0.02	2.05	0.02
B _{ash}		0.60	-	0.16	-	0.63	-

daf = Dry Ash Free, *a* = As received, *T_s* = softening temperature, *T_r* = resolidification temperature, *T_m* = temperature of maximum fluidity, *F_{max}* = Maximum fluidity expressed in dial division per minute [ddpm], *B_{ash}* = Basicity Index and *n.a* = not available

Quality of the produced metal, in terms of purity, is correlated with the amount of mineral inclusions in the coals. According to the values in Table 5.1, Blue Gem is a very pure coal as the ash level is only 1.5 %. Peak Downs contains the highest amount of ash (11.6 %) and composition of the ash is somewhat different from the other coals as the amount of acidic components like SiO_2 and Al_2O_3 amounts to almost 85 % of the total components.

Composition of the mineral matter in coal has been proven to affect the Boudouard reactivity in manganese production (**Kaczorowski 2006**). The basicity index is an indication of the amount of catalytically active components in the ash, and is calculated according to equation 5.1.

$$B_{ash} = \frac{(K_2O + Na_2O + CaO + MgO + Fe_2O_3)}{(Al_2O_3 + SiO_2)} \quad (5.1)$$

As the calculated basicity indices which are presented in Table 5.1, are giving information about the ratio of catalytically active components in the ash, a distinct difference between the Carboniferous coals and Peak Downs is observed. Close to 85 % of the mineral components in Peak Downs are not regarded as catalytically active in the blast furnace operation. Ash compositions of the Carboniferous coal samples are fairly similar which is confirmed by the basicity indices of the two samples.

Volatile matter has historically been used as an indicator of coal rank. Based on the reported values in Table 5.1, both Blue Gem and Staszic would be categorized as high volatile bituminous coals. Peak Downs contains less volatile matter and is hence of higher rank and represents a medium volatile bituminous coal.

According to **Todoschuk (2005)**, the North American coke producer's are aiming at lower values than 0.8 % of total sulfur in the coals, and all the analyzed coals fulfill this requirement.

The level of phosphorous is ranging from 30 – 570 ppm with the lowest value in Blue Gem and the highest in Peak Downs.

The Gieseler fluidity test provides information about the plastic properties of coals and is related to coal rank. As can be seen from the data in Table 5.1, the two high volatile bituminous coals have a lower temperature of initial softening, narrower plastic range and a lower fluidity than Peak Downs.

5.2 Coal Morphology Studies

In order to have an impression of the coal composition, surface observations of polished pellets prepared for petrographic examinations were carried out for each of the sample materials. The morphological studies were performed on the petrographic microscope illustrated in Figure 4.5, and are supplements to petrographic examinations such as maceral composition and vitrinite reflectance. Information like degree of homogeneity, arrangement and shape of different constituents of the coal and ease of differentiation of macerals are important results from morphological studies. In the present investigations,

focus was on maceral arrangement, appearance of the different maceral groups and sub-macerals as well as characteristic features such as degree of brecciation, amount of fines and possible oxidation.

5.2.1 Blue Gem

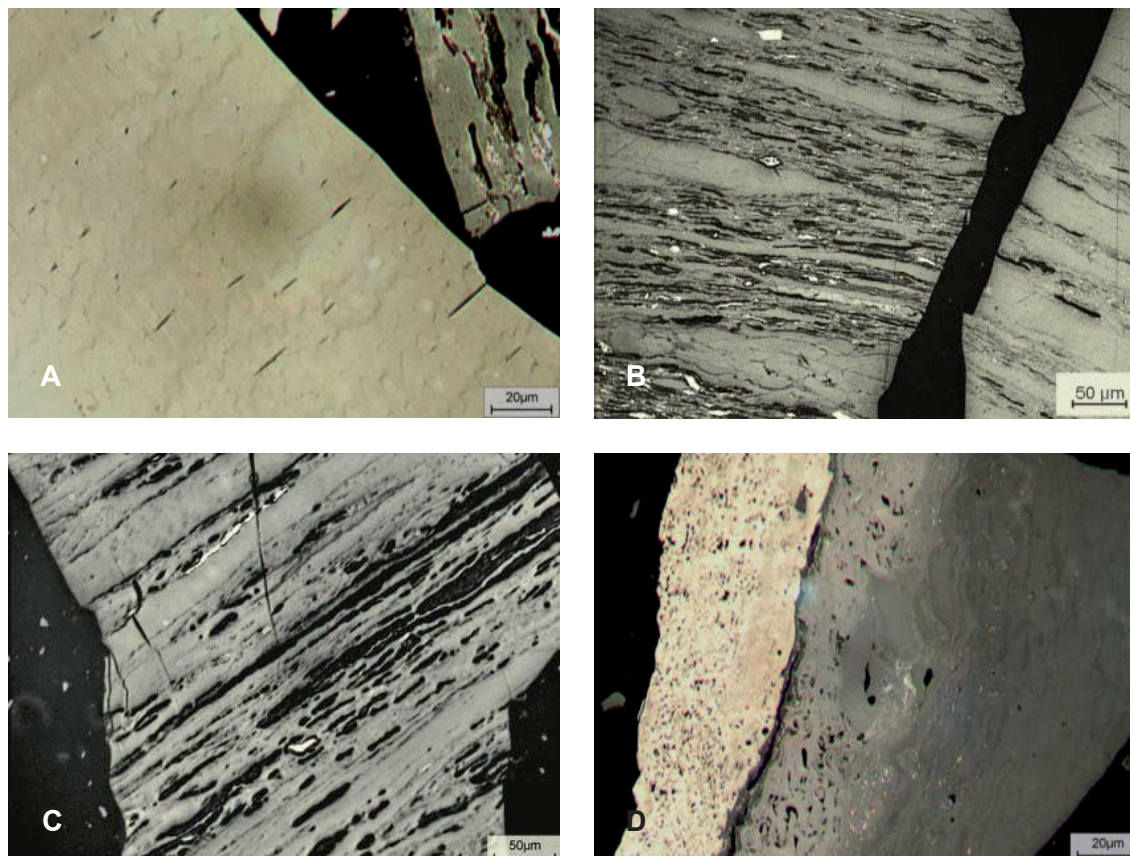


Figure 5.2: Microphotographs of typical morphological structures observed in Blue Gem.

Vitrinite is the dominant maceral group in Blue Gem. A relatively large ratio of the vitrinite is categorized as pseudovitrinite. Pseudovitrinite is easily observed based on the slightly higher reflectance than vitrinite as well as characteristic comma slits in the interior structure and stepped edges. In Figure 5.2 A) a homogenous particle of pseudovitrinite is observed on the left side whereas the particle in the upper right hand corner consists of sporinites embedded in the vitrinite matrix. Notice the higher reflectance of the pseudovitrinite particle.

Liptinites were often observed in the coal structure and both sporinite which constitute most of the liptinites, cutinite and resinite are easily observed. In Figure 5.2 C) cutinite is observed transversing the particle while the smaller black oval bodies are categorized as sporinites.

Macerals of the inertinite group are relatively scarce in Blue Gem, but small amounts of fusinite, semifusinite, micrinite and inertodetrinite are observed. Inertodetrinites can be recognized as small white fragments in Figure 5.2 B), while Figure 5.2 D) illustrates the

transition from vitrinite at the right through semifusinite to fusinite at the left side of the particle.

Pyrite, clay and shale are also observed in Blue Gem, and microphotographs of these inclusions can be seen in Appendix B.

Differentiation of maceral groups and minerals are straightforward in this coal sample as the boundaries between them are clear and the level of reflectance makes it evident to which group the components are belonging.

5.2.2 Peak Downs

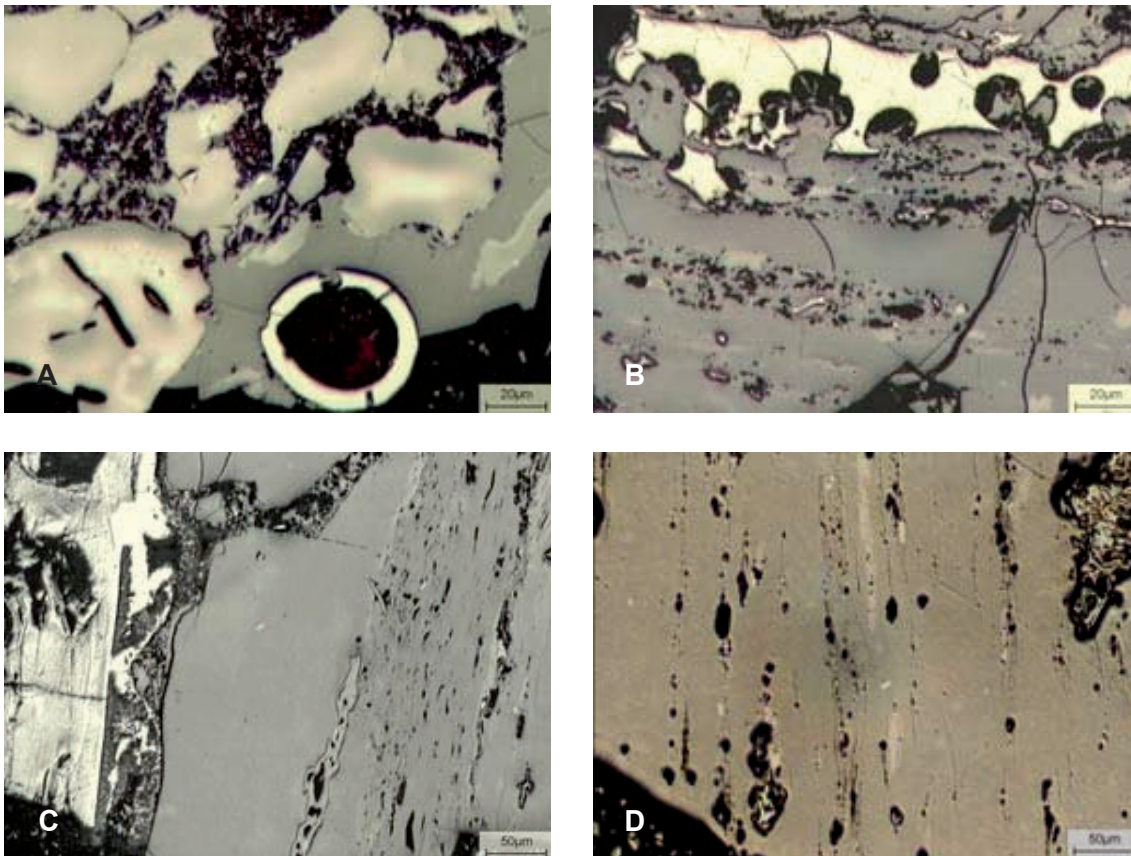


Figure 5.3: Microphotographs of typical morphological structures observed in Peak Downs.

The first impression of the Peak Downs coal sample is that it is more heterogeneous than Blue Gem. The macerals and minerals are more intertwined and some inert compounds which are not observed in Blue Gem are present.

Vitrinite is the most abundant maceral group in this coal, but the range of reflectance of the vitrinite grains is wider than for Blue Gem. Pseudovitrinite is present to a relatively large degree, and these grains are the most homogeneous in the sample.

In accordance to the rank of the coal based on the amount of volatile matter, liptinites are not present in Peak Downs. The black round or oval bodies that might resemble liptinite macerals in Figure 5.3 D) are clastic quartz grains which are embedded in the vitrinite matrix throughout the coal sample. These inclusions have a wide size range.

Macerals of the inertinite group are frequently observed. Fusinite, semifusinite, macrinite, micrinite and inertodetrinite as well as secretinite and funginite are among the macerals belonging to this group which are present in this sample. In Figure 5.3 A), a white fungal spore belonging to the funginite macerals is observed at the bottom of the figure. Secretinite macerals can also be seen in this microphotograph. These macerals are generally large, compact, homogeneous and slightly lower in reflectance than the fungal spores.

The inertinite macerals have a wide range of reflectance. In Figure 5.3 B), a highly reflecting fusinite is seen while some of the semifusinite might have similar reflectance to vitrinite (see Figure 5.3 C). This can make differentiation of the macerals more difficult as the boundaries between them are more diffuse.

5.2.3 Staszic

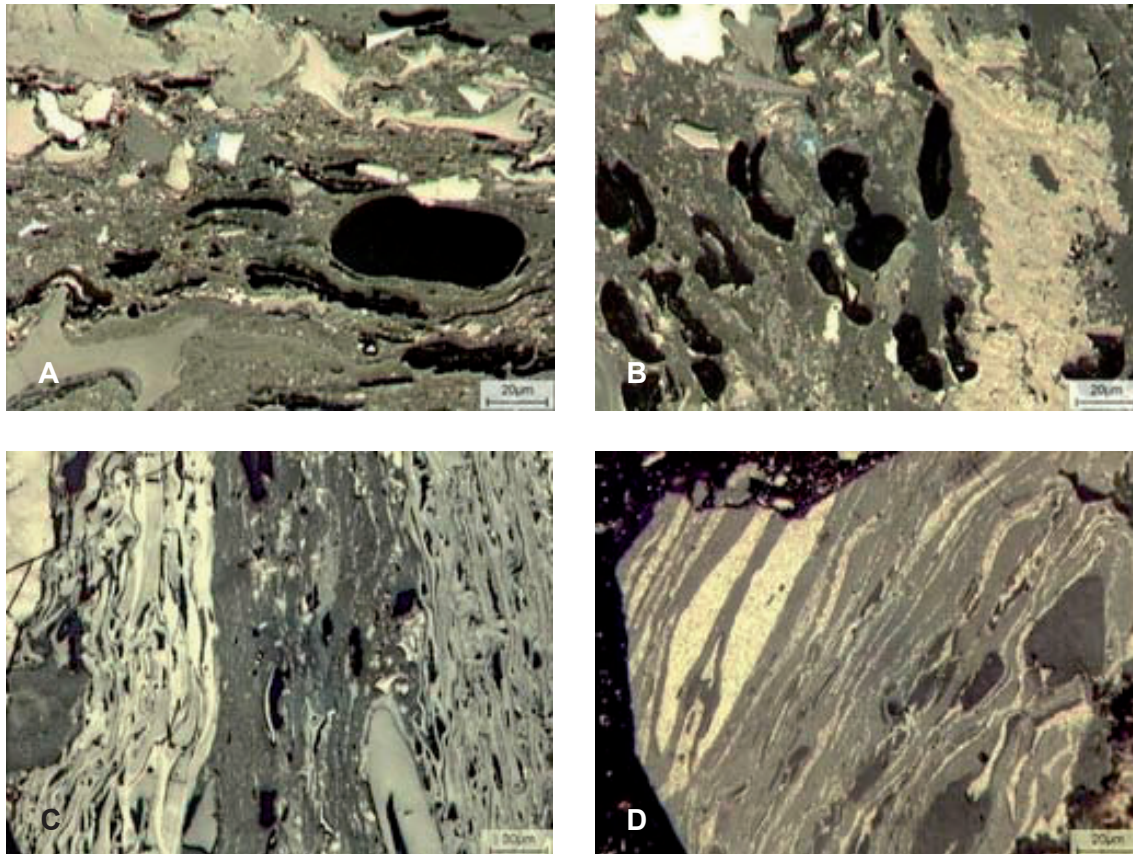


Figure 5.4: Microphotographs of typical morphological structures observed in Staszic.

Staszic is a very heterogeneous coal in which macerals and minerals are well mixed. Vitrinite is still the most common maceral group, but in comparison to Blue Gem and Peak Downs, the amount of pseudovitrinite is small and hardly noticeable. For the most part, vitrinite comprises the grey groundmass in which the other macerals and minerals are embedded.

Sporinite and resinite are the most common liptinite macerals, but cutinites are also present. A relatively large black oval resinite maceral can be identified in Figure 5.4 A), while typical dumb-bell shaped sporinite from the Lycopsida can be seen in the middle of Figure 5.4 B).

A large ratio of the components in Staszic belongs to the inertinite macerals. Compared to the other coal samples, especially semifusinite, micrinite and macrinite constitute a higher ratio of the components. Micrinite is present both as large cluster like in Figure 5.4 D), or more dispersed in the coal matrix. The reflectance of semifusinite covers a wide range in this coal as can be observed in Figure 5.4 C).

Identification of some macerals is more difficult in this coal sample as the level of reflectance is almost continuous from vitrinite to fusinite and the boundaries between the macerals are more diffuse. An illustration of this is the macrinite embedded in the vitrinite matrix in Figure 5.4 A). Macrinite has a slightly higher reflectance than vitrinite and appears to be quite homogeneous.

The mineral inclusions are mainly consisting of pyrite, clay and shale and occur both as discrete particles and embedded in the coal matrix.

5.3 Density Separation of the ROM Coal Samples

As one of the primary objectives of this work was to investigate how coals with different petrographic compositions influence the reactivity in the silicon process, the ROM coals were separated by density in order to obtain fractions with varying constitution. The ROM coal samples were crushed to minimum amount of fines and sieved to the size fraction 3.35 – 9.50 mm. Following the crushing and sieving, the unprocessed coal fractions were separated by density according to the sink – float procedure described in section 4.3. Separation of the ROM coals could maximum give four fractions of each coal and in the following these will be termed according to the denomination given in Table 5.2.

Table 5.2: Coal fractions after density separation.

Description	Termed	Specific density range [g/cm ³]
Low Density Fraction	<i>LD</i>	< 1.25
Medium Density Fraction	<i>MD</i>	1.25 – 1.35
High Density Fraction	<i>HD</i>	1.35 – 1.50
High Ash Fraction	<i>Ash</i>	> 1.50

Following the density separation, the coal samples were air dried and the yield in the specific density ranges were calculated. The yield for each density range was calculated based on the total amount of recovered coal, while the total yield was calculated by the difference in supplied and recovered coal. Total amount of processed coal and the respective yields are given in Table 5.3.

Table 5.3: Amount of coal recovered in different density fractions after separation.

Coals	Fraction	Weight in [kg]	Weight out [kg]	Yield* [%]
Blue Gem	LD		3.93	19.6
	MD		14.65	73.1
	HD		0	0
	Ash		1.46	7.3
	Total	20.05	20.04	100.0
Peak Downs	LD		0.51	5.1
	MD		4.35	43.5
	HD		4.42	44.3
	Ash		0.71	7.1
	Total	10.58	9.98	94.3
Staszic	LD		0	0
	MD		5.51	48.5
	HD		5.42	47.8
	Ash		0.42	3.7
	Total	11.88	11.35	95.6

* The total yield is calculated based on the total weight in and out, while yields of the different density fractions are calculated based on the amount of recovered coal.

From Table 5.3, it is evident that 87.8 % and 96.3 % of the coal is recovered in the density range 1.35 – 1.50 for respectively Peak Downs and Staszic. More than 90 % of the Blue Gem coal does however have a lower density than 1.35 g/cm³.

Based on the morphological studies (section 5.2) and the illustration of specific density variation with rank in Figure 3.14, the most possible explanation for the difference in recovery between Blue Gem and Staszic is the heterogeneous structure of the latter. Both inert components and mineral inclusions contribute to making the particle density higher, and as the Staszic coal is very inhomogeneous, all particles have a higher density than 1.25 g/cm³. Blue Gem on the other side is a very homogenous coal with low amounts of both minerals and inertinites and hence has the highest recovery in the lowest density fractions. Peak Downs can also be characterized as a relatively dull coal, but contains more pseudo vitrinite than Staszic. Particles with a high content of pseudovitrinite are homogenous and will contribute to an increased recovery in the lighter fractions.

In commercial operations, the coal recovered in the highest density fraction would be termed reject or tailings and deposited as it is not suitable for industrial utilization. Based on the data presented in Table 5.3, the total amount of reject would range from 3.7 – 7.3 %.

5.4 Petrographic Analyses of Coal Samples

Petrography has been widely used in the coke making industry in order to correlate coal properties with the desired properties of metallurgical coke. Primarily rank, but also the ratio of fusible to infusible macerals are of uttermost importance in order to make a coke that fulfils all the requirements from the blast furnace operation.

Analyses of carbonaceous reductants in the ferroalloy industry have historically been restricted to proximate- and ultimate analyses as well as ash composition. Petrographic analyses provide information about coal origin, composition, rank, mining operations and post mining influences like oxidation, and should thus render valuable information for the ferroalloy industry as well. In the last couple of years the carbonaceous materials have received increased attention, and petrographic analyses have become more common in trying to understand the correlation between coal properties and behaviour in the furnace.

In the present work, petrographic analyses determining composition of the coal, rank and microstructures not included in the standard maceral analysis have been performed.

5.4.1 Maceral analysis

Macerals are the smallest microscopically observable organic entities in coal, and are characterized by color, shape, size and association with other macerals. The different macerals are described in section 3.4.1 – 3.4.3 and microphotographs of the macerals observed in this work are presented in the form of an album in Appendix B.

As coal is an inhomogeneous material by nature, quantitative measurements should be statistically evaluated. The result of a standardized maceral analysis is given as the volumetric abundance of the constituents in coal determined by point counting (as described in section 4.2.1). The accuracy of the measurements is given as the standard deviation and repeatability according to **ISO 7404-3 (1994)**.

The theoretical standard deviation (σ) for the point count estimate of a petrographic component at the 95 % confidence interval is given in equation 5.2.

$$\sigma_i = \sqrt{\frac{p \cdot (100 - p)}{N}} \quad (5.2)$$

where p is the percentage of the components and N is the total number of counted points.

The difference between two single determinations of the petrographic composition of a coal sample is termed the repeatability (R), and is given by equation 5.3

$$R = 2 \cdot \sqrt{2} \cdot \sigma_i \quad (5.3)$$

The repeatability values listed in Table 5.4 and Table 5.5 define the theoretical spread, at the 95 % confidence level in repeat analyses of identical samples performed by the same analyst.

Estimates of standard deviation and repeatability only relate to the precision of the analyses and do not incorporate errors due to incorrect determination of the constituents in the sample.

5 EXPERIMENTAL RESULTS

Mineral matter is incorporated in the counting procedure, but is according to ASTM standards (ASTM D2799 1999) better approximated by applying a modified version of the Parr mineral matter equation. This formula has converted the Parr equation to a volume percent basis by assuming specific gravities of 1.35 and 2.80 g/cm³ for respectively the organic- and inorganic fractions of coal. Both counted values of inorganic matter as well as the estimated values by equation 5.4 are given in Table 5.4 and Table 5.5.

$$MM(vol\%) = \frac{100[(1.08A^d + 0.55S_t^d)/2.8]}{[100 - (1.08A^d + 0.55S_t^d)]/1.35 + (1.08A^d + 0.55S_t^d)/2.8} \quad (5.4)$$

where A^d and S_t^d are the weight percent of ash and total sulphur on a dry basis which are determined by proximate- or ultimate analyses (see section 4.1.1, 4.1.2 and Table 5.1).

Even though specific macerals were identified in the course of the maceral counting, the following categories were used for the ROM coals:

Vitrinite:	No subdivision
Liptinite:	No subdivision
Inertinite:	Fusinite, semifusinite, other inertinites
Minerals:	No subdivision

As the macerals have different mechanical hardness and stability, the petrographic composition is a function of grain size of the analyzed particles. According to Taylor et al. (1998), vitrinite will be concentrated in the fine fraction, while the inertinites are more abundant in the coarser grain sizes. In order to evaluate the effect of grain size on the petrographic constitution, polished pellets with different size requirements were prepared. Following the ASTM procedure for maceral analyzes, coal grains are crushed to < 850 µm. The petrographic compositions of the ROM coals prepared according to the ASTM standard are given in Table 5.4.

Table 5.4: Volumetric abundance of macerals in ROM coal samples prepared following the ASTM procedure i.e. particle size < 850 µm.

	Blue Gem			Peak Downs			Staszic		
	Volume [%]	α	R	Volume [%]	α	R	Volume [%]	α	R
Macerals									
Vitrinite	77.5	1.8	5.2	68.3	1.9	5.5	50.8	2.1	6.0
Liptinite	13.0	1.5	4.2	-	-	-	13.1	1.4	4.0
Fusinite	1.6	0.5	1.5	5.0	0.9	2.6	7.0	1.1	3.1
Semi fusinite	1.4	0.5	1.4	10.2	1.3	3.6	13.6	1.5	4.1
Inertinite	5.2	1.0	2.8	6.2	1.0	2.8	8.6	1.2	3.4
Mineral Matter									
Counted	1.4	0.5	1.4	10.3	1.3	3.6	6.8	1.1	3.0
Parr formula*	1.0			6.7			3.4		
Total Counts	515			580			557		

* The ash is corrected for moisture, but not total sulfur (i.e. values for as received is used for sulfur)

Results from the maceral analyses reveal that the assumptions from the morphological studies were justified. Vitrinite is the most abundant maceral in Blue Gem while

inertinites and minerals are scarce. This makes the grade of this coal very good. Inertinites and minerals are quite abundant in Peak Downs, but as the coal does not contain any liptinites due to the rank, vitrinite is still the most common group of macerals.

Staszic is a composite of the different maceral groups and in total about 30 % of the volume is occupied by macerals belonging to the inertinite group. The content of liptinite macerals is similar to Blue Gem while the amount of minerals is intermediate.

The petrographic constitutions of the ROM coal samples prepared in the size range 1 – 2 mm are given in Table 5.5.

Table 5.5: Volumetric abundance of macerals in ROM coal samples in the size range 1 – 2 mm.

	Blue Gem			Peak Downs			Staszic		
	Volume [%]	α	R	Volume [%]	α	R	Volume [%]	α	R
Macerals									
Vitrinite	83.9	0.5	1.5	73.1	1.7	4.8	56.7	0.7	2.0
Liptinite	10.5	0.5	1.3	-	-	-	10.5	0.4	1.2
Fusinite	1.5	0.2	0.5	7.0	1.0	2.8	4.2	0.3	0.8
Semi fusinite	0.7	0.1	0.4	8.6	1.1	3.1	16.6	0.5	1.1
Inertinite	2.5	0.2	0.7	5.4	0.9	2.5	9.3	0.4	1.5
Mineral Matter									
Counted	0.9	0.1	0.4	5.9	0.9	2.6	2.7	0.2	0.6
Parr formula*	1.0			6.7			3.4		
Total Counts	4559			673			5154		

* The ash is corrected for moisture, but not total sulfur (i.e. values for as received is used for sulfur)

In order to evaluate the effect of grain size on the petrographic composition of the ROM coal samples, results from maceral analyses with different grain sizes are compared in Figure 5.5.

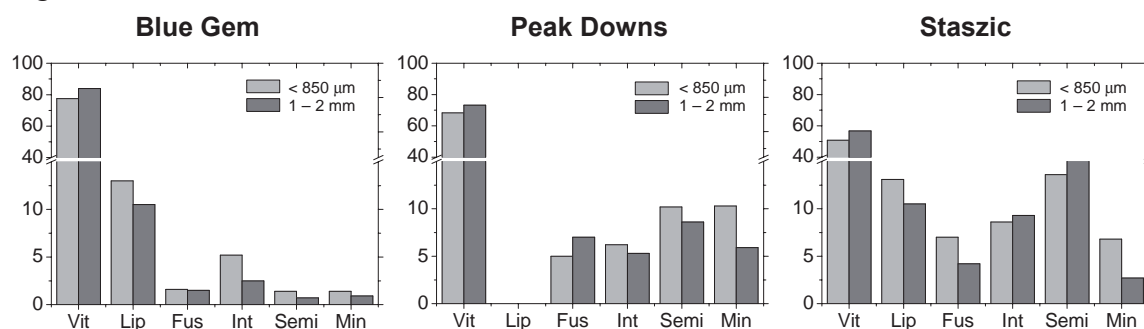


Figure 5.5: Effect of grain size on the petrographic constitution of the ROM coal samples.

Based on the results illustrated in Figure 5.5, vitrinite has a higher volumetric abundance in the coarsest grain fraction while the amount of minerals is highest in the smallest fraction for all the analyzed coal samples. Liptinite contents in Blue Gem and Staszic indicate that these macerals have an affinity towards the finer fraction of coal. Inertinite macerals tend to concentrate in the finest fraction, although the trend is not unambiguous. Fusinite is more abundant in the coarsest fraction of Peak Downs while the remaining inertinite macerals are concentrated in the finest size range. The opposite is true for the Staszic samples.

These results contradict the predicted trends proposed by **Taylor et al. (1998)**. According to these authors, the main reason for the increased content of vitrinite in the finer fraction of coal is the high concentration of the sub-maceral telovitrinite in this fraction. The level of both detrovitrinite and gelovitrinite remain fairly constant with varying grain size. During the maceral analyses in this work, the sub-macerals of the vitrinite group were not differentiated and it is thus hard to estimate the ratio of telovitrinite to the other vitrinite macerals. When the fine fraction is less than 100 μm , there is a sharp decline in the vitrinite content and a corresponding rise in the level of inertinites. The ASTM procedure for preparing samples for maceral identification defines the grain size of the coal particles as less than 850 μm . Fragments of fusinite and semifusinite have a tendency to accumulate in the finest size fraction thus lowering the amount of vitrinite.

As described in the previous section, the ROM coals were separated into different density fractions. The purpose of the density separation was twofold:

1. Separation of the coal samples into density fractions with different petrographic compositions.
2. To concentrate the mineral matter in the highest specific density fraction.

In order to investigate the effect of the density separation of the ROM coal samples, the petrographic composition of the recovered density fractions were examined. Polished pellets were made following the ASTM procedure, and standard maceral analyses were performed. During the counting procedure of the density separated fractions, fusinite and semifusinite were not differentiated and collectively counted under the term fusinites. The main reason for this is based on the structural similarities of these macerals. They are both porous and are thus more available for SiO gas during smelting operations. Results of the maceral counting procedure of the density separated coal fractions are presented in Table 5.6.

Table 5.6: Volumetric abundance of components in density separated coal fractions.

Coals		Specific density fractions			
		LD	MD	HD	Ash
Blue Gem	Vitrinite	77.6	85.9	-	17.6
	Liptinite	15.3	10.2	-	0.3
	Inertinite	2.4	2.0	-	0.1
	Fusinite	1.7	0.8	-	0.0
	Mineral Matter	3.0	1.2	-	82.0
	Total counts	2997	1711	-	1479
Peak Downs	Vitrinite	93.0	81.7	74.5	49.1
	Liptinite	0.0	0.1	0.0	0.0
	Inertinite	2.0	8.1	9.6	6.9
	Fusinite	1.5	6.3	9.6	5.8
	Mineral Matter	3.5	3.8	6.2	38.2
	Total counts	1379	1710	1493	1488
Staszic	Vitrinite	-	70.6	61.6	30.3
	Liptinite	-	12.6	8.3	2.2
	Inertinite	-	7.9	13.1	4.0
	Fusinite	-	6.6	10.5	8.5
	Mineral Matter	-	2.3	6.7	55.0
	Total counts	-	2430	1769	1664

According to **Stach et al. (1982)**, the density of the components in bituminous coals increases in the order: liptinite < vitrinite < inertinite < mineral matter which also is illustrated in Figure 3.14. This implies that the relative ratio of inertinite macerals and minerals should increase with density whereas the opposite would be expected for liptinites and vitrinite. In order to graphically illustrate how the maceral composition varies with specific density and investigate if the purpose of the separation is fulfilled, the results from Table 5.6 are plotted in Figure 5.6.

For both Peak Downs and Staszic there is a steady decrease in the content of vitrinite with increasing specific density. In the Blue Gem samples, the level of vitrinite is increasing from the Low Density fraction (LD) to the Medium Density fraction (MD). This increase in vitrinite might be due to the higher level of liptinite macerals present in the LD fraction. As liptinite has a lower specific density than vitrinite, dull particles of vitrinite and liptinite should have a lower density than homogenous particles of vitrinite. If this postulate is correct, we would expect to find a higher ratio of pseudovitrinite in the MD fraction.

From Figure 5.6, there almost seems to be a linear decrease in the amount of liptinite macerals with increasing specific density. This assumption is based on the results from Blue Gem and Staszic as liptinites are not encountered during the counting procedure of Peak Downs.

For inertinite macerals, analytical results from Blue Gem are ignored as the amount of these constituents are too low to see any trends. The amount of inertinites in Peak Downs and Staszic are relatively abundant and based on the results in Figure 5.6, these macerals tend to accumulate in the HD fraction of the coals.

5 EXPERIMENTAL RESULTS

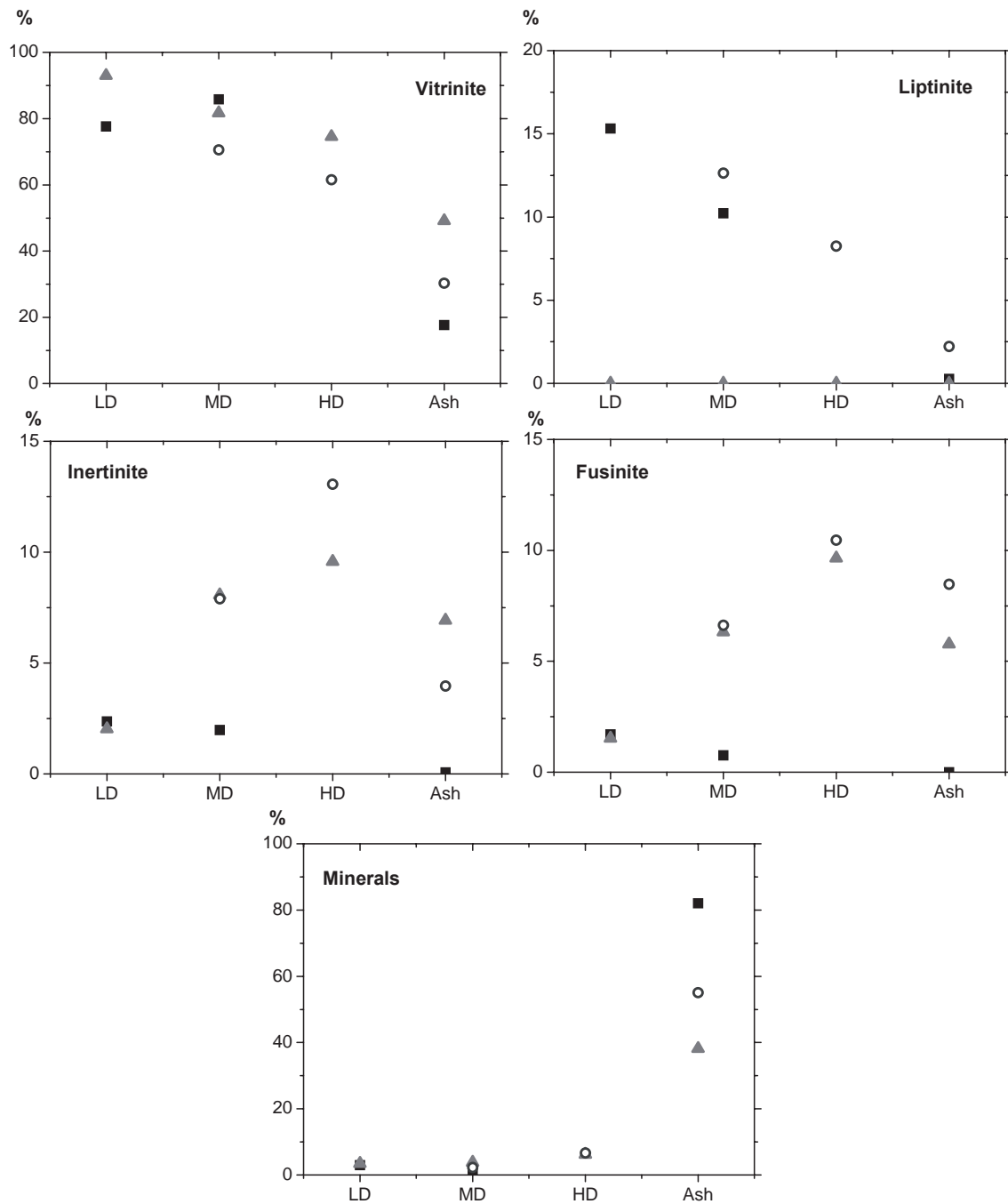


Figure 5.6: Graphical illustration of how the maceral composition varies with density. Filled squares (■) are Blue Gem, filled triangles (▲) are Peak Downs and open circles (○) are Staszic.

Mineral matter is concentrated in the highest density fraction for all the coal samples, and for Blue Gem more than 80 % of the counted constituents in this sample were identified as various minerals.

Based on the results presented in Table 5.6 and Figure 5.6, conclusions can be drawn on whether the purposes of the density separation are fulfilled. The mineral matter in all the

coal samples is concentrated in the Ash fraction and even though the amount varies from about 38 % in Peak Downs to 82 % in Blue Gem, this purpose is accomplished.

If the reject of the separation (Ash fraction) is disregarded, there is a tendency for the minerals and inertinite macerals to accumulate in the higher density fractions while the opposite is true for liptinite and vitrinite macerals. Blue Gem is a very homogeneous coal, which results in fairly similar composition of the different fractions. Based on the nature of the coal samples, the second purpose of density separation of the ROM coals is also fulfilled.

5.4.2 Vitrinite reflectance

Rank is the most important petrographic parameter for assessing the industrial application of coals. The production of metallurgical coke requires coals of bituminous rank as these fuse upon heating and re-solidify to make a strong coke. According to **Raness and Gray (1995)**, **Patalaky et al. (1995)** and **Raness (2001)** rank is one of the parameters that has the most significant effect upon the reactivity of carbonaceous materials towards SiO gas according to the reaction:



The most acknowledged measure of rank is reflectance of vitrinite. In the present work, random reflectance of vitrinite was measured on polished pellets of the coal samples according to the procedure described in section 4.2.2. Results from the vitrinite reflectance measurements are presented in the form of histograms in Figure 5.7.

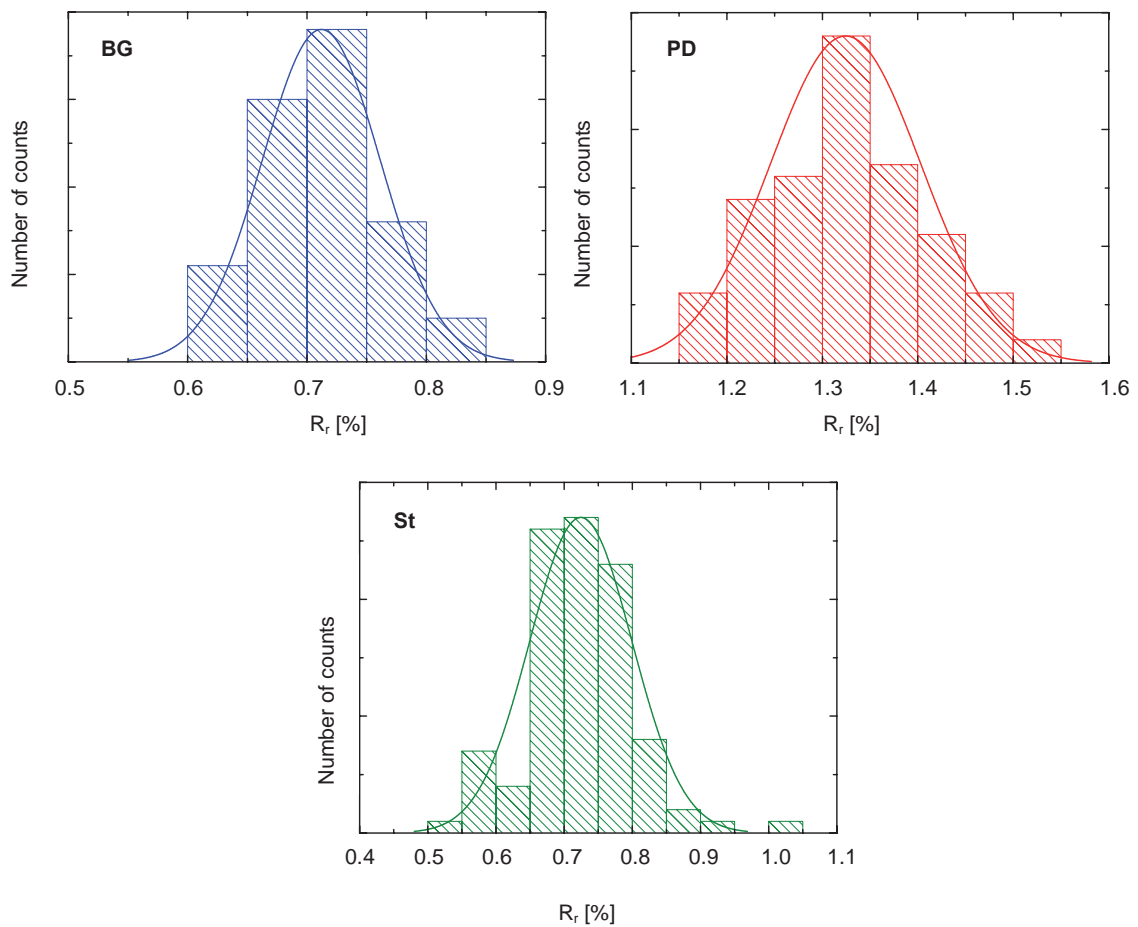


Figure 5.7: Histograms showing the random reflectance of vitrinite (R_r) of the coal samples.

The bin size in the histograms was set to 0.05 % reflectance for all measured samples. In order to make comparison of the samples more straightforward, normal distribution plots of all the measured coal samples are given in Figure 5.8.

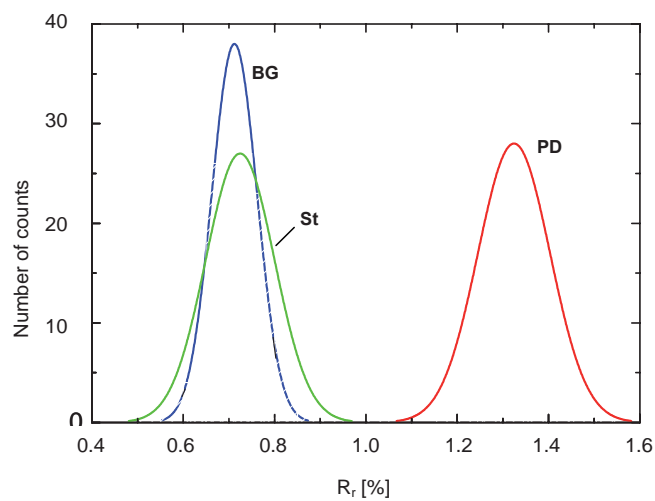


Figure 5.8: A comparison of the normal distribution acquired from the histograms shown in the figure above.

From the data presented in Figure 5.7 and Figure 5.8, it can be seen that the average vitrinite reflectance for Blue Gem and Staszic are very similar, while the Australian coal has a significantly higher value.

The scatter of the recorded reflectance values is correlated to the specific sub-macerals of vitrinite which is encountered during the analyses. According to **Taylor et al. (1998)**, variability of the readings can be reduced by limiting the measurements to one specific type of vitrinite (telovitrinite). **Ting (1989)** has also proved that vitrinite reflectance of coals with the same rank can vary due to differences in the plant material from which the coals were formed. Dull particles of vitrinite and liptinite may also cause the reflectance readings to be slightly lower. The dull structure of Staszic compared to the homogeneous Blue Gem is responsible for the higher spread of measurements for the Polish coal. The scatter of the measurements is represented by the standard deviation which is given in Table 5.7.

According to **Gray (1976)** and **Gray and Devanney (1986)**, the reflectance of vitrinite is directly correlated to the carbon forms in the coke texture. This correlation is even described in an ASTM standard, **ASTM D5061 (1997)**. In order to predict the carbon forms in the binder phase of the carbonized samples, the reflectance of vitrinite is listed in groups of vitrinoid types (V-types) in Table 5.7. Each V-type represents a span of 0.1 % reflectance. Thus V-Type 8 includes all measurements between 0.80 through 0.89. Microphotographs of the different carbon forms encountered in the present work are presented in Appendix F. The relative ratios of vitrinoid types for the investigated coal samples are presented in Table 5.7 as well as the average random reflectance (R_r) and the standard deviation of the measurements.

Table 5.7: Vitrinite reflectance and V-Types of the coal samples.

Vitrinoid V – Types	Vitrinite Reflectance	Blue Gem	Peak Downs	Staszic
V 5	0.50 – 0.59	-	-	8
V 6	0.60 – 0.69	41	-	30
V 7	0.70 – 0.79	54	-	50
V 8	0.80 – 0.89	5	-	10
V 9	0.90 – 0.99	-	-	1
V 10	1.00 – 1.09	-	-	1
V 11	1.10 – 1.19	-	-	-
V 12	1.20 – 1.29	-	20	-
V 13	1.30 – 1.39	-	44	-
V 14	1.40 – 1.49	-	28	-
V 15	1.50 – 1.59	-	8	-
Reflectance, R_r		0.71	1.32	0.72
Standard deviation		0.05	0.08	0.08

The original correlation between vitrinite reflectance and carbon forms in the resulting coke / char was based on mean – maximum reflectance (R_{max}), while random reflectance was used to measure the coals selected for the purpose of this work.

Reflective properties of vitrinite grains are uniaxial, which implies that that the vertical axis is shorter than the horizontal axis. This is due to the pressure of the overlaying sediments during the time of deposition. Practically this means that the reflectance is highest when the polarized light is parallel to the bedding plane and lowest when the incident light is perpendicular to the bedding plane. Coal rank assessments in the USA

5 EXPERIMENTAL RESULTS

are usually reported based on the mean maximum reflectance as this procedure will give a lower value for standard deviations than the corresponding random reflectance of vitrinite.

There exist several correlations between random- and mean maximum reflectance. In addition to the proposed relationships by **Price (2005)** and **Komorek and Morga (2002)** which are quoted in section 4.2.2, **Diessel and McHugh (1986)** have reported the following relation:

$$R_{\max} = 1.07 \cdot R_r - 0.01 \quad (5.5)$$

Sakurovs et al. (1987) reported that the maximum reflectance of vitrinite is linearly proportional to the temperature of maximum fluidity (T_m) according to equation:

$$R_{\max} = \frac{T_m - 381.43}{62.86} \quad (5.6)$$

According to **Miura (1978)**, the content of volatile matter on a dry ash free basis (V^{daf}) can also be used to assess the maximum reflectance of vitrinite:

$$R_{\max} = 2.46 - 0.04 \cdot V^{daf} \quad (5.7)$$

The quoted relationships between random- and maximum reflectance are compared to the analyzed results in Table 5.8.

Table 5.8: Comparison of the measured results of random vitrinite reflectance to the quoted correlations.

	Blue Gem	Peak Downs	Staszic
Random reflectance, R_r			
Measured value	0.71	1.32	0.72
Maximum reflectance, R_{\max}			
Price	0.75	1.40	0.76
Komorek and Morga	0.72	1.39	0.73
Diessel and McHugh	0.75	1.40	0.76
Sakurovs*	0.76	1.31	0.76
Miura*	0.96	1.55	1.07

* Values for the temperature of maximum fluidity (T_m) and amount of volatile matter (V^{daf}) are given in Table 5.1.

The calculated values of R_{\max} given in Table 5.8 show that all the correlations are in quite good agreement apart from the values calculated based on the amount of volatile matter which render significantly higher values of maximum reflectance for all the coal samples.

As most of the correlations between vitrinite reflectance and carbon forms in coke are based on R_{\max} , the quoted relationships should enable us to evaluate the carbon forms in the resulting char by transferring the measured values of R_r .

The vitrinite reflectance confirms that Staszic and Blue Gem are high volatile bituminous of rank while Peak Downs is grouped as a medium volatile bituminous coal.

5.4.3 Non-maceral analysis

The maceral analysis gives information about the relative ratios of the different macerals and minerals in coal. It does however not give any information about the degree of homogeneity of the coal samples nor does it reveal any information about mining operations or possible oxidation. These factors might influence the industrial application of coal, and the coal samples in this work were thus subjected to a non-maceral analysis. Following the procedure described in section 4.2.3, non-maceral microstructures were quantified on the same pellets used for the standard maceral analysis. The non-maceral microstructures in the ROM coals are presented in Table 5.9.

Table 5.9: Volumetric abundance of non-maceral microstructures in ROM coals.

	Blue Gem	Peak Downs	Staszic
Normal Coal			
<i>Vitrinite</i>	1.8	7.8	3.2
<i>Semi-fusinite</i>	1.4	16.0	10.2
<i>Fusinite</i>	0.4	3.6	1.6
<i>Bright attrital</i>	30.4	23.2	22.8
<i>Intermediate attrital</i>	19.2	9.8	11.6
<i>Dull attrital</i>	18.8	17.4	32
Pseudo-vitrinite	24.6	9.2	0.6
Fines	2.8	8.2	3.8
Oxidized	-	0.6	-
Microbrecciation	-	1.2	-
Minerals	0.4	3.0	14.0
Miscellaneous	0.2	-	0.2

As microstructures identified in the non-maceral analysis have different densities, counting procedures were performed for the density separated coal fractions as well. Results from non-maceral analysis of the density separated coal fractions are presented in Table 5.10.

Table 5.10: Volumetric abundance of non-maceral microstructures in density separated coal fractions.

	Blue Gem			Peak Downs				Staszic		
	LD	MD	Ash	LD	MD	HD	Ash	MD	HD	Ash
Normal Coal										
<i>Vitrinite</i>	4.2	2.0	-	15.9	5.4	3.1	1.0	2.4	1.0	1.2
<i>Semi-fusinite</i>	0.6	1.4	0.2	2.0	5.8	11.6	9.7	10.8	11.2	8.5
<i>Fusinite</i>	1.2	0.6	1.4	2.0	3.8	8.8	6.8	1.2	6.2	9.5
<i>Bright attrital</i>	38.8	41.0	4.4	28.0	40.0	25.4	14.3	30.6	14.8	5.6
<i>Intermediate attrital</i>	18.4	18.4	6.0	7.4	14.0	12.2	11.5	22.2	16.4	5.6
<i>Dull attrital</i>	13	10.4	42.5	2.2	10.2	15.5	26.2	25.8	39.6	24.5
Pseudo-vitrinite	22	23.6	3.0	19.1	13.0	5.2	-	4.2	5.2	1.0
Fines	1.4	2.6	2.0	15.7	4.2	10.3	8.9	1.6	3.0	2.5
Oxidized	0.2	-	-	0.2	0.2	0.6	0.2	-	0.4	0.6
Microbrecciation	0.2	-	-	7.0	3.0	3.6	1.2	0.2	0.2	-
Minerals	-	-	40.5	0.6	-	3.8	19.9	0.6	2.0	40.8
Miscellaneous	-	-	-	-	0.4	-	0.2	0.4	-	0.2

In order to graphically illustrate how non-maceral microstructures vary with specific density and to further investigate the effect of the separation process, results from Table 5.10 are plotted in Figure 5.9.

5 EXPERIMENTAL RESULTS

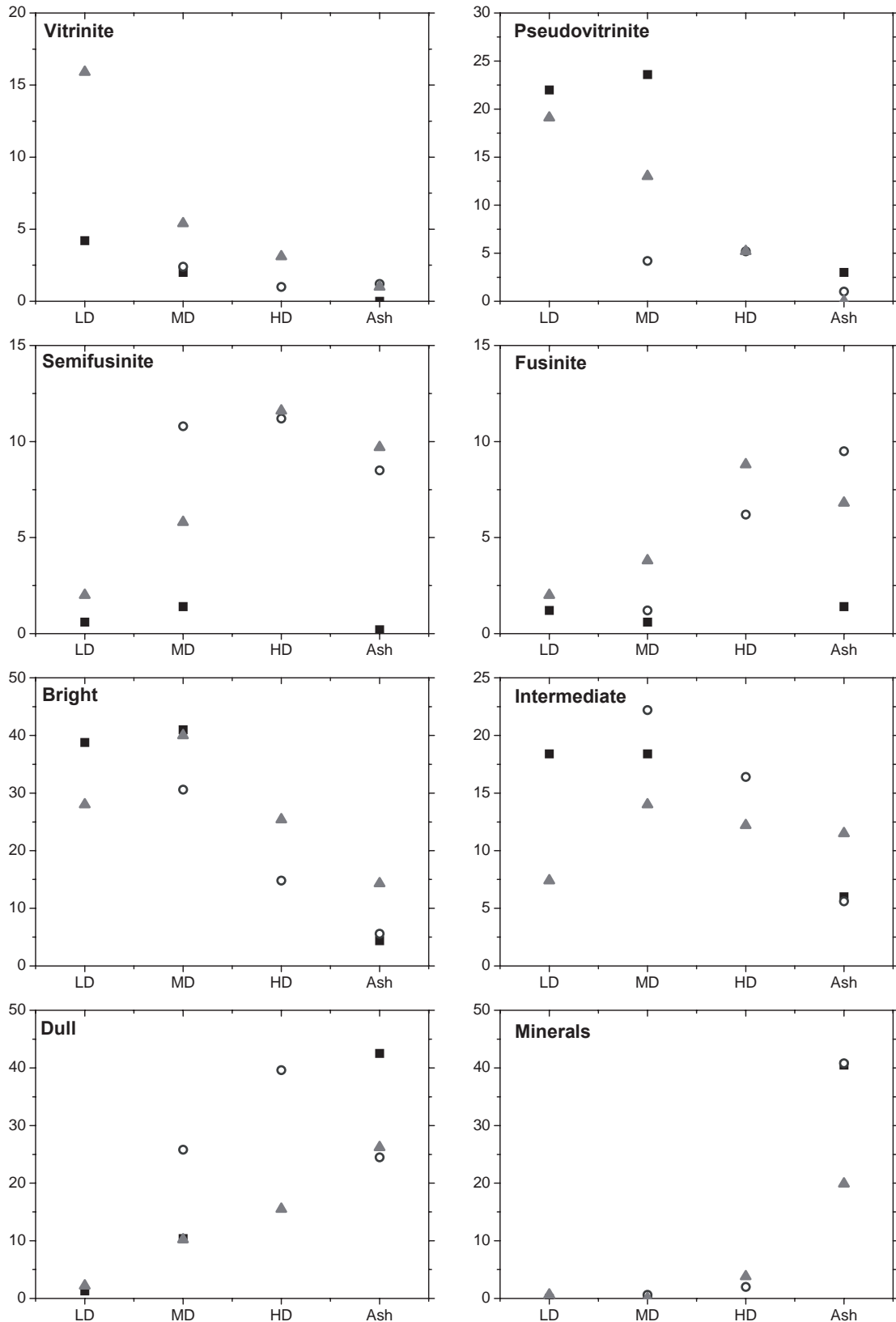


Figure 5.9: Graphical illustration of how the most abundant non-macerated microstructures vary with specific density. Filled squares (■) are Blue Gem, filled triangles (▲) are Peak Downs and open circles (○) are Staszic.

Attrital coal is a term used for heterogeneous coal particles and is, as described in section 4.2.3, divided into bright, intermediate and dull particles based on the volumetric amount of vitrinite in the considered particle. The constituents contributing to the attrital coal apart from vitrinite are however not identified. This implies that a dull particle can consist of a large amount of either mineral, liptinites, inertinite macerals or a combination of all the constituents. Differentiation of attrital coal is just a measure of the degree of homogeneity of the coal.

Similar to the macerals, the different constituents identified during the non-macerals counting procedure act differently upon carbonization. A high amount of vitrinite and bright attrital coal will produce a porous coke / char with low strength. Evenly distributed inertinites are known to act as a reinforcement contributing to increasing strength of the carbonized products.

Based on the data given in Table 5.9, both Blue Gem and Peak Downs can be categorized as relatively homogenous coals as the sum of vitrinite, pseudovitrinite and bright attrital coal is high. Staszic is however a very inhomogeneous coal with both liptinites, inertinites and minerals well embedded in the vitrinite matrix, thus contributing to the dull attrital category.

A quite surprising result is the high amount of minerals encountered in Staszic (14.0 %). Based on the amount of ash from the proximate analysis (see Table 5.1), Peak Downs was expected to have the highest level of mineral inclusions. The high amount of minerals in the polish coal compared to Peak Downs might be an indication of the origin of the minerals in the two coal samples. The results indicate that we find a large amount of discrete minerals in Staszic, which might be possible to remove by coal processing, while the minerals in Peak Downs to a larger degree are embedded in the coal structure i.e. syngenetic minerals.

The amount of fines is a function of coal rank (**Berkowitz 1994**), and the recorded readings of fines during the counting procedure proves that Peak Downs contain a substantially higher amount of fines than the lower rank coals.

According to the plots in Figure 5.9, both the amount of vitrinite and pseudovitrinite are decreasing with increased specific density. The variation of pseudovitrinite with density also confirms the assumption that the level of this microstructure is present to a higher degree in the MD- than the LD fraction in the Blue Gem coal (see page 101).

The number of readings of semifusinite and fusinite in Blue Gem are so scarce that it is hard to see any trends based on this sample. In Peak Downs both of these structures seem to accumulate in the HD fractions even though the level is nearly as high in the ash fraction. Semifusinite is present in similar quantities in all the density fractions of Staszic while the level of fusinite almost seems to have a linear increase with increasing density.

Regarding the attrital coal, densities of the inhomogeneous particles are dependent upon the nature of the constituents which are incorporated in the vitrinite matrix. Liptinites

will decrease the particle density while the opposite is true for inertinite and mineral inclusions. Bright attrital coal does however seem to concentrate in the fractions with lowest specific gravity, while dull particles are more common in the fractions with highest density.

Determination of minerals in the non-maceral analysis is exclusively counting discrete minerals as the particles that are embedded in the coal structure contribute to increasing the ratio of attrital coal. There is a clear tendency for the discrete minerals to concentrate in the Ash fraction, but the coal sample with the highest amount of ash based on the proximate analysis (see Table 5.1), has the lowest amount of discrete particles in this fraction. During the morphological studies of the coal samples, plentiful clastic quartz inclusions were identified in Peak Downs which might be an explanation to this discrepancy.

Microbrecciation is caused by movements of the coal seam usually induced by tectonics and are identified as highly fractured particles. Coal samples with a high portion of brecciation have a higher surface area and are thus more susceptible to oxidation. Rheological properties of coals are affected by brecciated particles and this will influence the carbonized product. This microstructure is hardly present in any of the analyzed fractions of the high volatile coals, but Peak Downs contain 7 % of microbrecciated coal in the LD fraction.

The amount of oxidized coal is important as oxidation will decrease coking properties as well as the heating value of coals. Coal will oxidize when it is exposed to air or water which might occur in the seam, during handling or storing of the coals. A staining procedure is often employed to detect oxidized coal (**Lowenhaupt and Gray 1980**), but only small amounts were counted in our samples.

Microphotographs of non-maceral microstructures identified in coal samples used for the purpose of this work are presented in Appendix D.

5.5 Carbonization

Based on the amount of coal recovered from the density separation, the fractions with sufficient amount of coal (>300 g) were carbonized using the SINTEF procedure which is described in section 4.4. The carbonization yields for the density fractions are listed in Table 5.11.

Table 5.11: Carbonization yields.

		Blue Gem		Peak Downs		Staszic	
		LD	MD	MD	HD	MD	HD
Parallel 1							
Weight in	g	310.6	314.4	314.7	314.5	309.2	313.3
Weight out	g	186.3	195.1	255.7	256.1	195.5	206.1
Yield	%	60.0	62.1	81.3	81.4	63.2	65.8
Parallel 2							
Weight in	g	312.6	315.3	316.2	327.6	307.0	315.5
Weight out	g	186.9	196.1	254.0	264.7	195.1	210.2
Yield	%	59.8	62.2	80.3	80.8	63.6	66.6
Average	%	59.9	62.1	80.7	81.1	63.4	66.2
Standard dev.		0.1	0.1	0.7	0.4	0.2	0.6

Having in mind the different rank and petrographic constitution of the analyzed coals, we would expect the yield from the carbonization process to be varying.

During a standard carbonization process, vitrinite macerals fuse and become plastic, liptinites are mainly decomposed and produce large amounts of gases which are generating pores in the product, while most of the macerals belonging to the inertinite group retain their shape and structure (see section 3.5.1 – 3.5.3). As most of the volatile components in coal are driven off as gases during carbonization, the yield of coke / char is correlated to the amount of volatiles in the coal samples. Based on this assumption, Peak Downs should render the highest yield of carbonized product. The data from Table 5.11 is graphically presented in Figure 5.10.

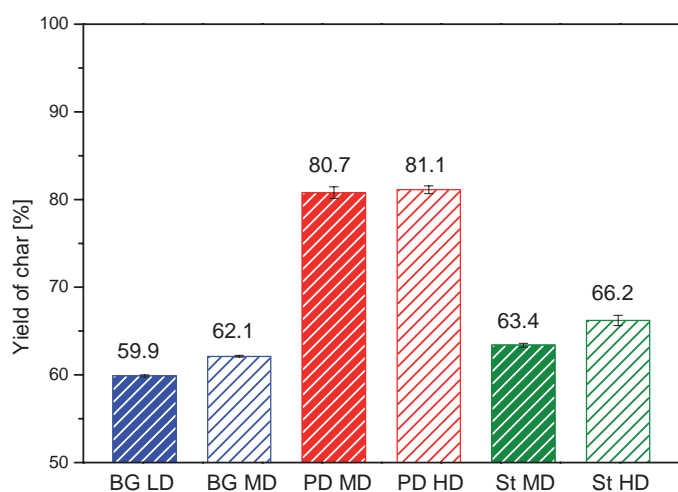


Figure 5.10: Yield of char after carbonization.

From the bar plot it can be seen that the carbonization yield of Peak Downs is significantly higher than the two lower rank coals which have similar values. The highest density fraction of the respective coals also gives a slightly higher yield of coke / char. A possible explanation for this is that the lowest density fractions of Blue Gem and Staszic have a higher content of liptinites which for the most part will decompose to gas. Regarding Peak Downs, the difference between the density fractions is within the limits for the standard deviation, but the content of vitrinite is highest in the MD fraction.

5.6 Characterization of the Carbonized Coal Samples

The second part of this work involved characterization of carbonized samples both in order to evaluate properties which are important in the silicon process and to monitor the coal to char transformation. Microscopical studies of the carbonized samples have involved measurements of microstructure and microtexture. Properties determining microstructure, like porosity, pore size distribution, pore wall thickness and surface area have been assessed by using image analysis, mercury intrusion, absorption techniques and pycnometers. Analyzing microtextures involve determining composition of the pore walls, i.e. ratio of binder- and filler phase and molecular ordering of the carbon forms in the binder phase. Analytical procedures used to quantify these properties involve coke petrography and X-ray diffraction.

5.6.1 Morphology of samples

Before quantifying any parameters of the carbonized samples, typical features and characteristics have been investigated during morphological studies. Polished samples of the carbonized materials have been investigated under the petrographic light microscope (see Figure 4.5). In order to distinguish the different carbon textures, crossed polarized light and a phase sensitive accessory plate were used to enhance these contrasts with color.

Results from the morphological studies of the carbonized materials are presented below.

Blue Gem

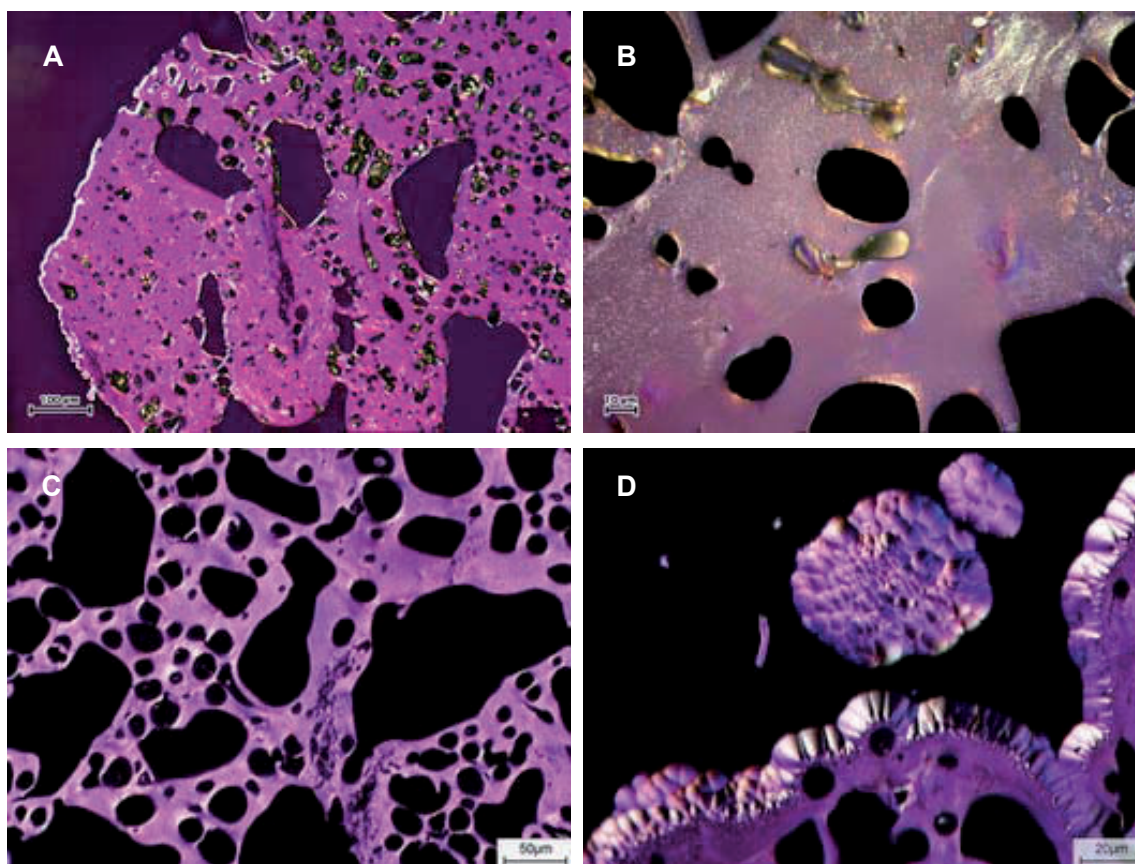


Figure 5.11: Morphology of carbonized coal samples of Blue Gem.

Both the standard maceral analysis and the quantification of the non-maceral microstructures show that fusible components are plentiful in Blue Gem. As fusible components constitute the binder phase in the carbonized materials, the produced char should mainly consist of binder phase. From pictures A – C in Figure 5.11, it is hard to see any filler phase at all, but both infused macerals and mineral inclusions were observed during the morphological studies (see Appendix F).

Measurements of vitrinite reflectance indicate that the binder phase should in large consist of isotropic to fine circular domains. The observed degree of crystallinity during the morphological studies proved that the prediction based upon vitrinite reflectance is

valid. The incipient structure is well illustrated in Figure 5.11 C), while a transition from incipient to fine circular structure can be observed in Figure 5.11 B). In this picture some strain anisotropy is also visible around the pores. This type of anisotropy is due to the tension exerted on the fused coal by the enlarging pores.

An unusual high proportion of the sample is covered by depositional carbons. These are typically encountered on the periphery of the particles and on the pore walls (see Figure 5.11 A and D). Depositional carbons are generated when gases evolved during carbonization crack on a hot surface leaving almost pure carbon as a solid residue. Depositional carbons are highly anisotropic and the structure resembles that of carbon black. A large amount of depositional carbons is in the coke making industry an indication of too high wall temperatures. As the depositional carbons have a relatively dense structure with a high degree of anisotropy, they are believed to affect the reactivity towards gases.

From picture A) in Figure 5.11 which is taken at a relatively low magnification, large pores of more than 100 μm are observed as well as more abundant smaller pores. The pore wall thicknesses are quite large and the pore shapes are relatively uniform.

Peak Downs

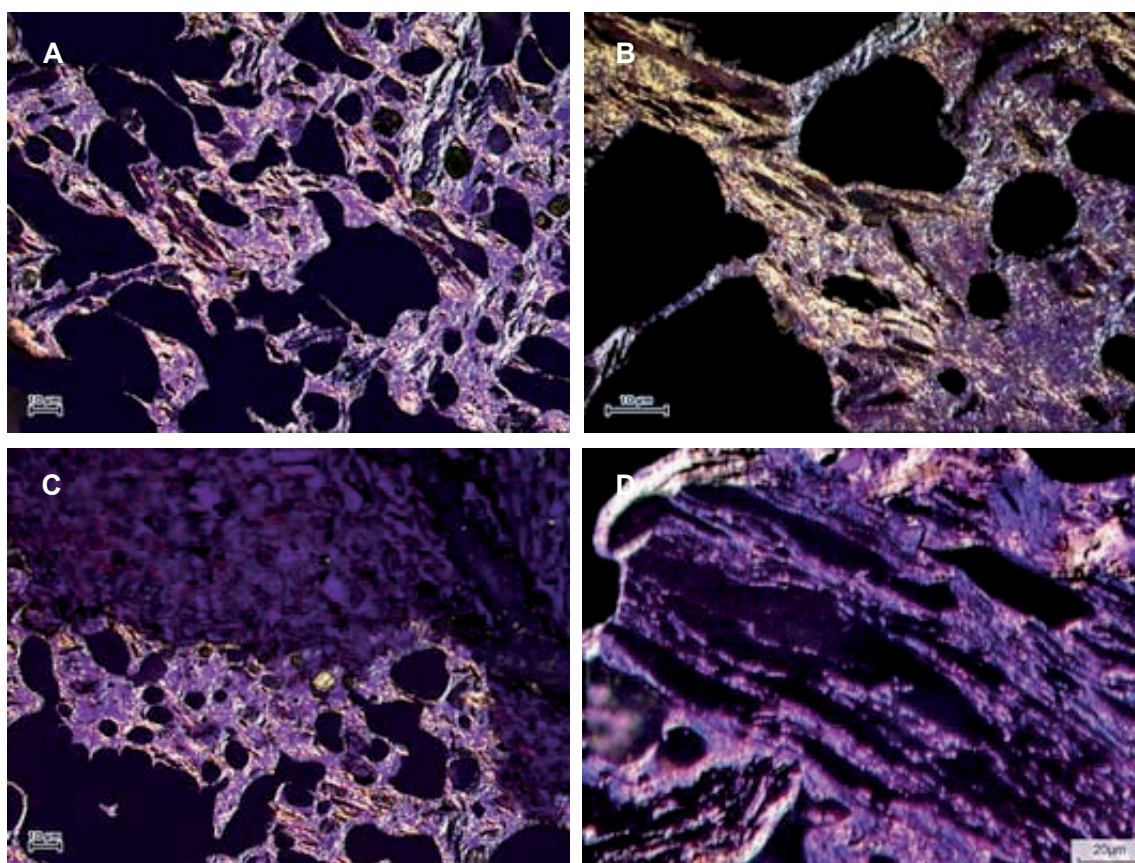


Figure 5.12: Morphology of carbonized coal samples of Peak Downs.

5 EXPERIMENTAL RESULTS

Peak Downs is a medium volatile bituminous coal, and according to the data in Table 5.7, most of the readings are categorized as a V-Type 13. Even after transferring random reflectance measurements to values of maximum reflectance, most of the readings are in the interval V 12 – V 15. The morphological studies showed that the degree of crystallinity is higher than in the carbonized Blue Gem sample, and dimensions of the anisotropic domains fulfill the requirements for the lenticular category. The amount and shape of the crystallites are illustrated in Figure 5.12.

Most of the carbonized sample consists of crystalline components, but the morphological studies also revealed infused macerals and minerals. Regarding the filler phase originating from the organic fraction of coals, especially large inclusions were observed. A coarse filler phase component originating from fusinite can be seen in Figure 5.12 C). During characterization of the coal samples abundant clastic quartz inclusions were observed. These particles are not easily detected in the carbonized samples, but large mineral inclusions were seen (Figure 5.12 D).

Based on the morphological studies, the structure can be characterized with relatively high amount of large pores and thin pore walls.

Staszic

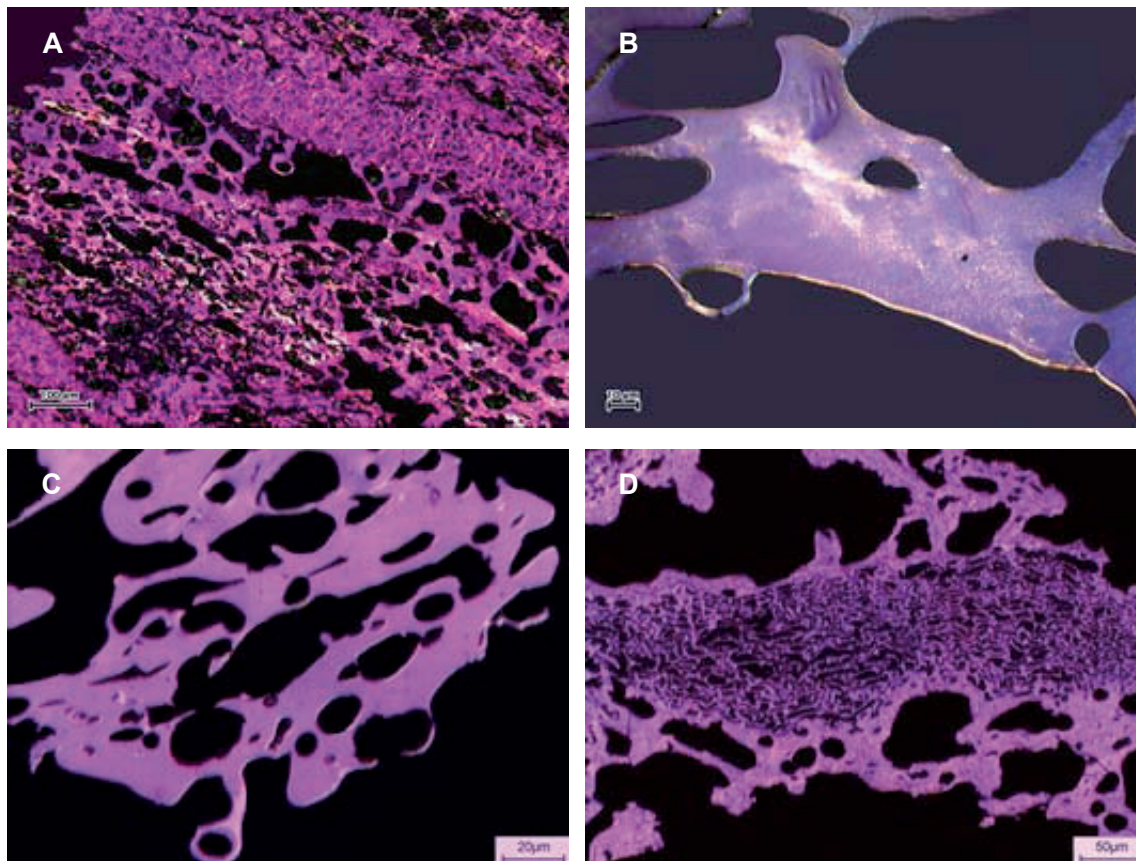


Figure 5.13: Morphology of carbonized coal samples of Staszic.

Staszic is characterized as a dull coal where inclusions of inertinite macerals, liptinites and minerals are embedded in the vitrinite matrix. The shape and size of pores in chars produced from dull coals are governed by the orientation and packing of the infusible components in coal. In Figure 5.13 A), the elongated pores in Staszic are illustrated.

Even though the rank of Staszic is almost identical to that of Blue Gem, the range is wider (see Figure 5.8). This should imply that more carbon forms were present in the carbonized sample material. Based on the morphological studies, there seems to be a larger fraction of isotropic carbon (Figure 5.13 C), but also larger domains of circular anisotropy are observed in Staszic (Figure 5.13 B). As most of the binder phase is isotropic to incipient, the division between isotropic binder phase and infusible macerals is harder to make. Large filler phase originating from fusite can still be easily recognized, as is illustrated in Figure 5.13 D). Small filler phase components embedded in the binder phase is harder to categorize.

Composition of the minerals is known to influence the degree of anisotropy of the binder phase. According to **Gray and Gray (2005b)**, alkali minerals will tend to give a lower degree of anisotropy than the rank suggests while the opposite is true for acidic mineral matter. Even though Staszic has the highest Basicity Index (B_{ash}) of the analyzed samples, there are probably some acidic minerals present in the sample. This statement is based on the fact that in the vicinity of some mineral inclusions, a significantly higher anisotropy was observed than in the bulk of the sample.

Some depositional carbons are also observed (Figure 5.13 B), but not close to the quantities in Blue Gem.

5.6.2 Textural analysis

Coke and char, which both can be products of carbonization of coal, consist of pores and a solid residue which constitute the pore walls. Microtextures of the carbonized material are the carbon forms that make up the walls. These are primarily dependant upon coal type and rank as described in section 3.5.1 and 3.5.2, but also process parameters like heating rate. Rank of the coal determines the degree of anisotropy where sizes of the anisotropic domains are increasing with increasing rank. Distribution of binder- and filler phase in the carbonized product is dependant upon the coal type and ratio of fusible to infusible macerals in the coal. The heating rate during carbonization influences the devolatilization characteristics which again define the fluid properties of coal. Maximum fluidity and width of the plastic range are important parameters in development of anisotropy.

The petrographic procedure for microtexture analysis involves determining the quantities of carbon forms that display different anisotropic domain size and shapes ranging from isotropic to anisotropic. According to **Gray and Gray (2005b)**, the results can be used to predict coke strength as well as reactivity of the carbonized material towards gases like CO₂ and SiO.

There are several systems describing nomenclature of carbon forms in coke (see Appendix E). Even though these systems were developed for the purpose of analyzing

5 EXPERIMENTAL RESULTS

metallurgical cokes, the ASTM standard (ASTM D5061 1997) has been used to quantify the microtextures of the carbonized samples in this work. The procedure for petrographic determination of microtextures in coke is described in section 4.2.4.

Distributions of microtextural components in the carbonized coal fractions according to the ASTM nomenclature are given in Table 5.12.

Table 5.12: Coke carbon forms according to the ASTM procedure.

	Blue Gem		Peak Downs		Staszic	
	LD	MD	MD	HD	MD	HD
Binder Phase						
Isotropic	12.1	10.3	-	-	18.6	34.9
Incipient	49.3	45.4	-	-	48.1	40.9
Fine Circular	36.3	41.7	-	-	31.0	18.1
Medium Circular	2.3	2.6	-	-	2.3	4.8
Coarse Circular	-	-	-	-	-	1.2
Fine Lenticular	-	-	2.7	0.8	-	-
Medium Lenticular	-	-	57.9	61.4	-	-
Coarse Lenticular	-	-	39.1	36.6	-	-
Fine Ribbon	-	-	0.4	1.2	-	-
Total	100	100	100	100	100	100
Filler Phase						
Binder Phase	95.1	87.1	73.7	59.0	65.1	55.7
Fine Inerts	1.9	2.8	8.3	8.4	14.0	11.4
Coarse Inerts	1.9	8.2	12.4	16.9	17.5	16.5
Fine Minerals	0.2	0.2	2.6	7.5	1.7	6.6
Coarse Minerals	0.4	1.2	3.0	6.0	1.7	9.3
Pyritic Minerals	-	0.2	-	2.0	-	0.5
Miscellaneous Inerts	0.6	0.2	-	0.2	-	-
Total	100	100	100	100	100	100
Miscellaneous						
Normal Coke	85.3	80.9	96.4	96.3	93.8	97.5
Pyrolytic carbon	(6.8)	(8.5)	(3.1)	(3.1)	(4.4)	(2.1)
Spherulitic carbon	(7.9)	(10.6)	(0.5)	(0.6)	(1.7)	(0.3)
Depositional Carbon	14.7	19.1	3.6	3.7	6.2	2.5
Total	100	100	100	100	100	100

The correlation between rank of the coals and the size of the anisotropic domains in the binder phase of the carbonized product is quite obvious from the data given in Table 5.12. Blue Gem and Staszic which are almost identical in rank, have similar distributions of carbon forms in the binder phase, ranging from isotropic to circular. Measurements of random reflectance of vitrinite showed that there was a higher degree of scattering in the Polish coal. This should result in a wider distribution of carbon forms identified during counting of binder phase components. For both density fractions of Blue Gem as well as the MD part of Staszic, about 80 % of the carbon forms are identified as incipient or fine circular. The HD fraction of Staszic do however show a wider distribution of anisotropy with a higher ratio of isotropic binder phase, but also some coarse circular carbon forms were counted. Peak Downs was determined to be a medium volatile coal by rank and practically all counts of binder phase components in the char were categorized as lenticular with the majority classified as medium and coarse by size. The total amount of binder phase in the different density fractions are plotted in Figure 5.14.

Identification of filler phase carbon forms is important in determining the strength of the carbonized product. Fine inclusions of filler phase components are known to increase the pore wall thickness and thus the strength and stability, while coarser components might initiate crack propagation which eventually leads to a weaker coke with lower stability. Both mineral inclusions and infusible macerals are therefore classified as fine or coarse with the limit set at 50 μm . While development of different anisotropic textures in the binder phase is correlated to the rank of the parent coal, amount and type of filler phase components are related to the coal type which is determined by maceral- and non-maceral analyses. The filler phase composition (see Table 5.12) displays large differences between the coals and the density separated fractions. A majority of the macerals in Blue Gem was classified as fusible and the content of minerals was scarce. The coke petrographic analysis also shows that the filler phase to binder phase ratio is high for this material. A slightly higher amount of organic filler phase components are counted in the MD fraction. Data presented in Table 5.12 show that the level of binder phase is lower in Peak Downs than for Blue Gem. The difference between the density fractions is also more noticeable where the minerals are present to a higher degree in the material with highest density. Staszic is a very dull coal, and counting of microtextures in the carbonized fractions confirms that filler phase components are abundant. Organic inerts are equally distributed between the density fractions while mineral inclusions are concentrated in the HD fraction. The amount of infusible macerals (inerts) and minerals of the different fractions are plotted in Figure 5.14.

The coke petrographic analysis also revealed that there are significant amounts of depositional carbon in the Blue Gem samples. Both pyrolytic and spherulitic carbons were identified in large quantities and were typically deposited on the periphery of the particles and on pore walls. Generation of depositional carbon is correlated with the amount of volatile matter in the coal samples. The gases evolved during carbonization crack in contact with hot surfaces and leave solid carbon as a residue. Staszic contains about the same amount of volatile matter as Blue Gem. It is believed that due to the dull structure of this coal, volatile compounds have a greater possibility to escape the coal particle during heating hence not creating the same amount of depositional carbons. As the content of liptinites is highest in the lightest fractions of both of the high volatile bituminous coals, the amount of depositional carbons was expected to show the highest values in these fractions of the char. This is true for Staszic, but Blue Gem does not follow this assumption (see Figure 5.14). Equal amounts of depositional carbon are counted in both fractions of Peak Downs.

Among others, **Patalsky et al. (1995)** have reported that a high ratio of binder- to filler phase in char is beneficial for the reactivity towards SiO gas. In that respect Blue Gem should be the most reactive material while Staszic should prove to have the lowest reactivity. The degree of crystallization in the binder phase has also been reported to be of importance for this reaction. **Diessel and Wolff-Fischer (1987)** defined a Coke Anisotropy Quotient (CAQ) in order to quantify the degree of anisotropy in cokes:

$$CAQ = \frac{a + 2b + 3c + \dots nl}{a + b + c + \dots l} \quad (5.8)$$

5 EXPERIMENTAL RESULTS

where a, b, c, \dots, l represent ratios of carbon forms starting from isotropic (see Table 5.13).

In order to calculate the CAQ , the carbon forms presented according to the ASTM nomenclature in Table 5.12, have been rearranged and are presented in Table 5.13.

Table 5.13: Modified coke carbon forms.

		Blue Gem		Peak Downs		Staszic	
		LD	MD	MD	HD	MD	HD
Binder Phase							
Isotropic	a	9.9	7.3	-	-	11.3	19.0
Incipient	b	40.0	32.0	-	-	29.4	22.2
Fine Circular	c	29.4	29.4	-	-	19.0	9.9
Medium Circular	d	1.9	1.9	-	-	1.4	2.6
Coarse Circular	e	-	-	-	-	-	0.6
Fine Lenticular	f	-	-	1.9	0.4	-	-
Medium Lenticular	g	-	-	41.1	34.9	-	-
Coarse Lenticular	h	-	-	27.8	20.8	-	-
Fine Ribbon	i	-	-	0.3	0.7	-	-
Medium Ribbon	j	-	-	-	-	-	-
Coarse Ribbon	k	-	-	-	-	-	-
Depositional Carbon	l	14.7	19.1	3.6	3.7	6.2	2.5
Inerts	p	3.7	9.1	19.9	24.5	29.6	27.3
Minerals		0.5	1.3	5.4	15.0	3.2	15.9
Miscellaneous		-	-	-	-	-	-
Total		100.0	100.0	100.0	100.0	100.0	100.0
CAQ		4.21	4.81	7.60	7.67	3.70	3.61
R_{tex}		2.23	2.15	1.42	1.58	2.54	2.66
CRI		28.9	27.0	16.8	17.7	38.5	43.0

According to the cited authors, there is a linear relationship between CAQ and rank. From Table 5.13 we see that for the materials investigated in this work, Peak Downs do have a higher value than the lower rank coals. Staszic do however have a lower value than Blue Gem even though the rank is approximately equal. This is caused by the higher amount of filler phase in the Polish char. As these components are not included in calculating the coke anisotropy quotient, the respective content of binder phase is lower than for Blue Gem.

The Boudouard reactivity in the blast furnace operations is consuming carbon and increasing the energy consumption. A low reactivity towards CO_2 is thus favourable. To assess the reactivity of metallurgical coke, a Coke Reactivity Index (CRI) is often used. This index gives a value of how much carbon reacts with CO_2 in a time interval of two hours at a temperature of $1100^\circ C$. **Shiaraishi et al. (1985)** reports the following relationship between the carbon forms in the coke and CRI :

$$CRI = 41 - 37.5 \cdot R_{tex} + 14.4 \cdot R_{tex}^2 \quad (5.9)$$

where R_{tex} is the relative reactivity index which, according to the nomenclature in Table 5.13, can be expressed as:

$$R_{tex} = \frac{1 \cdot (f + g + h + i + j + k + l) + 1.8 \cdot (c + d + e) + 2.8 \cdot (a + b) + 3 \cdot p}{(a + b + \dots + l) + p} \quad (5.10)$$

Values for both *CRI* and R_{tex} are given in Table 5.13.

In equation 5.10, carbon forms are classified according to their reactivity. The highest weight is given to organic inerts (*p*), followed by isotropic and incipient carbon forms (*a* and *b*), while the most anisotropic domains, including depositional carbons, are regarded as the least reactive carbon forms. According to the values of *CRI* listed in Table 5.13, Peak Downs should have the lowest reactivity towards CO₂ followed by Blue Gem and Staszic. Cokes used for production of pig iron in the blast furnace have a *CRI* value of less than 30 %.

Carbon forms presented following the ASTM nomenclature (Table 5.12) are more differentiated, but data in Table 5.13 give values as percentage of the total texture. To graphically illustrate the variations between the density fractions, data from Table 5.13 are presented in Figure 5.14.

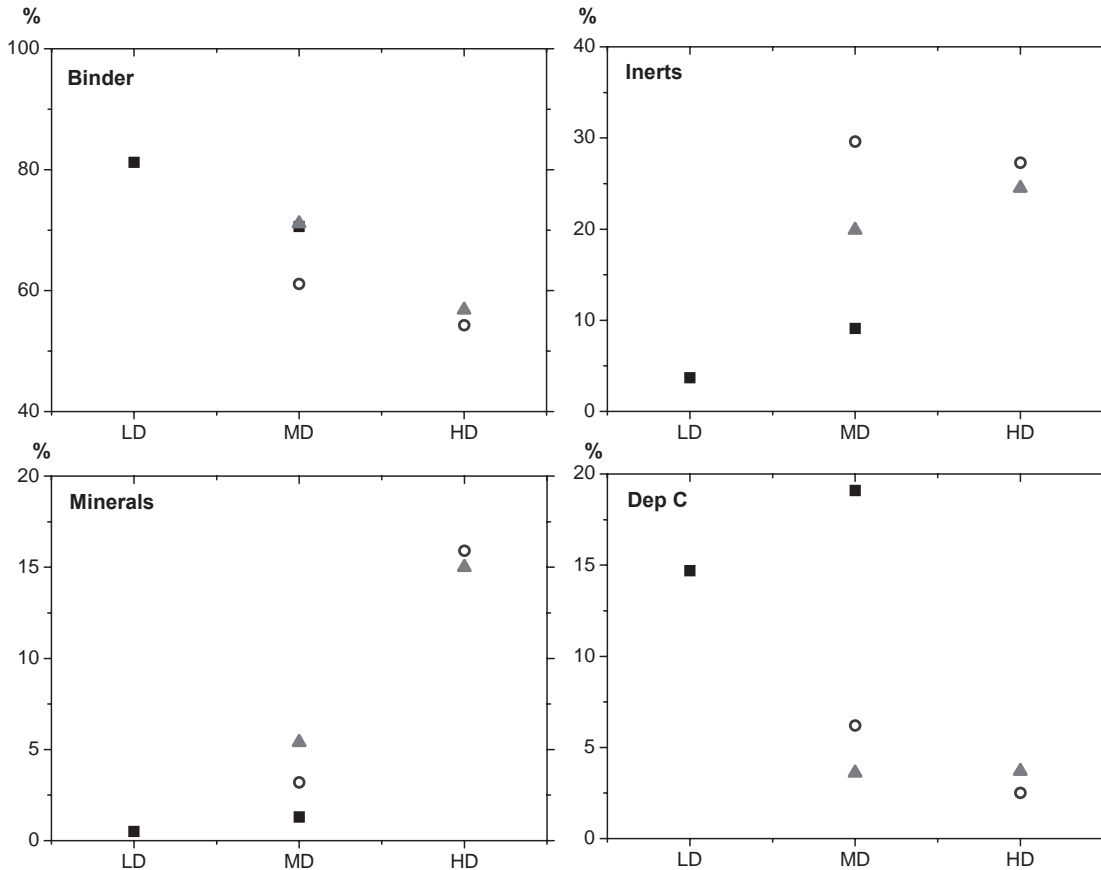


Figure 5.14: Graphical illustration of how binder phase carbons, organic inerts, minerals and depositional carbon (Dep C) vary with specific density. Filled squares (■) are Blue Gem, filled triangles (▲) are Peak Downs and open circles (○) are Staszic.

Microphotographs of microtextures identified in the carbonized samples are presented in Appendix F.

5.6.3 X-ray diffraction

In order to investigate dimensions of the carbon crystallites which the anisotropic domains are consisting of, an X-ray diffraction procedure, which is described in section 4.5.2, has been used. The observed and corrected X-ray profiles for the carbonized fractions are shown in Figure 5.15.

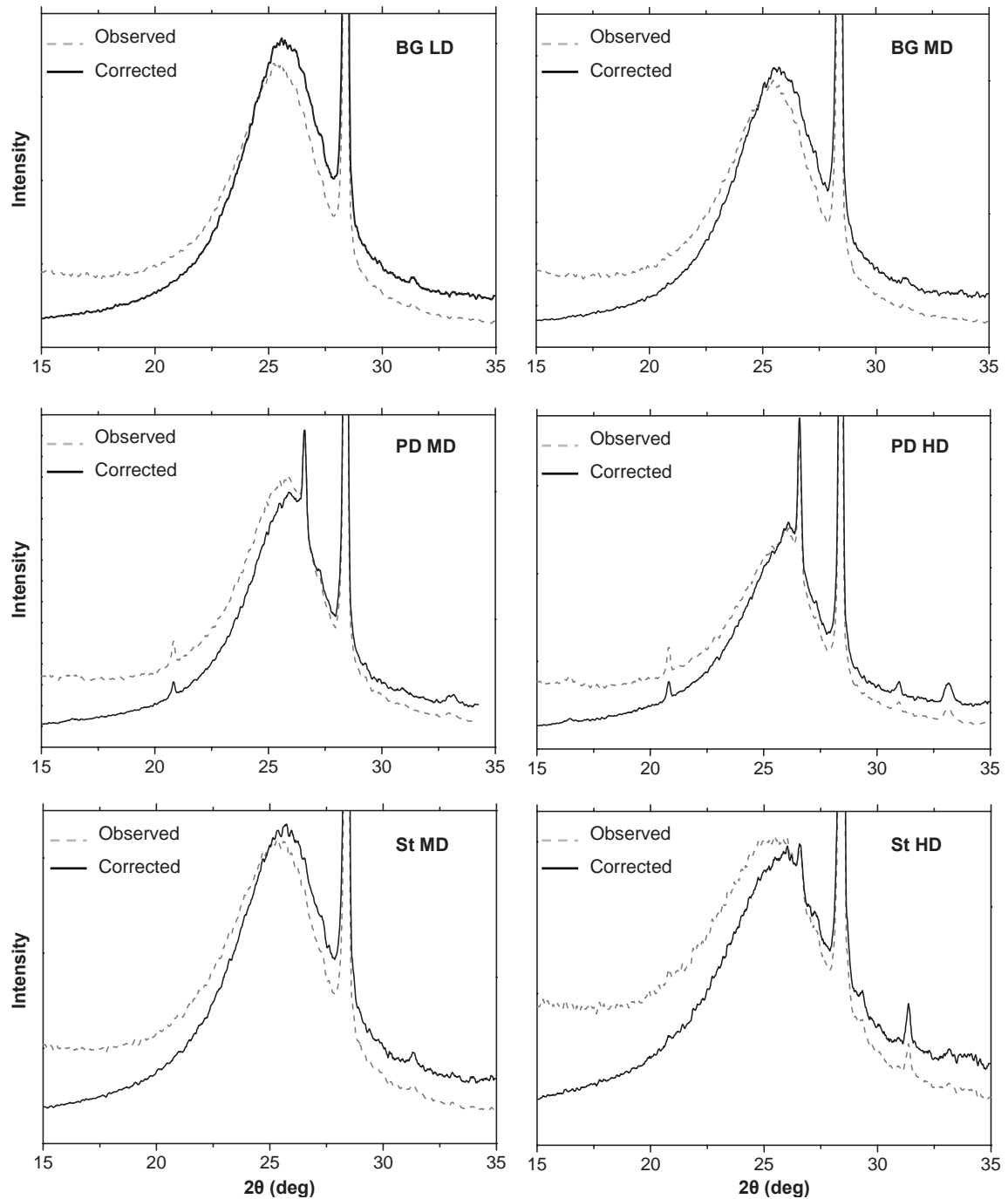


Figure 5.15: Diffraction profiles for the different density fractions of carbonized coals before and after FCT correction. The ordinate axes give an arbitrary intensity, while the x-axes give the value of 2θ in degrees. The profiles are smoothed using the Savitzky-Golay method.

Characteristic dimensions of the carbon crystallites are stack height (L_c) and interlayer spacing (d_{002}) which are illustrated in Figure 3.12. The procedure for calculating these parameters based on the obtained diffraction profiles is described in section 4.5.2.

For carbon compounds mixed with a silicon standard, we expect to find two main peaks – the broad carbon (002) peak and the sharp silicon peak (111). One characteristic feature of the diffraction profiles of the Peak Downs chars are the relatively intense peaks close to top of the carbon peaks. The 2θ values of these peaks are in the range $26.61 - 26.62^\circ$ and are due to the high amount of clastic quartz inclusions in this sample. According to **Kern and Eysel (1993)**, the main diffraction peak of quartz is at a 2θ value of 26.64° which is in good agreement with the observed values.

The disturbances in the profiles of Peak Downs and Staszic in Figure 5.15 are due to mineral inclusions. An indication of the effect of the density separation can be seen as the intensities of these peaks are increasing with density for the respective materials. From the diffraction profiles it is obvious that Blue Gem is a pure material without any noticeable minerals.

The lattice distance (d_{002}) is calculated using the Bragg equation and is based solely on the position of the carbon (002) peak of the intensity corrected diffraction profiles. By using the Scherrer equation, the average crystallite height (L_c) can also be assessed. Both the position and the width, expressed as the Full Width Half Maximum (*FWHM*), of the profiles are parameters in this equation. Intensity corrected diffraction profiles for the highest density fractions of the carbonized samples are compared in Figure 5.16.

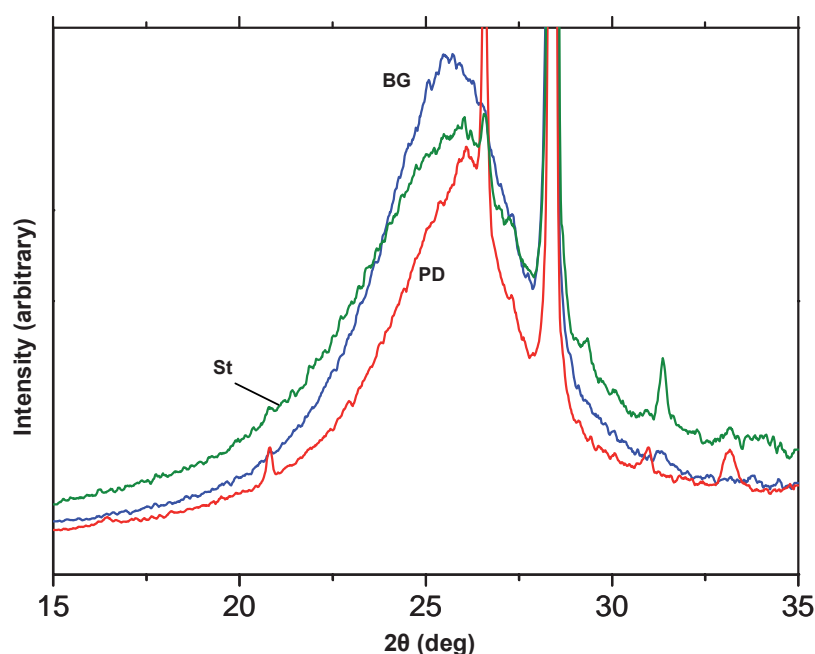


Figure 5.16: Intensity corrected X-ray diffraction profiles for the highest density fractions of each of the carbonized coal samples. Notice the difference in the width of the carbon (002) peak as well as the different peaks caused by mineral inclusions. The profiles are smoothed using the Savitzky-Golay method.

5 EXPERIMENTAL RESULTS

Based on the intensity corrected profiles in Figure 5.16, we would expect Blue Gem and Staszic to have similar values of d_{002} as the carbon peaks are very close, while Peak Downs has a slightly higher 2θ value and should thus have a correspondingly lower value of the interlayer spacing. The tested materials do however have quite different values of $FWHM$, and the crystallite height should thus show more significant differences with the broadest peak giving the smallest crystals.

Calculated dimensions of the carbon crystallites and observed values for $FWHM$ from two parallel runs are presented in Table 5.14.

Table 5.14: Structural parameters calculated from diffraction profiles.

		Blue Gem		Peak Downs		Staszic	
		LD	MD	MD	HD	MD	HD
Parallel 1							
FWHM	°	4.16	4.31	3.93	3.86	4.64	5.35
d_{002}	Å	3.47	3.47	3.45	3.42	3.47	3.46
Lc	Å	19.6	18.9	20.8	21.2	17.6	15.2
Parallel 2							
FWHM	°	4.18	4.31	3.87	3.74	4.50	5.29
d_{002}	Å	3.47	3.46	3.44	3.43	3.48	3.48
Lc	Å	19.5	19.1	22.0	24.2	17.8	15.4
Average							
FWHM	°	4.17	4.31	3.90	3.80	4.57	5.32
d_{002}	Å	3.47	3.47	3.45	3.43	3.47	3.47
Lc	Å	19.6	19.0	21.4	22.7	17.7	15.3

The results given in Table 5.14 are presented graphically in Figure 5.17.

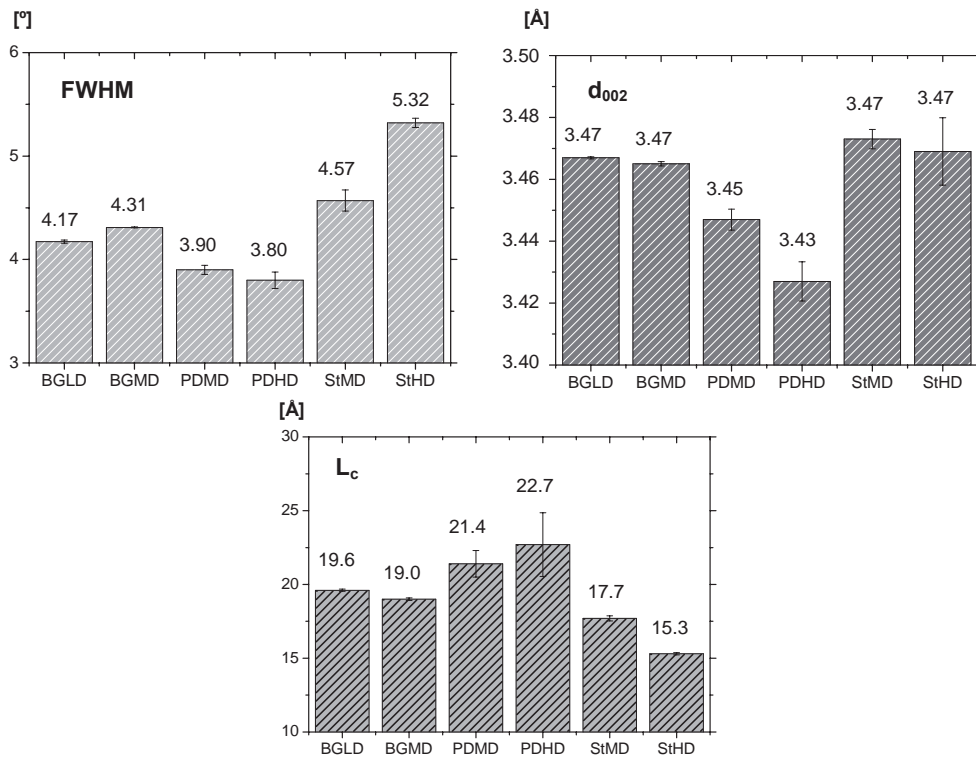


Figure 5.17: Full Width Half Maximum ($FWHM$) values from the intensity corrected diffraction profiles and calculated values for interlayer spacing (d_{002}) and stack height (L_c).

Figure 5.17 reveals that both the largest (highest value of L_c) and densest (lowest value of d_{002}) crystallites are present in Peak Downs. This implies that carbonized samples of Peak Downs have the most graphitic like structure of the tested chars. Chars produced from the high volatile bituminous coal samples have similar values of interlayer spacing with slightly larger crystals in Blue Gem.

L_c and d_{002} values obtained from X-ray data characterize the ordered structure of carbon. These crystallites would be impossible to see in a light microscope, and are thus a supplement to the petrographic procedure for determining optical domains in the binder phase of the carbonized material.

Too few samples have been tested during this work to give any general trends of how the characteristic dimensions of the carbon crystallites vary with composition of the density separated fractions. Based on the results from the available materials, there are no significant differences in the interlayer spacing between the density fractions of the Carboniferous coals. Similar values for stack height are obtained for both Blue Gem samples, while the HD fraction of Staszic results in the smallest crystals. A possible reason for the difference in L_c values between Blue Gem and Staszic can be contributed to the dull structure in the latter sample. The dull structure in Staszic with a large fraction being inertinite macerals might be considered as obstacles during the plastic stage when mobility of the fluid phase is high thus obstructing the ordering of crystallites. This would be particular obvious in the HD fraction as there are more infusible components present. The HD fraction of the char produced from the Permian coal sample both has a denser structure and larger crystals than the corresponding MD fraction.

5.6.4 Physical properties

Microstructure of the carbonized coal samples is believed to influence the reactivity towards gases. A large surface area will provide more available sites for reaction, the pore size distribution will influence the transport of gases to the reactive material and thickness of the pore walls is believed to affect the degree of conversion. Values for surface area and total porosities as well as absolute densities have been obtained using the procedures described in section 4.5.3. Results for all carbonized fractions are given in Table 5.15.

Table 5.15: Physical properties of the chars.

	Blue Gem		Peak Downs		Staszic	
	LD	MD	MD	HD	MD	HD
Total Porosity [%]	50.86	48.93	45.81	46.98	47.30	46.39
Absolute Density [g/cm ³]	1.78	1.79	1.89	1.94	1.79	1.82
Surface Area [m ² /g]	0.67	0.69	0.65	0.96	1.79	1.21

Data presented in Table 5.15 are shown as bar graphs in Figure 5.18.

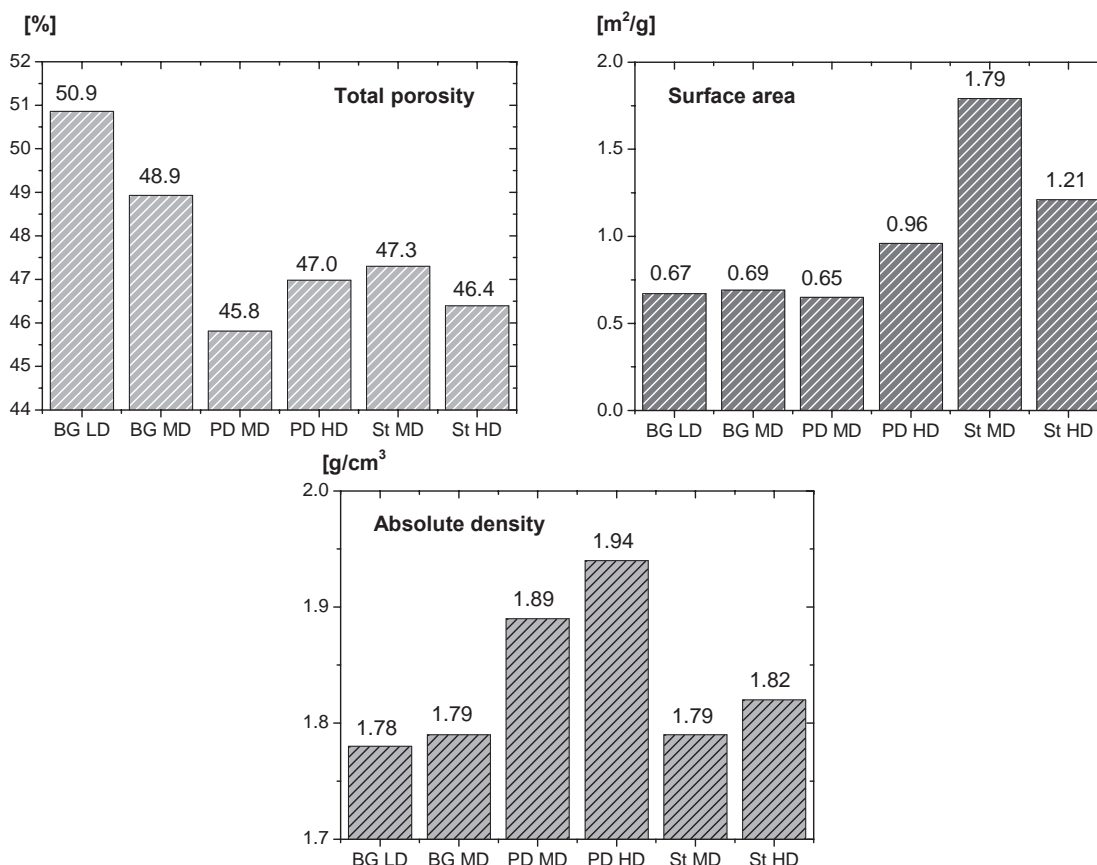


Figure 5.18: Physical properties of the chars.

From the results it can be seen that Blue Gem has the highest total porosity of all the samples. Values for Peak Downs and Staszic are in the same range. The highest density fractions for the Carboniferous coals have a slightly lower total porosity than the lightest fractions. According to the data presented in Table 5.6, the lightest fractions of both sample materials contain higher amounts of liptinites. As these macerals for the most part will decompose to gas during carbonization - hence creating pores, this might be an explanation for the higher values of total porosities. Samples of Peak Downs are showing the opposite trend with a higher porosity in the HD fraction. As there are no liptinites present in this coal which contribute to pore formation, there has to be another explanation. The content of fusinite, which is a maceral with visible pore structure (section 3.4.3), is increasing with density and might contribute to the observed differences between the density fractions.

Staszic clearly has the highest surface area of the analyzed materials, and especially the MD fraction which has almost three times the available surface area in Blue Gem. It is not possible to differentiate the density fractions of Blue Gem based on surface area. The HD fraction of the Australian char showed a higher porosity than the corresponding MD fraction, and the surface area is also higher in this fraction. Surface area in the MD fraction of Staszic is almost 50 % higher than in the HD fraction. If this is due to the higher value of total porosity, we would expect the MD fraction of this material to contain a significant amount of small pores. A possible explanation for the higher

surface area in the MD fraction might be that most of the liptinite macerals are associated with vitrinite in this fraction. This would still be characterized as a dull attrital coal, but during carbonization liptinite macerals are responsible for the formation of pores which contribute to increased surface area. The HD fraction contains a higher ratio of inertinite macerals and minerals. These constituents are contributing to a higher portion of the inhomogeneous structure of this fraction. Infusible macerals and minerals do not contribute in the formation of pores to the same degree as liptinite macerals, and the surface area is thus lower in this fraction.

Carbonized samples from the highest density fractions of the separated coals have the highest values of absolute density.

5.6.5 Pore size distributions and thickness of pore walls

Image analysis (IA) is a widely applied technique used for assessing microstructure of carbonized materials. The method can gather large data sets in the form of digital pictures in a short time thus giving statistically reliable results. Both size and shape of pores as well as pore wall thickness and in some cases degree of crystallinity can be analyzed. Resolution of the microscope is a restriction of the method, and only pores larger than about 5 μm can be analyzed with precision.

As described in section 4.5.1, the carbonized material was impregnated with a fluorescent epoxy resin which penetrated the open pores. Closed pores were not impregnated by the epoxy and appeared dark under the microscope. Porosity values from the IA are given as percentage of the particle surface. In the present work image analysis techniques were applied to measure pore size distribution of open- and closed pores as well as thickness of the pore walls.

Pore size distributions of pores open for impregnation by the fluorescent epoxy are given in Figure 5.19.

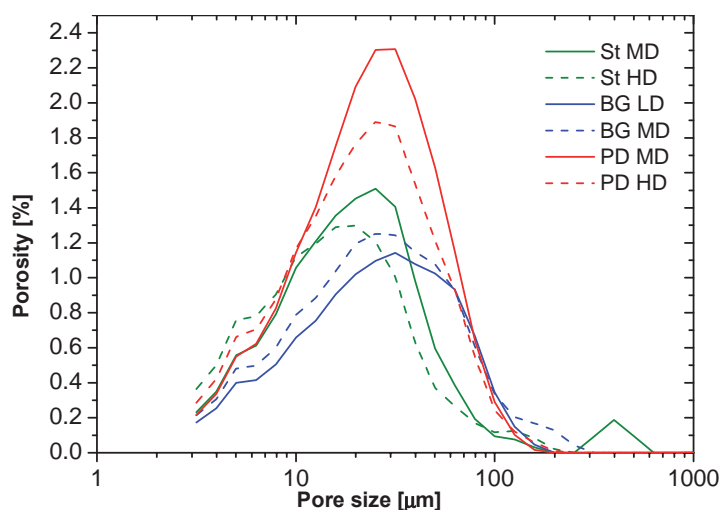


Figure 5.19: Pore size distributions of pores open for impregnation of fluorescent epoxy of the carbonized coal samples.

Measurements of open pores are fairly accurate as the contrast between the fluorescent epoxy and the carbon texture is high.

Based on the graphs in Figure 5.19, it can be seen that distribution of the pores are similar for all the samples. The majority of pores in all fractions are in the range 10 – 100 μm . Peak Downs has the highest amount of open pores with a slightly higher value for the MD fraction. The distributions have their peaks at about 30 μm which is an indication that most of the pores are in this order of magnitude. The distributions of open pores are fairly similar for both fractions of Blue Gem, which prove to have the lowest values of open pores. Distribution peaks are at slightly higher values than for Peak Downs. Values for total open porosity in the Staszic samples are intermediate, but the peaks tend to be at a lower value. A higher amount of smaller pores might be an indication of the high surface area of this material. One pore with a size of approximately 400 μm is responsible for the peak observed for the MD fraction.

The pore size distributions for closed pores are illustrated in Figure 5.20.

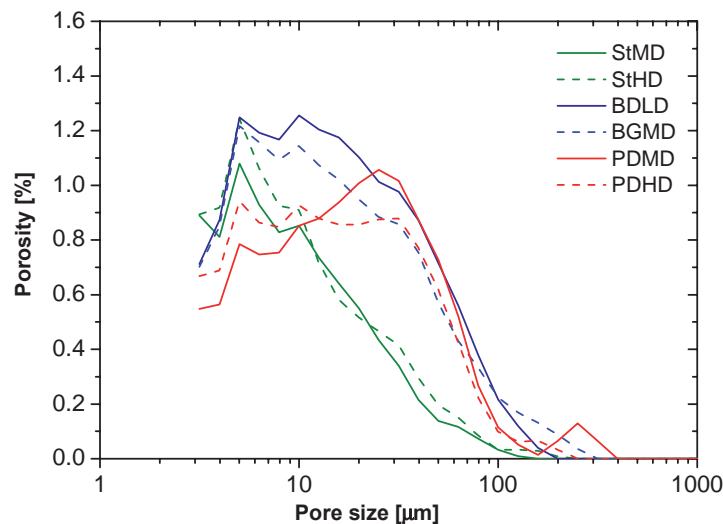


Figure 5.20: Pore size distributions of pores closed for impregnation of fluorescent epoxy of the carbonized coal samples.

Determination of closed pores by the image analysis technique is prone to higher inaccuracy than for open pores, and is more dependent upon preparation. The reason for this is that closed pores appear dark under the microscope. Contrast to the carbon texture is thus not as good as for the impregnated pores and relief or other flaws during preparation of the polished samples might be misinterpreted as closed porosity.

Based on the graphs in Figure 5.20, there are no clear peaks in the distributions and they are oscillating more than the corresponding distributions for open pores. All the materials contain pores from the detection limit of the microscope to about 100 μm . One large pore is identified in the MD fraction of Peak Downs. Distributions for Blue Gem and Peak Downs are similar with a slightly higher ratio of small pores in the former material. The most obvious trend in Figure 5.20 is that the distributions of closed pores in Staszic are shifted towards the smaller sized pores compared to the other materials.

In order to evaluate the total porosity distributions of the carbonized materials, distributions for open- and closed porosities are combined and plotted in Figure 5.21.

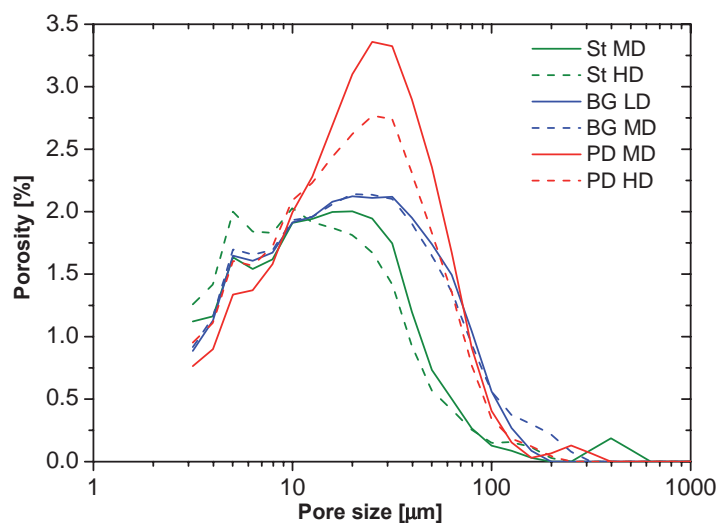


Figure 5.21: Pore size distributions of all pores of the carbonized coal samples.

As pores in the carbonized material develop during the plastic stage of carbonization, the observed differences in pore size distributions are related to processes in this temperature interval. Peak Downs has the highest porosity in the size interval analyzed by the IA method and according to data presented in Table 5.1 this coal has the widest plastic range which allows pores to coalesce and grow. The Carboniferous coal samples are of the same rank and can not be differentiated based on plastic properties. The pore size distributions are however quite different with Staszic tending to have a higher ratio of small pores. This difference has to be attributed to the structure of the coals. Staszic is an inhomogeneous coal with numerous inclusions of infusible macerals and minerals which influence both the size and orientation of the generated pores. Blue Gem is on the other side a very homogenous coal in which the pores are free to expand without any constraints.

Cumulative values for open-, closed- and total porosity analyzed by image analysis are presented in Table 5.16.

Table 5.16: Porosity of the char samples evaluated by the IA procedure

	Blue Gem		Peak Downs		Staszic	
	LD	MD	MD	HD	MD	HD
Open Porosity [%]	11.6	13.1	19.4	17.2	13.3	12.2
Closed Porosity [%]	14.8	13.7	12.0	11.6	8.7	9.5
Total Porosity [%]	26.4	26.8	31.4	28.8	22.0	21.7

There are no distinct differences between the density fractions of Blue Gem and Staszic. Regarding Peak Downs, the MD fraction has the highest porosity. As vitrinite is regarded as a reactive maceral which fuses during carbonization and contributes to the formation of pores, the higher ratio of this maceral is believed to be the reason for the observed differences in porosity. Total porosity values from the image analysis are consistently lower than the results obtained with a pycnometer (see Table 5.15). One

reason for this is that pores that are smaller than the detection limit of the microscope contribute significantly to the total porosity measured with a pycnometer.

In addition to pore size distributions, the image analysis also assessed the distances between the pores. This parameter directly describes the thickness of pore walls and is believed to be of importance in determining parameters related to the reactivity towards SiO gas. As reaction between carbon and SiO gas produces a coherent layer of silicon carbide which the gases have to diffuse through in order for the reaction to progress, the thickness of pore walls have a direct impact on the length of diffusion before the carbon is fully converted.

Cumulative distributions of distances between pores for the carbonized fractions are presented in Figure 5.22.

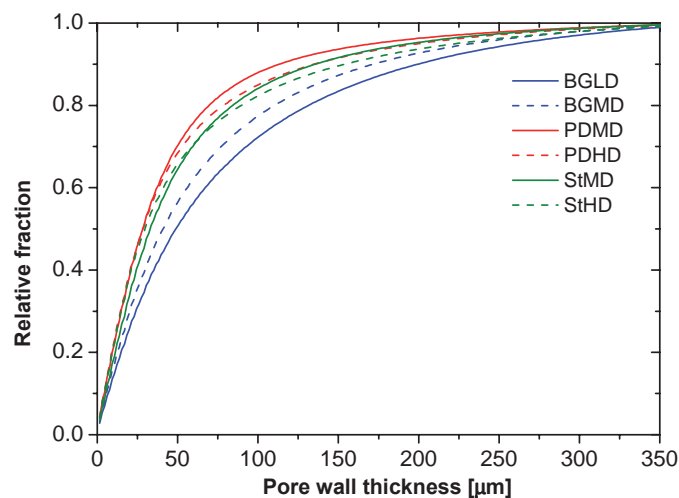


Figure 5.22: Relative fractions of pore wall thickness in the carbonized samples.

Although the graphs seem to be pretty well grouped in Figure 5.22, there are actually large differences in the pore wall thickness. As an example, 50 % of the pore walls in the LD fraction of Blue Gem have a thickness of less than 50 μm while the corresponding value for the MD fraction of Peak Downs is 70 %. Based on the data presented in Figure 5.22, the highest ratio of thin pore walls are found in Peak Downs. Distributions of both fractions of Staszic indicate that the carbonized samples have slightly thicker pore walls than Peak Downs. Blue Gem contains the highest ratio of thick pore walls, with the highest percentage in the LD fraction.

Pores in the carbonized material can be classified based on size and according to **Price (2005)**, the size range covered by the image analysis constitute mainly of coarse pores ($> 20 \mu\text{m}$). According to **Szekely et al. (1976)**, transport of gaseous species through the porous network in a solid material plays an important role in gas – solid reactions. Pores detected by IA can be compared to highways into the interior of the carbonized materials and most of the gas transport is due to convection. In order for the conversion of the material to be high, the reactive gases have to be further distributed to the carbon structure. It is thus of importance to analyze the network of smaller pores.

Mercury intrusion is a procedure which is commonly used to evaluate macro porosity (according to the definitions in section 3.5.5) of materials.

The pore size distributions of the carbonized materials from mercury intrusion are obtained according to the procedure described in section 4.5.4 and the results are given in Figure 5.23.

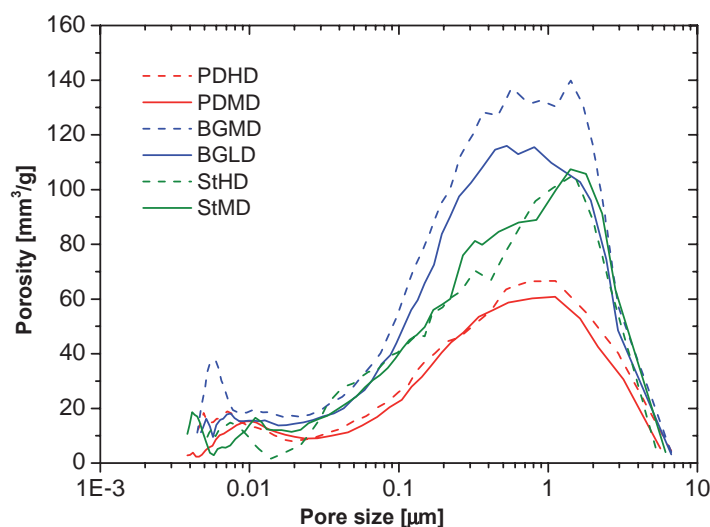


Figure 5.23: Pore size distributions from Hg-porosimetry.

According to the results in Figure 5.23 pore sizes from approximately 5 nm to almost 10 µm are analyzed by the mercury intrusion procedure. Accuracy of the measurements in both ends of the size range is however not good. In order to penetrate the smallest pores in the material, the pressure of mercury has to be very high. This will modify the porous structure by breaching of pore walls and thus the results at this end of the size range are not in compliance with the original microstructure of the material. According to **Marsh (1989)**, the lower limit for mercury porosimetry is set at 76 nm. Results from the analysis show that the porosity has a sharp decline at pore sizes larger than approximately 1 - 2 µm. The reason for this sharp decline in all tested materials is connected to the wetting of pores in this size range by mercury at atmospheric pressure. Values for porosity measurements above 1 - 2 µm are not trusted to be reliable.

A comparison of the total pore size distribution obtained by IA (Figure 5.21) with results from the mercury intrusion procedure reveals that Peak Downs, which has the highest amount of coarse pores, has the lowest content of macro pores. Blue Gem proved to have the highest values with the peak at about 1 µm for both fractions. Staszic has intermediate values for macro porosity with most of the volume contained in pores with sizes of approximately 2 µm.

In order to compare the total volume occupied by macro pores, cumulative pore size distributions are plotted in Figure 5.24.

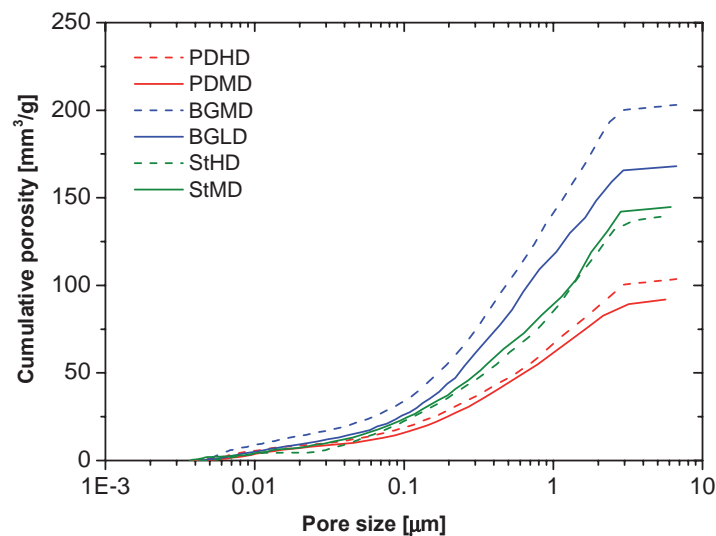


Figure 5.24: Cumulative porosity in carbonized samples from Hg-porosimetry.

From Figure 5.24 it can be seen that the MD fraction of Blue Gem, which has the highest value of total porosity in the size range covered by the mercury intrusion procedure, contains about twice the amount of pores as the Peak Downs samples. The density fractions of Staszic are almost identical and have intermediate values. During his doctoral work, **Myrhaug (2003)** measured the pore size distributions of both fossil- and biological carbon materials by mercury intrusion. Values for cokes and calcined coals are slightly higher than the reported values in Figure 5.24 in the same range of pore sizes. The charcoal samples do however have a wider range of macro porosities with the most porous material having a value for cumulative porosity approximately ten times higher than the MD Blue Gem sample.

In conclusions, both the image analysis technique and the mercury intrusion method give valuable information about size distribution of pores. The image analysis seems to be particularly well suited for measuring coarse pores and especially pore size distributions for pores larger than approximately 10 μm . Measurements of closed pores are also possible by this method. The macro pores generally denotes pores that are available to gases for diffusion into the carbonaceous structure and will thus be very important for the reactivity towards SiO gas and the effective diffusivity of the material. Mercury intrusion is well suited for analyzing macro pores in the size range 20 nm to approximately 1 μm . Based on the procedures used to acquire pore size distributions in this work, pores in the size range 1 – 10 μm are not properly analyzed. According to **Stenstad (2007)**, this could have been avoided by using a low pressure mercury porosimetry procedure. By the use of this procedure, pore sizes up to 50 μm could have been analyzed with precision.

5.7 SINTEF SiO- Reactivity

The third part of this work involved exposing the carbonized samples to SiO gas under controlled conditions in order to evaluate the reactivity of the materials. As discussed in section 2.3, there are several possible methods in which the SiO reactivity can be assessed. In this work, the SINTEF SiO reactivity test has been exclusively used. The SINTEF SiO reactivity test has been commercially available since the development in the 1970's. In a paper where carbon reactivity tests for various ferroalloys were evaluated, only the SINTEF procedure was mentioned for the production of silicon and ferrosilicon production. **Pistorius (2002)**.

Coal and carbonization products like char or coke are heterogeneous by nature. Repeatability has always been a major challenge in dealing with reactivity measurements of inhomogeneous materials. The SINTEF SiO reactivity test was recently revised and improved. According to **Lindstad et al. (2007)**, the reproducibility of the test is currently better than 10 % for all samples ranging from highly reactive charcoal to relatively inert cokes. Even though all of the reactivity tests in this work were carried out in the improved version of the test, a minimum of two parallel runs were conducted for each density fraction of the carbonized materials.

The reactivity of a carbonaceous material is evaluated based on the *R10 corrected* value. This value expresses the amount of SiO gas in volume (ml SiO) which passes the reactor chamber (in which the carbon material is placed) without being converted to SiC as the concentration of CO in the outlet gas decreases from 18 - 10 %. The apparatus, procedure and reactivity measures used in the SINTEF procedure are described in section 4.6. Corrected values of *R10* are calculated from the CO concentration profiles which are corrected for the back reaction in the condensing chamber (see *reaction -1.12*). Corrected values are not calculated until the measured CO concentration in the off gas drops below 18 %. As the original curves might contain information about the material composition which will not be included in the corrected profiles, both the measured relationship between time and CO concentration as well as the corrected graphs are given for all the tested density fractions in Figure 5.25.

5.7.1 CO – concentration as a function of time

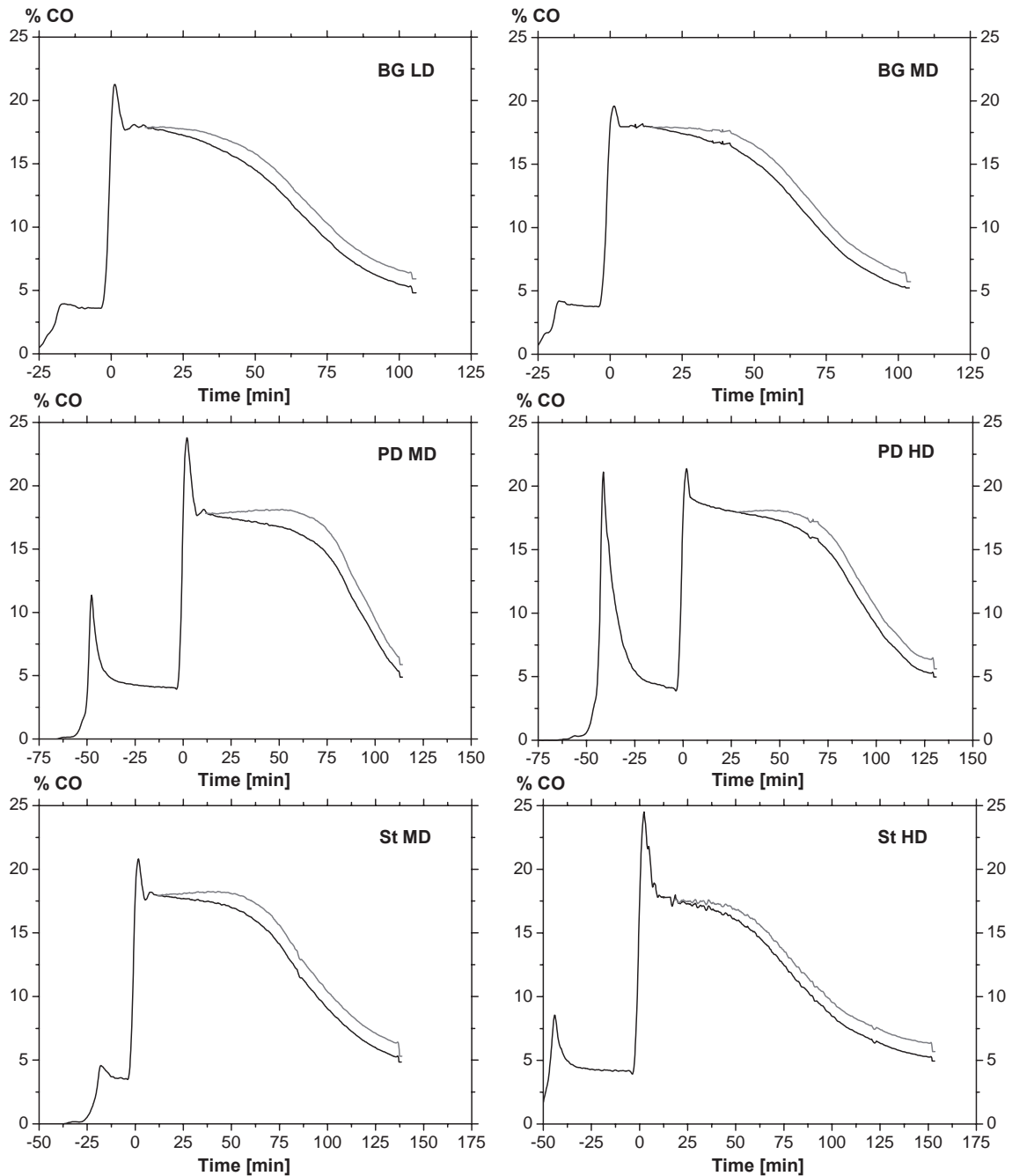


Figure 5.25: CO concentration as functions of time for the carbonized coal fractions. Measured CO concentration is given as black graphs while corrected CO level as a function of time is illustrated as grey curves. The profiles are smoothed using the Savitzky-Golay method.

In Figure 5.25 relations between measured curves and corrected profiles are compared for the different density fractions of the tested materials. Notice that the time scale is identical for density fractions of the same material, but varying between sample materials of different origin. Initiation of the test (time = 0) is defined as the time when the CO level first exceeds 18 % at a temperature above 1550°C.

As long as the CO level remains at 18 %, all of the produced SiO gas is converted to SiC according to *reaction 1.5*. Condensation of SiO gas according to *reaction 1.6* can not occur until some SiO gas is passing unreacted through the reaction chamber, which is detected by a drop of the measured concentration of CO in the outlet gas. Presence of silicon in the condensing chamber is a requirement for correction of the CO concentration (see *reaction -1.12*). As can be seen from the plots, onset of the corrected curves is identical to the time where the measured concentration of CO drops below 18 %. The designated end point of the test is when the measured CO level in the outlet gas is 5.2 %. As can be seen from the plots in Figure 5.25, gaps between the measured and corrected curves seem to be of the same magnitude at this point. According to equation 4.17, the value for the corrected curve should be 6.3 %, and this value is observed in all the tests.

The corrected profiles are used to calculate the reactivity measure from the SINTEF test (*R10 corrected*), and will be further dealt with in the next section.

As part of the SINTEF test procedure, the sample is heated to approximately 1500°C to reduce a maximum amount of minerals without exceeding the temperature for SiO generation. A high amount of reducible mineral inclusions at this temperature will lead to a sharp peak of measured CO in the outlet gas. Based on the measured profiles in Figure 5.25 large differences between both different density fractions and sample materials of different origin are observed.

Blue Gem has been characterized as a very homogeneous coal of high grade (i.e. low amount of impurities) both by chemical- and petrographical analyses. The reduction peaks from the SINTEF test is also in compliance with these results and the two density fractions can not be differentiated on this basis.

From the proximate analysis (Table 5.1), it can be seen that Peak Downs is the sample material with the highest amount of minerals. Based on the non-maceral analysis, a large amount of the minerals in this material was determined to be incorporated in the coal matrix rather than being discrete. Morphological studies also revealed numerous quartz inclusions in Peak Downs. These inclusions should however not contribute to the pre-reduction peak as there is no reaction between quartz and carbon under these conditions. The strong reduction peaks in both fractions of the tested samples do however indicate that there are large quantities of reducible minerals as well. Peaks of the HD fractions were stronger than the corresponding MD fractions and reached a value exceeding 20 % in both parallels.

Staszic is determined to be a very heterogeneous coal sample where macerals of different origin and minerals are well agglomerated. Petrographical analyses of both coal (Table 5.6) and the carbonized samples (Table 5.12) show that the amount of mineral matter is significantly higher in the highest density fraction. The pre-reduction peaks during the SINTEF test also had higher values for the HD fractions.

Reactivity curves for all the tested parallels are available in Appendix G, and data from reactivity experiments are presented in Appendix I.

5.7.2 Time adjusted corrected reactivity curves

The factor for evaluating kinetics in the reaction between carbon and SiO gas according to *reaction 1.5* is termed *R10 corrected* in the SINTEF procedure. This factor is directly calculated from the relationship between the corrected concentration of CO and time, and is illustrated in Figure 4.11. As the reactivity measure is an integral between 18 % and the corrected profile in the interval where the CO concentration is between 18 – 10 %, shapes of the corrected profiles can give valuable information about the reactivity of the materials. A material which has a steep slope in this interval will render a low value of *R10 corrected* and thus be characterized as a reactive material. The opposite is true for materials with gentle slopes.

From Figure 5.25 it can be seen that the corrected profiles have a range of variation in both time of onset and especially when the profiles are in the range of interest for calculation of the *R10 corrected* parameter. In order to compare the slopes and shapes of the corrected profiles, they were adjusted for time so that all of them are intersecting 12 % CO at the same time (90 minutes). This value was chosen as it is close to the point of inflection for most of the profiles. The time adjusted corrected reactivity curves are plotted in Figure 5.26.

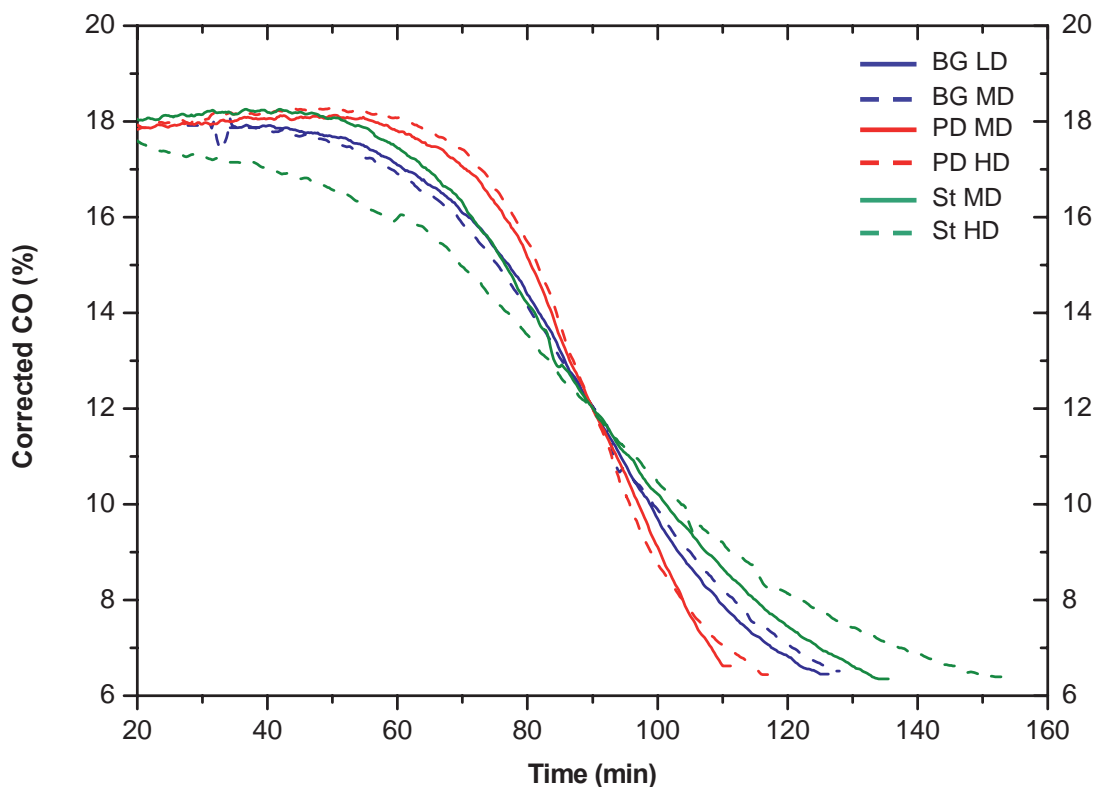


Figure 5.26: The corrected CO profiles are time adjusted to intersect 12 % CO at the same time.

As can be seen from the figure, the reactivity profiles of the tested materials can generally be grouped in three categories. Peak Downs has the highest rank of the tested sample materials, and should according to previous investigations be the least reactive material. Both fractions of Peak Downs do however have similar shapes and slopes, and

are classified as the most reactive materials in this work. Blue Gem and Staszic are both of similar rank (see Figure 5.8), but have significantly different maceral compositions. From Figure 5.26, it can be seen that both fractions of Blue Gem as well as the MD fraction of Staszic show similar behaviour during the course of reaction and are regarded as fairly reactive materials. The HD fraction of the Polish coal does however stand out as the least reactive material as the slope of the corrected profile is the most gentle of all the tested materials and constitutes the third category.

5.7.3 R10 corrected values

As discussed in the previous section, kinetics in the reaction between carbon and SiO gas is characterized by the *R10 corrected* parameter. This parameter is calculated according to equation 4.18 where the corrected CO profiles are plotted in Figure 5.26. Reactivity values for the tested materials are illustrated as an average of two parallels with the standard deviation indicated in Figure 5.27.

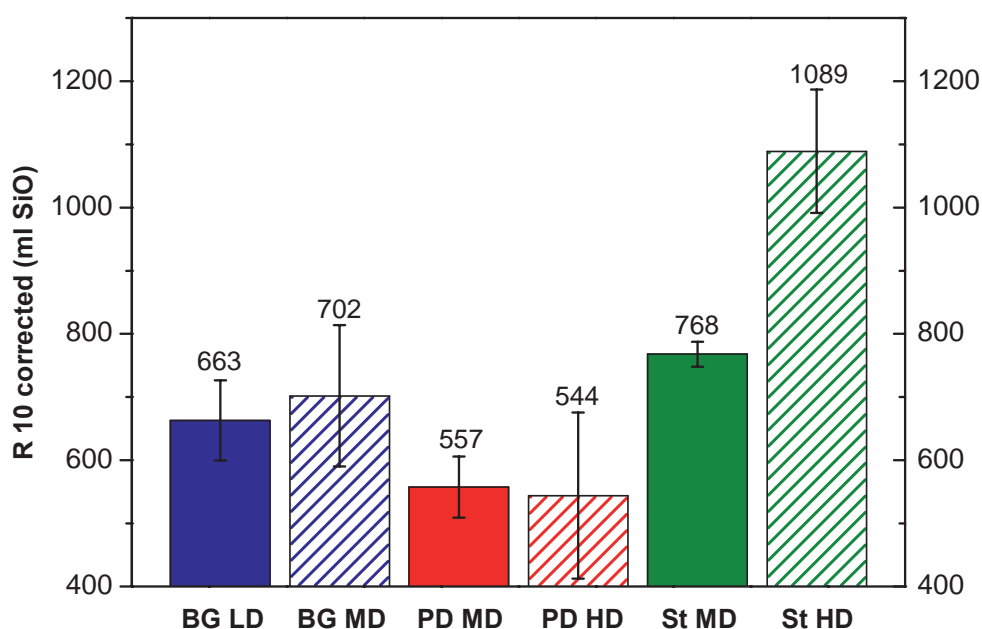


Figure 5.27: R10 corrected values for the density fraction of the tested materials.

When the results from Figure 5.27 are evaluated, it is important to keep in mind that a high value of *R10 corrected* is indicating a material with a low reactivity towards SiO. Based on the calculated reactivity values given in Figure 5.27, distinct differences can be seen between the tested materials.

Blue Gem is a homogeneous coal and analyses of both coal and carbonized samples have proven that fractions of Blue Gem are hard to distinguish. Based on coal petrographic procedures (section 5.4), there is a slightly higher ratio of pseudovitrinite in the MD fraction while the lowest density fraction has a higher content of liptinite macerals. Both fractions are scarce in inertinite macerals and mineral inclusions. Petrographic determination of texture in the carbonized material revealed that the LD fraction is containing a higher amount of binder phase. Filler phase microtextures and minerals are slightly more abundant in the MD fraction. Even though both fractions

have significant amounts of depositional carbons, there was a higher portion of these in the MD fraction. Depositional carbons have a dense structure similar to carbon black and are believed to retard the reactivity towards gases. Based on the *R10 corrected* values in Figure 5.27, the MD fraction has a slightly higher average value. Due to the standard deviation of 9.6 % and 15.9 % for respectively the LD- and MD fraction, the samples can not be separated based on the reactivity values. Both fractions are regarded as fairly reactive.

Previous studies (see section 2.3) have proven that rank correlates well with reactivity towards SiO gas. As Peak Downs is medium volatile bituminous of rank ($R_r = 1.32$ %) while the other samples in this work are of lower rank, the Permian sample was expected to give the highest values of *R10 corrected*. As can be seen from Figure 5.27, Peak Downs actually proved to be most reactive of the tested materials. Petrography of the coal samples revealed that the HD fraction of this material had the highest amount of both inertinite macerals and minerals as well as a higher ratio of fines. In addition, the texture was more inhomogeneous. Analyses of the carbonized fractions verified these findings with the highest amount of binder phase as well as a lower ratio of both filler phase and minerals in the MD fraction. Evaluation of physical properties of the carbonized material (i.e. char structure), showed that the lowest density fraction had the highest coarse porosity and lowest distances between pores. The results of these analyses indicate that there should be a noticeable difference in the reactivity of the two density fractions. The reported *R10 corrected* values for the two fractions are however almost identical and due to the relatively large standard deviation, the two fractions can not be told apart based on reactivity values. Peak Downs is regarded as a highly reactive material, and the main reason for this is believed to be due to the quartz inclusions.

Staszic is of the same rank as Blue Gem, but compositions of the two Carboniferous coal samples are distinctly different. Petrographic analyses have shown that Staszic is a very dull coal. Based on the maceral composition (Table 5.6), the MD fraction contains a higher amount of vitrinite and liptinite macerals than the corresponding HD fraction. The content of inertinite- and mineral inclusions are however significantly higher in the highest density fraction. Both fractions can be regarded as dull compared to the other sample materials, but the HD fraction is the most inhomogeneous. Attrital coal is classified as bright, intermediate and dull based on the volumetric abundance of macerals and minerals associated with vitrinite. The categorization does not separate between origins of the agglomerated constituents. Based on the standard maceral analysis and results from the non-maceral microtextures, a higher amount of dull coal in the highest density fraction is believed to consist of inertinite macerals and minerals, while liptinites are more commonly associated with vitrinite in the MD fraction. Analysis of coke carbon forms (Table 5.12) showed that the level of binder is slightly higher in the MD fraction while contents of infusible inert macerals have similar values in both fractions. The HD fraction does however contain a significantly higher amount of minerals. Regarding the char structure, the MD fraction of Staszic proved to have the highest surface area of all the analyzed samples – almost 50 % higher than the HD fraction. Significant differences between the two fractions of Staszic have been identified through analyses and these are expected to influence the measured reactivity values. As can be seen from Figure 5.27, the lowest density fraction has an average *R10*

corrected value slightly higher than the two fractions of Blue Gem and can be characterized as fairly reactive. The HD fraction does however have the highest value for all the tested samples and is the only investigated fraction that is characterized as a low reactive material.

Based on the tested samples, the repeatability is varying to a high degree. The highest value of standard deviation is reported from testing the HD fraction of Peak Downs with a value of 24.2 %. If this value is discarded, the average standard deviation in this work is 9.2 % and thus barely within the 10 % limits reported by **Lindstad et al. (2007)**.

5.7.4 Degree of conversion

In industrial production of silicon metal, the operation is not only dependant upon reactivity of the materials, but also on the degree of conversion. The *R10 corrected* value gives information about the ability a reduction material has to “filter” SiO gas which is an intermediate compound in the process. This value does not give any information about the conversion of the materials. When unreacted carbon from the upper part of the furnace is entering the crater zone of the furnace, SiO gas will react with carbon according to *reaction 1.5*, eventually causing a decrease in the silicon yield. In order to evaluate the suitability of a reduction material for the silicon process both reactivity and degree of conversion should be considered.

One of the improvements in the revised SINTEF test is that the degree of conversion is chemically analyzed and reported on the same basis as the reactivity measure. The carbonized samples are analyzed for total- and free carbon before and after the reactivity test. The degree of conversion is subsequently calculated according to equation 5.11:

$$X = \frac{2 \cdot (C_{2,tot} - C_{2,free}) \cdot m_2}{C_{1,tot} \cdot m_1} \cdot 100\% \quad (5.11)$$

where C_{tot} and C_{free} are total- and free carbon, respectively. Mass of the tested sample is denoted m and the indices 1 and 2 to refer to before and after the test, respectively.

In the original SINTEF reactivity test, the degree of conversion was evaluated solely on the measured weight increase during reaction. The maximum obtainable theoretical weight increase is calculated from reaction 1.5:

$$\frac{m_2 - m_1}{m_1} = \left(\frac{Mm_{SiC}}{2 \cdot Mm_C} - 1 \right) \cdot 100\% = 67\% \quad (5.12)$$

where Mm_{SiC} and Mm_C are the molecular masses of silicon carbide (40.1 g/mol) and carbon (12.0 g/mol), respectively. This value is only obtainable if the reductants consist of pure carbon and is totally converted. Mineral inclusions in the tested materials are synonymous with a decreased amount of carbon available for reaction. In addition some carbon will be consumed by reduction of the minerals. For reduction materials low in

minerals, measurements of weight increase can correlate well with conversion. In order to calculate the degree of conversion with precision for all reduction materials, the analytical procedure in the SINTEF procedure should be followed.

In order to evaluate the degree of conversion in the modified SINTEF test, analyses of total- and free carbon are conducted by an external laboratory. These are both costly and time consuming, and the degree of conversion has in this work thus been evaluated based on weight increase and morphological studies of the reacted samples.

Weight increase for the tested materials are illustrated as an average of two parallels with standard deviations indicated in Figure 5.28.

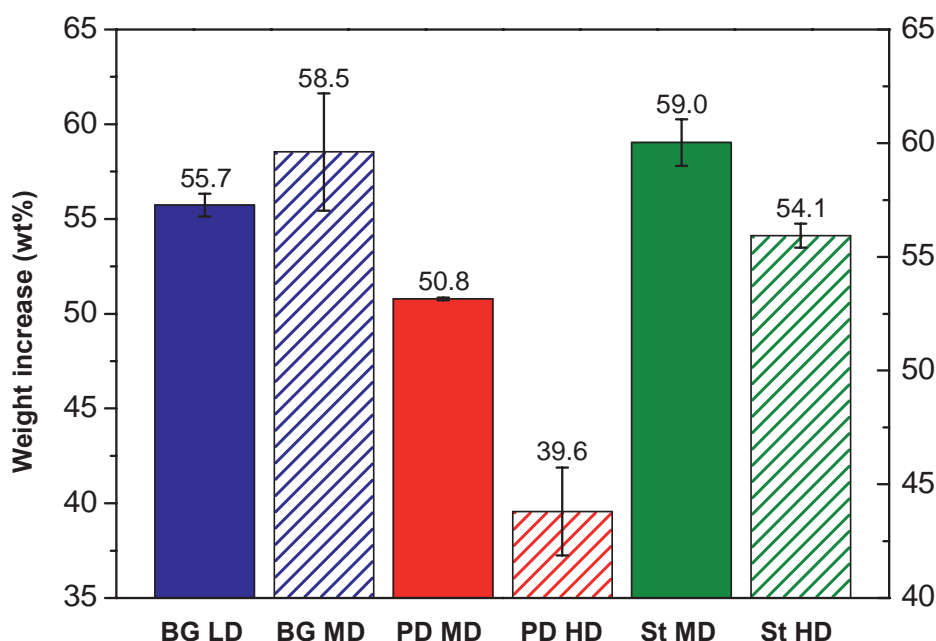


Figure 5.28: Measured weight increase for the reactivity tested materials.

As can be seen from Figure 5.28, none of the tested samples are close to the theoretical limit of 67 % weight increase. The sample materials are however natural heterogeneous fossil materials and conversions of 100 % can not be expected based on measurements of weight increase.

Mineral inclusions in fractions of Blue Gem are scarce and are not believed to be the reason for incomplete conversion based on the measured weight increase. Figure 5.28 reveals that the MD fraction of Blue Gem has a higher average conversion than the corresponding LD fraction. The main differences between the fractions were mentioned in the previous section, but the factor contributing to the relatively large dissimilarities when it comes to degree of conversion is the pore wall thickness. From Figure 5.22 it can be seen that the pore wall thickness in the lowest density fraction of Blue Gem is the largest of all the analyzed materials. By assuming that all the pores are open and available for SiO gas, large distances between pores imply that the gas will have a substantially thicker layer of silicon carbide to diffuse through before it will meet unreacted carbon. Even though the MD fraction of Blue Gem also has relatively thick

pore walls, this parameter is believed to be the main reason for the observed difference in weight increase.

Based on the measured weight increase, the MD- and HD fractions of Peak Downs would have conversions of 75.8 % and 59.0 %, respectively. This sample material does however contain the highest amount of mineral inclusions (see Table 5.1). Numerous inclusions of clastic quartz were identified during the morphological studies of this coal. These inclusions were harder to identify in the carbonized samples, but as the temperature during carbonization did not exceed 1200°C, quartz inclusions will remain in the material. During counting of microstructures in the carbonized samples, relatively high amounts of minerals were identified, especially in the HD fraction. Presence of these minerals will reduce the calculated weight increase. In addition, the reactivity profiles in Figure 5.25 prove that there is a high amount of reducible minerals. These will consume carbon and hence reduce the amount of carbon available for reaction with SiO gas. The observed difference in weight increase between the density fractions is due to the higher amount of minerals in the highest density fraction.

The highest weight increase of all the tested materials is observed for the MD fraction of Staszic. The degree of conversion is close to 90 % based on the measured increase in weight during reaction with SiO gas. Minerals have been identified during petrographic analyses of both coal- and carbonized samples with the majority in the highest density fraction. Measured CO levels during pre-reduction of the samples (Figure 5.25) show that reducible minerals are relatively more abundant in the HD fraction. Thin pore walls as well as the highest available surface area of the tested materials are structural properties that might indicate a high degree of conversion. The higher content of minerals in the HD fraction is believed to account for the observed difference in weight increase.

In order to have a supplement to the measured data for weight increase, morphological studies of the reacted materials were performed. Polished pellets of the reacted materials were prepared and subsequently examined by use of a petrographic microscope (See Figure 4.5). Settings of the microscope were identical as during the coke petrographic procedure which is described in section 4.2.4. Use of crossed polarized light and a tinted gypsum plate made identification of the different constituents in the reacted samples possible. From coke petrography it is known that binder phase carbon forms display a range of microtextures from optically isotropic to anisotropic. Filler phase microtextures are identified based on shape, size, texture, relief and association with other components. Infusible macerals are usually isotropic while minerals might have a range of anisotropies dependant on the crystal structure. As silicon carbide is isotropic under the microscope, the reaction front is easily observable in anisotropic binder phase microtextures. The differentiation is harder between reacted material and organic filler phase components and isotropic binder phase carbon forms.

During morphological studies of the reacted samples, identification of typical features of the sample materials was the main objective and differentiation between density fractions are thus not made in the following microphotographs.

Blue Gem

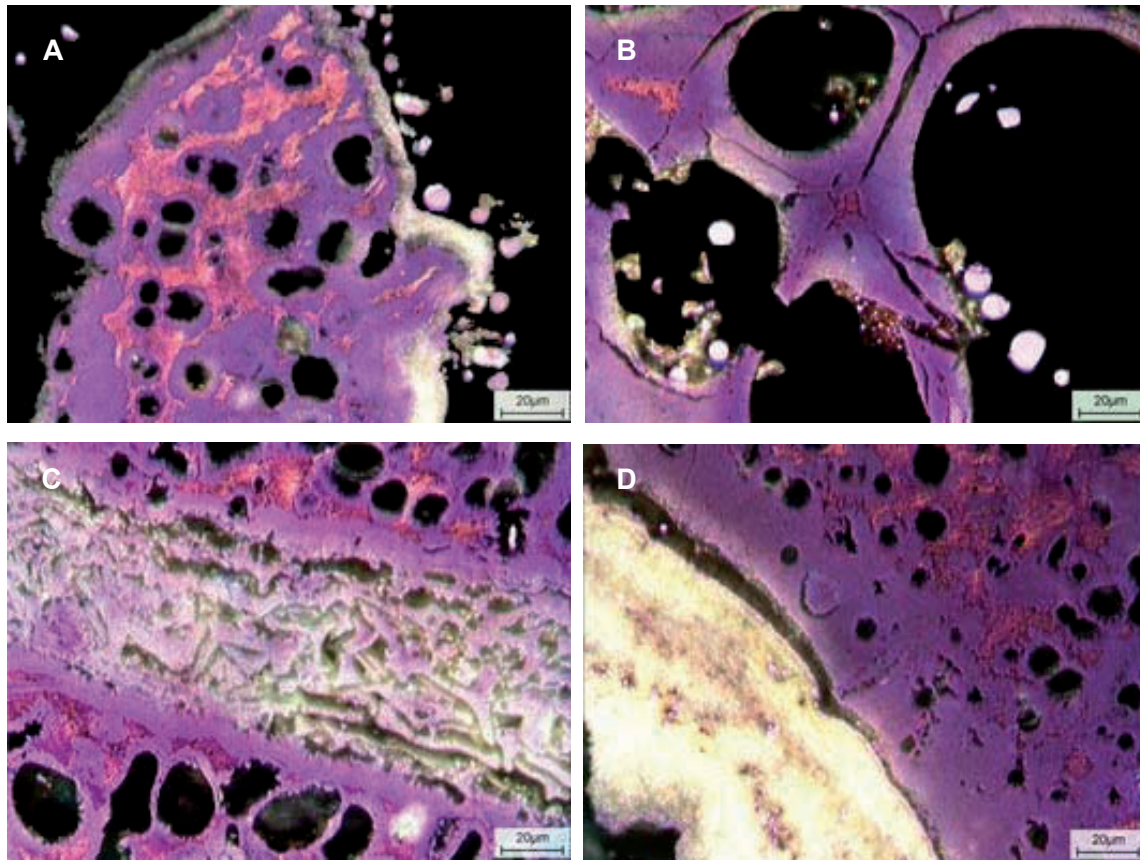


Figure 5.29: Microphotographs illustrating morphology of the reacted Blue Gem samples.

Data from the coke petrographic procedures indicate that the carbonized samples of Blue Gem mainly consist of binder form microtextures showing incipient and circular anisotropies. Infusible macerals are scarce in the lowest density fraction, but coarse organic filler phase components were relatively abundant in the MD fraction. Depositional carbons are abundant in both fractions.

As can be seen in Figure 5.29, differentiation between constituents in the reacted samples is straightforward in Blue Gem. Unreacted carbon still displays incipient to circular carbon forms and can be identified based on the pinkish color in all microphotographs in Figure 5.29. Carbon which has been converted to silicon carbide has an isotropic texture (purple or blue) and can be observed around pores and close to the periphery of the particles. In Figure 5.29 A), the reaction front is easily observable as the contrast between incipient carbon forms and isotropic silicon carbide is relatively high. At the rim of the particle, bright condensate as well as some metal droplets can also be seen.

When reaction fronts from adjacent pores meet, a crack will be induced in the structure of the reacted material. These cracks will enhance transport of reactive gases into the carbon structure thus contributing to increased conversions. This process is well illustrated in Figure 5.29 B).

Filler phase components classified as fine during counting of coke carbon forms are contributing to increased pore wall thicknesses. Large infusible macerals and minerals can initiate crack propagation during carbonization and thus contribute to increased surface area. Several authors have reported that a high ratio of filler phase components has a negative influence on reactivity towards SiO gas (see section 2.3). A large fusinite maceral which has retained its shape can be seen in Figure 5.29 C). This fusinite maceral is distributing SiO gas to the carbon structure as can be observed by the reaction front progressing from this component. Similar colors are observed for fusinite and converted carbon. Based on the morphological studies, filler phase components accessible to SiO gas are considered to be converted to silicon carbide.

Depositional carbons have a high degree of anisotropy and were easily detected in the carbonized samples. Both pyrolytic and spherulitic carbons were observed. During morphological examinations of the reacted samples these carbon forms were not identified. Figure 5.29 D) illustrates what is believed to have been depositional carbons. In this figure it seems to have been a preferred site for condensation reactions. According to Schei et al. (1998), the condensate in the process consists of SiO₂ and Si and in some cases also SiC. In the microphotographs, condensate is seen as a diffuse green or yellow highly reflecting component.

Peak Downs

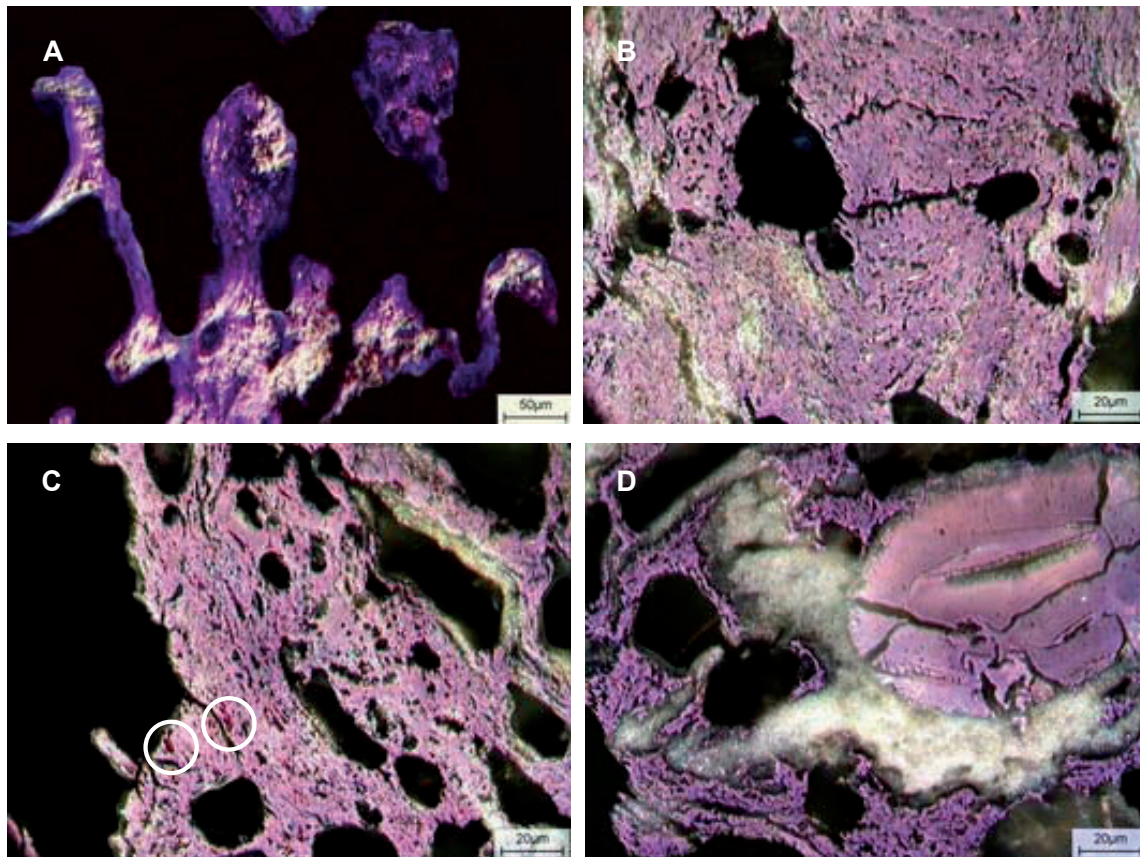


Figure 5.30: Microphotographs illustrating morphology of the reacted Peak Downs samples.

Binder phase carbon forms in the carbonized samples of Peak Downs have the highest degree of anisotropy with a majority of lenticular microtextures. Unreacted binder phase microtextures should thus be easily observable in the reacted samples as can be seen in Figure 5.30 A) and Figure 5.12.

Based on both the rank of the coal and on the measured weight increase, a substantial amount of unreacted carbon was expected to be observed during morphological studies of the reacted samples. These were however rarely encountered. By systematically investigating the reacted samples, hardly any unreacted binder phase microtextures were observed. In Figure 5.30 C), some small carbon crystallites can be identified as having a slightly darker color than the converted ground mass. In crossed polarized light, anisotropy of these crystals will be more evident by rotating the sample stage. The conclusion which can be drawn based on the morphological investigation is that binder phase carbon forms in Peak Downs are close to completely converted to silicon carbide.

Both fractions of Peak Downs have relatively high amounts of filler phase carbon forms. Compared to the Carboniferous coals, high amounts of secretinite and funginite macerals were identified in Peak Downs (see Figure 5.3 A). These macerals can be quite large and dense and are thus believed to have a low reactivity and degree of conversion. Differentiation between infusible macerals and SiC can be hard as both components are isotropic and of same color. In Figure 5.30 D), converted carbon can be identified as purple groundmass with a significant amount of small pores and fissures. In the upper right corner of the picture a secretinite maceral is observed. The particle has cracked and thereby increased the surface area available to reactive gas. Based on the morphological studies, a majority of the infusible macerals in Peak Downs are also considered to be converted.

Minerals are abundant in Peak Downs and metal formation was visually observed in the reacted samples. Numerous components with a high degree of anisotropy and ordered crystal structure were identified during morphological studies. These are believed to originate from the reducible minerals which are quite abundant based on the intensity of the pre-reduction peaks from the reactivity profiles (see Figure 5.25).

Mercury intrusion porosimetry rated Peak Downs as the material with the lowest amount of macro pores (Figure 5.23). During morphological studies of the reacted material, small pores were observed throughout the sample (see Figure 5.30 B, C and D). Both the high degree of conversion and generation of macro porosity are due to reaction of clastic quartz inclusions identified throughout the coal samples. At the reaction temperature, quartz inclusions will react with surrounding carbon. The reaction between quartz and carbon as well as the impacts of this reaction is further elucidated on in the next section.

Staszic

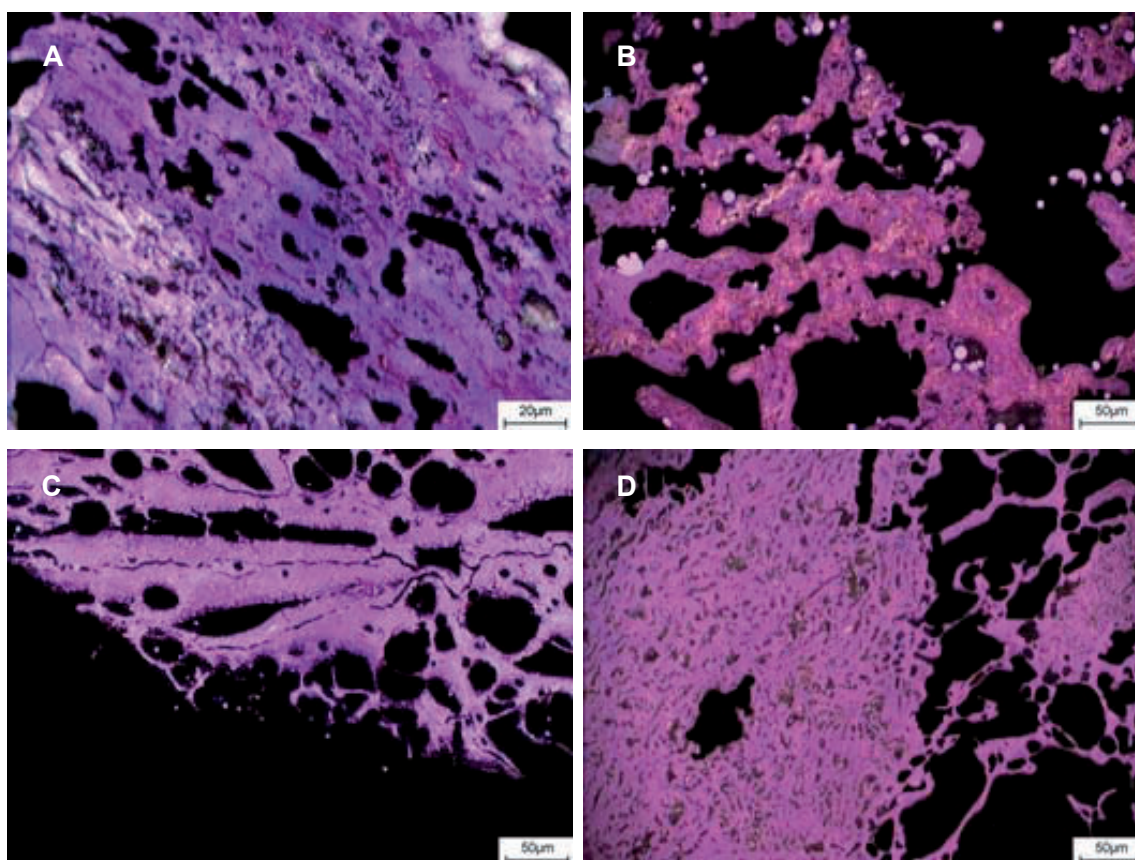


Figure 5.31: Microphotographs illustrating morphology of the reacted Staszic samples.

Due to the inhomogeneous structure of Staszic, the reaction front is not as continuous and easy to identify as for the Blue Gem samples. As the two Carboniferous coal samples are similar in rank, the degree of anisotropy of the binder phase microtextures are related. A microphotograph of a dull particle can be seen in Figure 5.31 A). Unreacted carbon can be identified based on color (dark pink) and displays isotropic to incipient anisotropy. Converted carbon has a blue to purple color and is isotropic. Some condensate can also be observed.

Metal formation was not visually observed in any of the reacted samples of Staszic, but on several occasions metal droplets were observed under the microscope. Formation of metal droplets is illustrated in Figure 5.31 B) where the highest degree of anisotropy of the binder phase also can be observed.

The presence of infusible macerals can influence the pore shapes in dull coals, and a higher ratio of elongated pores were observed in Staszic compared to Blue Gem which on the contrary is a very homogeneous coal. The dull structure is however generating a high surface area during carbonization. The elongated pores, high surface area and relatively thin pore walls are all factors that contribute to a high degree of conversion. A completely converted particle is illustrated in Figure 5.31 C), where both the elongated pores and the cracks where the reaction fronts met are easily identifiable.

Staszic is the sample material with the highest content of inertinite macerals. Morphological studies of the coal samples revealed that semifusinite covered a wide range of reflectance, which is an indication that some semifusinite is fusible during carbonization. A high amount of organic filler phase components was however identified and counted during the coke petrographic procedure. During morphological studies of the reacted samples especially large infused macerals were identified. Small fragments of inertodetrinite as well as incorporated macerals like micrinite and macrinite (which to some degree are categorized as reactive during carbonization) were not observed. This is mainly due to the dull structure of the reacted particles. Small fragments of infused macerals are also hard to distinguish from the SiC and isotropic binder phase carbon forms. In Figure 5.31 D), a large fusinite maceral which seems to have been converted to SiC can be seen.

Based on the morphological studies and the measured weight increase of the reacted samples, qualified estimates of conversion degrees are proposed. The measured weight increase is assumed to correlate fairly well with the degree of conversion for the Blue Gem samples. This material has the highest pore wall thickness of all the tested materials, and unreacted carbon is easily detected in the reacted samples. In validation of the improved SINTEF test, Blue Gem was used as a reference material. This reference material consisted of a mixture of the LD- and MD fractions from the density separation. The degree of conversion was analyzed according to the suggested procedure in the improved SINTEF test and was in the range 80 – 85% (Hansen 2005).

According to the measured weight increase, samples of Peak Downs have the lowest degree of conversion. During the morphological studies, it was however hard to find unreacted carbon in the samples. A blend of the MD- and HD fractions of Peak Downs was also used as a reference material in establishing the improved SINTEF test. Conversion degrees in the range 95 – 100 % were chemically analyzed for these samples.

Measured weight increase for reacted samples of Staszic indicated a degree of conversion similar to the Blue Gem samples. The content of mineral inclusions is however higher in the Polish coal samples and based on Figure 5.25, some of the available carbon is used for reduction of some of these minerals. These factors result in a lower amount of carbon available for reaction to SiO gas, and the degree of conversion is thus higher than the recorded weight increase. Unreacted carbon was observed during the morphological studies, but more scattered in dull particles compared to the Blue Gem samples.

Estimates of conversions for the tested materials are given in Table 5.17.

Table 5.17: Degrees of conversion (%) based on measured weight increase and morphological studies of the reacted samples.

Samples	Specific density fractions		
	LD	MD	HD
Blue Gem	80 – 85	85 – 90	-
Peak Downs	-	95 – 100	95 – 100
Staszic	-	90 – 95	85 – 90

5.7.5 Effect of heat treatment of Peak Downs

As both the measured reactivity and obtained degree of conversion of both fractions of Peak Downs are substantially different from the expected behaviour based on former research (see section 2.3), further investigations into this material was deemed necessary.

As mentioned in the previous section, the main reason for the observed behavior of Peak Downs is believed to be caused by the numerous clastic quartz inclusions. During petrographic investigations of the coal samples, these inclusions were identified throughout both the MD- and HD fractions of Peak Downs. They appeared black under the microscope, were round to oval shaped and had a relatively wide size range (see Figure 5.3 D). Qualitative analyses of mineralogy are however more reliable by the use of transmitted light. In order to positively identify the quartz inclusions, thin sections of the ROM coal were prepared and examined. Microphotographs of the quartz inclusions in both reflected- and transmitted light are presented in Figure 5.32.

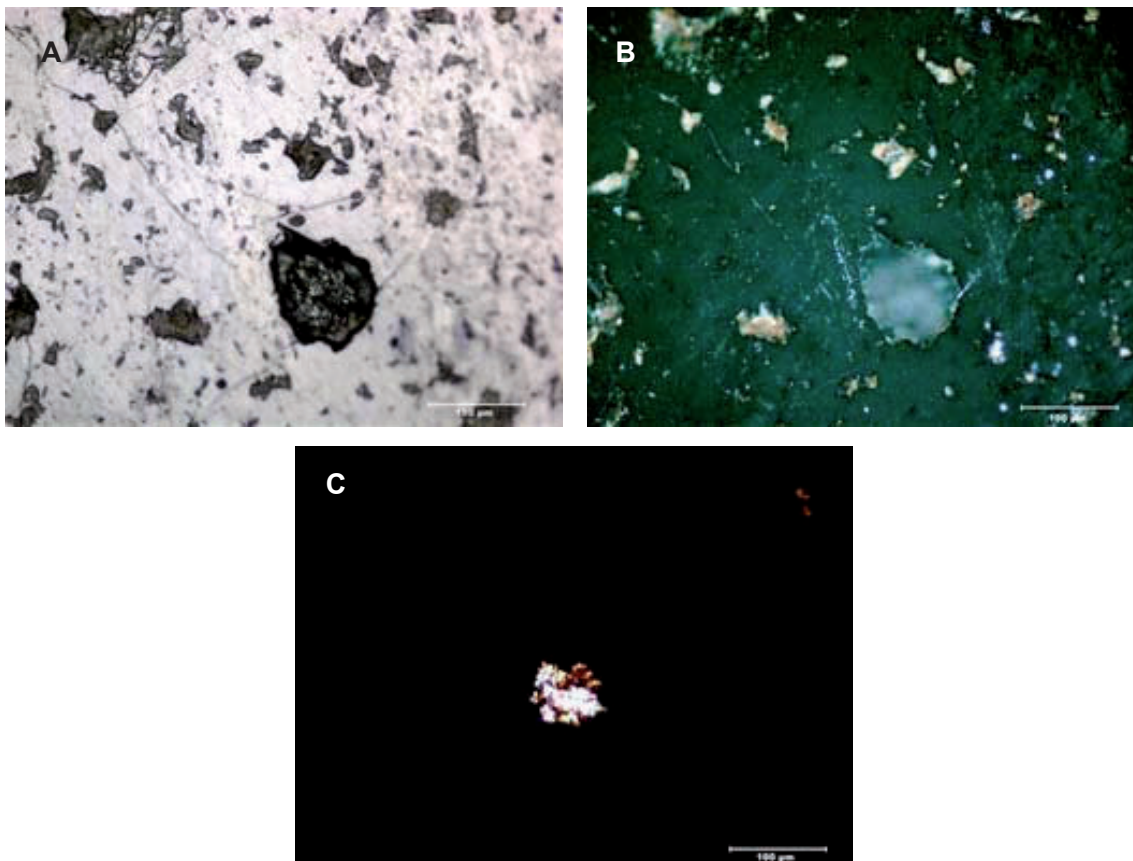


Figure 5.32: Identification of quartz grains in thin sections. All photos are from the same section.

A) Reflected white light, B) Reflected white cross polarized light and C) Transmitted light.

During preparation of the pellets used for petrographic investigations some of the quartz grains can have been removed from the sample. In such cases, the observed inclusions are imprints of the original quartz grains. Quartz inclusions can be identified by petrographic procedures in reflected light by use of cross polarized light where they

show internal reflectance. In transmitted light the quartz inclusions display interference colors with extinctions four times during one rotation of the sample stage.

A high relief between the largest quartz grains and the coal matrix was also observed in the thin sections. As a result of this, Figure 5.32 A) is stitched together from two pictures where one was focusing on the coal matrix and the other on the largest quartz inclusion. This picture was taken in reflected white light which is commonly used during coal petrographic procedures. Quartz grains are observed as dark inclusions in the bright coal matrix. In Figure 5.32 B), the same section can be seen in reflected white cross polarized light. By the use of these setting, the internal reflectance of the quartz grains is observable. Notice the high difference in relief for the largest quartz grain in the middle of the microphotograph. Presence of iron compounds in some of the inclusions is inducing a brownish tint which can be observed in the figure. This brownish tint is also visible in Figure 5.32 C) which is taken in transmitted light. Examination of thin sections enabled a positive identification of quartz inclusions.

From the microphotographs presented in Figure 5.30, it can be seen that the quartz inclusions are inducing a high degree of porosity in the reacted samples. At the reaction temperature in the SINTEF reactivity test, quartz inclusions will react with surrounding carbon and the generation of porosity can be seen as a combination of the following reactions:



According to **Wiik (1990)**, the reaction between carbon and quartz in powdery mixtures has significant rates from 1400°C in vacuum or in a stream of argon. The modification of quartz was however reported to have an impact on reaction rate with the high temperature modification (cristobalite) showing the highest rate. As can be seen from the reactions, formation of SiC can occur in coal samples high in quartz inclusions even without external access to SiO gas.

Formation of porosity in the samples due to quartz inclusions results in mechanically weak particles which may involve excessive formation of fines in the industrial production of silicon. In a report by **Gill and Dubrawski (1984)**, physical degradation of cokes in blast furnaces was contributed to the formation of SiC. The authors investigated SiC formation in eight widely used blast furnace cokes at various conditions. They claimed that the quartz content in the original samples was insufficient to account for the amount of SiC formed, and suggested that some of the SiO₂ originally associated with clay minerals in coal takes part in the reaction.

In order to investigate the influence of temperature on the structure of Peak Downs, a representative sample of the highest density fraction was heated to the reaction temperature without access of SiO gas. As the intention of the thermal treatment was to examine effects of the reaction between carbon and quartz, the pre-reduction step in the original procedure was by-passed. Massive formation of CO was observed, exceeding

the limit of the CO-analyzer (35 %). The reactor was cooled when the concentration of CO dropped below 5.2 %.

Following thermal treatment, macro porosity of the sample was analyzed by mercury intrusion. A comparison of pore size distributions and cumulative porosities of the sample before and after thermal treatment is illustrated in Figure 5.33.

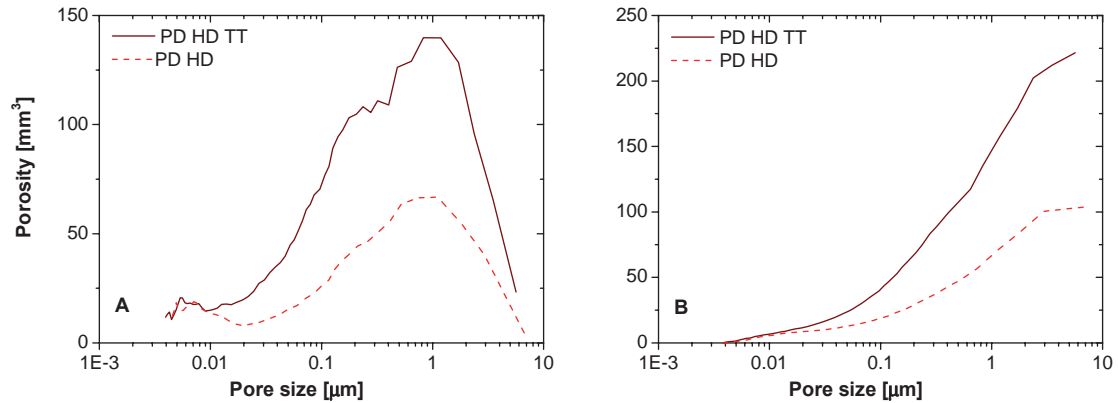


Figure 5.33: Pore size distribution (A) and cumulative porosity (B) by mercury intrusion of Peak Downs before (PDHD) and after (PD HD TT) thermal treatment.

As can be seen from plots, thermal treatment had a significant effect upon the porosity of the sample. The cumulative macro porosity following thermal treatment was more than doubled, and resulted in higher total macro porosity than the MD fraction of Blue Gem (see Figure 5.24). These results imply that even before the reaction with SiO gas initiates, samples of Peak Downs have the highest values of both coarse- and macro porosity as well as having the thinnest pore walls. Pores generated from quartz inclusions larger than the limits of the mercury intrusion procedure will contribute to an even higher coarse porosity.

In order to investigate if the thermal treatment had any effect upon reactivity, the heat treated sample was subjected to a reactivity test according to the SINTEF procedure. A comparison of the reactivity profiles before- and after thermal treatment is given in Figure 5.34.

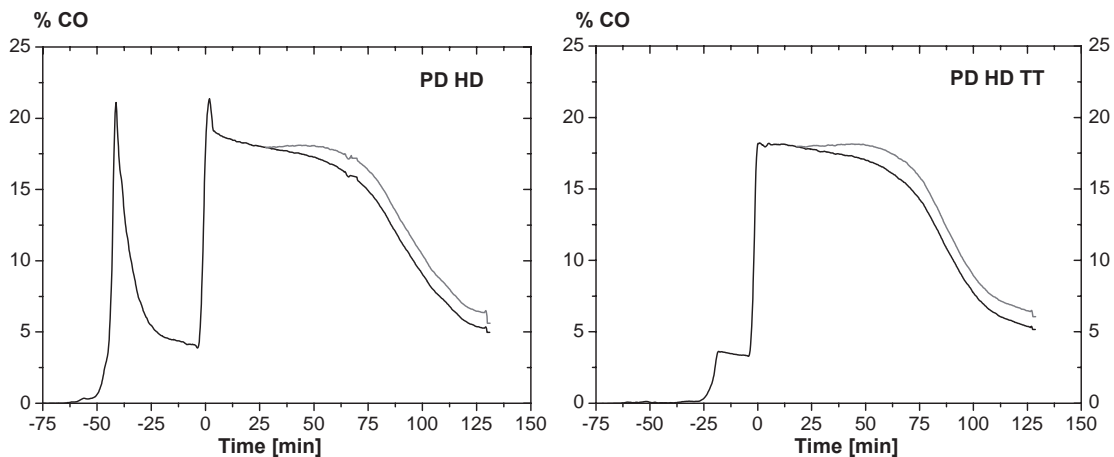


Figure 5.34: CO profiles before (PD HD) and after heat treatment (PD HD TT).

The most noticeable difference in Figure 5.34 is that the strong pre-reduction peak occurring in the original sample of Peak Downs has completely vanished in the heat treated sample. The result is an indication of a successful heat treatment procedure as there are no reducible minerals left in the sample following thermal treatment. A recorded weight loss of 12.4 % during thermal treatment is affirming this statement.

To further examine if the thermal treatment affected the reactivity, the corrected reactivity profiles are plotted in Figure 5.35.

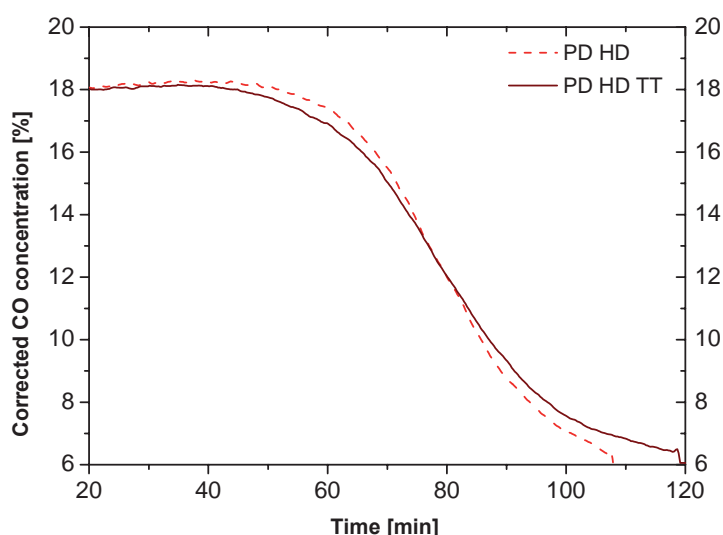


Figure 5.35: Comparison of CO profiles of the high density fraction of Peak Downs (PDHD) before and after heat treatment.

Based on the corrected reactivity curves plotted in Figure 5.35, the sample should be slightly more reactive prior to thermal treatment. A *R10 corrected* value of 538 ml SiO was calculated for the heat treated sample, while the average value of the original sample was 544 ml SiO (Figure 5.27). Thermal treatment had thus no effect upon reactivity of the sample as reduction of quartz inclusions and pore generation occur during the conventional SINTEF reactivity test.

Similar to the original samples, modest amounts of unreacted carbon was observed during morphological investigations of the reacted sample following thermal treatment. The measured weight increase should be more consistent with the degree of conversion for the heat treated sample as the amount of reducible minerals has been significantly reduced. A measured weight increase of 61.2 % corresponds to a conversion of 91.4 % and is the highest of all the tested materials (see Figure 5.28).

5.7.6 Tangent in point of inflection as alternative reactivity measure

The commonly reported reactivity measure from the SINTEF SiO reactivity test, *R10 corrected*, is a measure of the amount of SiO gas (volume in ml) that escapes the reaction chamber from the CO concentration drops below 18 % until it reaches 10 %. As this test has been commercially available for almost three decades, this reactivity measure is accepted and understood by the customers.

As mentioned in section 5.7.2, shapes and slopes of the CO profiles contain information about the reactivity of the tested materials. A reactive material has a narrow reaction zone and the concentration of CO will decrease rapidly after breakthrough. The reactivity profile will thus have a steep slope for reactive materials, while the opposite is true for slowly reacting materials.

Based on these observations, a mathematical reactivity value is proposed solely based on the corrected concentration of CO as a function of time. A 3rd order polynomial is fitted to the reactivity curve:

$$\%CO = A + Bt + Ct^2 + Dt^3 \tag{5.14}$$

where %CO is the corrected concentration of CO, t is time and A , B , C and D are constants from the fitting procedure.

The second derivative of the fitted function will give the point of inflection.

$$\frac{d^2(\%CO)}{dt^2} = 2C + 6Dt \tag{5.15}$$

As the slope of the CO profile is correlated to the thickness of the reaction zone in the reaction chamber and hence the reactivity of the carbonaceous material, the slope of the tangent in the point of inflection can be used as an alternative measure of reactivity. This slope is calculated based on values from either the fitted polynomial or the corrected graph (preferably the first option as there are some disturbances in the recorded data). In Figure 5.36, an illustration of the procedure is given.

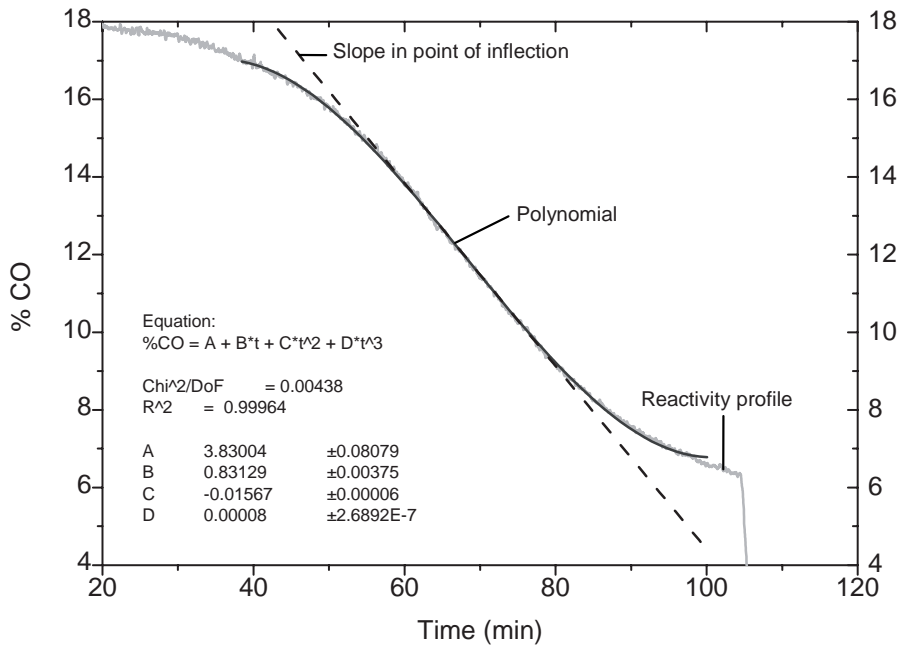


Figure 5.36: An illustration of the procedure of acquiring the tangent in the point of inflection for the corrected CO concentration as a function of time.

Curve fitting was performed for both parallels of the tested fractions in this work. Special attention was taken to assure a best possible fit in the range 14 – 10 % CO which includes the points of inflection for a majority of the tested samples. Goodness of the fitted polynomials was evaluated by the R^2 parameter. The lowest recorded value was 0.9962 which implies that the fitting procedure was performed with sufficient accuracy. In order to investigate how the calculated slopes correlated with the *R10 corrected* values, they were plotted in Figure 5.37.

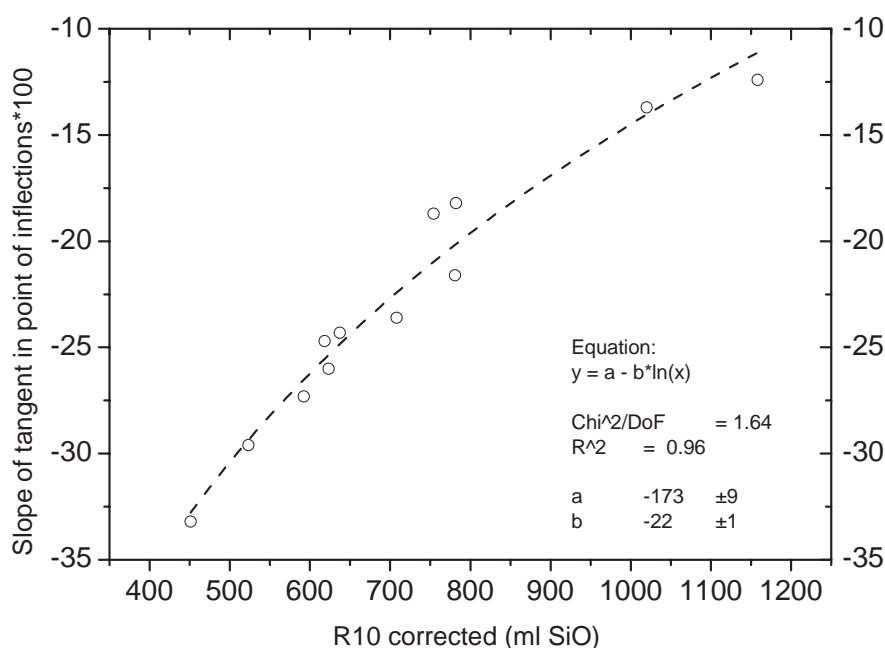


Figure 5.37: Correlation of R10 corrected and slopes of tangents in the points of inflection.

A logarithmic function seems to be the most logical function to express the relationship between the corrected reactivity values and slopes in the points of inflection. For materials that do not react with SiO gas, the CO profile will be steady at a value of 4.5 % thus giving a *R10 corrected* value approaching infinity and a not existing slope. For a “super” reactive material, we can imagine the slope of the curve to be vertical thus rendering a reactivity value close to zero. In Figure 5.37, a logarithmic function is fitted to the data points with fairly good precision ($R^2 = 0.96$).

5.8 Kinetic Parameters

As can be seen in section 2.2, kinetic parameters like effective diffusivities, D_E , and reaction rate constants, k_C , are important in determining which step is rate determining in gas - solid reactions. In addition, the kinetic parameters can be used to predict the behaviour of a given reduction material in a packed bed such as the silicon furnace which has been demonstrated by Myrhaug (2003).

Based on the origin and properties of the coal samples used in this work, they are considered to be of interest for ferroalloy producers, and especially for industrial utilization in the silicon process. Mathematical modeling of behavior in the furnace is

often preceding actual testing of carbonaceous materials in industrial operation. In order for the modeling to give accurate results, the kinetic parameters needed to be evaluated.

5.8.1 Thermo gravimetric experiments

In principle, the easiest way to obtain kinetic parameters of the sample materials would be to prepare particles of a defined geometry (F_p) and record the weight change during reaction with SiO gas in a thermogravimetric apparatus. In his doctoral work, **Myrhaug (2003)** performed TG experiments on single spheres with diameters in the range 8 – 25 mm of both charcoal and fossil carbonaceous materials. Values for both effective diffusivities (D_E) and reaction rate constants (k_C) could subsequently be calculated based on different kinetic models (see section 2.3.2).

Disregarding the fact that use of a single particle might cause problems with statistical significance; the thermogravimetric procedure seemed appealing to try. Adopting data from TG experiments to different kinetic models necessitates a defined geometry of the particles. In order to meet this criterion, the largest particles after carbonization were screened out and selected for TG experiments. During the carbonization procedure used for the purpose of this work (section 4.4), no pressure was induced and the particles were thus free to swell. As the particle size of the charged coal was limited by the coal separation procedure (3.35 – 9.50 mm), the largest particles following carbonization were not particularly well suited for inscribing a defined geometry (see Figure 5.38).



Figure 5.38: Best suited particles for TG experiments.

These problems could have been sidestepped by carbonizing larger coal particles or choosing another carbonization procedure. As one of the key objectives of this work was to investigate the influence of maceral composition on the reactivity towards SiO gas, evaluation of kinetic parameters had to be performed on both fractions of the density separated coals i.e. size range 3.35 – 9.50 mm. The carbonization procedure was developed to resemble the conditions coals experience during charging in an industrial process and was also evaluated as significant to the experimental work. Based on these findings, the thermogravimetric experiments were not suitable for the purpose of this work.

5.8.2 SINTEF test with reduced particle size

The SINTEF SiO reactivity test is widely used to assess the reactivity and degree of conversion for reduction materials used in the silicon process and for evaluating potentially new reductants. Kinetic constants are however not evaluated as part of the standardized test procedure.

5 EXPERIMENTAL RESULTS

To examine the effect of particle size on reactivity, carbonized particles in the size range 3.35 – 4.00 mm were prepared for all density fractions and tested according to the SINTEF procedure.

Corrected reactivity profiles from the conventional tests (4.00 – 6.30 mm) are compared with profiles obtained from tests with reduced sizes (3.35 – 4.00 mm) in Figure 5.39.

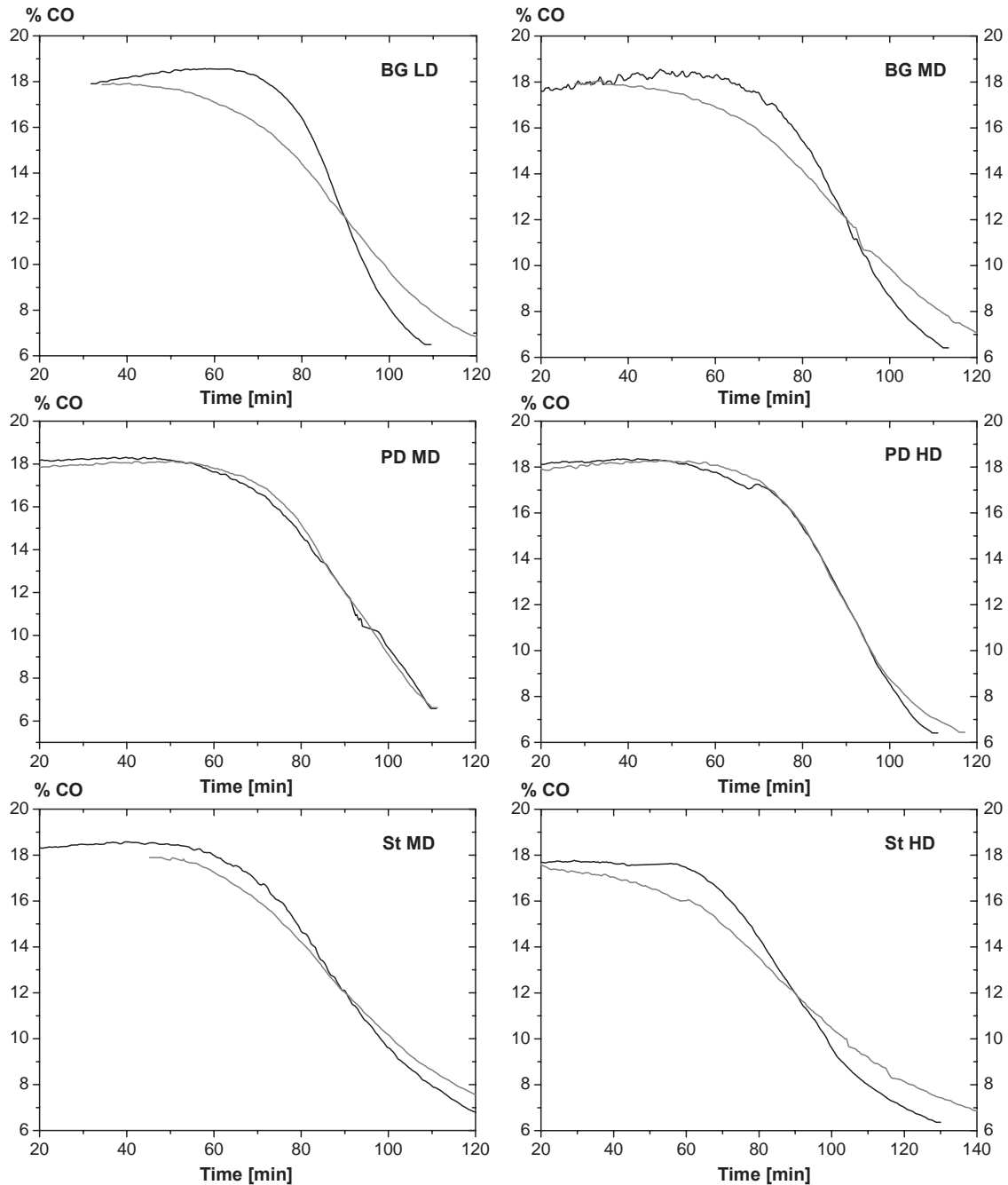


Figure 5.39: Corrected CO profiles from conventional tests (4.00 - 6.30 mm) – grey graphs compared with graphs obtained with smaller particle sizes (3.35 – 4.00 mm) – black graphs. The profiles are time adjusted to cross 12 % CO at the same time.

Degree of conversion as function of time is given for the most relevant gas – solid reaction models in section 2.2. As can be seen in both of them, the degree of conversion is a function of particle size with a smaller size inducing an increased reaction rate.

As can be seen from Figure 5.39, the reduction in particle size is significantly affecting the reactivity of the Carboniferous samples, but has little or no effect on Peak Downs. To further illustrate the influence of particle size on reactivity towards SiO gas, the *R10 corrected* values from the tests are compared in Figure 5.40.

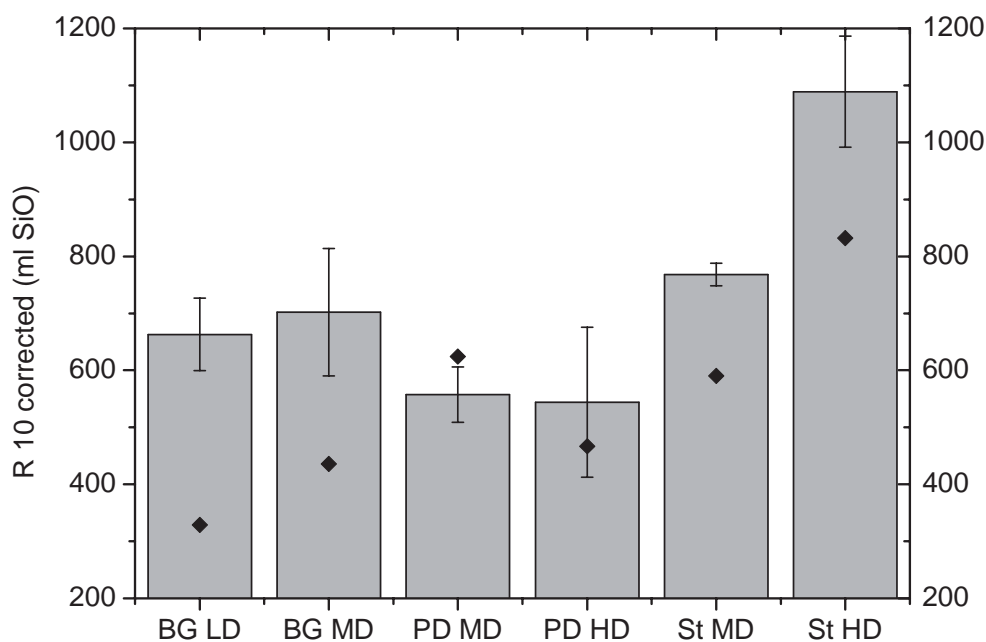


Figure 5.40: Comparison of *R10 corrected* values from the conventional tests (grey bars) and values obtained with smaller particles (black diamonds).

For particles in the size range 3.35 – 4.00 mm, a single test was performed and thus no standard deviation is indicated in Figure 5.40. As can be seen from the figure, significantly higher reactivities are observed due to reduced particle size in all fractions of Blue Gem and Staszic. Size reduction did not have any positive effect on the reaction rate for the Peak Downs samples, and did in fact increase the *R10 corrected* value for the MD fraction. These results are suggesting that none of the gas – solid reaction models described in section 2.2 is suitable for describing the reaction of Peak Downs with SiO gas. Disregarding Peak Downs, reactivity results obtained with smaller particles are consistent with trends from conventional test where the lowest density fractions proved to be the most reactive.

Reduced particle size will, according to the relations listed in section 2.2, result in a higher degree of conversion given equal reaction time. The SINTEF reactivity test is however terminated as the concentration of CO drops below 5.2 %, and reaction times of the smallest particles are thus shorter than the conventional tests. Measured weight increase for reactivity tests with reduced particle sizes are compared with the conventional tests in Figure 5.41.

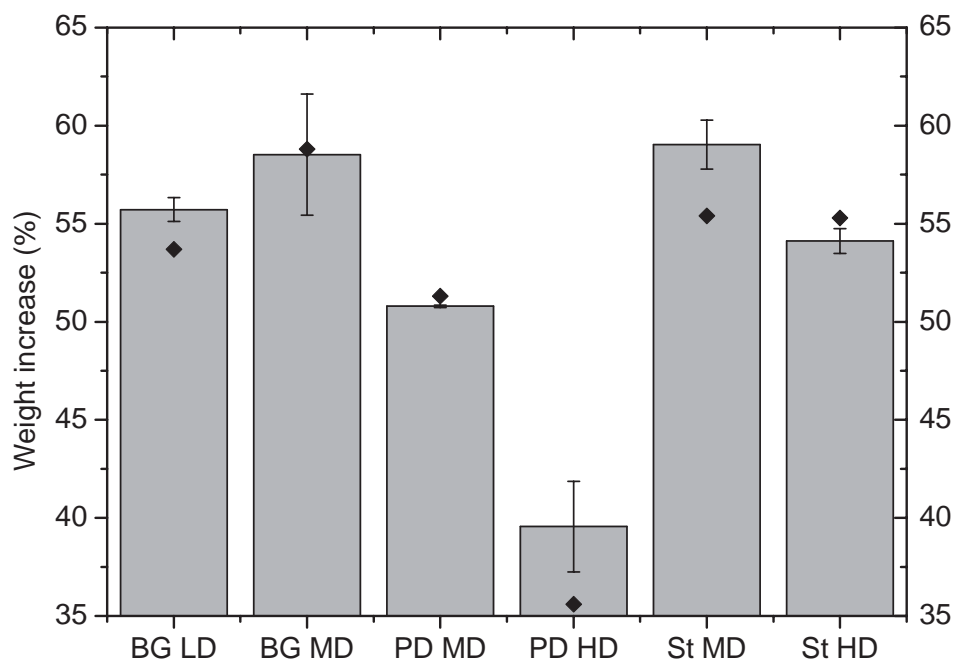


Figure 5.41: Comparison of measured weight increase from conventional tests (grey bars) and values obtained with reduced particle sizes (black diamonds).

From Figure 5.41 it can be seen that the measured weight increases for the reduced size fractions are in fairly good agreement with the conventional tests. Slightly lower values are measured for the lowest density fractions of the Carboniferous samples while a lower weight increase is noticed for the HD fraction of Peak Downs.

As mentioned in the previous section, reactions of both biological- and fossil carbonaceous samples with SiO gas were thoroughly examined in a thermo gravimetric apparatus by **Myrhaug (2003)**. Spheres of different sizes were prepared from the sample materials and the weight change recorded as a function of time. Based on the recorded weight change, a direct relationship between time and degree of conversion was found. Based on this relationship a number of different gas – solid reaction models were fitted to the experimental data, and the shrinking core model came out as the best option for both biological- and fossil samples (see section 2.3.2).

Formulas for gas – solid reactions in packed beds combined with the shrinking core model for individual particles are presented in **Szekely et al. (1976)**. By combining kinetic parameters obtained from thermo gravimetric experiments and these formulas, **Myrhaug (2003)** developed a model for the SINTEF SiO reactivity test. This model provides a tool for predicting reactivity profiles based on kinetic parameters.

As kinetic parameters are material properties, the model should give accurate results independent on particle size. In this work, the model developed by **Myrhaug (2003)** was used to assess the kinetic parameters of the tested sample materials. A set of kinetic parameters were manually tuned in such a way that the model described experimental reactivity profiles for both particle sizes. When the best set of values for effective diffusivities and reaction rate constants were implemented, the model accurately

predicted the reactivity profiles for all the tested fractions. An example of a well fitted model is given for the highest density fraction of Staszic in Figure 5.42.

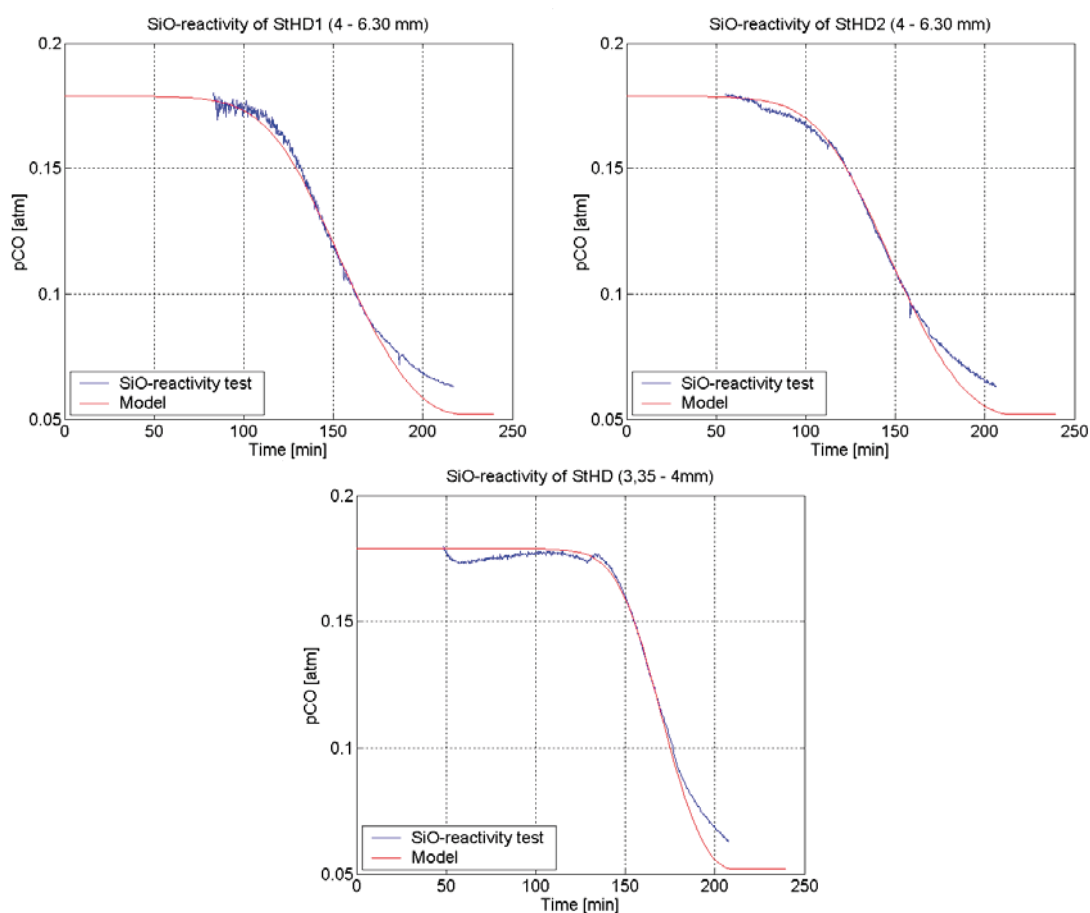


Figure 5.42: Model fitting for two conventional (4.00 - 6.30 mm) SINTEF SiO reactivity tests of St HD as well as a test with reduced particle size (3.35 – 4.00 mm). The kinetic constants are the same in all models: $D_e = 2.4 \cdot 10^{-5} \text{ m}^2/\text{s}$ and $k_c = 0.06 \text{ m/s}$.

The major concern when tuning the kinetic constants was to get the best possible fit between the modeled curves and the experimental reactivity profiles in the interval where the CO profiles are steepest i.e. from 15 – 10 % CO. As can be seen from Figure 5.42, the chosen values for D_E and k_C in the model are explaining the experimental profiles very well. In all the plots presented in Figure 5.42, a discrepancy between the model and the experimental profiles are observed towards the end of the experiments. The model is designed to simulate the measured reactivity curves, while the blue curves in Figure 5.42 are the corrected profiles. As pointed out in section 5.7.1, the difference between the measured- and corrected profiles when the reactivity test is terminated is 1.1 % CO. The model could be adjusted to fit the corrected reactivity curves, but as long as there is an accurate fit in the steepest part of the profiles, the kinetic constants would remain unaffected.

As the reactivity model is developed based on the assumption that individual carbon particles are following the shrinking core model, the modeled reactivity profiles are functions of particle size. Figure 5.39 revealed that reduced particle sizes resulted in a

5 EXPERIMENTAL RESULTS

significantly increased reactivity for all fractions of Blue Gem and Staszic. This is consistent with predictions from the shrinking core model, and density fractions of these materials were thus modeled with accurate precision. Illustrations of all the modeled reactivity profiles are presented in Appendix H.

Reduction in particle size did not significantly affect the reactivity of the Peak Downs fractions. From Figure 5.40, it can be seen that the MD fraction even showed a higher value of R10 corrected following size reduction. These findings are not compatible with the shrinking core model, and hence the reactivity model was not able to find suitable values for kinetic parameters of this material. Figure 5.43 illustrates the best obtainable tuning of kinetic parameters for Peak Downs.

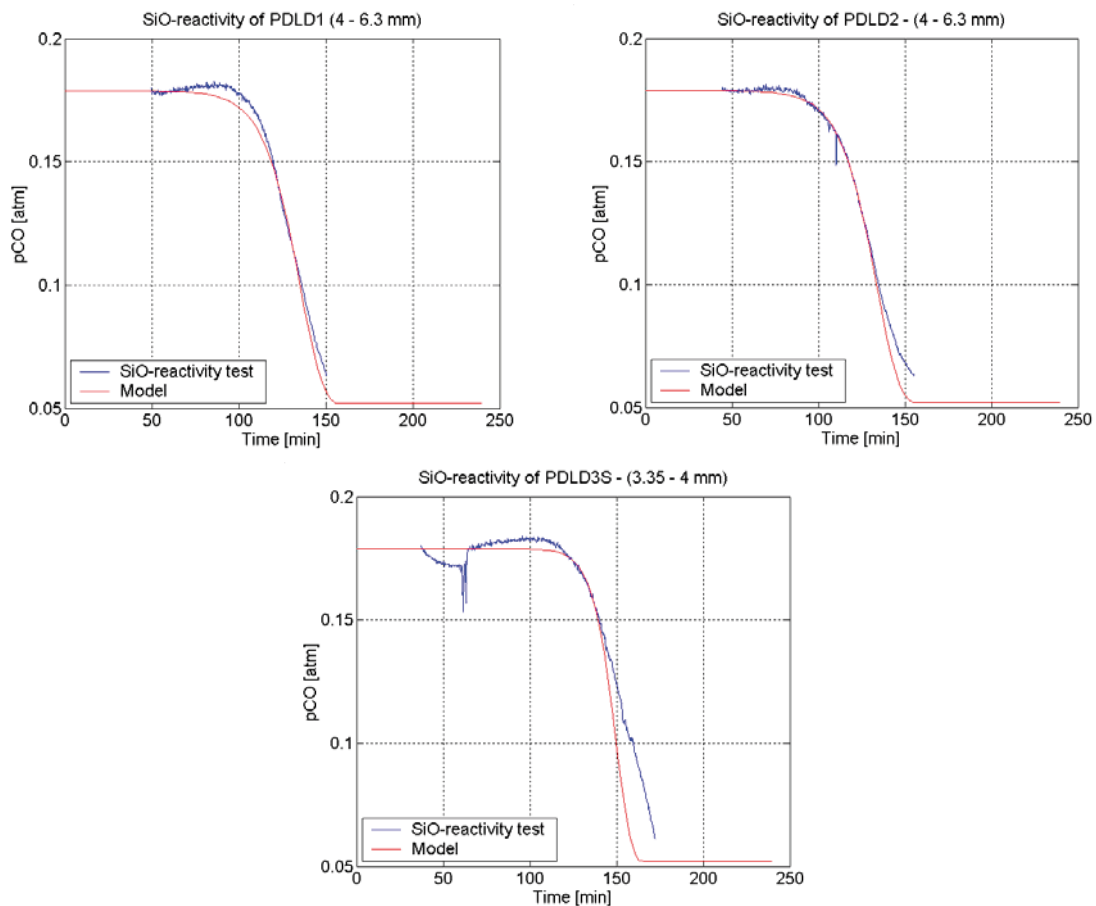


Figure 5.43: Model fitting for two conventional (4.00 - 6.30 mm) SINTEF SiO reactivity tests of PDL as well as a test with smaller particle size (3.35 – 4.00 mm). The kinetic constants are the same in all models, and are set to: $D_e = 3.5 \cdot 10^{-4} \text{ m}^2/\text{s}$ and $k_c = 0.08 \text{ m/s}$.

Values of D_E and k_C which give fairly good fits between the model and the corrected reactivity profiles for both parallels in the conventional reactivity test can be observed in Figure 5.43. As reduced sizes of the reacting particles will result in a higher reactivity according to the shrinking core model, an accurate fit for this particle size range is impossible as long as the observed reactivity was independent on particle size.

Based on tuning kinetic constants in the reactivity model to accurately fit the corrected profiles for two sets of particle sizes, estimates of effective diffusivities and reaction rate constants are presented in Table 5.18.

Table 5.18: Estimated values for kinetic constants

Kinetic parameters		Blue Gem		Peak Downs		Stazic	
		LD	MD	MD	HD	MD	HD
D_E	[m ² /s]	$4.50 \cdot 10^{-5}$	$3.25 \cdot 10^{-5}$	-	-	$3.65 \cdot 10^{-5}$	$2.40 \cdot 10^{-5}$
k_c	[m/s]	0.085	0.090	-	-	0.065	0.060

The estimated values are in the same order of magnitude as the values **Myrhaug (2003)** reported for the fossil carbonaceous samples in his doctoral work ($0.0676 < k_C < 0.0712$ and $1.81 \cdot 10^{-5} < D_E < 2.67 \cdot 10^{-5}$). One of the advantages with the procedure used in this work compared to the thermo gravimetric method is that a more representative sample is evaluated. In the TG experiments, a single particle of a defined geometry is reacting with SiO gas and the kinetic parameters of the material are evaluated based on the recorded weight change during reaction of this single particle. By proper sampling procedures, a representative amount of the tested materials are evaluated in the SINTEF SiO reactivity test, and the reported values of kinetic parameters are hence more statistically significant.

6. DISCUSSION

In the previous chapter, results from characterization of coal- and carbonized samples were presented as well as reactivity values from the SINTEF SiO reactivity apparatus and estimated degrees of conversion. The following chapter is divided into three parts. In the first part, analyzed properties of the coal samples presented in this work are compared with other reported values and typical features of Carboniferous- and Permian coals are discussed. Different conditions under carbonization are known to influence properties of the carbonized materials. The second section of this chapter includes comparison of textural- and structural properties of Blue Gem, Peak Downs and Staszic based on different conditions during carbonization. In the third part of this chapter, reactivity results obtained in this work are compared to parameters which in former studies have been proven to affect the reactivity of carbonaceous materials towards SiO gas.

6.1 Carboniferous- and Permian Coal Samples

The most important factors during deposition of peat were described in Chapter 3. Geological age is often used to describe different occurrences of coal. As coals originating from the same geological periods often were deposited in a restricted geographical area, under a limited range of climatic conditions with the same flora, this seems to be a valid division. Grouping of coals on the basis of geological age allows the Carboniferous coals of Europe and North America and the Permian coals of Australia, India, South Africa, South America and Antarctica (Gondwana) to be considered as two separate groups.

According to **Taylor et al. (1998)**, Carboniferous coals are often of bituminous rank and consist largely of vitrinite- and liptinite macerals, while contents of macerals belonging to the inertinite group are higher in Permian coals. Based on petrographical analyses of samples used in this work, Blue Gem and Peak Downs would be characterized as typical for respectively Carboniferous- and Permian coals.

Of all the analyzed coal samples in this work, Staszic contains the highest amount of inertinite macerals and is in that respect not typical for the Carboniferous coals. **Hyde et al. (1991)** related high inertinite content in Carboniferous coal samples from Newfoundland to periods of relatively low water table. **Misiak (2006)** have shown petrographic changes due to oscillating ground water table for a coal sample belonging to the Orzesze Beds in the Siltstone series (see Figure 4.19) in the Upper Silesian Coal Basin. A low ground water table might have contributed to the numerous inertinite macerals observed in Staszic.

Another typical feature of the Permian coals is according to **Taylor et al. (1998)**, the tendency for much mineral matter to be distributed throughout the seams, generally in a fine state. Both kaolinite and quartz are common mineral inclusions in Gondwana coals. Finely distributed quartz inclusions were observed throughout the coal samples during morphological studies of Peak Downs. These inclusions are believed to be the main reason for the observed reactivity and degree of conversion for this sample.

Semifusinite is the most common inertinite maceral in Permian coals and are reported to have a wide range of reflectance which can make differentiation to vitrinite more difficult. This corresponds very well with the typical features observed during morphological studies of the Peak Downs coal sample (section 5.2.2) where a microphotograph (Figure 5.3 C) is illustrating the gradation between vitrinite and semifusinite. In the same microphotograph, a component of wood can be seen. According to **Taylor et al. (1998)**, well defined cell structures of wood including annual growth rings are commonly observed in Permian coal samples. The same authors claim that funginite is comparatively common in Permian coals. A microphotograph of funginite inclusions is given in Figure 5.3 A.

Based on morphological studies of the coal samples and petrographic analyses, Blue Gem and Peak Downs are typical samples for their respective geological ages. The dull structure of Staszic with plentiful inclusions of both inertinite macerals and minerals is not representative for the bulk of the Carboniferous coals. As the Carboniferous coals cover a large depositional province, there were local differences in the depositional environment contributing to the diversity of coal properties. Fluctuation of the ground water table might have been a factor contributing to the relatively high ratio of inertinite macerals as well as the numerous discrete minerals observed during the non-maceral analysis.

6.1.1 Blue Gem

As discussed in section 4.7.1, the Blue Gem coal bed is part of the central Appalachian Basin and stratigraphically belonging to the Pond Creek coal zone. Coal from the Blue Gem coal bed is mined in Knox, Whitley and Bell counties in the south-eastern part of Kentucky. The sample used in the purpose of this work originated from Knox County, but it was however not possible to trace the sample back to the exact location of mining. Nor was information about whether the coal sample was gathered from the base-, middle- or top of the seam provided. During the analyses performed in this work Blue Gem was characterized as a high volatile bituminous coal with random reflectance of vitrinite of 0.71 %. The coal was very homogeneous and mineral inclusions scarce, thus characterized as a coal of high grade. A relatively large ratio of pseudovitrinite was observed in the sample.

An extensive report regarding the Pond Creek coal zone in the Central Appalachian Basin is presented by **Ruppert et al. (2001)**. In this report, resources of the Pond Creek coal zone have been assessed as well as geochemistry and detailed information concerning concentration of the most important trace elements. A number of samples covering the entire coal zone have been analyzed and are presented as figures and tables. In Table 6.1 parameters that can be compared with analyses performed in the present work are given.

6.1 CARBONIFEROUS- AND PERMIAN COAL SAMPLES

Table 6.1: Properties of coal samples from the Pond Creek coal zone in Knox County, Kentucky. Values are reported in Ruppert et al. (2001).

	W ^a [%]	A ^a [%]	Q _s ^a [Btu/lb]	S _t ^a [%]
Min	2.17	1.06	12450	0.47
Max	6.38	12.83	14370	4.40
Average	3.31	4.18	13830	1.39

Data referred to in Table 6.1 are collected from the entire Knox County and samples obtained close to the outcrop of the Pond Creek coal zone tend to have higher values of both ash yield and total sulfur. The authors claim that samples of Blue Gem generally have a very low ash yield (< 8 %) and amounts of total sulfur (< 1 %) which corresponds to the values presented in Table 5.1. The reported values are averages of the whole coal bench on an as-received basis, and 8 % ash yield for Blue Gem samples must thus be an absolute maximum value.

Rank is not reported based on vitrinite reflectance. Classification of rank according to the ASTM system of the entire Pond Creek coal zone is provided in Figure 6.1.

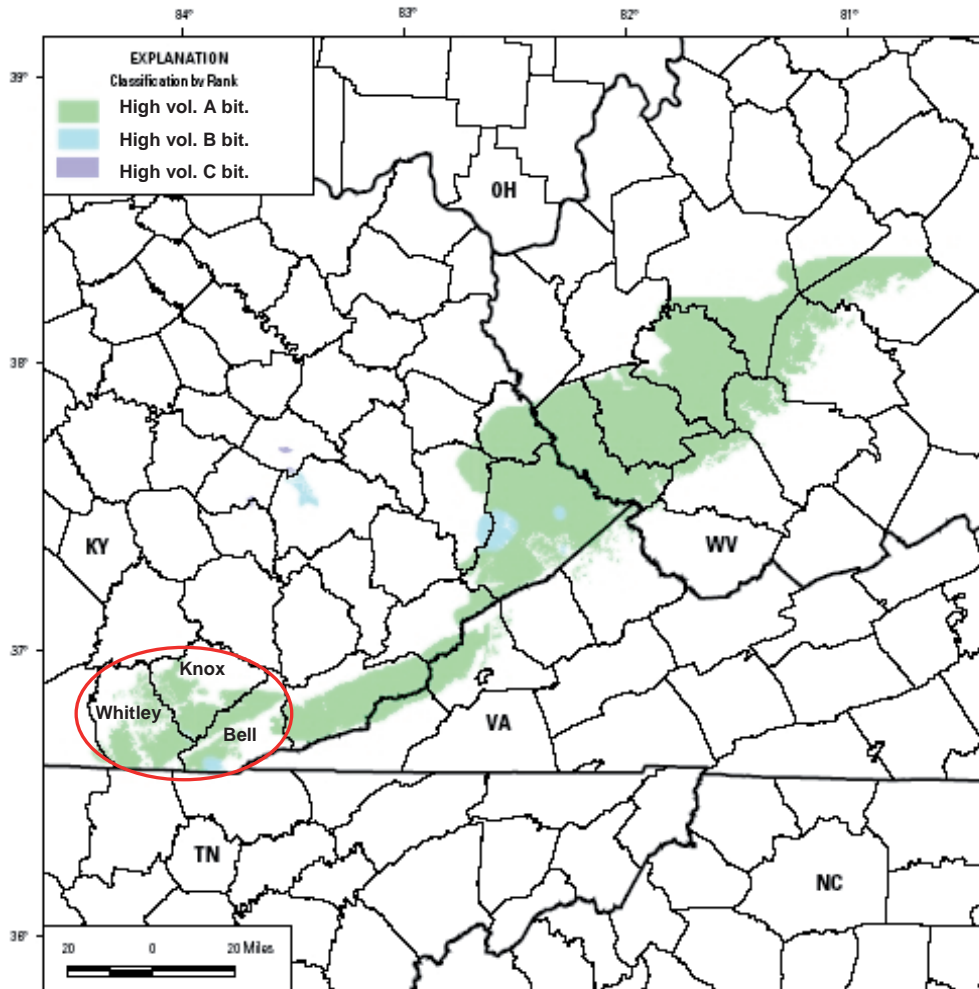


Figure 6.1: Rank classification of the Pond Creek coal zone based on 327 samples. The red circle indicates the position of the Blue Gem coal bed. Modified after Ruppert et al. (2001).

Almost the entire coal zone is according to Figure 6.1 classified as high volatile A bituminous coals. From Table 3.2 it can be seen that this classification corresponds to a random reflectance in the range 0.77 – 1.11 %. Measurements performed in this work concluded that Blue Gem had a value of 0.71 % random reflectance of vitrinite. Based on the analyzed value in this work, Blue Gem would be characterized as a high volatile B bituminous coal. From Figure 6.1, it can be seen that there are samples from the Blue Gem coal bed of this classification, but the majority of these samples are from Bell County.

As Blue Gem is a very homogeneous coal with low amount of mineral inclusions and sulfur, it has been a valuable coal for silicon producers in Norway. According to **Ruppert et al. (2001)**, it is also sold to coal fired power plants using bottom scrubbers at a very high price due to its low ash fusion temperature (which is related to the basicity value). The favorable properties of the Blue Gem coal bed has resulted in several publications about this coal measure.

The Geochemistry of the Blue Gem coal bed in Knox County was investigated in a paper by **Hower et al. (1991)**. In the course of these investigations, amount and composition of mineral matter and trace elements in 18 bench scale coal samples representing the Blue Gem coal bed in Knox County were analyzed. In order to observe trends during the time of deposition, samples from the different locations were separated based on vertical position in the seam. Based on the analytical results, an average thickness of the seam was reported to be approximately 70 cm. The seam is divided into a basal bench which is approximately 10 cm (> 1 % ash; enrichment in TiO₂), a middle part of 45 cm (< 1 % ash, relatively high CaO) and a top bench which is about 15 cm (> 1 % ash; relatively high SiO₂). The authors conclude, based on the analytical results, that the Blue Gem peat swamp was ombrotrophic through at least part of its geological history (section 3.4.4).

Rimmer et al. (2000) investigated the petrography and palynology of the Blue Gem coal bed in Knox County and came to the conclusion that the coal bed was divided into two separate zones. The lower part consisted of well preserved vitrinite while macerals in the top section were degraded to a larger degree. These findings confirmed the predictions of an ombrotrophic peat swamp as the peat swamp was domed in the final stages of peat accumulation.

A more thorough investigation of one specific mine in Knox County was reported by **Hower et al. (1994)**. In this report, samples representing the entire thickness of the seam were split into benches based on the position in the seam and analyzed. Chemical-, petrographic- and geochemical investigations of the samples were performed. In addition, the samples were crushed and separated by density according to the Density Gradient Centrifugation (DGC) procedure described by **Dyrkacz and Horowitz (1980)**. Proximate- and ultimate analyses of the bench samples prove that there are relatively large variations through the coal seam with a higher content of ash (~ 10 %) and sulfur (~ 2 %) in the top segment of the seam. Based on the discrepancy between the reported values for the top bench of the seam and the analyzed values in this work (see Table 5.1), we expect that the sample used in this work was mined from

the middle- or bottom part of the seam which has ash values in the range 0.4 - 1.6 % and total sulfur 0.61 – 0.78 %. Petrographically, the bench samples have vitrinite content in the range 77.6 – 87.3 % and a slightly higher amount of inertinite macerals than were counted during the maceral analysis in the present work. This specific coal sample was characterized as a high volatile A bituminous coal with a maximum reflectance of vitrinite of 0.88 %. Based on the correlations between random- and mean maximum reflectance presented in sections 4.2.2 and 5.4, this value corresponds to a random reflectance slightly above 0.8 % which is more than 10 % higher than the analyzed value of 0.71 %. This discrepancy in vitrinite reflectance is an indication that the sample in the present work is not originating from the same mine as the bench sample analyzed by **Hower et al. (1994)**.

6.1.2 Peak Downs

The Peaks Downs mine is owned and operated by BHP Billiton Mitsubishi Alliance, which is the largest coal mining company and exporter in Australia. According to information on the company web page (<http://www.bmacoal.com/>), a total annual tonnage of 9 million tons is mined from the Dysart- and Harrow Creek sequence of medium volatile hard coking coal seams. According to **Michaelsen and Henderson (2000)**, these are the two lowermost seams within the Moranbah Coal measures (see Figure 4.16). Apart from the rank, which is in agreement with measurement performed in this work, no technical information about coal properties is provided.

An extensive review of coal quality variations in Late Permian coal measures of the Bowen Basin is however reported by **Kahraman and Esterle (2001)**. In this report, amount of volatile matter, vitrinite reflectance, content of vitrinite and inertinite macerals are reported as well as ash chemistry and amounts of total sulfur and phosphorous. Values given in the report are referring to coals which are washed and blended. As the sample of Peak Downs used for the purpose of this work was received from the SSAB coking plant, it should resemble values in the report. The reported values for Peak Downs can be seen in Table 6.2.

Table 6.2: Vitrinite reflectance, maceral composition, amount of ash, volatile matter, total sulfur- and phosphorous as well as calculated values for basicity for Peak Downs. Values reported by Kahraman and Esterle (2001).

R _{max} [%]	Maceral composition		A ^a [%]	V ^{dar} [%]	S _t ^a [%]	P _t ^a [%]	B _{ash} [*]
	Vitrinite	Inertinite					
1.4	68	27	9.9	23	0.55	0.04	0.06

* The basicity is calculated based on the reported values of Fe₂O₃, CaO, K₂O and MgO. The remaining ash components are supposed to consist of either SiO₂ or Al₂O₃.

A comparison between values presented in Table 6.2 and analyzed in the course of this work shows a reasonable good correlation. Rank is reported based on maximum reflectance of vitrinite in **Kahraman and Esterle (2001)**. From the correlations between random- and maximum reflectance of vitrinite given in Table 5.8, an analyzed value of 1.32 % of random reflectance correlates very well with the reported value of 1.4 % for maximum reflectance of vitrinite.

In this work, petrographic composition of the ROM coals was investigated in two separate size ranges (Figure 5.5). The amount of vitrinite in the coal sample containing the finest size fraction corresponds better with the reported value in Table 6.2 than the coarser particles. Content of inertinite is however on the lower side in both size fractions compared to the value given in Table 6.2. The quoted values for volatile matter as well as amounts of total sulfur and phosphorous are well correlated with the values given in Table 5.1.

6.1.3 Staszic

Even though information including both the exact mine and seam from which the coal sample was extracted were known, typical properties of coals mined from the Anticlinal beds in the Upper Silesian Sandstone Series were harder to find than for the other sample materials. The Staszic mining concession is belonging to the Kompania Węglu Kammiengo and general information like size ranges, calorific values, ash contents, amounts of total sulphur, levels of moisture and amounts of volatile matter are available on the company web page (<http://www.kwkstaszic.pl/>). These values are however related to the commercial products from the mine, and the data are most likely given for washed coals. As the information was limited and the fact that the sample used in this work was ROM coal, a direct comparison was not made.

Parzentny and Róg (2000) have analyzed 110 channel samples from the 510 seam, which is the seam from which the coal sample in this work was extracted from. The reported samples are gathered from three regions in the Upper Silesian Coal Basin of which Staszic is belonging to the central region. Rank, maceral composition, proximate analysis as well as calorific values are reported for a total of 70 samples in this region. Results from the analyses are presented in Table 6.3.

Table 6.3: Random vitrinite reflectance, maceral composition, results from proximate analyses and calorific values for 70 samples mined from the 510 seam in the central part of the Upper Silesian Coal Basin. Values reported by Parzentny and Róg (2000).

	R _r [%]	Maceral composition			W ^a [%]	A ^a [%]	V ^{dal} [%]	Q _s ^{dal} [Mj/kg]	S _t ^a [%]
		Vit	Lip	Int					
Min	0.60	17	5	12	1.26	2.49	29.85	30.20	0.18
Max	1.08	81	26	70	9.08	18.69	39.04	36.20	1.66
Average	0.79	42	12	46	3.92	5.21	34.06	33.78	0.54

As the data in Table 6.3 is gathered from 70 samples in the region of interest, the range of reported values are wide. The characteristic properties from the sample used in this work are however fairly similar to the average values presented in the Table 6.3.

6.2 Effect of Different Carbonization Procedures

Properties of metallurgical coke are known to depend on both coal properties and the carbonization conditions. In this work, the coals have been carbonized in a procedure resembling the conditions coals experience as they are charged to an industrial silicon furnace (section 4.4). This procedure is completely different from the industrial production of metallurgical coke in several aspects: heating rate, pressure induced during carbonization, “coking” time and grain size of the coal particles.

During his PhD work, **Kaczorowski (2006)** investigated, among other things, how coal- and coke properties influence the Boudouard reactivity in the production of manganese alloys. Undersized coke from the blast furnace operation is commonly used as a reducing agent in the production of manganese alloys. In addition to analyzing industrial cokes, Kaczorowski also looked into the coal to coke conversion. In order to gain insight into factors which might affect reactivity in the manganese production, he analyzed three ROM coal samples and subsequently carbonized those in a laboratory furnace resembling conditions in a slot oven before the reactivity tests were performed. As both projects had the same professor, the ROM samples in his work are identical to the coals which have been used in the present work. Thus, in order to investigate how different carbonization procedures affect properties of coke / char, reported analytical data of the produced cokes in **Kaczorowski (2006)**, are compared to properties of products following the SINTEF carbonization procedure (section 5.5 – 5.6). In the following sub-chapters the lowest density char is used as a term for the char produced from the coal fraction with the lowest specific density for the sample materials. This corresponds to LD for Blue Gem and MD for Peak Downs and Staszic. Correspondingly, the term highest density char is used for the MD fraction of Blue Gem and HD fractions of Peak Downs and Staszic. Values gathered from **Kaczorowski (2006)** are denoted as coke.

6.2.1 Physical properties

Physical properties of the carbonized products are compared based on different carbonization procedures in Figure 6.2.

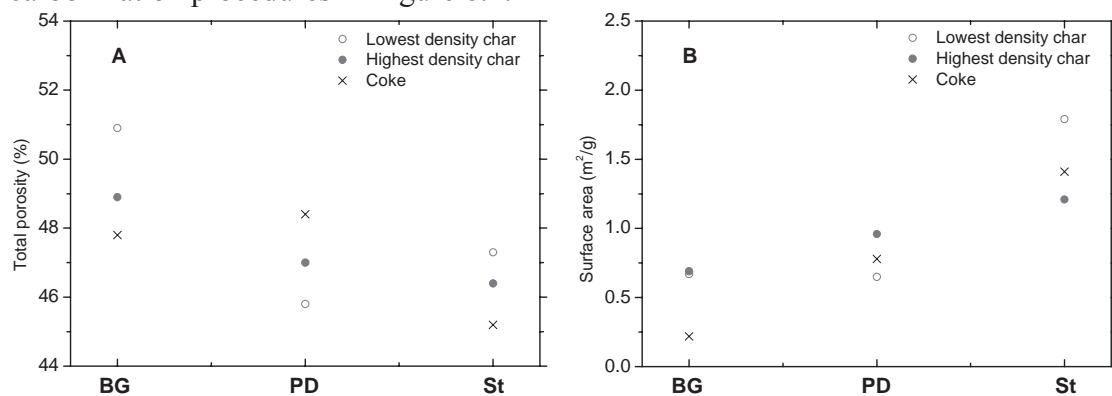


Figure 6.2: Comparison of total porosity (A) and surface area (B) of the carbonized materials based on different carbonization procedures.

From Figure 6.2 A, it seems like development of total porosity is a function of coal rank as well as the carbonization procedure. For the high volatile bituminous coal samples higher values for total porosity are obtained by the SINTEF procedure. These coals have relatively large amounts of volatile matter which for the most part is released during carbonization. In the SINTEF procedure the coals are free to swell as there is no pressure applied during carbonization. In addition, the temperature gradient experienced by the charged coals is very high and a rapid development of gases might lead to higher porosity values. The cokes used by **Kaczorowski (2006)** were produced in a crucible of fixed dimensions and were hence not able to expand in the same manner. As the procedure was supposed to resemble the industrial production of metallurgical coke, a

significantly lower heating rate was applied during carbonization. These factors are believed to be the main reasons for the observed trend regarding the high volatile bituminous coal samples.

Peak Downs is medium volatile bituminous of rank and does not contain the same amount of volatile matter as the lower rank coals (Table 5.1). Based on the content of volatile matter, a release of volatile components during charging similar to Blue Gem and Staszic is not expected. As porosity is developed by reactive components in the plastic range, duration of plasticity is probably a factor that might account for the observed differences in total porosity for this sample. The widest plastic range is detected for Peak Downs (Table 5.1). By applying a low heating rate, time in the plastic range is prolonged and pores developed by reactive components thus have more time to coalesce and grow. This assumption is confirmed by the pore size distributions obtained by image analysis where the samples in Kaczorowski's work all tend to have higher fractions of coarse pores. The pore size distributions of macro pores were however not analyzed during his work.

Values for surface area given in Figure 6.2 B do not show the same trends. The combination of higher values of total porosity combined with a larger ratio of smaller pores in Blue Gem by using the SINTEF procedure should also render a higher surface area which can be observed in the figure. Following the same argumentation, available surface area of Peak Downs should give approximately the same values independent of carbonization procedure, as can be seen in the figure. By far the highest surface area was found in samples of Staszic (Figure 5.18). This was contributed to the dull structure of the coal where attrital coal including liptinite macerals will produce carbonized particles of higher porosities than when inertinite or mineral inclusions are contributing to the attrital microtextures. In this work the coal samples were separated by density thus concentrating the attrital coal associated with liptinites in the MD fraction. Inertinite macerals and minerals contribute to a higher particle density and a higher fraction of the attrital coal recovered in the HD fraction of the coal is believed to consist of these components. As the ROM coal, analyzed in **Kaczorowski (2006)**, will be a combination of these microtextures, a value of available surface area in between what is observed for the MD- and HD fractions was anticipated.

The effect pyrolysis conditions on char structure are of interest to coal fired power plants and have been investigated in several papers. Very fine grained coal particles and high heating rates are common parameters in these examinations.

Zygourarakis (1993) has pyrolyzed coal particles varying in size from 125 – 710 μm at heating rates from 0.1 - 1000°C/s and analyzed both total porosity and pore shapes. An increased heating rate resulted in chars with higher values of total porosity, more open pore structure and larger surface area. In addition, the author states that large particle swelling occurs at high heating rates leading to particles with very high porosity. Coal particle size did not affect the sample porosity, but changed the shape of the pores which might influence the surface area of the carbonized products. These results are in accordance with the values illustrated in Figure 6.2.

Tang et al. (2005) separated six Australian coal samples varying in rank from 0.44 – 1.02 % random reflectance of vitrinite in the size range 45 – 63 μm by a sink – float procedure into density fractions corresponding to the MD-, HD- and Ash fractions used in the present work. The MD- and HD fractions were subsequently pyrolyzed in a drop tube furnace with heating rates of 100,000 K/s before porosity of the produced chars were evaluated by image analysis. All the chars produced from the MD fractions had higher values of average porosity than the corresponding HD fractions.

Conclusions from the quoted authors above largely agree with the results presented in Figure 6.2 even though different grain sizes and heating rates have been applied.

6.2.2 Coke petrography

To examine if the carbonization procedure affects composition of microtextures, the most abundant carbon forms in the carbonized products are plotted in Figure 6.3.

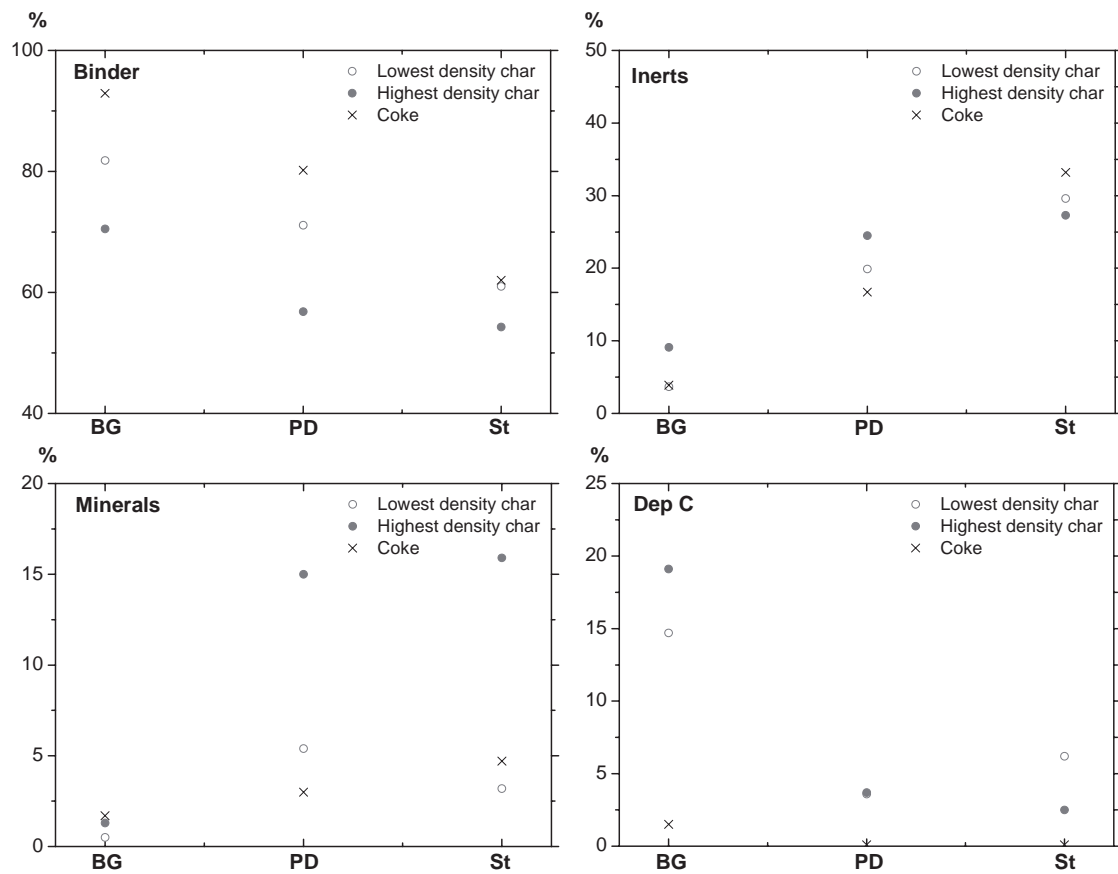


Figure 6.3: Abundance of microtextural components in the carbonized products based on different carbonization procedures.

Petrographic identification of microtextures in coke is a more difficult procedure than the corresponding maceral analysis for coal samples. If the coal rank dictates a high degree of anisotropy in the carbonized product, differentiation of binder phase components and organic inerts are performed with relative ease. Isotropic binder phase and semi-fusible macerals are factors making differentiation between binder- and filler phase microtextures harder. As discussed in 5.6.1, the abundant quartz inclusions

observed in coal samples of Peak Downs are not distinguishable in the carbonized product. Anisotropy of the chars and cokes produced from this coal make it very difficult to identify these inclusions. Even though guidelines to dimensions and shapes of the observed anisotropic domains are given in the ASTM standard (ASTM D5061 1997), determination of these microtextures is still to a certain degree subjective.

Based on Figure 6.3, it can be seen that cokes analyzed by Kaczorowski (2006) all have a higher content of binder phase than the analyzed chars. The main reason for this difference can to some extent be contributed to a higher level of depositional carbons in the chars produced by the SINTEF carbonization procedure. Following the density separation of coals, ash fractions which were containing mostly minerals were discarded and did not contribute to the carbonized products. Especially minerals and to some extent infusible macerals were thus anticipated to be more abundant in carbonization products from the ROM coals than in the chars produced from the density separated coals. For the Blue Gem samples this assumption seems to hold water, apart from the fact that the amount of organic inerts is higher in the HD char than in the coke. For Peak Downs, a significantly higher content of both mineral inclusions and infusible macerals are observed in both char samples compared to the coke. These findings are puzzling, and especially the large differences in observed mineral inclusions. The most probable explanation is a misidentification of these components during analyses. Unusually high amounts of mineral inclusions are identified in the highest density fractions of both Peak Downs and Staszic. The reduction peaks in the measured CO profiles during reactivity tests in the present work (Figure 5.25) are however indicating that there are higher amounts of minerals in these fractions. As the cokes produced by Kaczorowski have not been tested in the SINTEF SiO reactivity test, it is hard to conclude about the level of minerals in these materials.

6.2.3 X-Ray diffraction

According to Gray (2005), heating rate during carbonization is known to affect the degree of crystallinity in the products. Heating rates applied during industrial production of metallurgical coke are significantly lower than the one coals experience during charging to an industrial silicon furnace, thus prolonging time in the plastic range. A high heating rate influences composition of the plastic layer and might result in incomplete release of volatile tar components. These components will enhance fluidity and hence contribute to larger carbon crystals.

In order to investigate whether degree of crystallization is influenced by the carbonization procedure, structural parameters obtained from X-ray diffraction procedures are compared in Figure 6.4.

Based on values for interlayer spacing and stack height in Figure 6.4, carbonization conditions do not influence the d_{002} values to any significant degree. This value is calculated from the Bragg equation (4.12) and is only dependant upon position of the intensity corrected carbon peak (002). The Scherrer equation (4.13), which is used for calculating L_c values, includes both position- and width of the carbon peaks (FWHM). As can be seen from Figure 6.4, wider carbon peaks for the cokes are indicating smaller crystals than for the chars produced from the SINTEF procedure.

Oya et al (1983) have prepared cokes from five Chinese coals ranging in rank from 0.71 – 1.66 % R_{max} . A maximum temperature of 1000°C and a heating rate of 4°C/min were used as carbonization parameters. In general, increasing rank is resulting in decreasing interlayer spacing and increasing crystallite height. Reported values are in the range 3.41 – 3.45 Å and 16 – 20 Å for respectively interlayer spacing and stack height. As can be seen from Figure 6.4, the carbonized materials analyzed in this work generally have slightly higher values for both d_{002} and L_c . Values for stack height analyzed by Kaczorowski (2006) corresponds well with the reported values while interlayer spacing are tending to be slightly higher in his work as well.

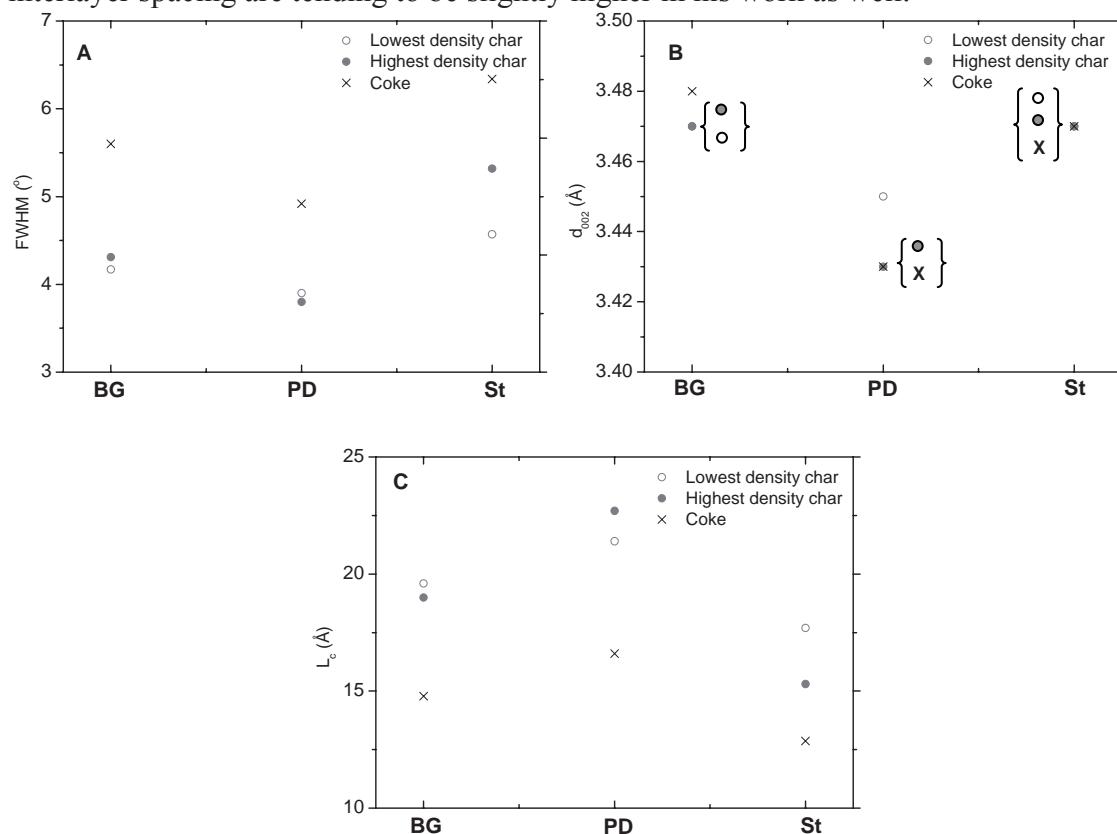


Figure 6.4: Comparison of how structural parameters of the carbonized coals depend upon the carbonization procedure. Full Width Half Maximum (A), interlayer spacing (B) and stack height (C).

6.3 Material Properties and Reactivity Towards SiO gas

The reaction between carbonaceous materials and SiO gas has been extensively studied. Based on the studies referred to in section 2.3, rank and ratio of fusible to infusible macerals are the two most important petrographic parameters of coals which affect reactivity. According to these studies, low rank and high amounts of “reactive” macerals are correlated with an increase in reactivity. Some of the studies are reporting a low degree of anisotropy and high binder- to filler phase ratio in the carbonized products to be beneficial for a high reactivity. These properties are determined by rank and maceral composition of the coals, and are thus directly related to the former predictions.

Coal rank can be evaluated based on several parameters (section 3.3.1), but the most acknowledged measure of rank is the reflectance of vitrinite. Measurements of random reflectance of vitrinite (Figure 5.8 and Table 5.7) divide the coal samples used in the present work in two groups. Blue Gem and Staszic have similar values of random reflectance and are characterized as high volatile bituminous coals. Peak Downs has a significantly higher reflectance value and is a medium volatile bituminous coal in rank according to the American classification. Based solely on rank, Peak Downs should, according to the quoted studies in section 2.3, have the lowest reactivity of the tested coals. The measured reactivity values obtained in this work (Figure 5.27) do however reveal that Peak Downs is the most reactive of all the tested samples and thus contradict the previous studies. Blue Gem and Staszic can hardly be differentiated based on the reflectance measurements, and should thus have similar reactivity values based solely on rank. As can be seen in Figure 5.27, the MD fraction of Staszic and Blue Gem samples have similar reactivity values, while the HD fraction of Staszic has the lowest reactivity of all the tested samples. These differences are however not related to rank.

Composition of the coal samples have in this work been evaluated by standard maceral analyses (5.4.1) supplemented by non-maceral analyses in order to among other things evaluate the degree of heterogeneity of the coal samples (5.4.3). These analyses revealed large differences in the ROM coal samples (Figure 5.5). Blue Gem was characterized as a very homogeneous coal (bright), high in vitrinite and liptinite and scarce in inertinite macerals and mineral inclusions, thus having a high fusible to infusible macerals ratio. Staszic on the other side was proven to be a very dull coal especially high in inertinite macerals well embedded in the vitrinite matrix. Based on the rank of Peak Downs, macerals belonging to the liptinite group are not identifiable in this coal sample. There were however observed plentiful inclusions of clastic quartz throughout the sample, which was one of the characteristic features for this coal.

In addition to the original differences in petrographic composition, a density separation of the ROM coal samples were performed in order to produce fractions of the same coal with different petrographic constitution. The objective of the density separation was to concentrate inertinite macerals and minerals in the highest density fractions while vitrinite and liptinite macerals should have a higher content in the lightest density fractions. As can be seen in Figure 5.6, the objective of the procedure was accomplished. The influence of petrographic composition of the coal samples on reactivity can thus be evaluated.

As Blue Gem is a homogeneous coal from nature, the density fractions of this sample were fairly similar in petrographic composition (Table 5.6 and Figure 5.6). If vitrinite and liptinite are regarded as reactive macerals and the remaining components in Table 5.6 are believed to be infusible during carbonization, a higher content of fusible macerals is present in the MD fraction of Blue Gem. This is mainly due to a higher amount of vitrinite (pseudovitrinite) in the MD fraction while liptinite macerals are present in a higher amount in the LD fraction. As petrographic composition of the density fractions are fairly similar, they are anticipated to have reactivity values in the same range. Textural analysis of the carbonized samples did however reveal a higher

content of organic inerts and depositional carbons in the MD fraction which indicates a slightly higher *R10 corrected* value for this fraction. Based on the measured reactivity (Figure 5.27), the MD fraction has a 5.9 % higher average *R10 corrected* value than the corresponding LD fraction. This is within the standard deviation of the test and reactivity of the samples can thus not be separated.

The density separation resulted in a higher amount of infusible macerals as well as minerals in the HD fraction of Peak Downs compared to the MD fraction (Table 5.6). As textural analysis of the carbonized fractions also revealed that filler phase carbon forms are present to a higher degree in this fraction, the HD fraction should thus, according to the studies in section 2.3, have a higher value of *R10 corrected* than the MD fraction. As can be seen in Figure 5.27, measured reactivities of the density separated fractions are almost identical thus indicating that the petrographic composition does not have any influence on reactivity of this sample material. The reason for this is due to the numerous quartz inclusions in both density fractions. These inclusions will render the physical properties of the carbonized material at reaction temperatures according to *reaction 1.3*, increasing both surface area and porosity. The effects of these inclusions are thus suppressing any effects of the difference in petrographic composition between the different density fractions.

Maceral analysis of the density separated fractions of Staszic revealed a significantly higher ratio of fusible to infusible components in the MD- than HD fraction. Both fractions are however characterized as dull attrital coals, but the attrital coal in the MD fraction is believed to consist of a higher content of liptinite macerals than the corresponding HD fraction. This is confirmed by the higher surface area and total porosity in this fraction (Figure 5.18). Textural analysis of the carbonized fractions also proved that there is a higher amount of binder phase carbon forms in the MD fraction. According to the petrographic differences of the density fractions, the HD fraction should be less reactive than the MD fraction of this coal sample. The reactivity results confirm that there is a significant difference in reactivity between the two fractions with the HD fractions having a value of *R10 corrected* close to 30 % higher than the MD fraction. The higher content of fusible components (especially liptinite) in the MD fractions is believed to be the main cause for the higher reactivity of this fraction, and is thus in accordance with the studies referred to in section 2.3.

In previous studies of the reaction between fossil carbonaceous materials and SiO gas, mineralogy has not been considered to be a factor contributing to the reactivity, mainly because the reaction is believed to be limited by transport processes rather than catalytic phenomena. Results presented in this work do however emphasize the importance of identifying mineral components and their distributions in the coal in addition to petrographical properties. The clastic quartz inclusions which are finely distributed throughout the samples of Peak Downs are the main cause for the high reactivity and degree of conversion for this sample, and are thus contradicting the conclusions from previous studies as neither rank nor petrographic composition influences the reactivity of this sample.

As mentioned in section 5.7.4, both Blue Gem and Peak Downs have been used as standard materials in validation of the improved SINTEF SiO reactivity test. **Lindstad et al. (2007)** and **Hansen (2005)**. These authors have reported *R10 corrected* values in the range 567 – 606 and 519 – 580 ml SiO for Blue Gem and Peak Downs, respectively. The reported reactivity values for Peak Downs are agreeing very well with the values presented in this work, while Blue Gem is slightly more reactive in validation of the SINTEF test than the results in the present work indicate. As Blue Gem is a fairly well known coal for the Norwegian silicon producers, it has previously been tested in the SINTEF reactivity test. According to **Hansen (2005)**, reactivity values obtained before modification of the test can be correlated to the *R10 corrected* values from the improved SINTEF SiO reactivity test by multiplying the “old” values by a factor 0.75. As **Patalsky et al (1995)** have reported an “old” *R10* value of 921 ml SiO this corresponds to a *R10 corrected* value of 701 ml SiO. This value is better correlated with the results presented in this work than by **Hansen (2005)**.

7. CONCLUSIONS AND FURTHER WORK

The main objectives of this work have been to establish methods suitable for examinations of fossil reduction materials in the silicon process and to correlate the material properties to the reactivity towards SiO gas.

In order to accomplish these objectives, three run of mine (ROM) single seam coals which are particularly well suited for ferroalloy production were selected. Both Blue Gem and Staszic are Carboniferous coals from USA and Poland, respectively. By measuring the reflectance of vitrinite, these samples were determined to be almost identical in rank. Measured values of random reflectance were 0.71 % and 0.72 % for respectively Blue Gem and Staszic, and are thus categorized as High Volatile Bituminous B according to the American coal classification. Peak Downs is a Permian coal from the Bowen Basin in Australia and was determined to be medium volatile bituminous in rank with a random reflectance of vitrinite of 1.32 %.

The ROM coals were characterized by standard coal analyses including proximate- and ultimate analyses as well as ash composition and evaluation of the thermoplastic properties (Gieseler fluidity). In addition, the petrographic properties were determined by standard maceral analyses, vitrinite reflectance and non-maceral analyses. Non-maceral analysis was included in order to assess properties in the coal samples which are not accounted for during a standard maceral analysis. By combining the results from these analyses, Blue Gem can be characterized as a very homogeneous coal with low amounts of mineral inclusions. A relatively high amount of pseudovitrinite was detected in these coal samples. Even though Staszic is almost identical in rank and deposited in the same geological age, the composition of this coal is quite different. Proximate analysis revealed an ash content of 5.9 % which is an intermediate value of the tested coals. Composition of the ash is however similar to that of Blue Gem (determined by the basicity value). Petrographic composition of the coal is however distinctly different from Blue Gem. Staszic is the most inhomogeneous coal of the tested samples, and macerals from the major groups as well as minerals were typically very well mixed in this sample material. The highest ash content was detected in Peak Downs (11.6 %). Compared to the Carboniferous samples, the level of SiO₂ in the ash was significantly higher. Petrographical analyses revealed several typical features of Permian coals in this coal sample. Macerals of the inertinite group which were not present (or in very low amounts) in the Carboniferous coals, were fairly abundant in Peak Downs (funginite and secretinite). The level of reflectance was in many cases similar for vitrinite and some inertinite macerals (especially semifusinite) which made positive identification of these macerals somewhat harder than in the Carboniferous samples. Based on the rank of Peak Downs, liptinite macerals were not identified in this coal. Numerous inclusions of clastic quartz were observed well distributed throughout the coal texture.

As petrographic composition of the coal samples was one of the factors believed to affect the reactivity towards SiO gas, density fractions of the ROM coals were prepared by a sink – float procedure. Three aqueous solutions of ZnCl₂ with specific density 1.25, 1.35 and 1.50 g/cm³ were prepared and compositions of the density fractions were

analyzed by petrographic procedures. The purpose of the density separation was to accumulate inertinite macerals and minerals in the fractions with highest specific density and consequently vitrinite- and liptinite macerals in the lightest fractions. Even though recoveries of the + 1.50 g/cm³ fractions in all cases were below 10 %, they had a content of 38 – 82 % of mineral matter. The most significant differences between density fractions were obtained with the most inhomogeneous ROM coals. As Blue Gem is a very homogeneous coal, the density fractions were fairly similar, while a better separation was observed for both Peak Downs and Staszic.

Succeeding the separation procedure, the two density fractions of each coal with highest recovery were carbonized according to the SINTEF method. Structural properties of the carbonized samples were assessed by image analysis, mercury porosimetry, BET method and X-ray diffraction. Blue Gem proved to have the highest total porosity and mercury porosimetry identified both density fractions of this sample to have the highest amount of small pores. Values of surface area were however highest in the other Carboniferous coal sample, and especially in the lowest density fraction of Staszic. This is due to the inhomogeneous particles consisting mostly of vitrinite- and liptinite macerals. Peak Downs was determined to have the highest density of the tested samples, which correlated well with results from X-ray diffraction where this sample was determined to consist of the largest and densest carbon crystallites. Quantification of microtextures in the carbonized samples was determined by a petrographic counting procedure. The results correlated well with composition of the coal samples where fusible macerals will constitute the binder phase while infusible macerals and minerals will constitute the filler phase. Surprisingly large quantities of depositional carbons were accounted for in both Blue Gem samples. Depositional carbons are produced when volatile gases evolved during carbonization crack on a hot surface. They were typically observed on the pore walls and periphery of the particles.

Reactivity of the carbonized samples towards SiO gas was assessed by the SINTEF SiO reactivity procedure. The reactivity measure from this procedure is termed the *R10 corrected* value and is given as the volume of SiO gas which passes unreacted through a packed bed of carbon particles as the CO concentration in the effluent gas decreases from 18 – 10 %. A low value of *R10 corrected* is thus indicating a reactive material and vice versa. A minimum of two parallels of each density fraction was tested in order to secure consistency and evaluate the reproducibility of the test procedure. Former studies of the reaction between carbon and SiO gas have come to the conclusions that low rank and high amounts of fusible macerals are correlated with a high reactivity. Peak Downs was thus expected to be the least reactive material and the highest density fractions were believed to be less reactive than the corresponding lightest density fractions.

Results from the SINTEF test did however reveal that Peak Downs was the most reactive material of the tested samples, and it was not possible to differentiate between the density fractions. The reason for the observed behavior of Peak Downs is due to the abundant quartz inclusions in the coal matrix. These inclusions will react with carbon at the reaction temperature of 1650°C to produce SiC and CO. In addition, the reaction will increase porosity and surface area of the material thus contributing to easier access for reacting gases which in turn will result in an increased reactivity and degree of conversion. Petrographic examinations of the reacted samples did in fact conclude with

a degree of conversion close to 100 % as unreacted carbon hardly was observed. In order to evaluate the effect of the quartz inclusions on the physical properties, the highest density fraction of Peak Downs was heated to the reaction temperature without access to SiO gas. Porosity evaluated by mercury intrusion of the sample was more than doubled following the heat treatment.

Both density fractions of Blue Gem came out with similar reactivity values from the SINTEF test, and are termed intermediate of the tested materials. Blue Gem is a homogeneous coal, and there were no significant differences with regard to the petrographic composition of the density fractions. The effect of maceral composition on the reactivity towards SiO gas is thus hard to evaluate based on these samples. Unreacted carbon was easily detected by petrographic examinations of the reacted samples. Based on these investigations and the reported weight increase during reaction, a degree of conversion between 80 – 90 % is reported for the Blue Gem samples.

Staszic has been characterized as an inhomogeneous coal and the highest amount of infusible macerals and minerals are identified in the heaviest density fraction. The SINTEF SiO reactivity test revealed that there was a significant difference in reactivity between the two fractions. The highest density fraction of Staszic is the least reactive of all the tested materials and has a *R10 corrected* value more than 40 % higher than the lowest density fraction. As both fractions are of identical rank, the observed reactivity difference has to be caused by the higher amount of filler phase in the highest density fraction.

The effect of particle size on reactivity has been demonstrated by running the SINTEF SiO reactivity test with smaller particles (3.35 – 4.00 mm) than the conventional test procedure prescribes (4.00 – 6.30 mm). Reduced particle size resulted in an increased reactivity for both Blue Gem and Staszic while the effect was not noticeable in the density fractions of Peak Downs. In order to obtain kinetic parameters like the reaction rate constant and effective diffusivity for the tested materials, profiles from both the conventional tests and the tests with reduced particle size were fitted to theoretical reactivity curves obtained from the shrinking core model used for packed beds. Values for the kinetic parameters in the same order of magnitude as previously reported were obtained for Blue Gem and Staszic. Based on the results from experiments with reduced particle sizes, it was obvious that Peak Downs could not be modeled by the shrinking core model thus no kinetic parameters were obtained for these samples.

For the purpose of evaluating and differentiating properties of the fossil carbonaceous materials used in this work, a number of petrographic analyses have been employed. To summarize benefits, potential drawbacks and range of applications for the methods, an evaluation is in order. The standard maceral analysis is the only procedure which is quantifying the constituents (macerals and minerals) in the coal and is thus very useful. In order to gain more information about the nature of a specific coal, this analysis should however be combined with morphological studies and / or non-maceral analysis. A combination of these procedures will render much more information than by using the standard maceral analysis on a stand alone basis. Information like oxidation of coal which affects the thermoplastic properties and hence development of porosity, nature and distribution of mineral inclusions and degree of inhomogeneity of the coals should also be provided.

Quantification of attrital coal in the non-maceral analysis should probably be more diverse in order to give more specific information to determine properties of the carbonized products. Attrital coal consisting for the most part of vitrinite and liptinite macerals will produce a porous coke / char while this is not necessarily true for agglomerates of vitrinite and inertinite and / or minerals.

Petrography of the carbonized products will give the ratio between binder- and filler phase which for the most part is equal to the ratio between fusible- to infusible macerals in the coal. The procedure can however give information about the carbonization procedure as amount and type of depositional carbons. The depositional carbons have a significantly different structure than coke / char and might affect the reactivity in the process.

In this work, petrography of the reacted samples has also been carried out. These examinations have given useful information about the degree of conversion, which macerals have predominantly been converted to SiC and preferred sites for condensation. Based on the examinations carried out in this work, all carbon forms seem to be converted to SiC as long as the supply of SiO gas is sufficient. In addition condensation was mostly observed on infusible macerals of fusinite and semifusinite as well as on depositional carbons on pore walls and the particle edges.

Even though mineral inclusions in the carbonaceous reduction materials are not believed to catalyze the reaction with SiO gas, findings in this work have determined that they might affect the structure and hence influence both reactivity and degree of conversion. In future studies of the reaction between carbon and SiO gas it is hence recommended to include the effect of mineral matter and especially the type and distribution of these.

Applications of silicon metal with low amounts of impurities and trace elements are expected to increase in the immediate future. A stable demand for pure raw materials to the process is a prerequisite for accomplishing the future demand of high purity silicon. In that respect, utilization of pure carbon materials like synthetic graphite or petroleum coke might expect a higher demand. These materials have a low reactivity towards SiO gas and are thus not suitable based on profitability of the process. Agglomerating these carbon materials with finely ground quartz might alter the process parameters to make these materials more suitable for the process. The major challenge is to maintain sufficient mechanical strength of the agglomerate. Tailor-made agglomerates that fulfil both process- and product requirements should be investigated further.

BIBLIOGRAPHY

- Andresen, B. (1995).** "Process model for carbothermic production of silicon metal". Trondheim, Universitetet i Trondheim, Norges tekniske høgskole, Metallurgisk institutt.
- Antal Jr, M. J. and Grønli, M. (2003).** "The Art, Science and Technology of Charcoal Production", *Ind.Eng.Chem.Res.* vol. 42, pp. 1619 – 1640.
- ASTM D2795 (1999).** "Standard Practice for Preparing Coal Samples for microscopical Analysis by Reflected Light". Philadelphia, USA.
- ASTM D2798 (1999).** "Standard Test Method for Microscopical Determination of the Reflectance of Vitrinite in a Polished Specimen of Coal". Philadelphia, USA.
- ASTM D2799 (1999).** "Standard Test Method for Microscopical Determination of Volume Percent of Physical Components of Coal". Philadelphia, USA.
- ASTM D4371 (1998).** "Standard Test Method for Determining the Washability Characteristics of Coal". Philadelphia, USA.
- ASTM D5061 (1997).** "Standard Test Method for Microscopical Determination of Volume Percent of Textural Components in Metallurgical Coke". Philadelphia, USA.
- Bakken, J. A. (1969).** "Omsetningsgrad ved prosesser av typen $AB(g)+2C(s)$ $AC(s)+BC(g)$ ": rapport for Norges teknisk-naturvitenskapelige forskningsråd (In Norwegian). Trondheim, SINTEF. Avd. for metallurgi.
- Berkowitz, N. (1994).** "An introduction to coal technology". San Diego, Academic Press, pp. 398.
- Bhatia, S. K. and Perlmutter, D. D. (1980).** "A random pore model for fluid – solid reactions: I. Isothermal, kinetic control.", *AI Chem Eng. Journal.*, vol. 26, pp. 379 – 386.
- Bhatia, S. K. and Perlmutter, D. D. (1981).** "A random pore model for fluid – solid reactions: II. Diffusion and transport effects.", *AI Chem Eng. Journal.*, vol. 27, pp. 247 – 254.
- Bhatia, S. K. and Perlmutter, D. D. (1983).** "Unified Treatment of Structural Effects in Fluid – Solid Reactions.", *AI Chem Eng. Journal.*, vol. 29, pp. 281 – 289.
- BMA Coal (2007),** Retrieved 2007-07-11, from:
<http://www.bmacoal.com/opencms/export/sites/bccom/operations/PeakDowns/>

- Brown, N. A., Coin, C. D. A and Gill, W. W. (1982).** "Prediction of Coke Quality", BHP Technical Bulletin 23, pp. 27 – 30.
- Butler, J., Marsh, H. and Goodarzi, F. (1988).** "World coals: Genesis of the world's major coalfields in relation to plate tectonics." *Fuel*, Vol 67 (2), pp. 269 - 274.
- Byrne, J. F. and Marsh, H. (1995),** "Introductory overview" in "Porosity in carbons: characterization and applications", J. W. Patrick (Editor), Edward Arnold, London, ISBN 0-340-544732.
- Callcott, T. G. and Calcott, R. (1990).** "Review of coal characteristics of the Bowen Basin". In Beeston, J. W. (Ed), "Proc. Bowen Basin Symp. And GSA (Qld Division) Field Conf., pp 47 – 53, Mackay, Qld, Australia.
- Carstens, H. (2005).** "Energi for evigheten." *GEO* (6): 3.
- Chen, G. Z., Fray, D. J. and Farthing, T. W. (2000).** "Direct electrochemical reduction of titanium dioxide to titanium in molten calcium chloride." *Nature*, Vol. 407 (6802), pp. 361 - 364.
- Condie, K. C. (1989).** "Plate tectonics & crustal evolution". Oxford, Pergamon Press.
- Crelling, J. C. (1987).** In International conference on coal science. Elsevier, pp. 119 – 122.
- Cross, A. T. and Phillips, T. L. (1990).** "Coal-forming plants through time in North America." *International Journal of Coal Geology*, Vol. 16 (1-3), pp. 1 - 46.
- Diessel, C. F. K. and McHugh, E.A. (1986).** "Fluoreszenzintensität und Reflexionsvermögen von Vitriten und Inertiniten zur Kennzeichnung des Verkoksungserhaltens." *Glückauf-Forschungshefte: Zeitschrift zur Verbreitung von Forschungsergebnissen im Bergbau*, Vol. 47: 11.
- Diessel, C. F. K. and Wolff-Fischer, E. (1986).** "Vergleichsuntersuchungen an Kohlen und Koksen zur Frage der Inertinitreaktivität." *Glückauf-Forschungshefte: Zeitschrift zur Verbreitung von Forschungsergebnissen im Bergbau*, Vol. 47: 9.
- Diessel, C. F. K. and Wolff-Fischer, E. (1987).** "Coal and coke petrographic investigations into the fusibility of Carboniferous and Permian coking coals." *International Journal of Coal Geology*, Vol 9 (1), pp. 87-108.
- Dyrkacz, G. R., Bloomquist, C. A. A. and Ruscic, L. (1984).** "High-resolution density variations of coal macerals." *Fuel*, Vol. 63 (10), pp. 1367 - 1373.
- Dyrkacz, G. R. and Horwitz, E. P. (1982).** "Separation of coal macerals." *Fuel*, Vol 61 (1), pp. 3 - 12.

- ECE – UN (1988).** “International codification system for medium and high rank coals”. United Nations, New York, USA.
- EIA (2005)** "Energy Information Administration (EIA), Official Energy Information from the U.S Government." Retrieved 2007-07-11, from:
<http://www.eia.doe.gov/cneaf/coal/page/acr/table1.html>
- EIA (2007).** "Energy Information Administration (EIA), Official Energy Information from the U.S Government." Retrieved 2007-07-11, from
<http://www.eia.doe.gov/pub/international/iea2003/table82.xls>
- Ellis, P. J. and Paull, C. A. (1998).** “Tutorial: Delayed Coking Fundamentals”, unpublished, Great Lake Carbon Corporation, Port Arthur, Texas, USA.
- ENS (2007).** "European Nuclear Society." Retrieved 2007-08-21, 2007, from
<http://www.euronuclear.org/info/encyclopedia/coalequivalent.htm>.
- Evans, J. W. and Song, S. (1974).** “Application of a Porous Pellet Model to Fixed, Moving, and Fluidized Bed Gas-Solid Reactors” Ind.Eng.Chem., Process Des. Develop., Vol. 13, pp. 146-152.
- FAO (1985),** “Industrial Charcoal Making”, FAO Forestry Paper No. 63. Food and Agriculture Organization of the United Nations, Rome, Italy.
- Flores, R. M. et al. (1999).** ”1999 Resource assessment of selected Tertiary coal beds and zones in the Northern Rocky Mountains and Great Plain Region”. U.S. Geological Survey professional paper 1625-A, Washington D.C, USA
- Fomin, A. P. et al. (1973).** Coke and Chemistry (USSR), Vol. 10, pp. 11 – 12.
- Gaal, S. (2007).** Picture. Personal communication.
- Gabzdyl, W. and Probierz, K. (1987).** "The occurrence of anthracites in an area characterized by lower rank coals in the Upper Silesian Coal Basin of Poland." International Journal of Coal Geology, Vol. 7 (2), pp. 209 - 225.
- Gill, W. W. and Dubrawski, J. V. (1984).** "Silicon carbide in heat - treated cokes." Ironmaking & steelmaking, Vol. 11 (4): 5.
- Glagolev, A. A. (1934).** "Quantitative analysis with the microscope by the point method." Eng. Min. J. Vol. 135, pp. 399 - 400.
- Goodarzi, F. and Swaine, D. J. (1994).** "The influence of geological factors on the concentration of boron in Australian and Canadian coals." Chemical Geology, Vol. 118 (1-4), pp. 301 - 318.

- Gray, R. J. (1976).** "A system for coke petrography." Proceedings Illinois Mining Institute, Vol 28.
- Gray, R. J. (1982).** "A petrologic method of analysis of non-maceral microstructures in coal." International Journal of Coal Geology, Vol. 2 (1), pp. 79 - 97.
- Gray, R. J. (1991).** "Some petrographic applications to coal, coke and carbons." Organic Geochemistry, Vol. 17 (4), pp. 535 - 555.
- Gray, R. J. (2005).** Personal communication, Monroeville.
- Gray, R. J. and Bowling, C. M. (1995).** "Petrographic prediction of coking properties for the Curragh coals of Australia." International Journal of Coal Geology 27(2-4): 279-298.
- Gray, R. J. and Devanney, K. F. (1986).** "Coke carbon forms: Microscopic classification and industrial applications." International Journal of Coal Geology, Vol. 6 (3), pp. 277 - 297.
- Gray, R. J. and Gray, D. (2005a).** "Lithotypes, Microlithotypes and Nonmaceral Microstructures in Coal". Monroeville, Pennsylvania, USA. Unpublished work.
- Gray, R. J. and Gray, D. (2005b).** "Petrographic Analysis of Coke". Monroeville, Pennsylvania, USA. Unpublished work.
- Grigore, M. et al. (2005).** "Mineral Matter in Coke and Its Effect on gasification Rate", International Conference on Coal Science and Technology, Okinawa, Japan.
- Grigore, M., Sakurovs, R. and Sahajwalla, V. (2006).** "Influence of Mineral Matter on Coke Reactivity with Carbon Dioxide" Iron and Steel Institute of Japan (ISIJ) International, Vol. 46 (4), pp. 503 – 512.
- Grigore, M. et al. (2007).** "Effect of Carbonization Conditions on Mineral Matter in Coke". Iron and Steel Institute of Japan (ISIJ)_International, Vol. 47 (1), pp. 62 – 66.
- Gundersen, Ø. (1998).** "Modelling of structure and properties of soft carbons with application to carbon anode baking". Trondheim, Department of Engineering Cybernetics, Norwegian University of Science and Technology. **1998:70: XLVIII, 532 s.**
- Gurba, I. W. and van Schagen, F. (2003).** "Black Coal in Australia - Sustainable Coal Resource Management". 12th International Conference on Coal Science. Cairns, Australia.

- Hansen, S. (2005).** “Metoder, feilkilder og repeterbarhet for SINTEF SiO reaktivitetstest”. Trondheim, SINTEF Materialer og kjemi, STF80MKF05119 internal report, pp. 64.
- Hatch, J. and Affolter, R. H. (2002).** “Resource Assessment of the Springfield, Herrin, Danville and Baker coals in the Illinois Basin”. U.S. Geological Survey professional paper 1625-D, Washington D.C, USA
- Havlena, V. (1982).** “The Namurian deposits of the Upper Silesian coal basin”. Rozpravy Československé akademie věd - Řada matematických a přírodních věd. Praha, Academia, Praha. Vol. 92.
- Hower, J. C., Rimmer, S. M. and Bland, A. E. (1991).** "Geochemistry of the Blue Gem coal bed, Knox county, Kentucky." International Journal of Coal Geology, Vol. 18 (3-4), pp. 211 - 231.
- Hower, J. C. et al. (1994).** “Petrographic and Geochemical Anatomy of Lithotypes from the Blue Gem Coal Bed, Southeastern Kentucky”. Energy & Fuels, Vol 8 (3), pp. 719 - 728.
- Hyde, R. S., Kalkreuth, W. D. and Utting, J. (1991).** "Petrology, palynology and depositional environments of coals from Upper Carboniferous Barachois Group (Wesphalian A and C), southwestern Newfoundland " Canadian journal of earth sciences, Vol. 28: 20.
- ICCP (1998).** “The new vitrinite classification (ICCP System 1994)”, Fuel, Vol. 77 (5), pp. 349 – 358.
- ICCP (2000).** “The new inertinite classification (ICCP System 1994)”, Fuel, Vol. 80 (4), pp. 459 - 471.
- ICCTC (1982).** "International committee for characterization and terminology of carbon: first publication of 30 tentative definitions". Carbon, Vol. 20 (5), pp. 445 - 449.
- ICCTC (1983).** "International committee for characterization and terminology of carbon: first publication of further 24 tentative definitions". Carbon, Vol. 21 (5), pp. 517 - 519.
- Ishida, M. and Wen, C. Y. (1968).** “Comparison of Kinetic and Diffusional Models for Gas – Solid Reactions”, AIChE Journal, vol. 14, no. 2, pp. 311 – 317.
- ISO 7404-3 (1994).** “ Methods for the petrographic analysis of bituminous coal and anthracite, Part 3: method for determining maceral group composition”
- ITAM (2003)** "Coal in a Sustainable Future". Pp. 24, Osmond Earth Sciences, Adelaide, Australia

Iwashita, N. et al. (2004). "Specification for a standard procedure of X-ray diffraction measurements on carbon materials." *Carbon*, Vol. 42 (4), pp. 701 - 714.

Jacob, H. (1956). "Die Biochemische Inkohlungsphase und das Weichbraunkohlenstadium." (In German). *Chemie der Erde*, Vol. 18: 29.

Jacob, H. (1961). "Die Bildung der Kohlen unter besondere Berücksichtigung der biochemischen Phase." (In German) *Geol. Jb*, Vol. 78: 20.

Jensen, R. (2006). Drawing. Personal communication.

Johansen, S. T., Tveit, H., Grådahl, S., Valderhaug, Aa. and Byberg, J. Å. (1998). "Environmental aspects of Ferro-Silicon furnace operation – an investigation of waste gas dynamics", INFACON 8, Beijing, China.

Kaczorowski, J. (2006). "The Boudouard reaction in manganese production." Trondheim, Norwegian University of Science and Technology, Faculty of Natural Sciences and Technology, Department of Materials Science and Engineering. **2006:224:** XIII, 191 s.

Kahraman, H. and Esterle, J. S. (2001). "Review of coal quality variation in Late Permian Coal Measures of the Bowen Basin, Australia". 18'th Annual International Pittsburgh Coal Conference, Newcastle, New South Wales, Australia.

Kallfeltz, P. L. (2001), "Study prepared for Elkem ASA, Silicon Division, February 2001. " Use of Charcoal in the Silicon production (Draft)", Internal Report,

Kern, A. and Eysel, W. (1993). Mineralogisch-Petrograph. Inst., Univ. Heidelberg, Germany., ICDD Grant-in-Aid.

Kirchbaum, M. A. et al. (2000). "Geological Assessment of Coal in the Colorado Plateau: Arizona, New Mexico and Utah". U.S. Geological Survey professional paper 1625-B, Washington D.C, USA

Kobus, K. (2005). "The History of Cokemaking". 4'th McMaster Cokemaking Course. Hamilton, Ontario, Canada, Department of Materials Science and Engineering, McMaster University.

Koch, J. and Günther, M. (1995). "Relationship between random and maximum vitrinite reflectance." *Fuel*, Vol. 74 (11), pp. 1687 - 1691.

Komorek, J. and Morga, R. (2002). "Relationship between the maximum and the random reflectance of vitrinite for coal from the Upper Silesian Coal Basin (Poland)." *Fuel*, Vol. 81 (7), pp. 969 - 971.

- Kotarba, M. J. and Lewan, M. D. (2004).** "Characterizing thermogenic coalbed gas from Polish coals of different ranks by hydrous pyrolysis." *Organic Geochemistry*, Vol. 35 (5), pp. 615 - 646.
- Kozhevnikov, G. N., Vodopyanov, A. G. and Chufarov, G. I. (1972).** "Reactions between silicon monoxide and carbon". *Russian Metallurgy* (4) (English transl.), pp. 51 – 54.
- Kozhevnikov, G. N., Vodopyanov, A. G. and Nefedov, P. Ya. (1973).** "Influence of oxides in the ash on the reaction between carbon and silicon monoxide". *Russian Metallurgy* (5) (English transl.), pp. 24 – 26.
- Krevelen, D. W. van. (1961).** "Coal: typology, chemistry, physics, constitution". Amsterdam, Elsevier.
- Krevelen, D. W. van. (1993).** "Coal – typology, chemistry, physics, constitution". Amsterdam, Distributors for the U.S. and Canada, Elsevier/North Holland.
- Kårstad (2006).** Personal communication
- Levenspiel, O. (1999),** "Chemical Reaction Engineering", 3rd edition, J. Wiley and Sons, New York, USA.
- Levine, J. R. (1993).** "Coalification: the evolution of coal as a source rock and reservoir rock for oil and gas". In Law, B.E. and Rice, D. D. (Eds) "Hydrocarbons from coal", Amer. Ass. Petrol. Geol, stud in Geol. Ser., Vol. 38, pp. 39 – 77.
- Lide, D. R. (2002).** "CRC Handbook of chemistry and physics: a ready-reference book of chemical and physical data."... : a ready-reference book of chemical and physical data, 83rd Ed.
- Lindstad, T., Gaal, S., Hansen, S. and Prytz, S. (2007).** Improved SINTEF SiO-Reactivity Test. INFACON XI, New Dehli, India, IFAPA.
- Lowenhaupt, D. E. and Gray, R. J. (1980).** "The alkali-extraction test as a reliable method of detecting oxidized metallurgical coal." *International Journal of Coal Geology*, Vol. 1 (1), pp. 63 - 73.
- Marsh, H., Ed. (1989).** "Introduction to carbon science". London, Butterworths.
- Marsh, H. and Clarke, D. E. (1986).** "Mechanism of Formation of Structure within Metallurgical Coke and its Effect on Coke Properties", *Erdöl und Kohle, Erdgas Petrochemie vereinigt mit Brennstoff Chemie*, Vol. 39, pp. 113 – 122.
- McCartney, J. T. and Teichmuller, M. (1972).** "Classification of coals according to degree of coalification by reflectance of the vitrinite component". *Fuel*, Vol 51 (1), pp. 64 - 68.

- McClurg, P. (2001).** "Wyoming Coal." 2007, from <http://smtc.uwyo.edu/coal/>.
- Michaelsen, P. (2002).** "Mass extinction of peat-forming plants and the effect on fluvial styles across the Permian-Triassic boundary, northern Bowen Basin, Australia." *Palaeogeography, Palaeoclimatology, Palaeoecology*, Vol. 179 (3-4), pp. 173 - 188.
- Michaelsen, P. and Henderson, R. A. (2000).** "Facies relationships and cyclicity of high-latitude, Late Permian coal measures, Bowen Basin, Australia." *International Journal of Coal Geology*, Vol. 44 (1), pp. 19 - 48.
- Misiak, J. (2006).** "Petrography and depositional environment of the No. 308 coal seam (Upper Silesian Coal Basin, Poland)-a new approach to maceral quantification and facies analysis." *International Journal of Coal Geology*, Vol. 68 (1-2), pp. 117 - 126.
- Miura, Y. (1978).** "The science of coke making technology and its development in Japan." *Coke oven manager's yearbook 1978*.
- Moriyama, A. (1971).** "Analysis of Fluid-Solid Reaction in Fixed-Bed Reactors under Isothermal Conditions." *Transactions ISIJ*, Vol. 11: 8.
- Motzfeldt, K. (1961).** "An evaluation of the chemistry of the ferrosilicon process, with the special aim of increasing the silicon recovery" (in Norwegian), Report for Elkem from the Inst. Of Silicate Science / Inst. Of Inorganic Chemistry, NTH, Trondheim, Norway.
- Murphy, D. C. (2007),** from <http://www.devoniantimes.org>.
- Myrhaug, E. H. (2003).** "Non-fossil reduction materials in the silicon process: properties and behaviour". Trondheim, Department of Materials Technology, Norwegian University of Science and Technology. **2003:67: XVI**, 226 s.
- Nowak, G. J. (2004).** "Facies studies of bituminous coals in Poland." *International Journal of Coal Geology*, Vol. 58 (1-2), pp. 61 - 66.
- O'Brien, G. et al. (2003).** "Coal characterisation by automated coal petrography." *Fuel*, Vol. 82 (9), pp. 1067-1073.
- Olsen, S. E., Tangstad, M. and Lindstad, T. (2007).** Production of manganese ferroalloys. Trondheim, Tapir akademisk forl.
- Optima (2005).** *Optima*. Vol. 51.

- Otani, Y., Saito, K., Unsi, K and Chino, N. (1968).** "The inner structure of the submerged arc furnace", Paper N.112, discussion M117D, VIth International Congress of Electroheat, Brighton.
- Oya, A., Z., Qian, Z. and Marsh, H. (1983).** "Structural study of cokes using optical microscopy and X-ray diffraction." *Fuel*, Vol. 62 (3), pp. 274 - 278.
- Parzentny, H. and Róg, L. (2000).** "Petrographic and physiochemical properties of coal in seam 510 in the northern and central parts of the Upper Silesian Coal Basin (in Polish)." *Przegląd Górniczy*, Vol. 56 (2): 5.
- Patalsky, R. M., Gray, R.J., Raaness, O. and Todd, S. (1995).** "Results of Microscopic Evaluation of Coals Used to Produce Silicon Metal and Ferroalloys". Electric Furnace Conference, Vol 53. Orlando, Florida, USA.
- Paull, J. M. and See, J. B. (1978).** "The interaction of silicon monoxide gas with carbonaceous reducing agents." *Journal of the South African Institute of Mining and Metallurgy*, Vol. 78: 7.
- Pinheiro, P. C. C., Sampaio, R. S. and Rezende, M. E. A. (2001),** "Charcoal making: Fundamentals and practice" (in Portuguese), Carbonization short course, 1st International Congress on Biomass for Metal Production and Electricity Generation, Belo Horizonte, Brazil.
- Pistorius, P. C. (2002).** "Reductant selection in ferro-alloy production: The case for importance of dissolution in metal." *Journal of the South African Institute of Mining and Metallurgy*, Vol. 4.
- Potonié, H. (1920).** "Die Entstehung der Steinkohle und der Kaustobiolithe überhaupt". 6th Ed, , 233 pp, Borntraeger, Berlin, Germany.
- Poveromo, J. (2005).** "Coke in the Blast Furnace", 4th McMaster Cokemaking Course. Hamilton, Ontario, Canada, Department of Materials Science and Engineering, McMaster University.
- Price, J. (2005).** "Microscopy, Chemistry and Rheology - Tools to Determine Coal and Coke Characteristics". 4th McMaster Cokemaking Course. Hamilton, Ontario, Canada, Department of Materials Science and Engineering, McMaster University.
- Ragot, J. P. (1977).** "Contribution à l'étude de l'évolution des substances carbonées dans les formations géologiques". (In French). Univ. P.Sabatier, Toulouse, France, Thesis, 150 pp.
- Reznik, B. and Huttinger, K. J. (2002).** "On the terminology for pyrolytic carbon." *Carbon*, Vol. 40 (4), pp. 621 - 624.

- Rimmer, S. M. et al. (2000).** "Petrography and palynology of the Blue Gem coal bed (Middle Pennsylvanian), southeastern Kentucky, USA." *International Journal of Coal Geology*, Vol. 42 (2-3), pp. 159 - 184.
- Rodríguez-Reinoso, F. and Marsh, H. (2000).** "Sciences of carbon materials", Universidad de Alicante, Alicante, Spain.
- Roine, A. (1997),** "Outokumpu HSC Chemistry for Windows. Chemical Reaction and Equilibrium Software with Extensive Thermochemical Database. User's Guide version 3.0", Outokumpu research Oy., Finland.
- Roman, O. (1990).** "Geology of Poland vol. VI, Mineral deposits". Warsaw, Pub. House Wydawnictwa Geologiczne.
- Ruppert, L. F. et al. (2001).** "2000 Resource assessment of selected coal beds and zones in the Northern and Central Appalachian Basin coal regions". U.S. Geological Survey professional paper 1625-C, Washington D.C, USA
- Raanes, O. (2001).** "Kull ved produksjon av silisium og silisiumrike ferrolegeringer". (in Norwegian), Trondheim, SINTEF Materialteknologi, STF24 F01504 (internal report).
- Raanes, O. and Gray, R. J. (1995).** "Coal in the production of silicon rich alloys". INFACON 7. Trondheim, Norwegian Ferroalloy Research Organization (FFF): Bl. 201-219.
- Raanes, O., Kolbeinsen, L. and Byberg, J. Å. (1998).** "Statistical Analysis of Properties for coals used in the production of silicon rich alloys", INFACON 8, Beijing, China.
- Sakurovs, R. et al. (1987).** "Molecular mobility during pyrolysis of Australian bituminous coals." *Energy & Fuels*, Vol. 1 (2): 6.
- Sakurovs, R., French, D. and Grigore, M. (2007).** "Quantification of mineral matter in commercial cokes and their parent coals." *International Journal of Coal Geology*, Vol. 72 (2), pp. 81 - 88.
- Schapiro, N. and Gray, R. J. (1960).** "Petrographic classification applicable to coals of all ranks". *III Min. Inst. Proc.*, 68th year, pp. 83 – 97.
- Schapiro and Gray, R. J. (1964).** "The Use of Coal Petrography in Coke-Making", *J.Inst. Fuel*, Vol. 37, pp. 234 – 242.
- Schei, A. and Halvorsen S. H. (1991).** A stoichiometric model of the ferrosilicon process. Proceedings from the Kjetil Motzfeldt Symposium, Institute of Inorganic Chemistry, NTH, Trondheim, Norway.

- Schei, A., Tuset, J. K. and Tveit, H. (1998).** "Production of high silicon alloys". Trondheim, Tapir.
- Schopf, J. M. (1956).** "A definition of coal". *Economic Geology*, New Haven, Connecticut, Vol. 51 (6), pp. 521 - 527
- Schweinfurth, S. P. (2003).** "Coal - A complex Natural Resource"., U.S. Geological Survey circular 1143, pp. 39, Washington D.C, USA.
- Shiraishi, M. et al. (1985).** "Discussion of CSR of canadian coal." *Coke Circular* (Japan), Vol. 34: 4.
- Sohn, H. Y. (1997),** "Developments in gas – solid reaction analysis", *Proceedings of the Julian Szekely Symposium on Materials Processing*, Cambridge, Massachusetts, USA.
- Speight, J. G. (1994).** "The chemistry and technology of coal". New York, Marcel Dekker.
- Stach, E. et al. (1982).** "Stach's textbook of coal petrology, 3rd revised and enlarged edition". Berlin, Gebrüder Borntraeger.
- Steller, M., Arendt, P. and Kühl, H. (2006).** "Development of coal petrography applied in technical processes at the Bergbau-Forschung/DMT during the last 50 years." *International Journal of Coal Geology*, Vol. 67 (3), pp. 158 - 170.
- Stenstad, P. M. (2006).** Personal communication, Trondheim.
- Stenstad, P. M. (2007).** Personal communication, Trondheim.
- Stopes, M. C. (1935).** "On the Petrography of Banded Bituminous Coals." *Fuel*, Vol. 14, pp. 4 - 13.
- Swaine, D. J, (1994).** "Trace elements in coal and their dispersal during combustion". *Fuel.Proc.Techn*, Vol. 39, pp 121- 137.
- Szekely, J. and Evans, J. W. (1970),** "A structural model for gas – solid reactions with a moving boundary", *Chemical Engineering Science*, vol. 25, pp. 1091 - 1107
- Szekely, J., Evans, J. W. and Sohn, H. Y. (1976).** "Gas-solid reactions". New York, Academic Press.
- Tang, L. et al. (2005).** "The char structure characterization from the coal reflectogram." *Fuel*, Vol. 84 (10), pp. 1268 - 1276.

- Taylor, G. H. et al. (1998).** “Organic petrology: a new handbook incorporating some revised parts of Stach's Textbook of coal petrology”. Berlin, Gebrüder Borntraeger.
- Teichmüller, M. (1987).** “Organic material and very low-grade metamorphism”. In Frey, M. (Ed.) “Low Temperature Metamorphism”, Blackie, Glasgow, pp 114 – 161.
- Teichmüller, M. (1989).** “The genesis of coal from the viewpoint of coal petrology”. International Journal of Coal Geology, vol 12, pp. 1 – 21.
- Teichmüller, M. and Teichmüller, R. (1968).** ”Geological aspects of coal metamorphism“. In Murchison, D. G. and Westoll, T. S. (Eds), “Coal- and coal bearing strata”, Oliver & Boyd, Edinburgh, Scotland.
- Teichmüller, M. and Teichmüller, R. (1979).** ”Diagenesis of coal (coalification)“. In Larsen, G. and Chilingar, G. V. (Eds), “Diagenesis in Sediments and Sedimentary rocks”, pp. 207 – 246, Elsevier, Amsterdam.
- Ting, F. T. C. and Sitler, J. A. (1989).** "Comparative studies of the reflectivity of vitrinite and sporinite." Organic Geochemistry, Vol. 14 (3), pp. 247 - 252.
- Todd, S.J. and Hansen, H. (1995).** “Nature and Origin of Coal and Its Petrographic Characteristics”. Electric Furnace Conference Proceedings, Vol. 58, pp. 3 – 15, Orlando, Florida, USA.
- Todoschuk, T. W. (2005).** “Coke Oven Game”. 4th McMaster Cokemaking Course. Hamilton, Ontario, Canada, McMaster University.
- Tuset, J. K. and Raaness., O. (1976).** Reactivity of Reduction Materials for the Production of Silicon, Silicon-Rich Ferroalloys and Silicon Carbide. 34th Electric Furnace Conference, Missouri, USA.
- USEPA (1995).** “Reducing Methane Emissions From Coal Mines in Poland - A Handbook for Expanding Coalbed Methane Recovery and use in the Upper Silesian Coal Basin”, U.S. Environmental Protection Agency (USEPA) - Atmospheric Pollution Prevention Division 119, EPA/430-R 95-003, pp. 119.
- Valderhaug, Aa. (1992).** “Modelling and control of submerged-arc ferrosilicon furnaces”. Trondheim, Department of Engineering Cybernetics, Norwegian Institute of Technology. **1992:83:** xxvii, 348 s.
- Videm, T. (1995).** “Reaction rate of reduction materials for the (ferro)silicon process”, INFACON 7. Trondheim, Norwegian Ferroalloy Research Organization (FFF), pp. 221 - 230.

- Videm Buo, T., Gray, R. J. and Patalsky, R. M. (2000).** "Reactivity and petrography of cokes for ferrosilicon and silicon production." *International Journal of Coal Geology*, Vol 43 (1-4), pp. 243 - 256.
- Volkman, N. (2004).** "Practical Coal Petrology – Coal as a raw material in technical processes". Lecture notes from short course at NTNU March 16 – 24, 2004.
- WCI (2007).** "Coal Facts 2007 Edition with 2006 data", World Coal Institute. From: http://www.worldcoal.org/assets_cm/files/PDF/fact_card2007.pdf (November 6th, 2007)
- Wiik, K. (1990).** "Kinetics of reactions between silica and carbon". Trondheim, Institutt for uorganisk kjemi, Norges tekniske høgskole. 1990:16: 220 s.
- Yagi, S. and Kunii, D. (1955).** "Studies on combustion of carbon particles in flames and fluidized beds", *Proceedings of 5th (int.) Symposium on Combustion*, pp. 231 – 244, Reinhold, New York, USA.
- Yagi, S. and Kunii, D. (1961).** "Fluidized - Solids Reactors with Continuous Solid Feed I - III", *Chem.Eng.Sci*, vol. 16(3),
- Zygourakis, K. (1993).** "Effect of pyrolysis conditions on the macropore structure of coal-derived chars". Vol. 7, pp. 33 - 41.
- Øye, H. A. et al. (2000).** "Characterization of optical texture in cokes by image analysis". *Light Metals*, pp. 549 – 554.

APPENDIX B: COAL ALBUM

During the course of this work petrographic investigations of the coal samples have been performed. In the result section (Chapter 5), macerals and minerals were divided into groups believed to have the largest impact on the reactivity towards SiO gas. In the following appendix, microphotographs of specific macerals and minerals identified during petrographic investigations of the coal samples analyzed in this work are presented.

Petrographical studies were performed on the petrographic microscope illustrated in Figure 4.5. Most of the presented microphotographs were taken with a Kappa CF 20 DXC digital camera under normal reflected light and oil immersion. Magnifications used are 200x, 320x, and 500x and the scale bars are illustrated on the microphotographs. In order to illustrate the fluorescence of liptinites, some pictures are taken in this mode. These microphotographs were taken on a Leica DM RXE petrographic microscope.

Typical properties of macerals and minerals in coal are described in section 3.4.

The following notation is used to describe microtextures on the microphotographs:

Vitrinite macerals:

V: Vitrinite
PV: Pseudovitrinite

Liptinite macerals:

S: Sporinite
MS: Macro spores
Cu: Cutinite
R: Resinite
Li: Unidentified liptinites

Inertinite macerals:

F: Fusinite
SF: Semifusinite
W: Wood – Fusinite in Permian coals
Ma: Macrinite
Mi: Micrinite
ID: Inertodetrinite
Sc: Sclerotinite (Part of funginite)
FS: Fungal spore (Part of funginite)
Se: Secretinite

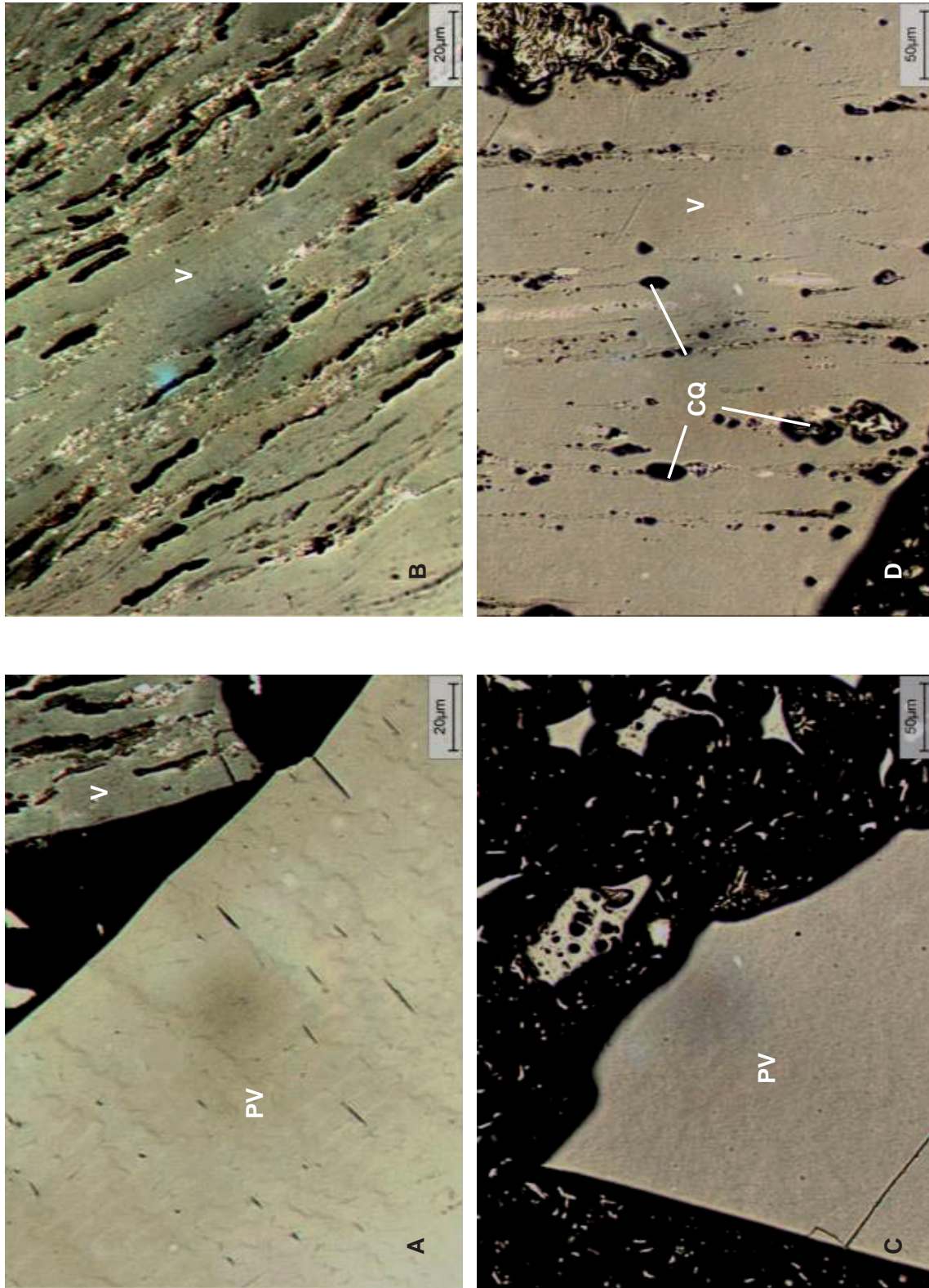
Mineral inclusions:

Py: Pyrite
CQ: Clastic quartz
Cl: Clay
Sh: Shale
Sd: Siderite
Ca: Calcite
BC: Bone coal
Min: Unidentified mineral

Miscellaneous:

ER: Epoxy Resin

Figure A.B.1: A) Pseudovitrinite in BG with characteristic slits and of higher reflectance than neighboring vitrinite particle. B) Liptinites (black, long axed) and inerts (white, small) imbedded in the vitrinite matrix of BG. C) Pseudovitrinite particle in PD D) Vitrinite matrix of PD with clastic quartz inclusions



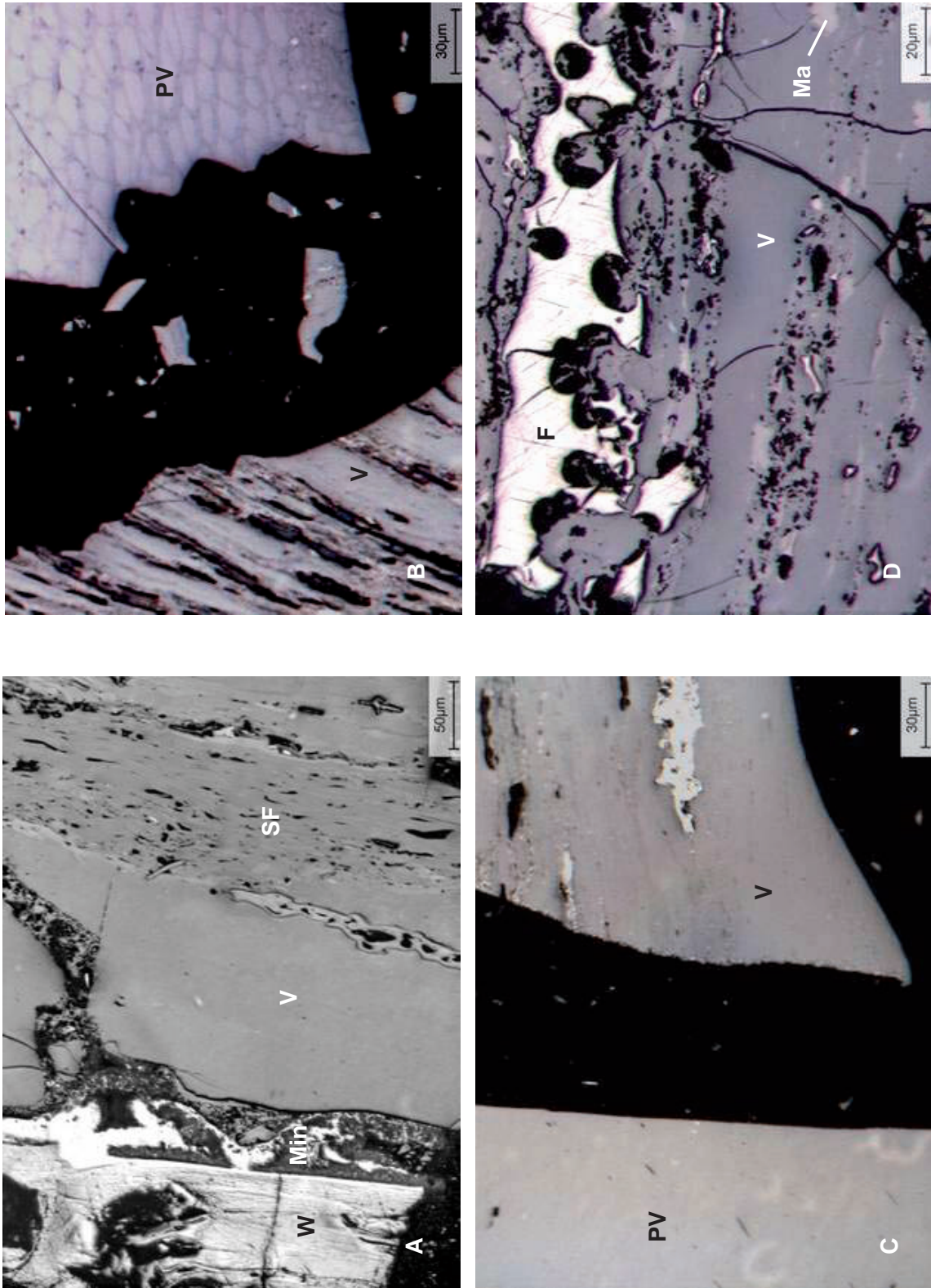
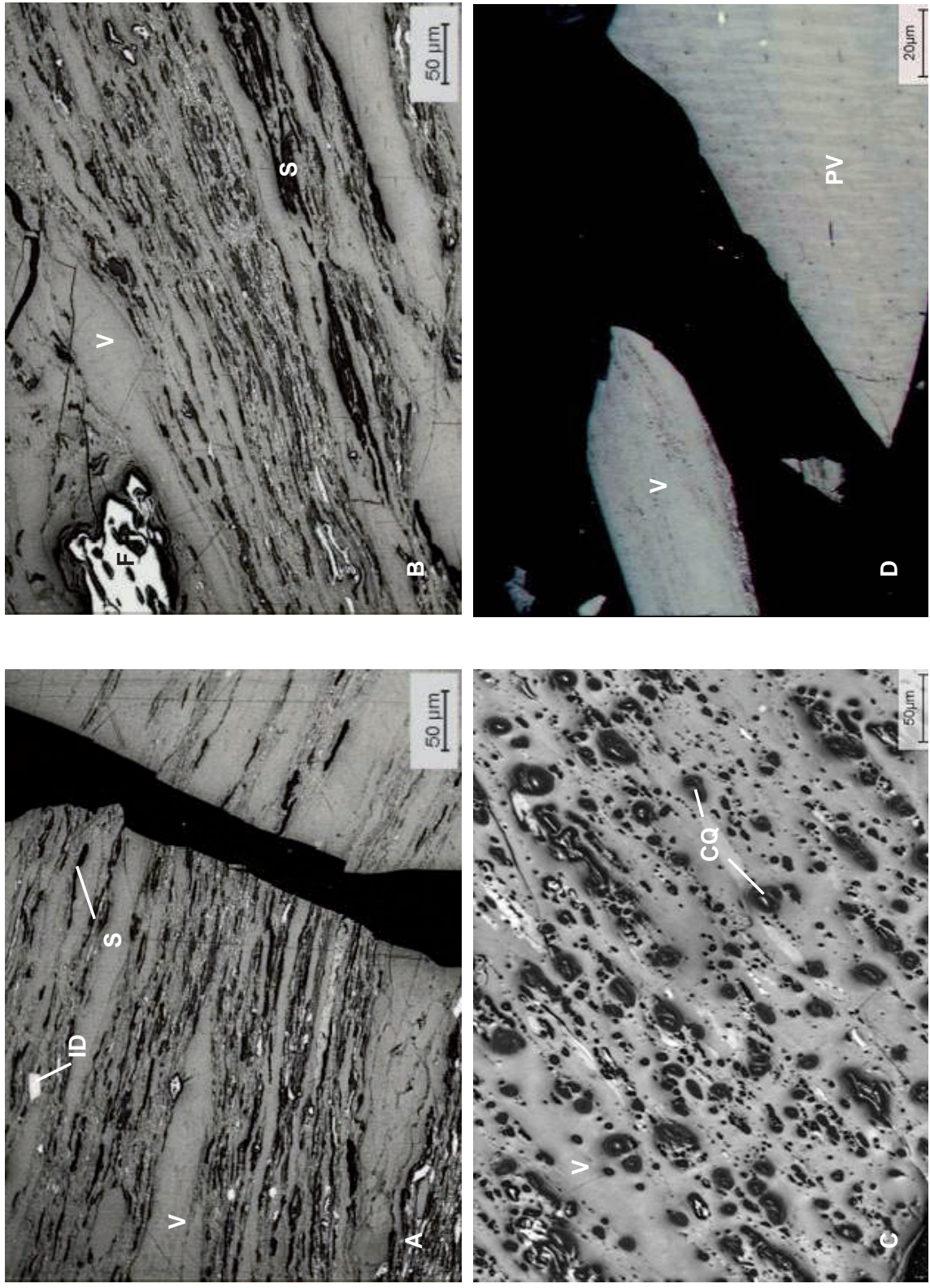


Figure A.B.2: A) Some precursor of vitrinite has been preserved during coalification. Also note the similar reflectance of vitrinite and semifusinite in PD. The wood identified to the left is typical for Permian coals. B) Pseudovitrinite with tellinitic structure in BG C) Pseudovitrinite and vitrinite in BG D) Vitrinite as the most common group of macerals in Staszic.

Figure A.B.3: A) Both liptinites (dark) and inerts (bright) are embedded in the vitrinite matrix of BG. B) Typical vitrinite particle of BG. C) A lot of clastic quartz inclusions in the vitrinite matrix of PD. D) Pseudovitrinite particle of PD. D) Pseudovitrinite particle and pointed edges next to a vitrinite particle of BG.



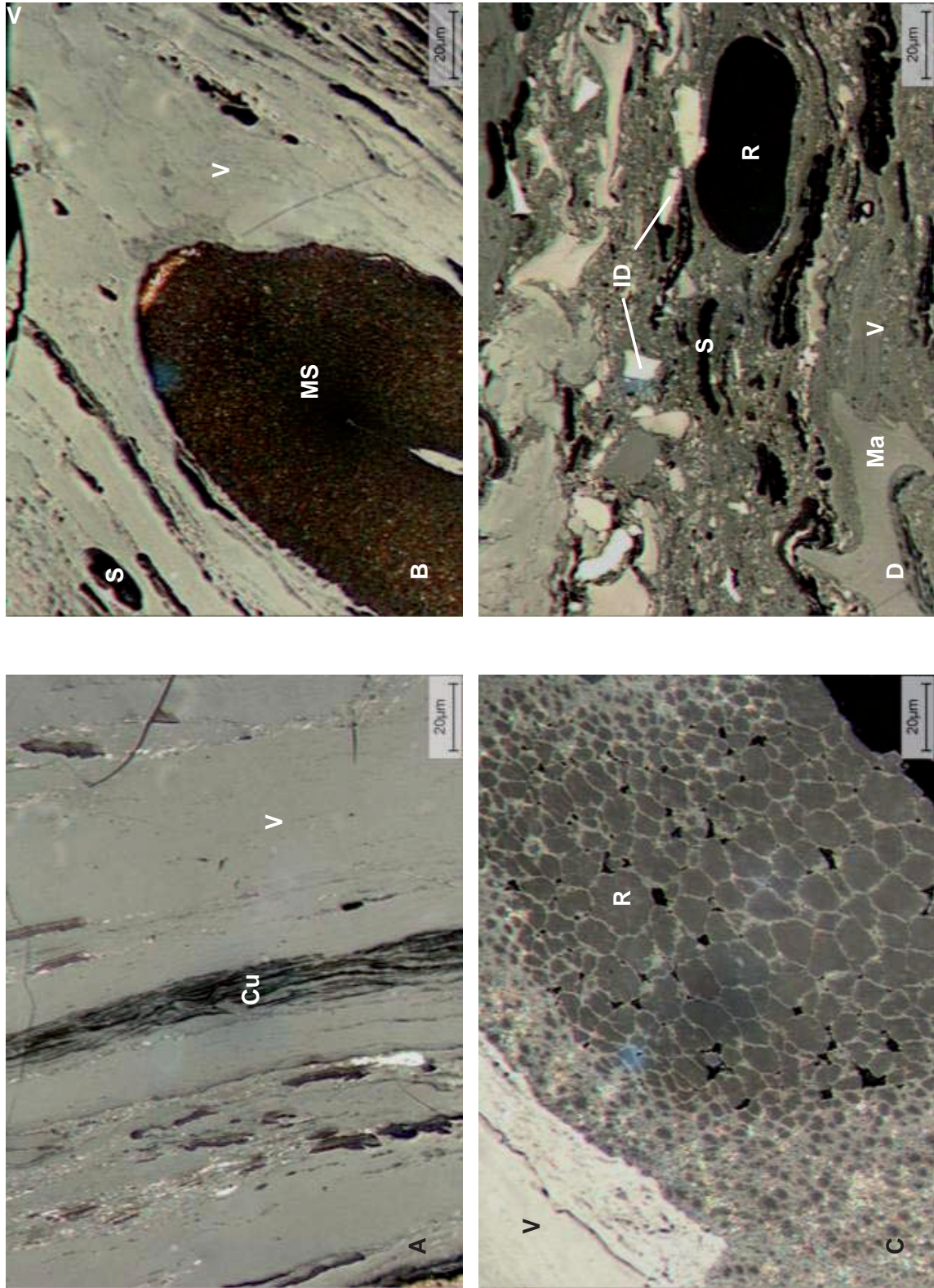
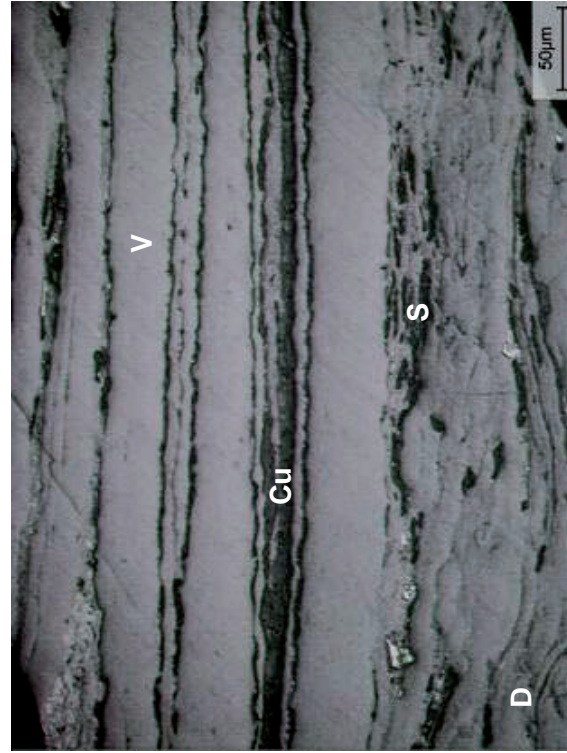
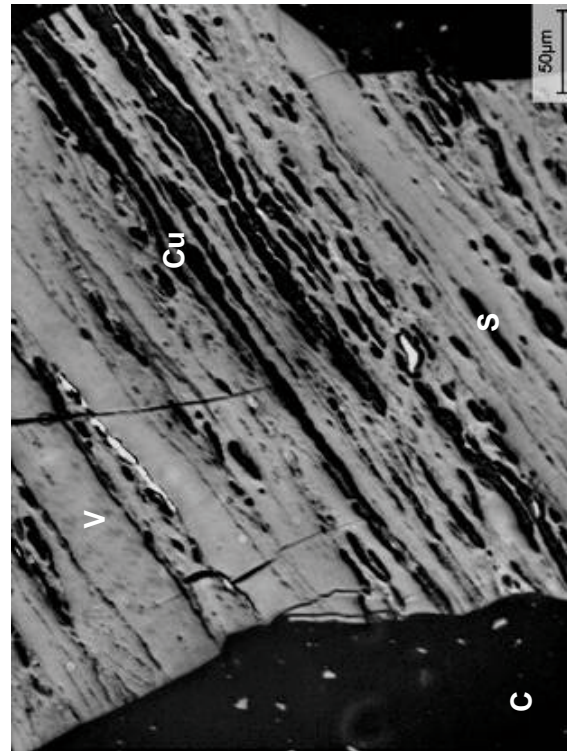
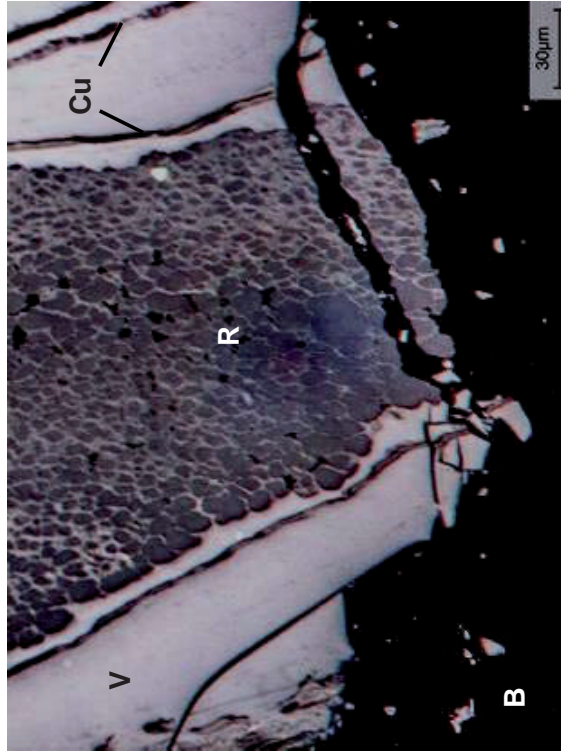
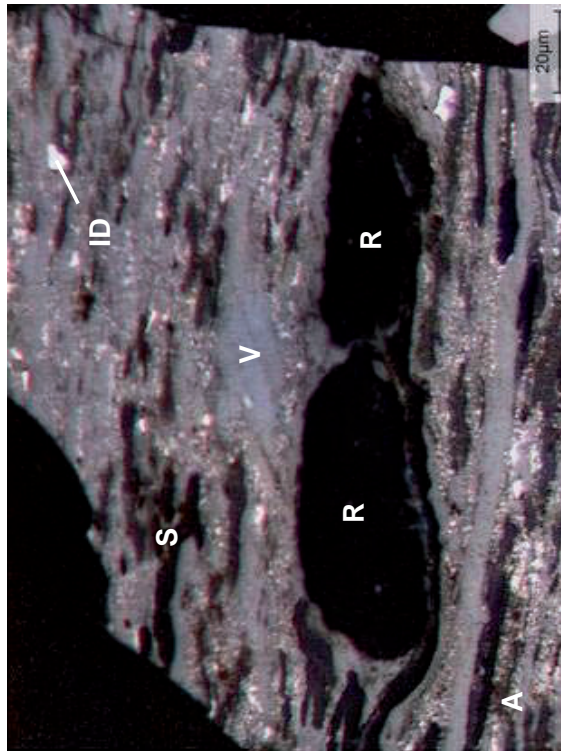


Figure A.B.4: A) Cutinite in BG. B) A macrospore and spores in a particle of BG. C) Resinite filling the cells of tellinite in BG. D) A very dull particle of St. A large resinite body, spores, inertodetrinite and some macrinite can be noticed.

Figure A.B.5: A) Two large resinite bodies in BG. Notice how the resinite is more resistant to compaction than the corresponding vitrinite. B) Resinite filling the cells of tellinite in BG. C) Cutinite transverse a particle of vitrinite in BG. D) Cutinite transverse a particle of vitrinite in BG. Notice the characteristic pattern of the cutinite.



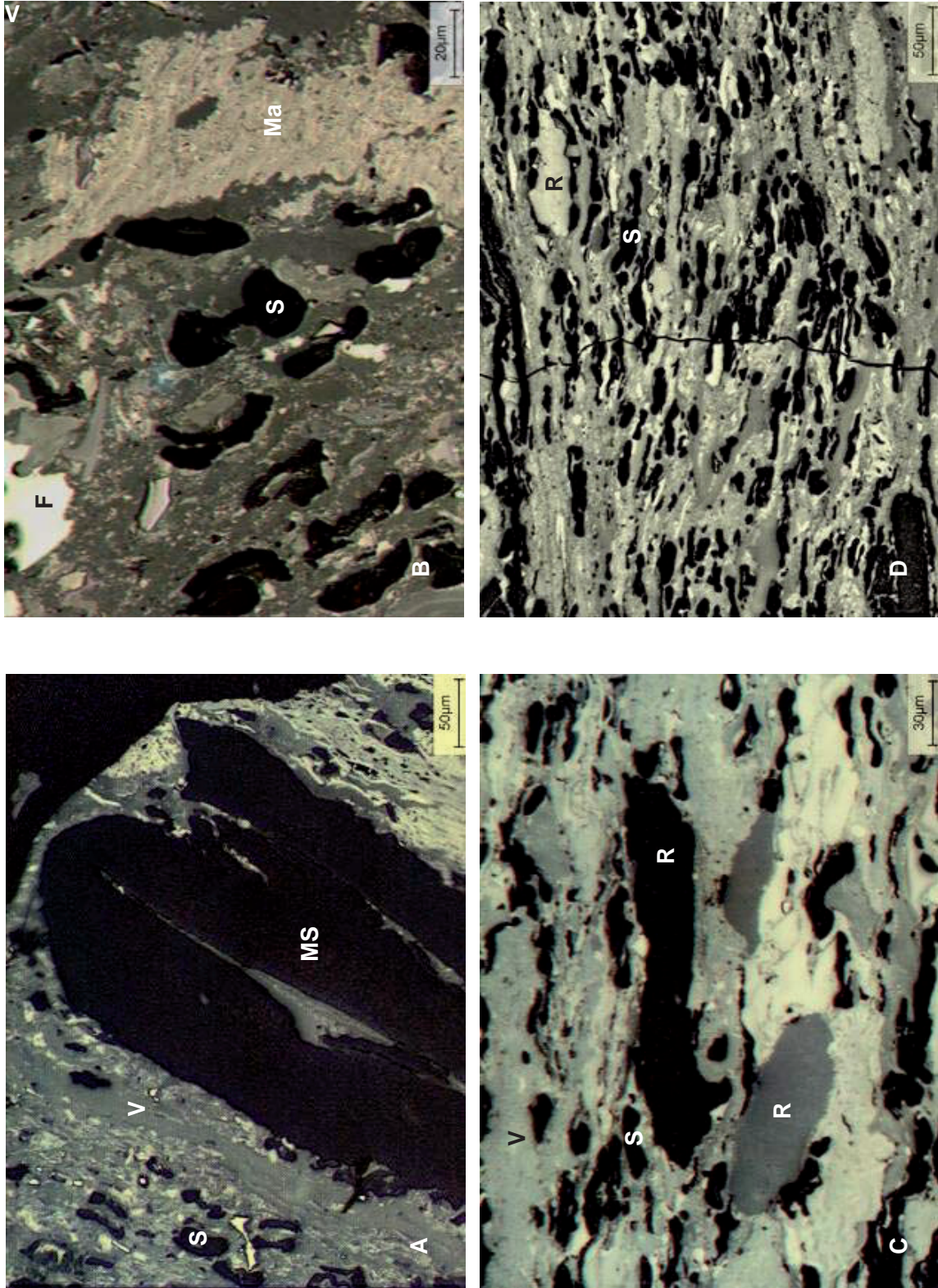
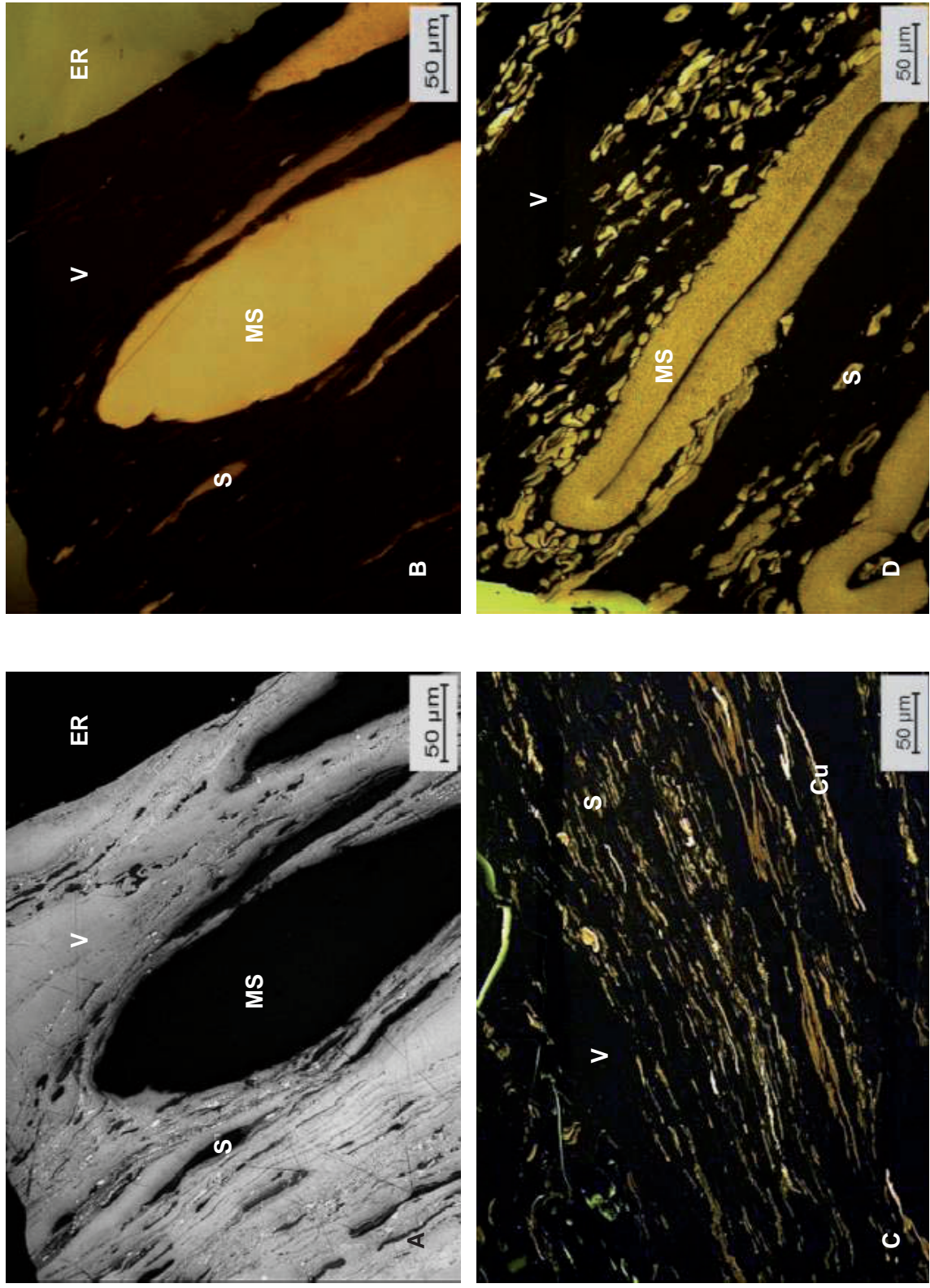


Figure A.B.6: A) A macrospore and spores in a particle of St. B) Spores in St. Notice the characteristic dumb-bell shape of the spore that refers to the plant Lycopsidea. C) Resinite and spores in a dull particle of St. D) Some bright resinite and spores are present in a dull particle of St. Notice the crack that transverse the particle almost perpendicular to the bedding plane.

Figure A.B.7: A) A Macrospore and spores in BG. B) Same picture as A), but in fluorescent light. Notice how the lipinites show excitation phenomena while the vitrinite appear black. C) Sporinites embedded in vitrinite groundmass in BG. Picture taken in fluorescent light. D) Macrospores and spores in St. Picture taken in fluorescent light.



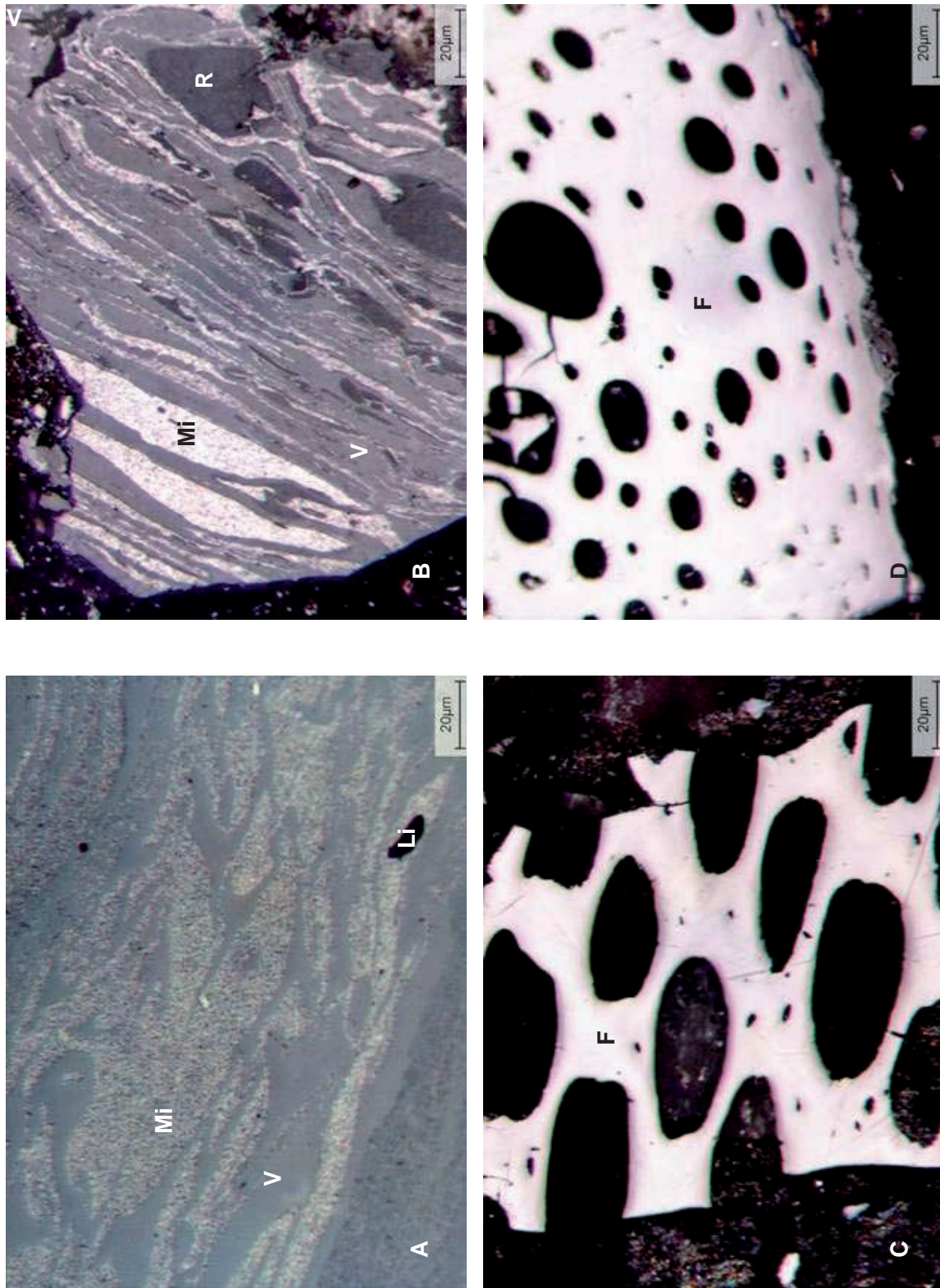
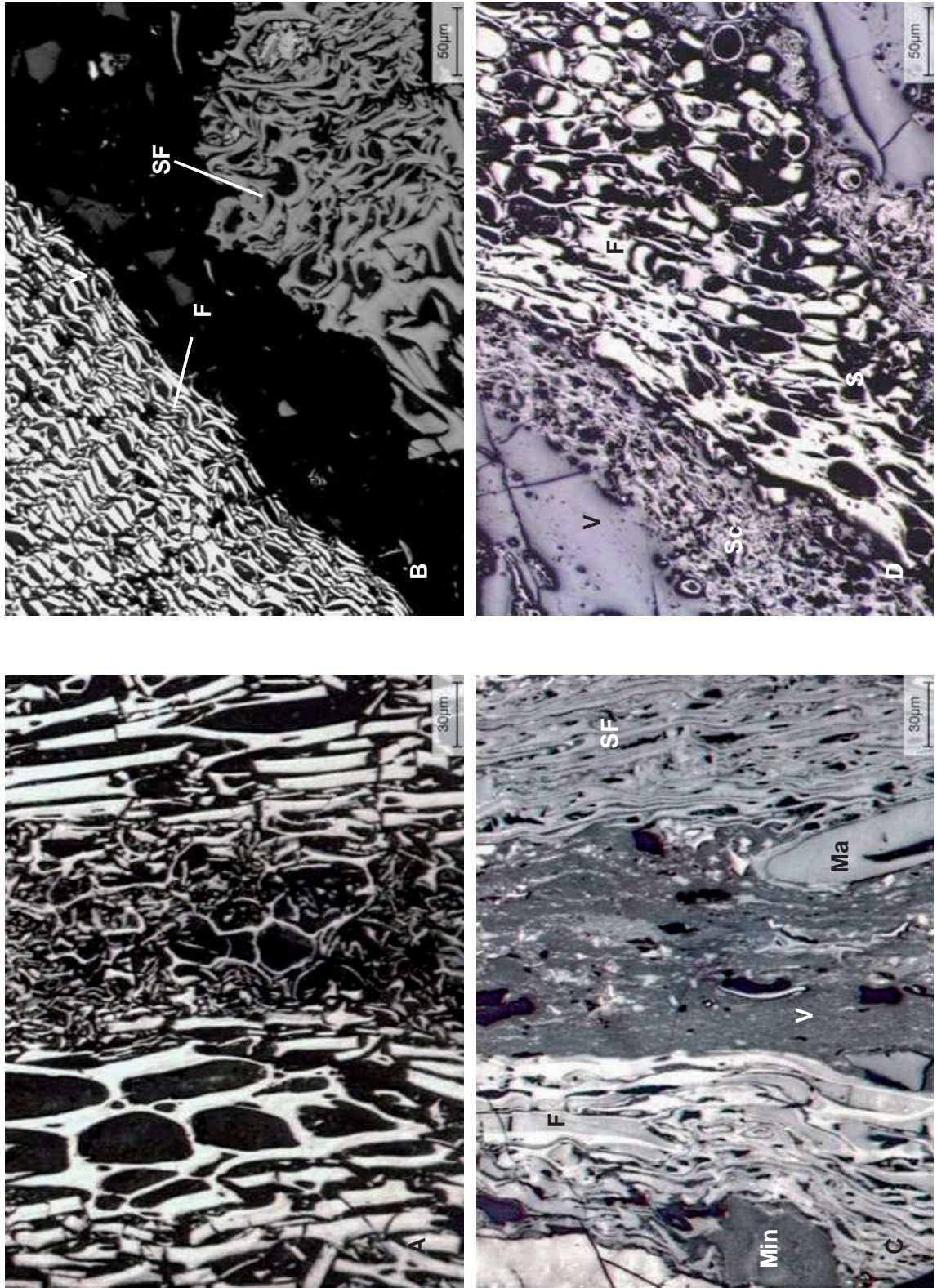


Figure A.B.8: A) Micrinite in St. Notice the lipinite (sporinite or resinite) that is in the process of being transformed to micrinite. B) Micrinite and resinite in a dull particle of St. C and D). Well preserved fusinite particles in St. The cell structure is well recognizable.

Figure A.B.9: A) Fusinite in St. Some of the cell structure is preserved while some is degraded. B) The difference in reflectance between fusinite and semifusinite is clearly illustrated in this picture from St. C). A dull particle of St where several of the macerals of the inertinite group are present. D) Fusinite and sclerotia in PD. Notice the level of reflectance between fusinite, sclerotia and vitrinite.



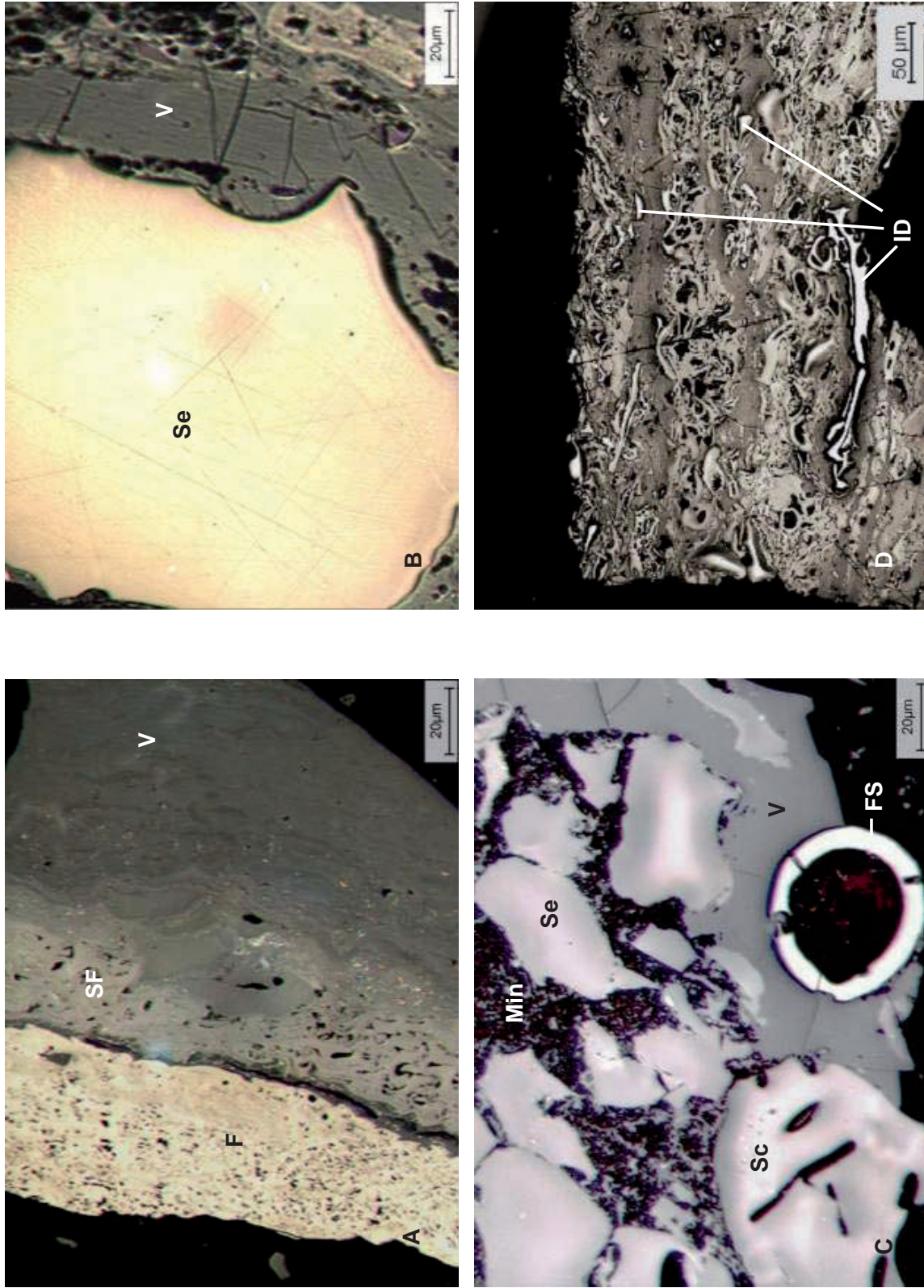
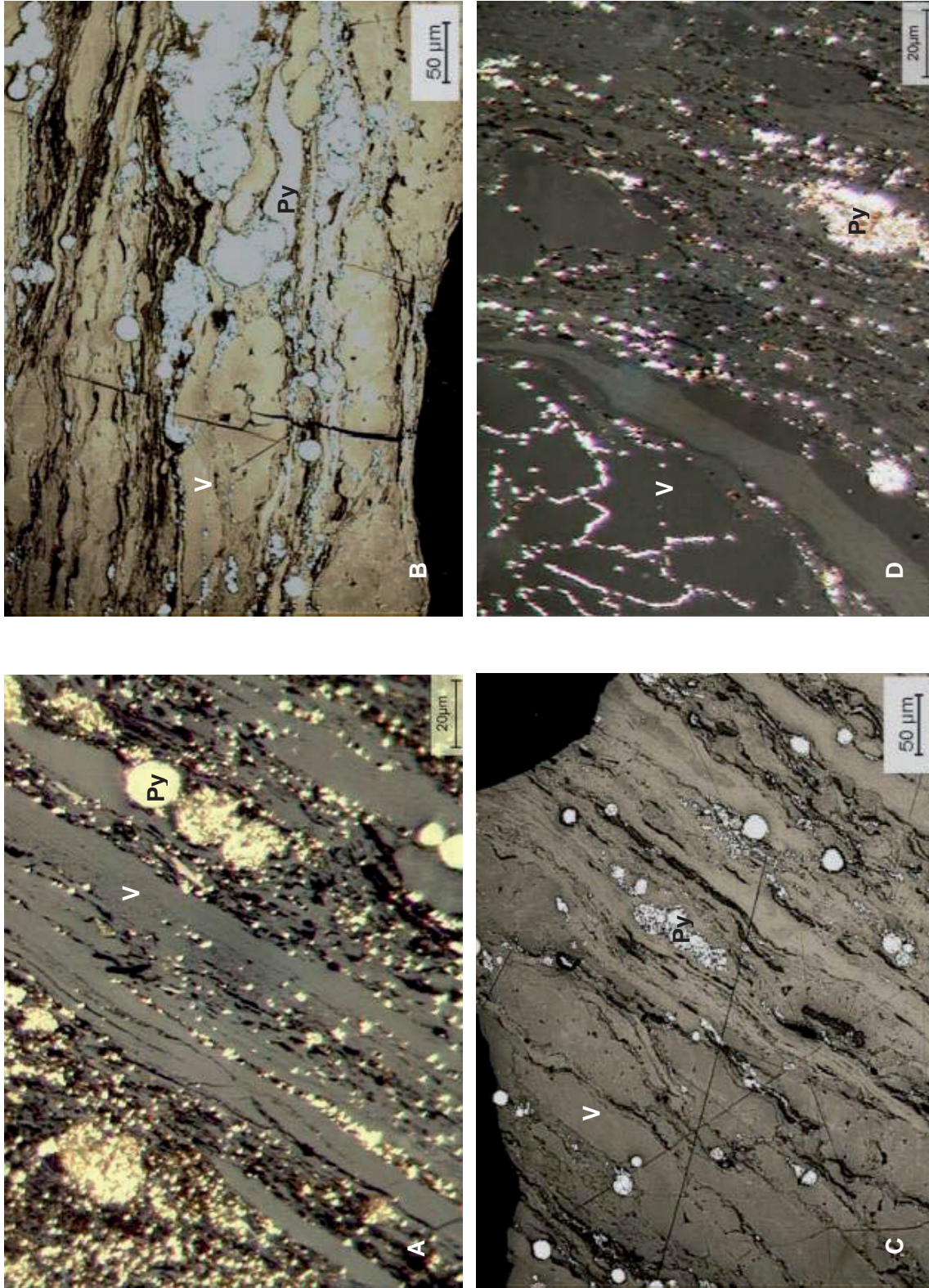


Figure A.B.10: A) Transition from vitrinite via semifusinite to fusinite in a particle of BG. B) A large dense particle of secretinite in PD. C) A highly reflecting fungal spore, sclerotinite and secretinite in a particle of PD. D) A very dull particle of PD showing vitrinite, plenty of semifusinite as well as several inclusions of inertodetrinite.

Figure A.B.11: Framboids of pyrite in Staszic. The individual crystals of FeS are particularly clear in photo A and D. All photographs from St.



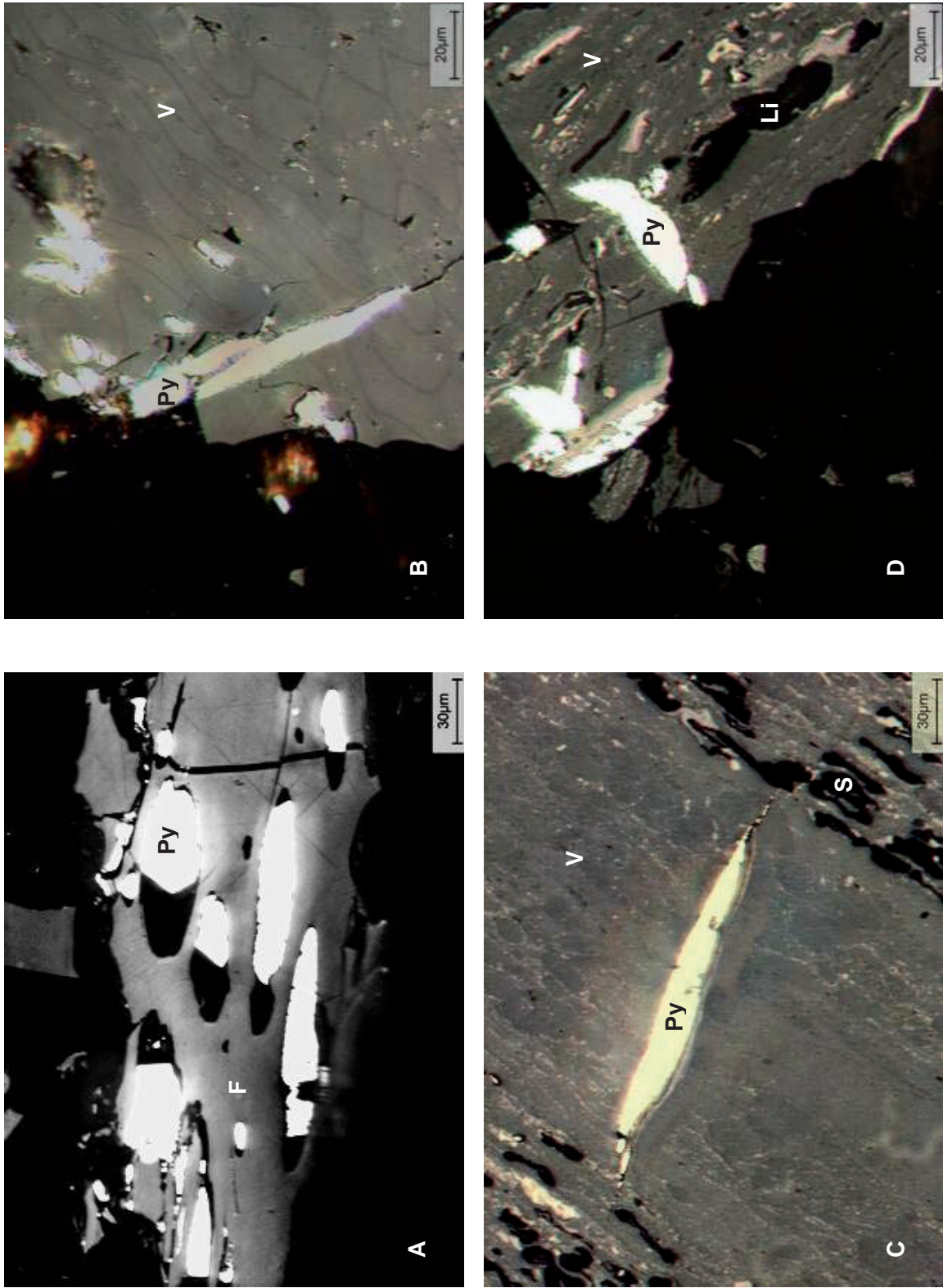
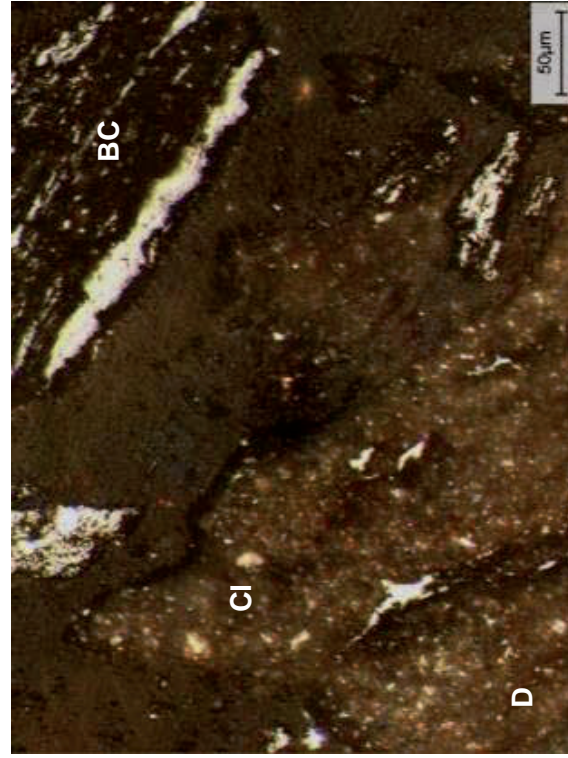
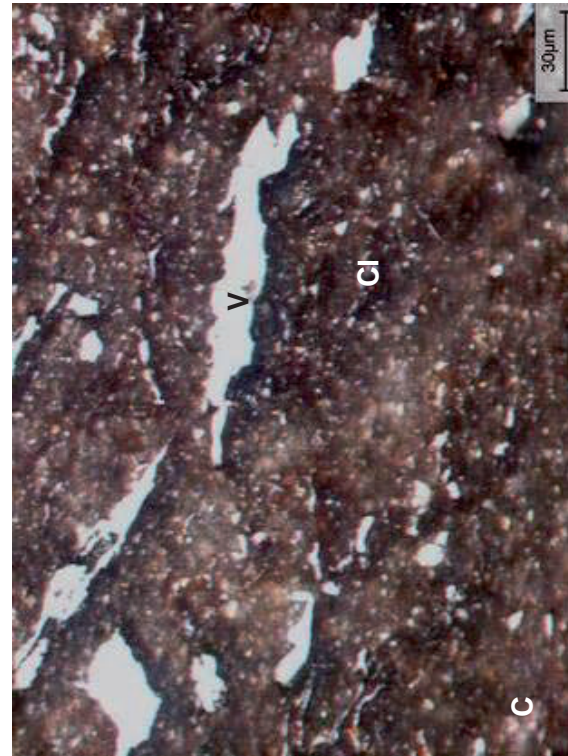
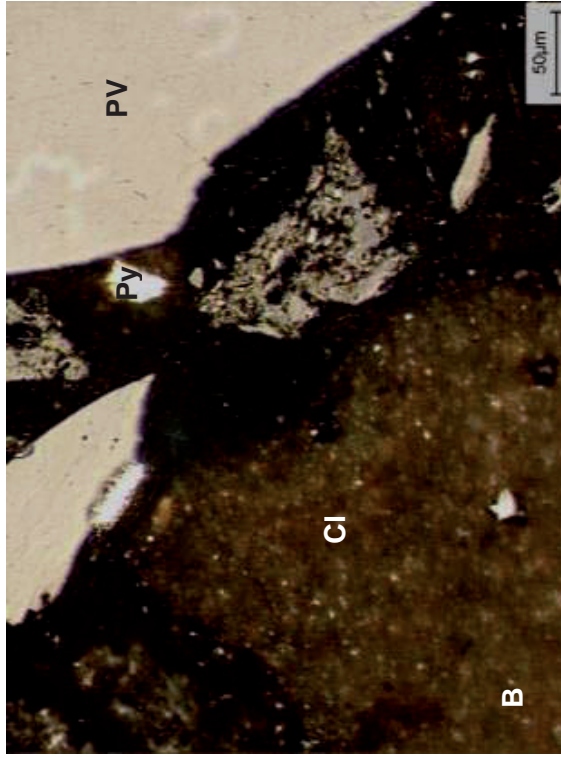
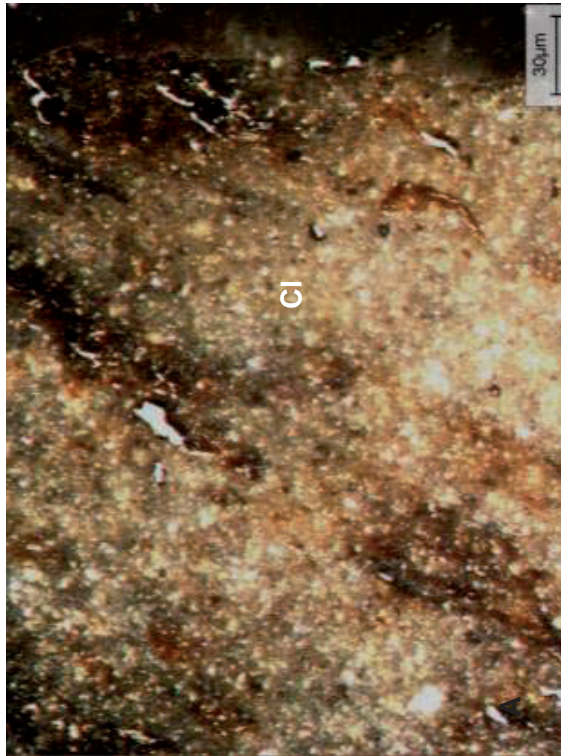


Figure A.B.12: Pyrite deposited in cracks and cleats. A) Pyrite filling the cells of a fusinite particle in BG. B) Pyrite deposited in a crack in BG. C) Pyrite deposited in a crack in St. D) Pyrite deposited in a crack in V. Notice the cellular structure of the vitrinite C, D)

Figure A.B.13: Clay minerals in coals. A) A large clay mineral in St. B) A large vitrinite and pyrite in BG. C) A large clay inclusion in St. Notice the bright particles of vitrinite. D) A clay particle close to a particle of bone coal in BG.



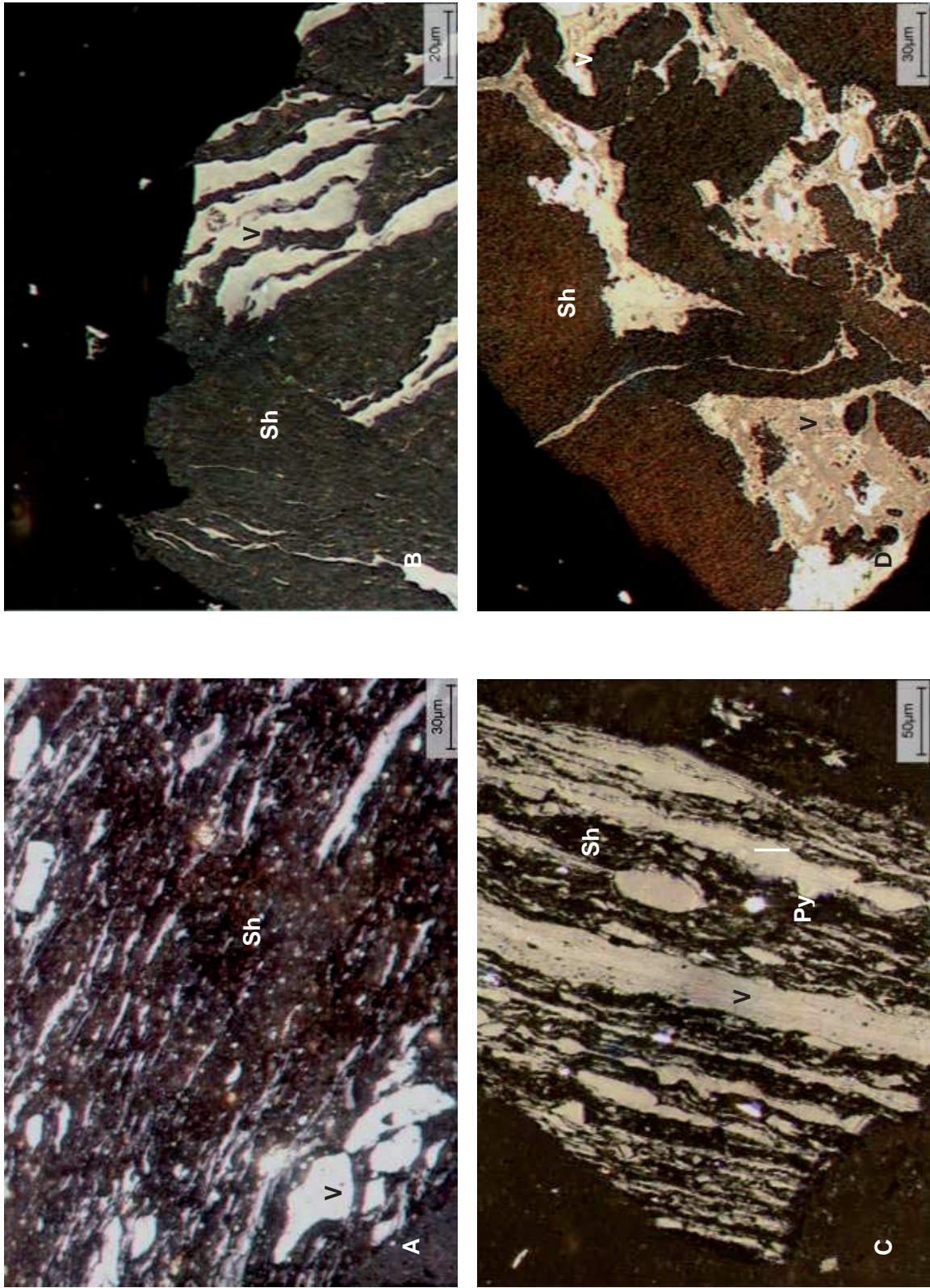
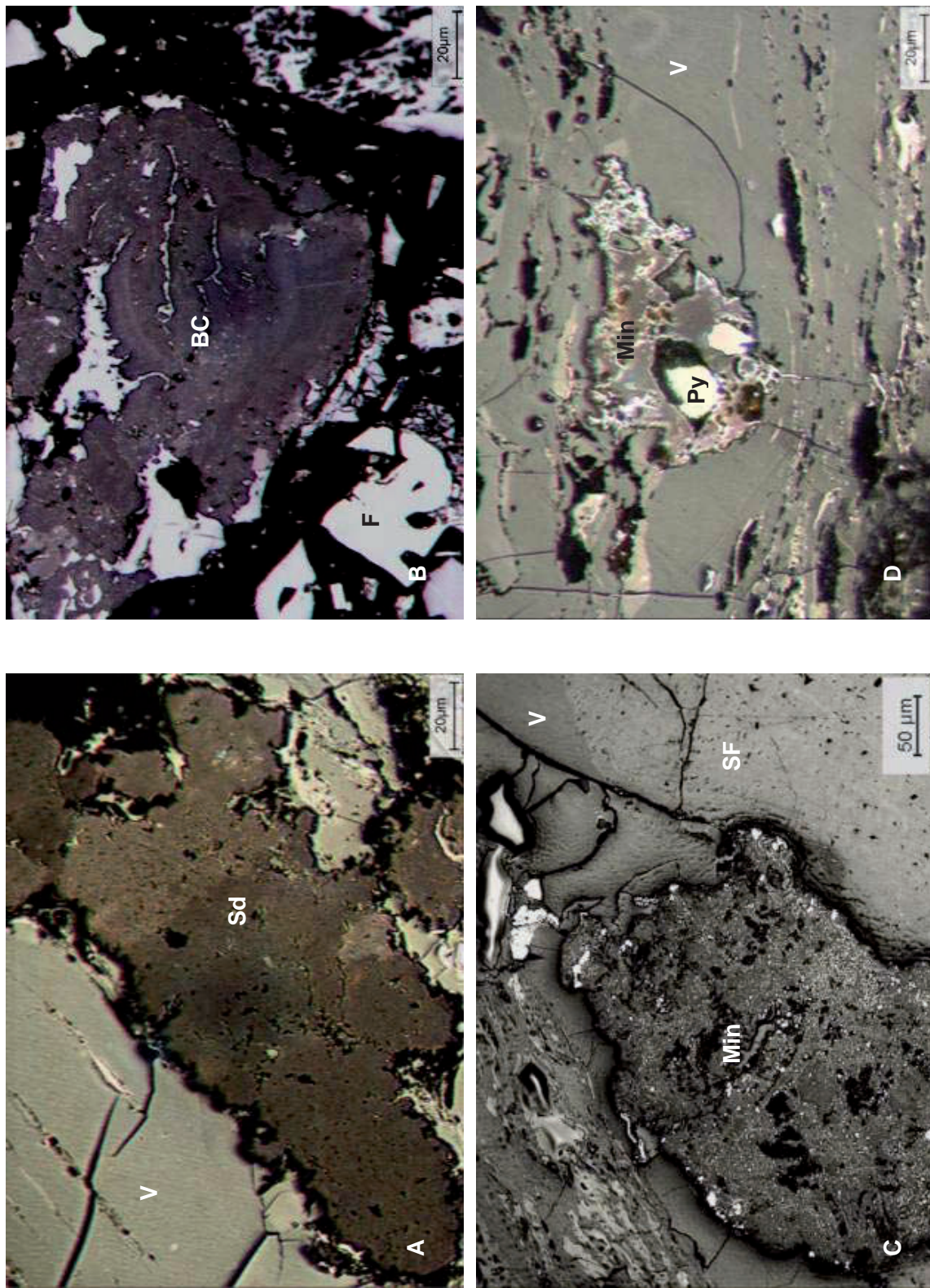


Figure A.B.14: Shale inclusions and bone coal of BG. In A) and C) there are some pyrite inclusions as well. D) Shale inclusions in a particle of St.

Figure A.B.15: A) A relatively large mineral inclusion of what is believed to be siderite in PD. B) Bonetcoal in BG. C) A large unidentified mineral inclusion in St. D) A mixture of different minerals in BG.



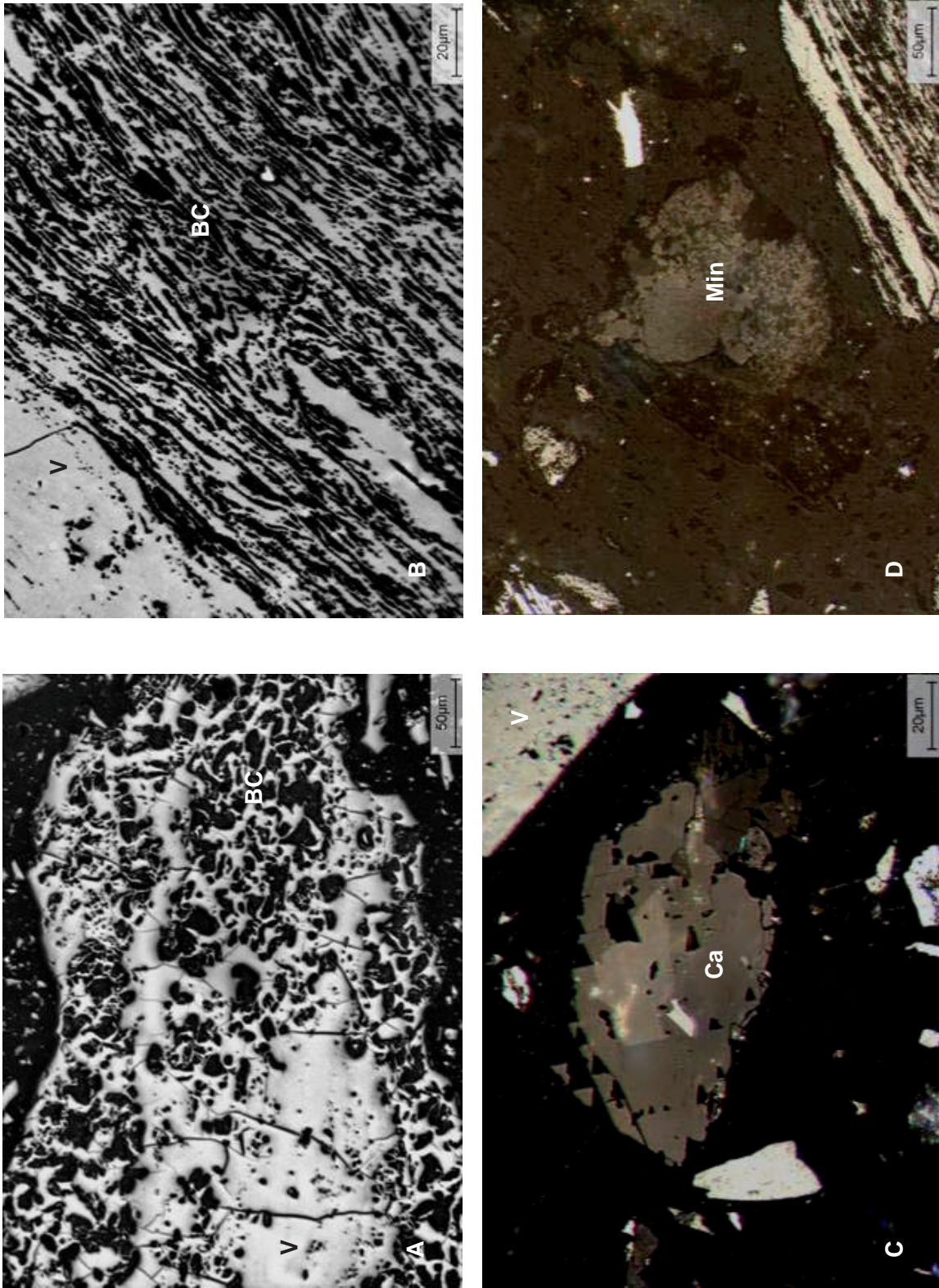


Figure A.B.16: A) and B) Inclusions of clay and clastic quartz in PD. C) A particle of calcite in St. D) Unidentified mineral particle with a high degree of anisotropy and pyrite in BG.

APPENDIX C: STANDARDS USED IN ANALYSES OF COAL SAMPLES

Table A.C.1: Standards used in this work for coal analyses and references to standards in other systems.

	Polish Norms (PN)	ISO standards	ASTM
Proximate Analysis:			
Moisture	PN-G-04560:1998	17246:2005	D3172-07
Ash	PN-G-04560:1998	17246:2005	D3172-07
Volatile Matter	PN-G-04560:1998	17246:2005	D3172-07
Ultimate Analysis:			
Carbon	PN-G-04571:1998	17247:2005	D3176-89(2002)
Hydrogen	PN-G-04571:1998	17247:2005	D3176-89(2002)
Nitrogen	PN-G-04571:1998	17247:2005	D3176-89(2002)
Sulfur	PN-G-04584:2001		D3177-02(2007)
Phosphorous:	Q/ZK/P/15/01/A		
Plastic properties: (Gieseler method)	PN-G-04565:1994	10329	D2639-04e1
Ash analysis:	Q/ZK/P/15/01/A	23380	D3682-01(2006)

APPENDIX D: NON-MACERAL MICROTEXTURES

In order to quantify microtextures of the sample materials which are not included in standard maceral analyses, non-maceral analyses have been performed in this work. Microphotographs of non-maceral microtextures identified during morphological studies of the coal samples analyzed during the course of this work are presented on the following page.

Morphological studies were performed on the petrographic microscope illustrated in Figure 4.5. All the presented microphotographs were taken with a Kappa CF 20 DXC digital camera under normal reflected light and oil immersion. Magnifications used are 200x, 320x, and 500x and are illustrated on the microphotographs.

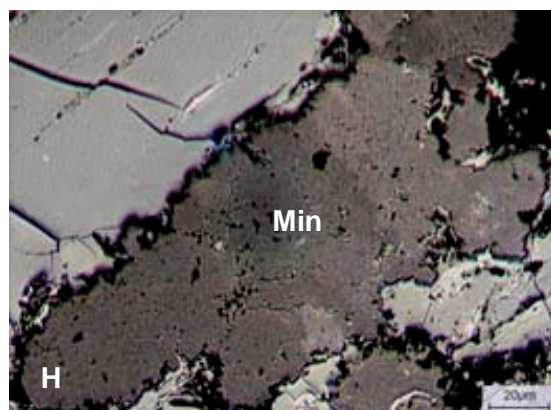
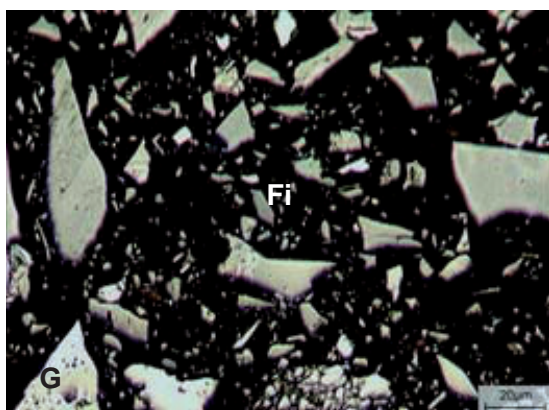
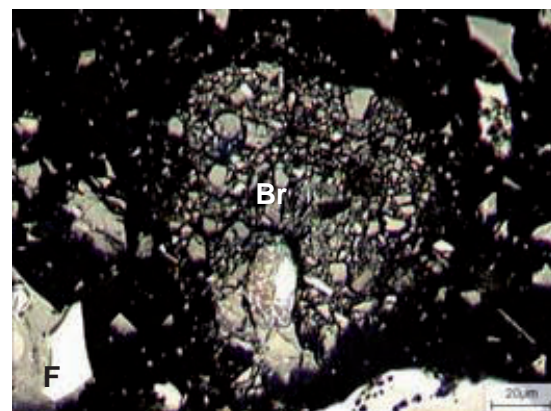
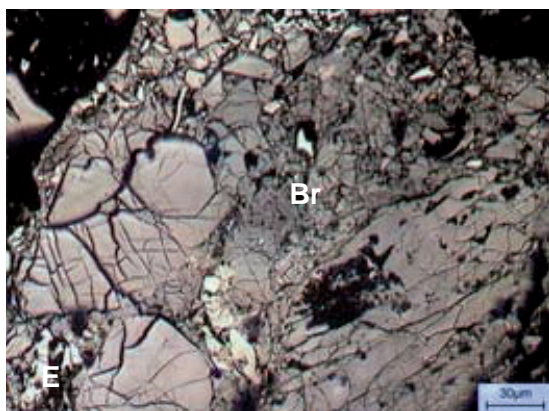
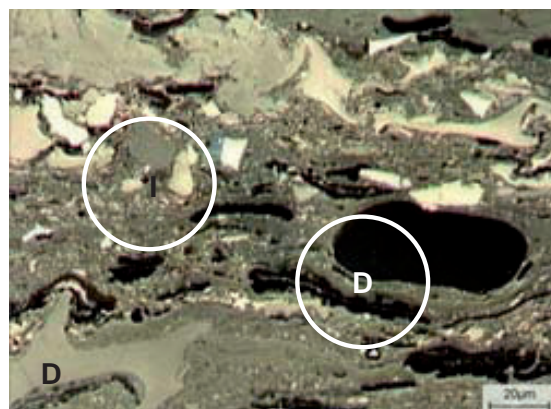
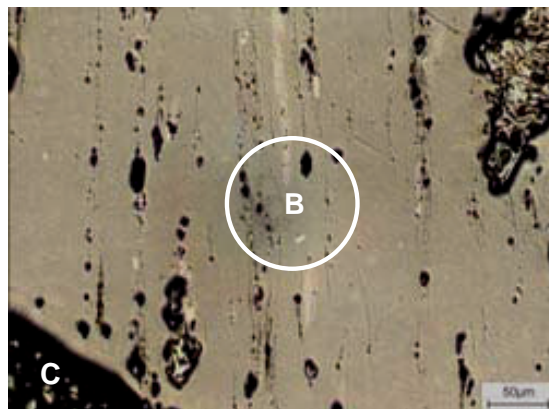
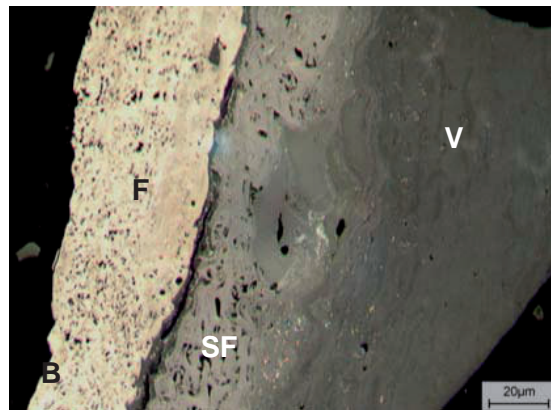
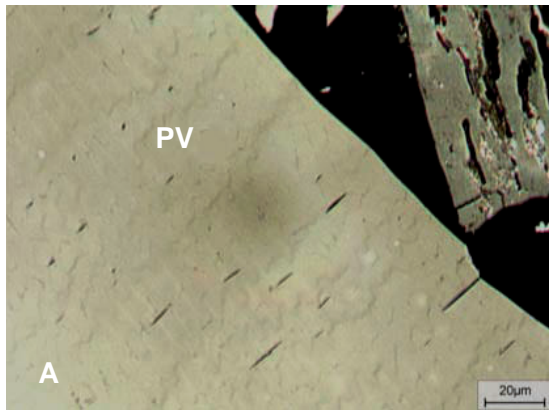
Classification of microtextures identified during non-maceral analysis is described in sections 4.2.3 and 5.4.3.

The following notation is used to describe microtextures on the microphotographs:

- V:** Vitrinite
- PV:** Pseudovitrinite
- F:** Fusinite
- SF:** Semifusinite
- B:** Bright attrital coal
- I:** Intermediate attrital coal
- D:** Dull attrital coal
- Br:** Brecciated coal
- Fi:** Fines
- Min:** Mineral inclusions

Non-maceral microtextures not identified in this work can be seen in **Gray (1982)** and **Gray and Gray (2005a)**.

APPENDIX D: NON-MACERAL MICROTEXTURES



APPENDIX E: SYSTEMS FOR COKE NOMENCLATURE

Coal Rank	Japan Steel Mills	Australia (Coin)	BCRA (Patrick)	ICCP	US Steell (Gray)		CANMET (Marsh)	
						R _m %		R _m %
Low rank coals	isotropic	Very fine grain anisotropic	isotropic	isotropic	Isotropic	0.65 – 0.75	Isotropic	0.70
					Incipient Fine circular	0.85 0.95	Very fine gr. anisotropic	0.85
HV coal Low fluidity	Fine mosaic	Fine grain anisotropic	Fine mosaic	Fine mosaic W ≤ 3 m	Medium circular	1.05	Fine gr. mosaic	0.95
					Coarse circular	1.15	Medium gr. mosaic	1.05
MV coal good coking	Coarse mosaic	Medium grain anisotropic	Medium mosaic	Coarse mosaic W = 3-10 m	Fine lenticular	1.25	Coarse gr. mosaic	1.15
					Medium lenticular	1.35	Fine flow l=2w, w < 1,5 m	1.25
	Fine fibrous	Coarse grain anisotropic	Coarse grain flow	Fibers L > 3W W < 10 m	Coarse lenticular	1.45	Coarse flow l=2w, w < 10 m	0.70
					Medium lenticular	1.35	Med flow l=2w, w < 5 m	1.35
Low volatile coking coal	Follated or leaflet	Follate anisotropy (vit & react. semi-fus)	Flow type anisotropy	Domains W > 10 m	Fine ribbon	1.55	Ribbon domain	1.55
					Medium ribbon	1.65	Undulating domain	1.65
					Medium ribbon	1.85	Flat flow domain	1.75
Semi-anthr. Anthracite			Basic anisotropy	Anthracitic textures	< 0.55 > 1.75	Basic anisotropy	< 0.55 > 1.75	
Inerts		Isotropic	Fine- and coarse inerts	Inertinite, Pyrolytic C, Pet. Coke, coke breeze	Inerts - Fine < 50 m - Coarse > 50 m	Fusinite, SF, alt vitrinite, depositional and spherulitic carbon		

APPENDIX F: ALBUM OF MICROTEXTURES IN CARBONIZED SAMPLES

Macerals behave differently upon carbonization. Some are characterized as fusible (reactive) and will constitute the binder phase in the carbonized product while others are infusible and make up the filler phase constituents. During the course of this work, petrographic investigations of the carbonized samples have been performed. In the result section (Chapter 5), binder phase carbon forms are classified according to their degree of anisotropy. Filler phase carbon forms are differentiated based on their origin (organic or inorganic) as well as size. Miscellaneous components are also part of the petrographic analysis and were in this work mainly composed of depositional carbons. In the following appendix, microphotographs of carbon forms identified during petrographic investigations of the carbonized samples analyzed in this work are presented.

Petrographical studies were performed on the petrographic microscope illustrated in Figure 4.5. Most of the presented microphotographs were taken with a Kappa CF 20 DXC digital camera under normal reflected light and oil immersion. Magnifications used are 200x, 320x, and 500x and scale bars are illustrated on the microphotographs. Some microphotographs are taken by the use of a metallurgical inverted microscope (Leica MeF3A) with dry objectives. These are recognized by having the scale bar in the lower left hand side corner.

The following notation is used to describe microtextures on the microphotographs:

Binder phase carbon forms:

- I:** Isotropic
- In:** Incipient
- Ci:** Circular
- Len:** Lenticular
- Ri:** Ribbon

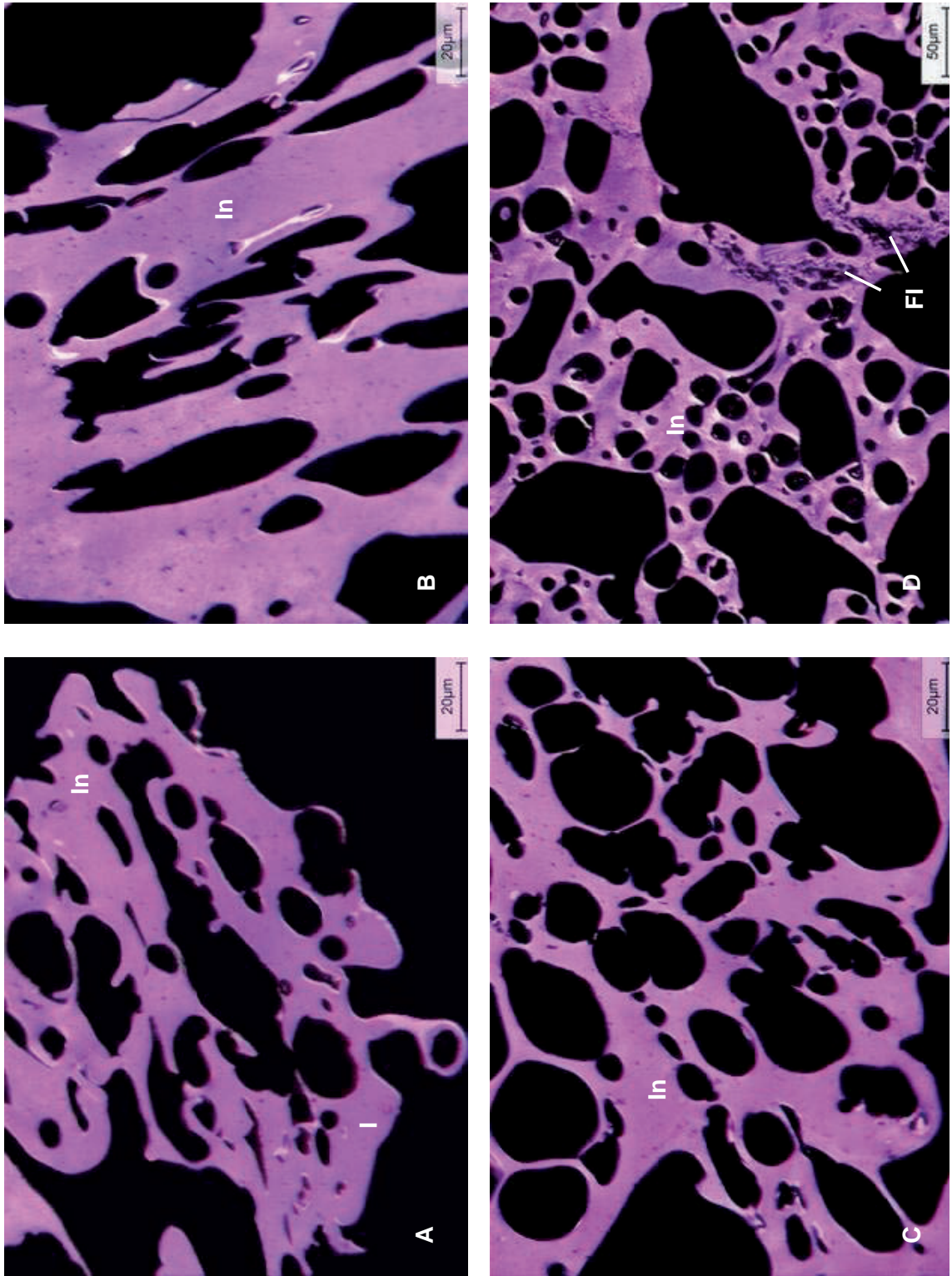
Filler phase carbon forms:

- FI:** Fine Inerts
- CI:** Coarse Inerts
- FM:** Fine Minerals
- CM:** Coarse Minerals

Depositional carbon forms:

- Py:** Pyrolytic
- Sph:** Spherulitic

Figure A.F.1: A) Isotropic and incipient carbon forms from a carbonized sample of St HD. This photomicrograph is from a relatively bright part of the sample. B) Incipient carbon forms from BG LD. Notice the slits from pseudovitrinite. C) Incipient microtextures from a BG LD sample. Notice the higher porosity compared to B). D) Incipient carbon forms and fine inert inclusions in BG HD.



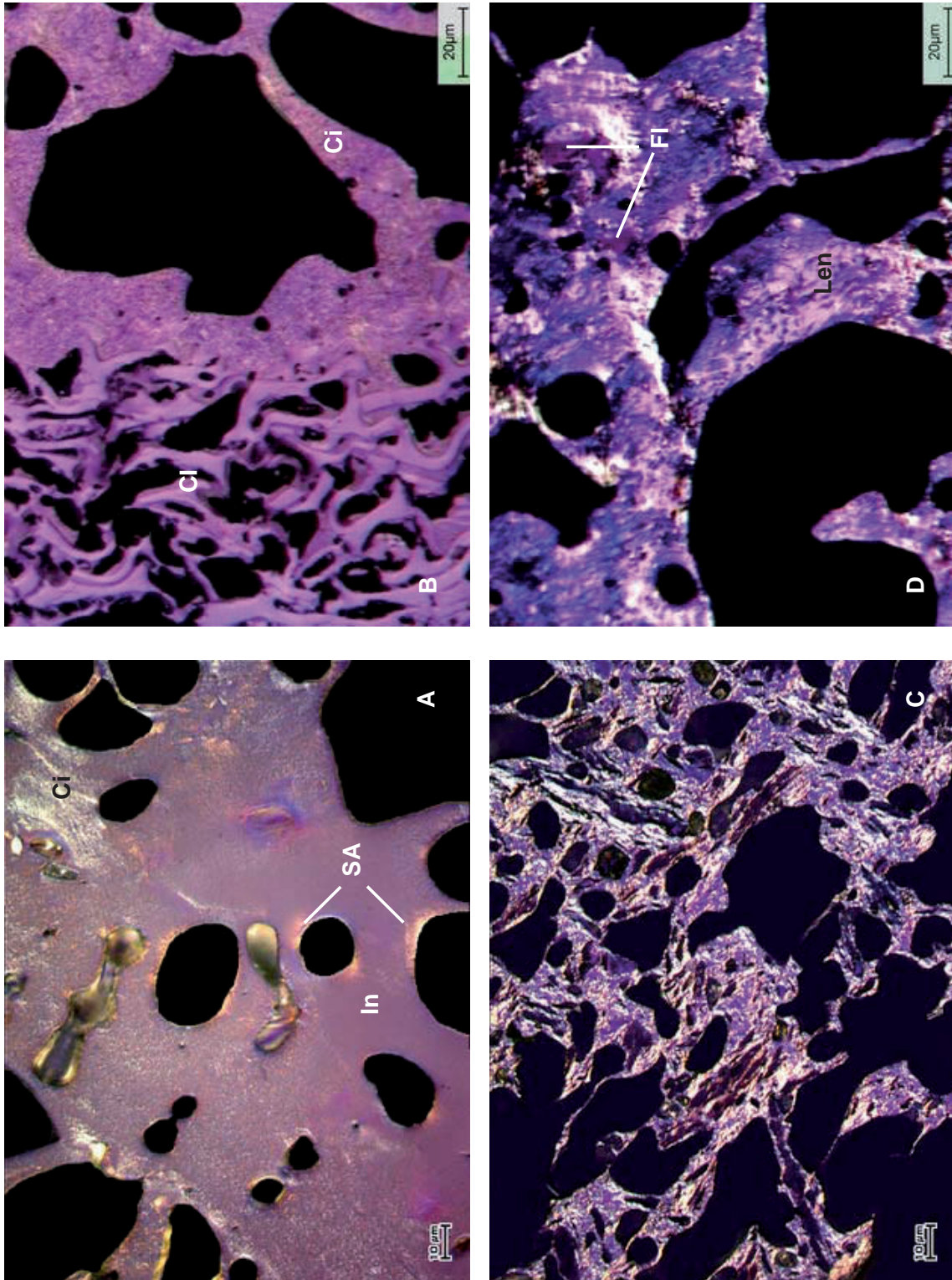
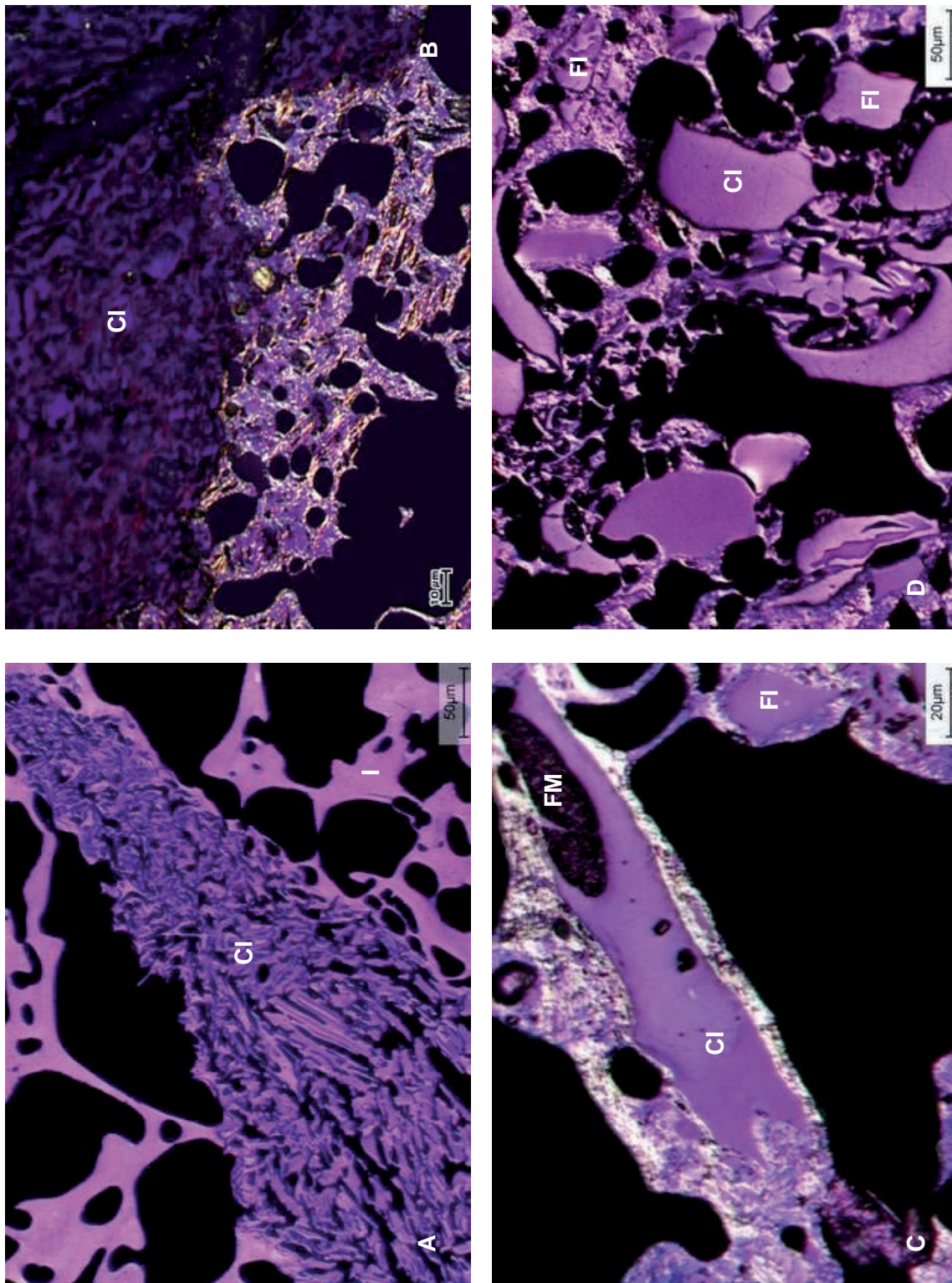


Figure A.F.2: A) Transition from incipient to fine circular carbon forms in BG L.D. Strain anisotropy around the pores are also visible. B) Circular microtextures and a coarse inert in a carbonized sample of St L.D. The higher degree of anisotropy in PD is clearly illustrated in C and D.

Figure A.F.3: Infusible inclusions from fusinite are present in respectively BG (A) and PD (B). C) Well embedded inerts in the binder phase of PD LD. The coarse inert also contains some mineral matter. D) Infusible remnants from the maceral secretinite in PD HD



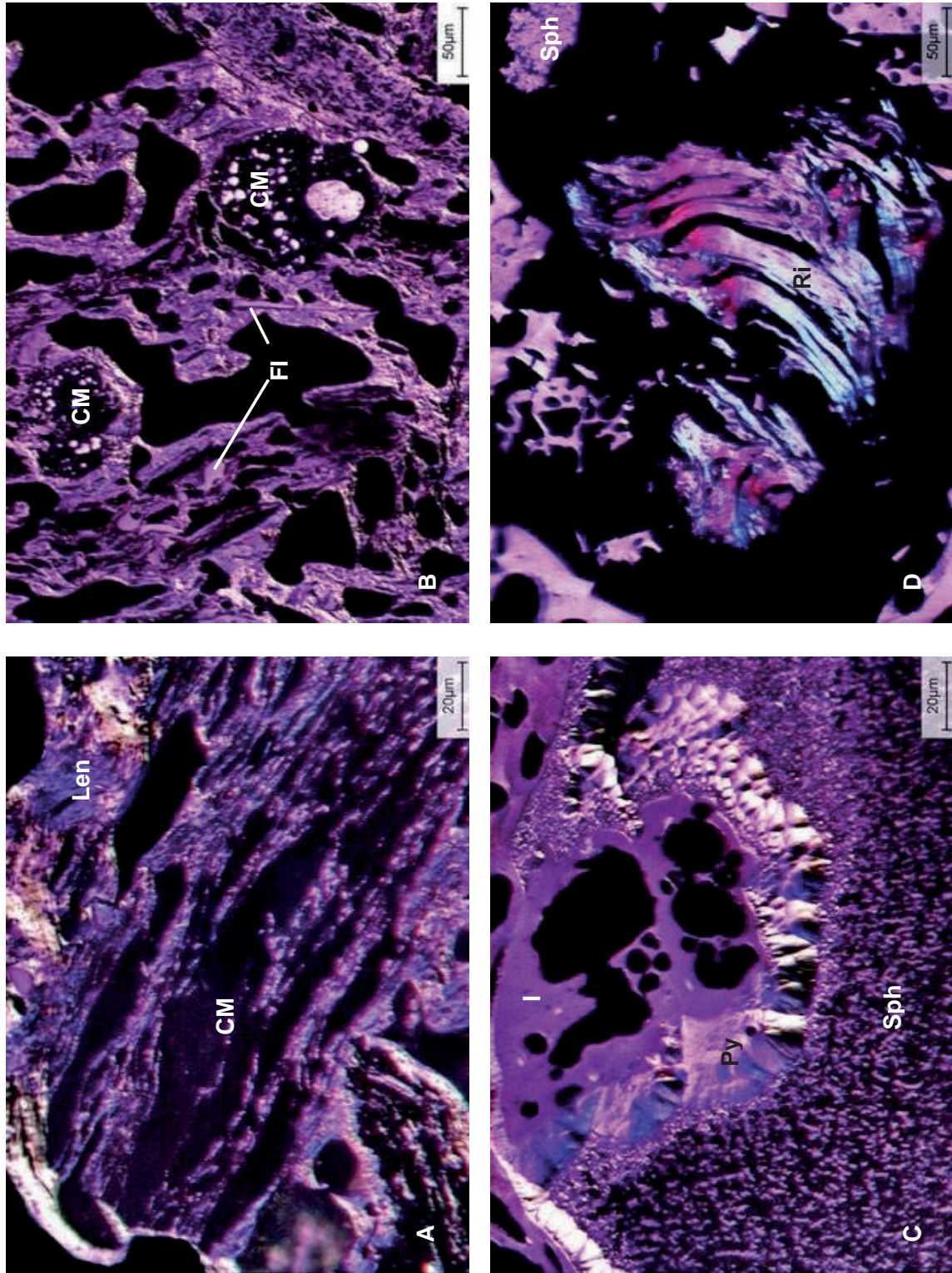


Figure A.F.4: A) A coarse mineral inclusion well embedded in the binder phase of PD HD. B) A mixture of different minerals and fine inert inclusions in PD HD. C) Depositional carbon forms in BG LD. D) Carbon forms with ribbon like anisotropy from BG LD. These most likely originated from condensation of oil like substances.

APPENDIX G: REACTIVITY PROFILES

Both measured- and corrected reactivity curves for all the tests performed in the SINTEF SiO reactivity test are illustrated in the following Appendix.

Blue Gem:

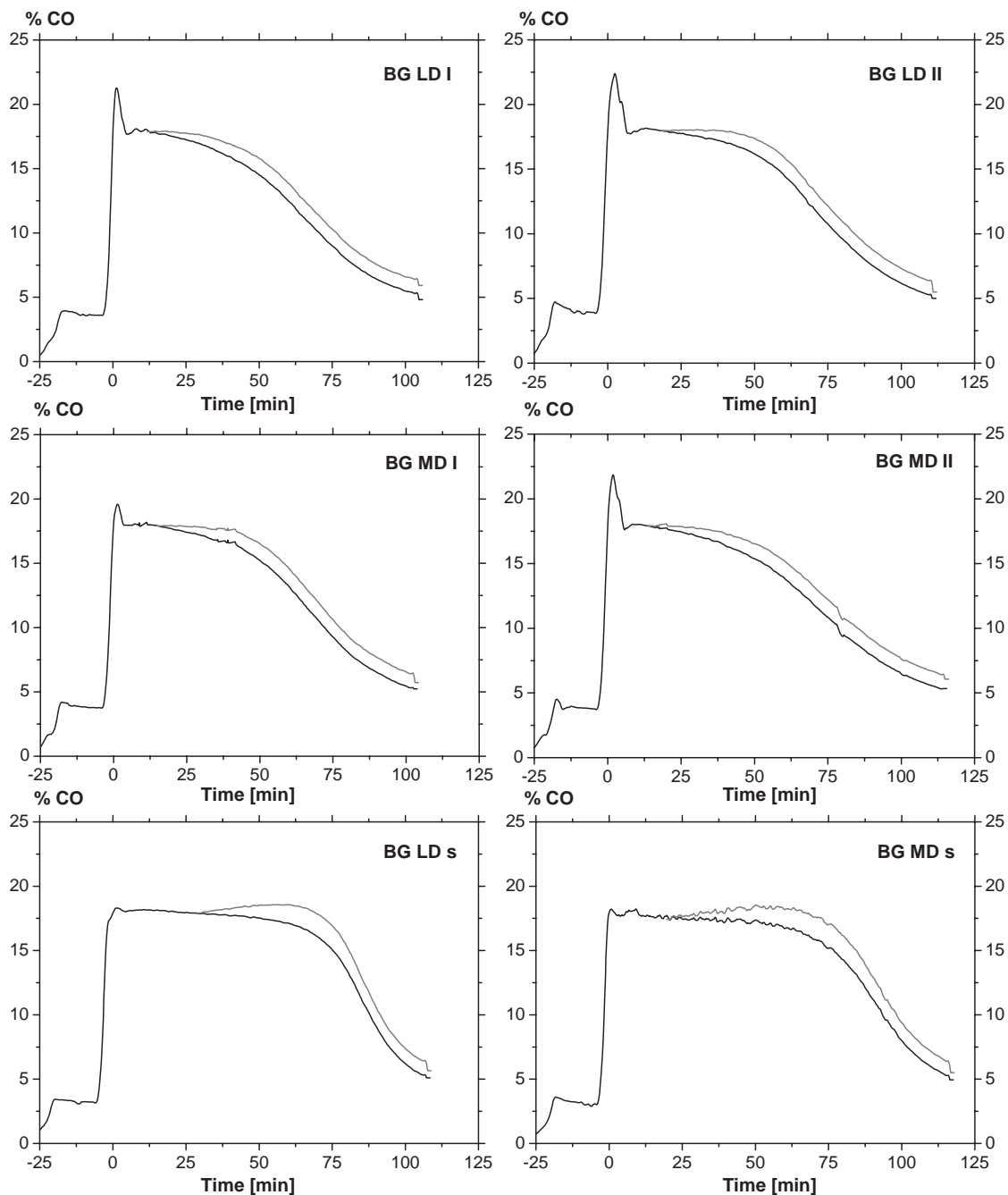


Figure A.G.1: Measured- and corrected reactivity profiles are black and grey, respectively. *LD* and *MD* refer to the Low- and Medium density fractions. *I* and *II* are parallels of the same fraction while *s* is used for test with reduced particle size.

Peak Downs:

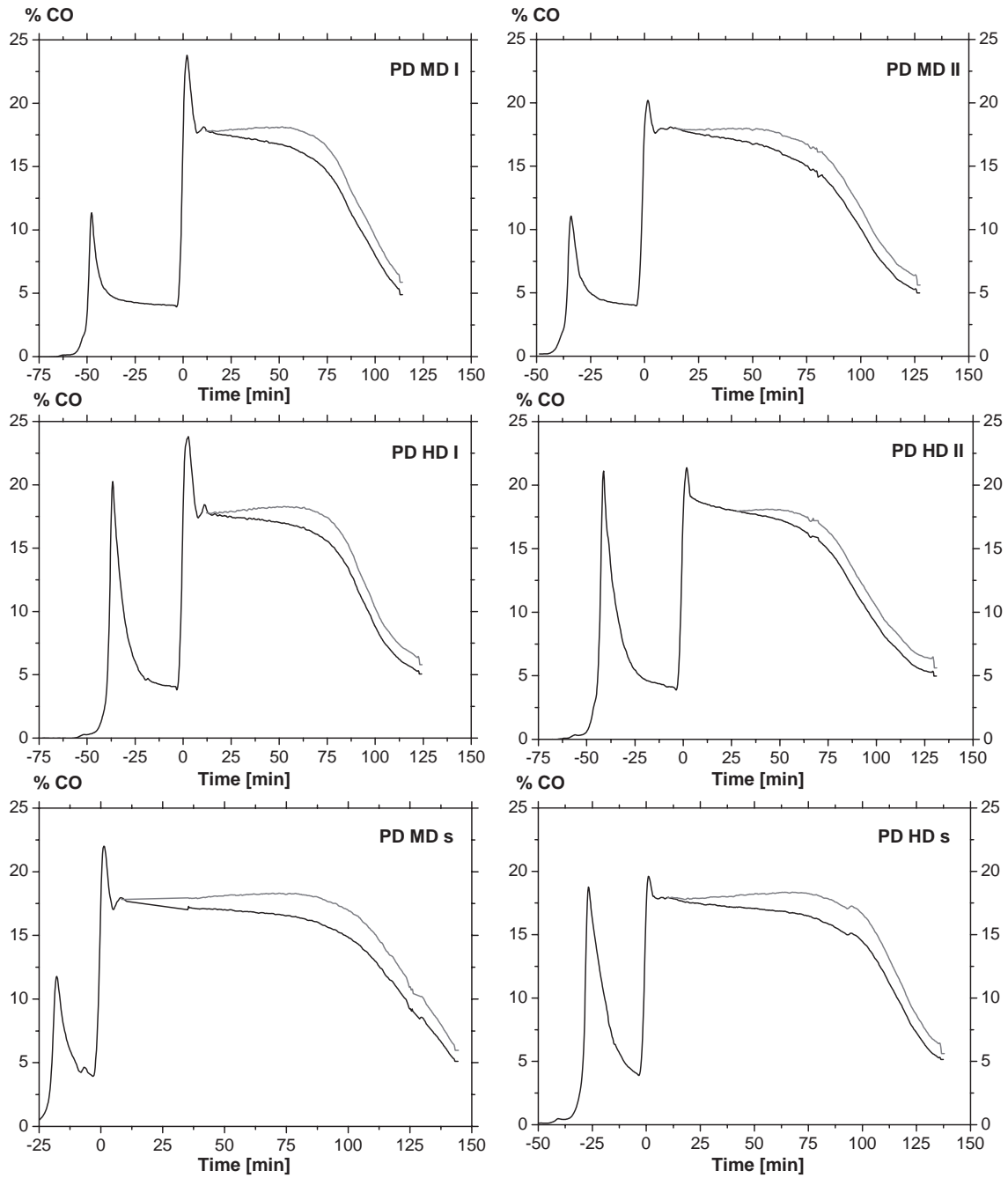


Figure A.G.2: Measured- and corrected reactivity profiles are black and grey, respectively. *LD* and *MD* refer to the Low- and Medium density fractions. *I* and *II* are parallels of the same fraction while *s* is used for test with reduced particle size.

Staszic:

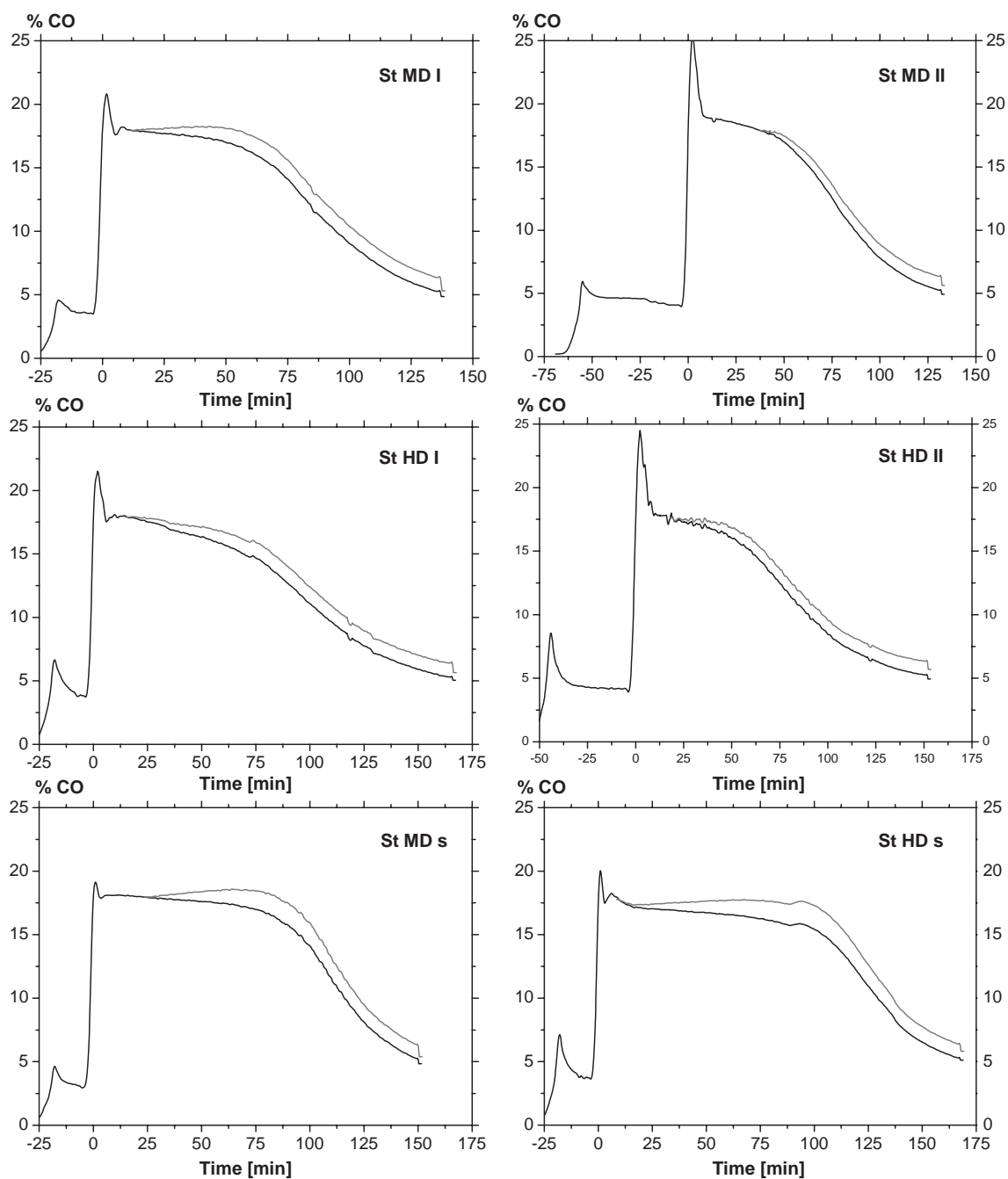


Figure A.G.3: Measured- and corrected reactivity profiles are black and grey, respectively. *LD* and *MD* refer to the Low- and Medium density fractions. *I* and *II* are parallels of the same fraction while *s* is used for test with reduced particle size.

APPENDIX H: EVALUATION OF KINETIC PARAMETERS

A procedure for obtaining kinetic parameters of the sample material was outlined in section 5.8.2, and the best fitted parameters were presented in Table 5.18. The model used to find the kinetic parameters has applied the full expression for the shrinking core model (equation 2.9) in a packed bed. This model was implemented in Matlab by **Myrhaug (2003)**. In order to illustrate how the chosen values for effective diffusivities, D_E , and reaction rate constants, k_C , in the reactivity model fit with the corrected reactivity curves, all the tests are illustrated in the present Appendix.

As mentioned in section 5.8.2, a good fit for both size fractions of the Peak Downs samples was not possible by keeping the kinetic parameters constant. The behaviour of this particular coal sample can not be predicted based on the shrinking core model (see Figure 5.39). As for the rest of the samples, the best possible fits were made for the samples whose parallels were the most accurate, i.e. low standard deviation. From Figure 5.27, it can be seen that the MD fraction of Staszic showed that lowest value of standard deviation. Correspondingly this sample showed the most accurate fit to the reactivity model.

Blue Gem:

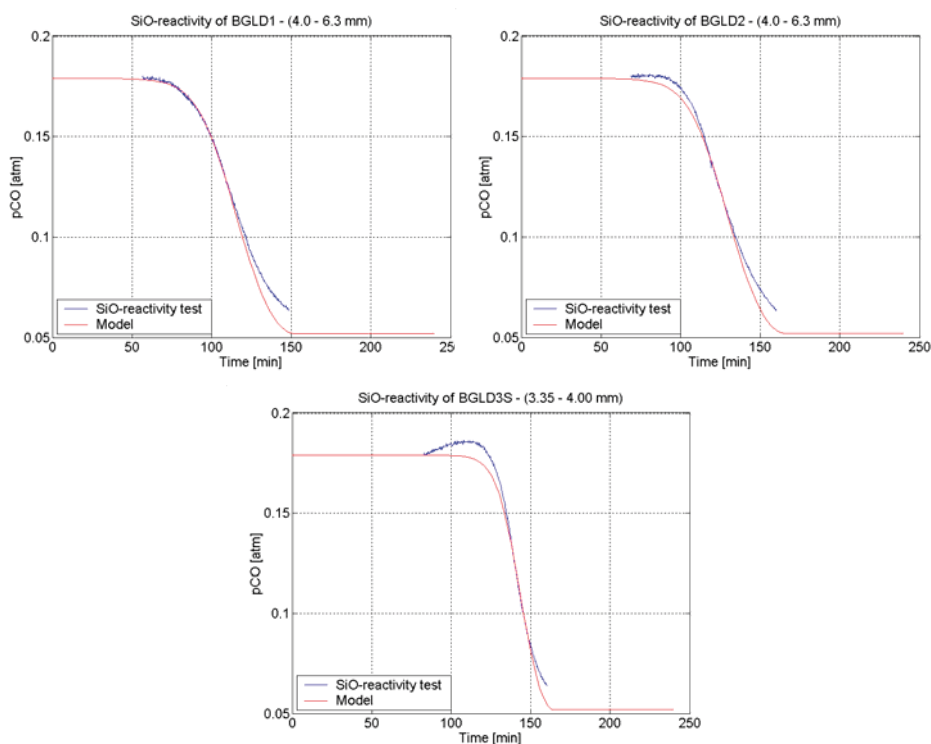


Figure A.H.1: Kinetic constants for BG LD: $D_e = 4.5 \cdot 10^{-5} \text{ m}^2/\text{s}$ and $k_c = 0.085 \text{ m/s}$.

APPENDIX H: EVALUATION OF KINETIC PARAMETERS

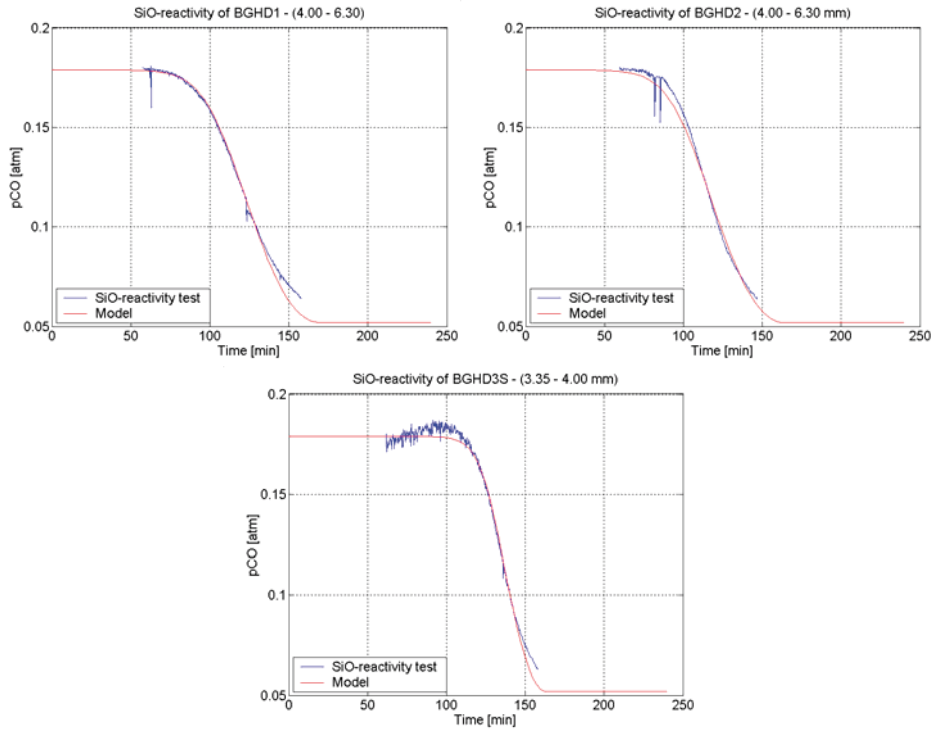


Figure A.H.2: Kinetic constants for BG MD: $D_e = 3.25 \cdot 10^{-5} \text{ m}^2/\text{s}$ and $k_c = 0.09 \text{ m/s}$.

Peak Downs:

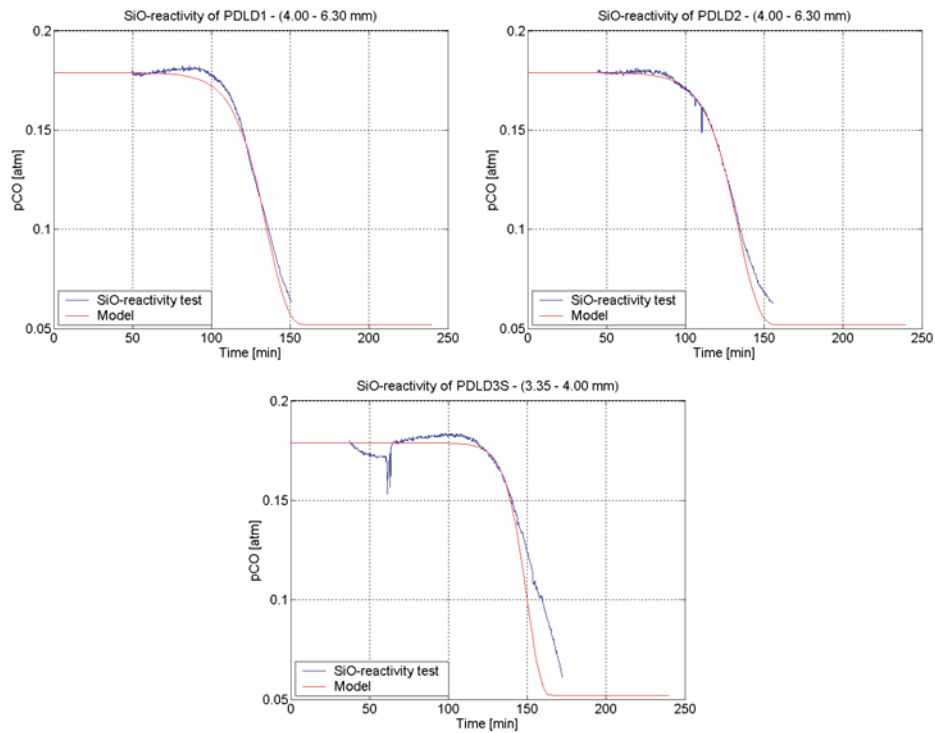


Figure A.H.3: Kinetic constants for PD MD: $D_e = 3.5 \cdot 10^{-4} \text{ m}^2/\text{s}$ and $k_c = 0.08 \text{ m/s}$.

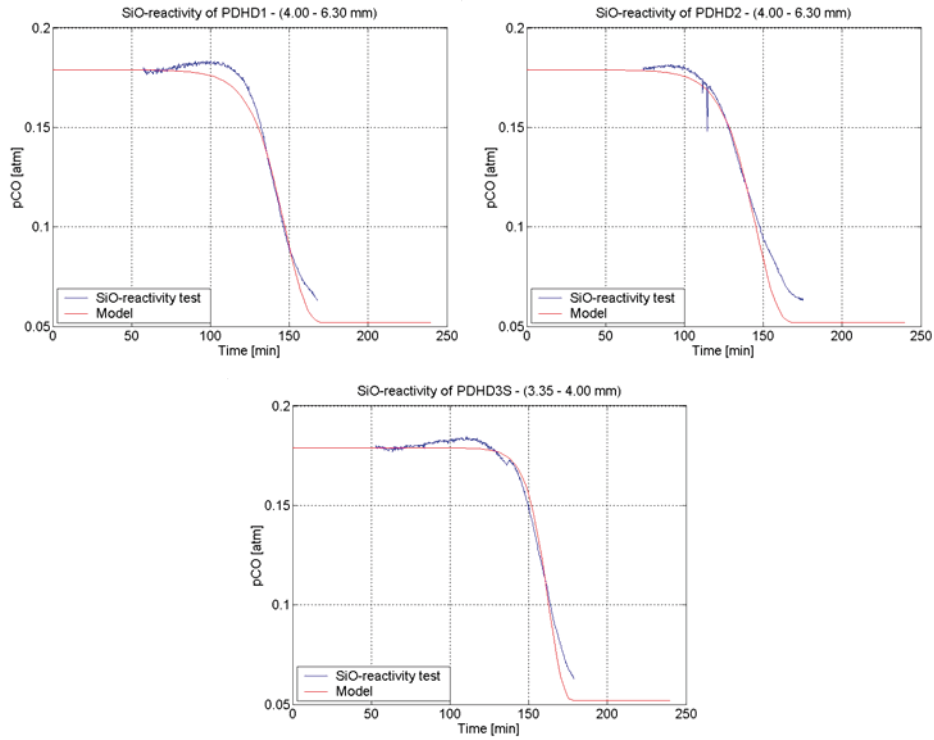


Figure A.H.4: Kinetic constants for PD HD: $D_e = 4.0 \cdot 10^{-4} \text{ m}^2/\text{s}$ and $k_c = 0.075 \text{ m/s}$.

Staszic

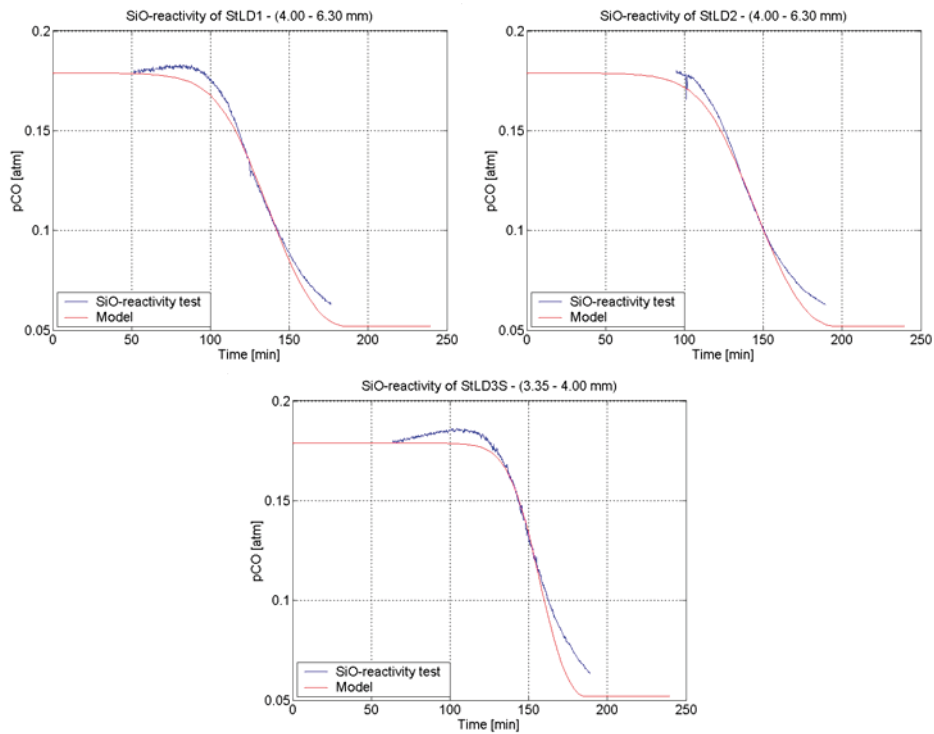


Figure A.H.5: Kinetic constants for St MD: $D_e = 3.65 \cdot 10^{-5} \text{ m}^2/\text{s}$ and $k_c = 0.065 \text{ m/s}$.

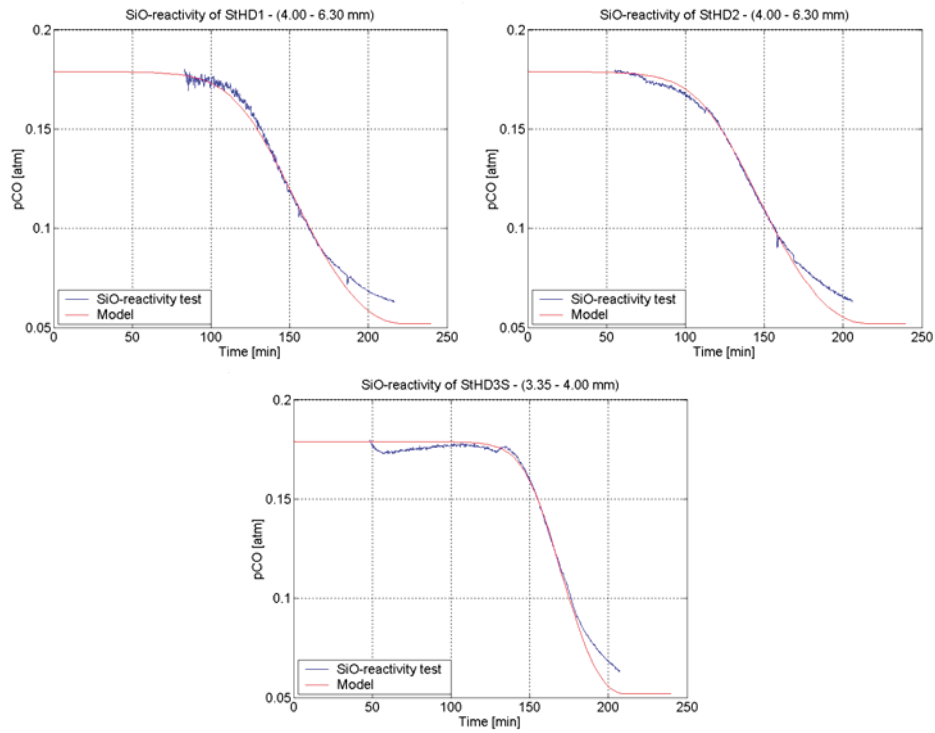


Figure A.H.6: Kinetic constants are the same in all models: $D_e = 2.4 \cdot 10^{-5} \text{ m}^2/\text{s}$ and $k_c = 0.060 \text{ m/s}$.

APPENDIX I: DATA FROM REACTIVITY EXPERIMENTS

Table A.I.1: Some of the data from reactivity experiments according to the SINTEF SiO reactivity test

Sample	Date	Weight in [g]	Weight out [g]	Weight Increase [%]	R10 corr [ml SiO]
<i>BGLD</i>	25.08.06	4.7667	7.4028	55.3	708
<i>BGLD</i>	31.10.06	5.3658	8.3785	56.1	618
<i>BGHD</i>	07.09.06	5.1882	8.4061	62.0	781
<i>BGHD*</i>	30.11.06	4.9709	7.7606	56.1	
<i>BGHD</i>	06.12.06	4.9590	7.8084	57.5	623
<i>PDL D</i>	06.06.06	6.2160	9.3759	50.8	523
<i>PDL D</i>	13.12.06	6.1386	9.2531	50.7	592
<i>PDHD</i>	05.07.06	7.1115	10.0899	41.9	451
<i>PDHD</i>	14.12.06	7.4680	10.2492	37.2	637
<i>StLD</i>	28.06.06	6.1943	9.9050	59.9	754
<i>StLD</i>	23.11.06	6.5620	10.3783	58.2	782
<i>StHD</i>	27.06.06	7.2253	11.1682	54.6	1158
<i>StHD</i>	22.11.06	6.9072	10.6146	53.7	1020
<i>BGLDs</i>	13.04.07	6.0192	9.2523	53.7	329
<i>BGHDs</i>	23.04.07	5.8400	9.2754	58.8	436
<i>PDL Ds</i>	17.04.07	7.0736	10.6997	51.3	624
<i>PDHDs</i>	02.05.07	8.1144	11.0046	35.6	467
<i>StLDs</i>	10.04.07	7.2314	11.2352	55.4	590
<i>StHDs</i>	30.03.07	7.9988	12.4183	55.3	832

* Due to computer problems, the reactivity data was not recorded for this experiment

